

dc\_303\_11

MTA Doktori Értekezés

**A humán kognitív, alvási és epilepsziás agykérgi elektromos  
tevékenység rétegelvezetéses vizsgálata**

Dr. Ulbert István

MTA Természettudományi Kutatóközpont  
Kognitív Idegtudományi és Pszichológiai Intézet  
Összehasonlító Pszichofiziológiai Csoport

Budapest, 2013

**TARTALOMJEGYZÉK**

BEVEZETÉS	3
CÉLKITŰZÉSEK	5
Módszertani kutatások	5
A kognitív funkciók rétegelemzéses vizsgálata	5
Az alvási oszcillációk rétegelemzéses vizsgálata	5
Az epilepsziás tüskézés rétegelemzéses vizsgálata	6
MÓDSZEREK	7
A rétegelektrodok	7
Az előerősítő	7
A potenciál gradiens elvezetés tulajdonságai	9
Az adatregisztráló rendszer	10
Adatanalízis	10
Áramforrás sűrűség elemzés	10
Egysejt és soksejt aktivitás elemzés	11
Spektrális analízis	12
Műtéti eljárások	12
Hisztológia	13
A kísérleti személyek összeállítása	13
A kutatáshoz kapcsolódó kockázatok	14
A kutatáshoz kapcsolódó előnyök	14
Kognitív feladatok	15
EREDMÉNYEK	16
A hemodinamikai és idegi tevékenység kapcsolata	16
A hemodinamikai és rétegelvezetési jelek egyidejű regisztrációja	16
Az elülső cinguláris kéreg kognitív funkciói	18
Az elülső cinguláris kéreg aktivitása a különböző feladatokban	19
Az anteroventrális temporális lebeny kognitív funkciói	20
Az ismétlés feldolgozása az anteroventrális temporális lebenyben	21
Az alvási oszcillációk rétegelemzéses vizsgálata	23
A K-komplex kérgi forrásai	26
A lassú oszcilláció kérgi forrásai	27
A lassú oszcilláció térbeli terjedésének vizsgálata	28
Az epilepszia hatása az alvási oszcillációkra	29
Az epilepsziás tevékenység rétegelemzéses vizsgálata	31
Az interiktális tüskézés tulajdonságai a hippocampusban	32
Az interiktális tüskézés tulajdonságai a szubikulumban	33
Az interiktális tüskézés tulajdonságai a kéregben	35
Az egysejt aktivitás és az interiktális tüskézés kapcsolata	36
ÖSSZEFOGLALÁS	38
KÖSZÖNETNYILVÁNÍTÁS	39
IRODALOMJEGYZÉK	40
AZ ÉRTEKEZÉS ALAPJÁUL SZOLGÁLÓ SAJÁT KÖZLEMÉNYEK	45
AZ ÉRTEKEZÉS TÉMÁJÁHOZ KAPCSOLÓDÓ EGYÉB KÖZLEMÉNYEK	46
A TELJES ÉLETMŰ TUDOMÁNYMETRIAI MUTATÓI	46
MELLÉKLETEK	47

**BEVEZETÉS**

Az élővilág evolúciójának egyik legösszetettebb eredménye az emberi agykéreg. Az emberi agykéreg nemcsak egy nagymértékben felskálázott állati rendszer, hanem unikális, az állatvilágtól eltérő sejtmorfológiai és ideghálózati összeköttetésbeli tulajdonságok jellemzik (Elston, 2003; Elston et al., 2006; Herculano-Houzel et al., 2007). Ezek a különleges tulajdonságok tették lehetővé többek között az absztrakt emberi gondolkodás kifejlődését, valamint ebben az összetett rendszerben kialakuló hibák okozhatnak bizonyos emberre jellemző betegségeket, például az epilepsziát.

Az állatvilágtól nagyban eltérő kognitív képességek a tagolt emberi nyelv kialakulásával teljesebben ki, mely képességek háttérében a memória fontos szerepet kapott. Különösen a tényekre irányuló memória az, ami segítheti a hatékony emberi kommunikáció kialakítását. A tényekre irányuló memória megszilárdítása emberben az alvás lassú hullámú fázisában történik, így az alvás és a kognitív folyamatok szoros összefüggésben állnak egymással (Huber et al., 2004; Vyazovskiy et al., 2008). Hasonló összefüggéseket találhatunk az alvás és az epilepszia vonatkozásában. Az egyik orvosi szállóige szerint „Az alvás és az epilepszia hálótársak.”. Az epilepsziák egy része előszeretettel manifesztálódik az alvás-ébrenléti ciklus határán, illetve a mély alvási fázisokban (Halasz, 2012; Steriade, 2003). Az állatvilágban a kutya kivételével az emberhez hasonló nem szimptomás epilepszia betegség természetesen csak igen ritkán fordul elő, ellentétben a számos mesterségesen előállított állatmodellel.

Megítélésünk szerint mind az emberi kognitív képességek, mind az emberi alvás, mind az emberi epilepszia nagymértékben különbözik az állatvilágban megjelenő hasonló képességektől, illetve állapotoktól. Ezért a kognitív, alvási és epilepsziás állatmodellek vizsgálatának eredményei az emberre mechanisztikusan nem vonatkoztathatóak.

A korrekt modellalkotás egyik kritériuma az, hogy egy bizonyos szinten ismerjük meg azt a rendszert, amiről modellt szeretnénk alkotni. Ha tehát összehasonlítható sejt illetve ideghálózati szintű modellt szeretnénk kidolgozni valamely fent említett funkció vizsgálatára állatban, akkor legalábbis megfigyelhetővé kellene tenni az adott funkcióban az emberi agykéreg sejt és hálózati szintű működését. A sejt és hálózati szintű működés megfigyelése olyan módszereket követel, amelyekkel megfelelő téri és időbeli felbontással rögzíthetjük az egyes elemi idegi folyamatokat: az akciós potenciálokat, a serkentő és gátló posztzinaptikus és egyéb transz-membrán áramokat.

Ezeknek az elemi idegi folyamatoknak a megismerésére használatos módszerek mind a mai napig invazív agyi behatolást igényelnek, tehát nem meglepő, hogy vizsgálatuk egészséges emberben nem megvalósíthatóak.

A gyógyszer rezisztens epilepszia betegség sebészi kezelése során olyan ablakot nyitottunk az emberi agyra, melyben invazív beavatkozások segítségével az elemi idegi működések egy részét közvetlenül regisztrálni tudtuk (Ulbert et al., 2001a; Ulbert et al., 2001b; Ulbert et al., 2004a; Ulbert et al., 2005).

Az agykéregben lejátszódó elemi idegi folyamatok megfigyelésére sokcsatornás rétegelektrod rendszert fejlesztettünk ki, melyhez hasonlóan korábban állatkísérletekben használtunk (Mehta et al., 2000a; Mehta et al., 2000b). A rétegelvezetések jelentősége abban rejlik, hogy az agykérgi rétegek szintjén nagy tér és időbeli felbontásban tudunk elektrofiziológiai adatokat rögzíteni a vizsgált kérgi régió idegi aktivitásáról. A rétegelektrodok segítségével lehetővé vált a szakirodalomban először a skalpon illetve az agy felszínén mért potenciálteret generáló áramforrások pontos agykérgen belüli, intrakortikális lokalizációja, valamint a kapcsolt sejtaktivitás pontos tér és időbeli dinamikájának leírása.

Az intrakortikális áramforrások és a sejtaktivitás elemzése segítségével meghatározhatjuk, mely elemi idegi folyamatok vesznek részt a vizsgált agyi elektromos tevékenység kialakításában. Az anatómiai és elektrofiziológiai adatok összevetésekor pedig megállapíthatjuk az elemi idegi folyamatok kérgi rétegek szerinti eredetét.

## **CÉLKITŰZÉSEK**

Kutatásaink elsődleges célja az volt, hogy felderítsük, milyen nagy léptékű és helyi hálózati és sejtszintű idegi mechanizmusok felelősek az emberi agykérgi kiváltott válaszok, oszcillációs jelenségek, valamint patológiás események kialakulásáért. Három alapvető agyi működési módot vettünk részletes vizsgálat alá; a kognitív az alvási és az epilepsziás folyamatokat. Kutatásaink felfedező, leíró jellegűek, hiszen eddig még mások által feltáratlan területet céloztunk meg. A következőkben összefoglalt konkrét feladatokat tűztük ki magunk elé kutatásaink során:

### **Módszertani kutatások**

- Az intraoperatív rétegelvezetések technikai kidolgozása és hazai bevezetése.
- A krónikus alvási rétegelvezetések technikai kidolgozása és hazai bevezetése.
- A rétegelvezetések valamint a klasszikus ECoG módszerek együttes alkalmazásának kidolgozása és hazai bevezetése
- Szimultán elektromos és hemodinamikai regisztráló rendszer kidolgozása.
- Az elektrofiziológiai és az anatómiai adatok fúziójának kidolgozása.

### **A kognitív funkciók rétegelemzéses vizsgálata**

- Az elülső cinguláris kéreg és az anteroventrális temporális lebeny kognitív feladatok alatti tevékenységének vizsgálata.
- A kognitív feldolgozásban résztvevő idegsejt populációk aktivitásának és a szinaptikus/transz-membrán áramok dinamikájának leírása.
- A kérgi mikro-régiók ingerfeldolgozási stratégiájának leírása.

### **Az alvási oszcillációk rétegelemzéses vizsgálata**

- Az alvási oszcillációk (K-komplex, lassú oszcilláció) rétegelvezetéses elemzőmódszereinek kidolgozása.

- A K-komplexhez kötött elektromos tevékenység szinaptikus/transz-membrán forrásainak és az akciós potenciál aktivitás dinamikájának agykérgi rétegek szerinti karakterizálása.
- A K-komplex nagyléptékű leírása ECoG elvezetések segítségével.
- A lassú oszcillációhoz kötött elektromos tevékenység szinaptikus/transz-membrán forrásainak és az akciós potenciál aktivitás dinamikájának agykérgi rétegek szerinti karakterizálása.
- A lassú oszcilláció terjedésének nagyléptékű leírása ECoG elvezetésekben, nemlineáris módszerek segítségével.

### **Az epilepsziás tüskézés rétegelemzéses vizsgálata**

- A interiktális tüskékhez kapcsolódó szinaptikus/transz-membrán és akciós potenciál tevékenység kérgi rétegek szerinti vizsgálata.
- A laterális temporális lebeny és a hippokampusz valamint a szubikulum aktivitásának elektrofiziológiai vizsgálata interiktális tüskézés alatt.
- Az interiktális tüskézés epilepsziás hálózatban betöltött funkciójának elemzése.
- Az interiktális tüskézéshez kapcsolódó akciós potenciál aktivitás leírása.

## MÓDSZEREK

### A rétegelektrodok

Négy különböző típusú rétegelektrodot fejlesztettünk ki, és használtunk tanulmányainkban. Az úgynevezett *rajzsög elektrodot* a szubdurális klinikai rács vagy szalag elektrokortikográfiás (ECoG) elektrodokkal együttes beültetésre terveztük, a *mély elektrodot* a klinikai mély iEEG (intrakraniális elektroencefalogram: iEEG) elektrodokkal való beültetésre szántuk, a *hippokampális elektrodot* az intraoperatív megfigyelésekre dolgoztuk ki, míg az *optód* alapvetően egy rajzsög elektrod, melyet optikai feltétellel láttunk el, így az alkalmassá vált az elektrofiziológiai és az agyi véráramlási paraméterek egyszerre történő mérésére is.

A rétegelektrodok átmérője 0.45 mm, 24 elvezető kontaktust tartalmaztak, melyek egymástól mért távolsága 0.15 mm. A rajzsög és a mély elektrod tüje polyimidből, míg a hippokampális elektrod tüje rozsdamentes sebészeti acélból készült. Az elvezető kontaktusok átmérője 40 mikrométer, melyet a polyimiddel szigetelt platina/irídium szálak elcsiszolt végei alkottak két-komponensű műgyantába ágyazva. A rajzsög elektrod fedő lapját sebészeti tisztaságú szilikon gumiból alakítottuk ki.

A felhasznált anyagok mindegyike, amelyik a szövetekkel érintkezett, így a polyimid cső, a rozsdamentes sebészeti acél cső, a két-komponensű műgyanta, a szilikon gumi valamint a platina/irídium huzal az Egyesült Államok Gyógyszerészeti Intézete által elfogadott szervezetbe ültethető minősítéssel rendelkezett. Az elektrodokat etilén-oxid gázban sterilizáltuk a klinikai protokolloknak megfelelően.

### Az előerősítő

Az előerősítő feladata az, hogy illeszti a rétegelektrod elvezetési kontaktusain detektálható feszültség jelet a külső erősítő bemenetére. Az előerősítőnek számos kritériumnak kell megfelelnie. Az egyik legfontosabb szempontunk a tervezésnél az eszköz mérete volt. Olyan megvalósítási módokat kerestünk, melyek lehetővé teszik az áramkörnek a páciens fejen található kötésben való elhelyezését. A kis alapterület elérése végett felületszerelt áramköri elemeket használtunk, valamint négy rétegben szereltük a nyomtatott áramköri lapokat. Így a könnyű, kötésbe helyezhető kisméretű eszköz viselése nem okozott

problémát a betegeknek. A pontos forrás lokalizációs mérések elvégzésére precíziós műszererősítő integrált áramköri elemeket használtunk az előerősítő megvalósításánál.

Mivel az elvezetési kontaktusok impedanciája igen magas (300-500 kOhm), olyan műszererősítő implementációt kerestünk, amely segítségével igen kis veszteséggel lehet illeszteni a kontaktus magas impedanciáját a külvilághoz. A precíziós kívánalmaknak megfelelően azt a célt tűztük ki, hogy az előerősítő bemeneti impedanciája legalább három nagyságrenddel legyen magasabb, mint a kontaktus impedanciája. Ebben az esetben a jel leosztódása az előerősítő bemenetén kisebb, mint 1/1000 (0.1 %), ami elfogadható precíziós kritériumnak.

Mivel az elvezetési kontaktusok igen kis területűek és így impedanciájuk igen magas, a megkívánt bemeneti impedancia csak junction field effect transistor (JFET) vagy complementer metal oxide semiconductor (CMOS) technológiájú eszközzel valósítható meg. A JFET alapú műszererősítők termikus zaja sokkal kedvezőbb a fiziológiában használt frekvencia tartományokban (0.1-20 kHz), különösen az alacsonyabb régióban (0.1-100 Hz), mint a CMOS alapú áramköröknek, így JFET alapú eszközt választottunk.

Az elektromágneses zavarok kivédése szintén alapvető tervezési kritérium volt az előerősítő elkészítésénél. Mivel a humán rétegelektrodok hossza meglehetősen nagy, az antenna hatás is igen nagymértékben jelentkezik. Így, az elektromos hálózati zaj (50 Hz és felharmonikusai) mellett az egyéb tranzienst és kommunikációs zajforrások például kapcsoló üzemű tápegységek, mobil telefonok is zavarják az agykérgi idegi tevékenység regisztrációját. Mivel az elektródák addicionális elektromágneses árnyékolása esetünkben nem kivitelezhető, mert az árnyékolás aránytalanul megnövelné az agyba ültetett eszköz méretét és így nagymértékű szövetkárosodást okozna, máshogyan kellett a külső elektromágneses zavarokat minimalizálni.

A szokásos mezőpotenciál elvezetéseknel legtöbbször egy külső referencia ponthoz viszonyítunk, mely a földelési ponttól különbözik. Ideális esetben a referencia ponton és az aktív elvezetési ponton a zavar jel megegyezik, és ezt a közös jelet az általánosan használt referenciális erősítők nagymértékben csillapítják. A csillapítás mértéke, vagyis a közös módusú zajelnyomás egy igen fontos paramétere az eszköznek. A modern erősítők közös módusú zajelnyomás paramétere elméletileg minimum 90 dB (törtben kifejezve: 1/31622, vagyis 1 V-os közös bemeneti zavar jel esetén a referenciális erősítő kimenetén 0.03162 mV-os jelet mérhetünk). A fenti 90 dB-es paraméter abban az esetben helytálló, ha az erősítő aktív és referencia bemenetére nagyon pontosan ugyanakkora impedancia kapcsolódik és a zavar jel is pontosan ugyanakkora a két mérőponton. Sajnálatos módon ezek a kritériumok a

gyakorlatban soha nem teljesülhetnek, mivel az élő szövetek dinamikusan változtatják fizikai tulajdonságaikat. Így sem a referencia valamint az aktív pontok azonos impedanciája sem a referencia valamint aktív pontok azonos feszültsége nem lehet ugyanaz. Következésképp a közös módusú zajelnyomás degradálódik, és referenciális erősítőknél a zavar jel gyakorlati biológiai alkalmazásokban mindig nagyságrendekkel nagyobb, mint ahogy azt az elméleti paraméterek sugallnák. Ez a zavar jel sokszor telíti a következő erősítési fokozatot, ezért az eredeti biológiai jel sajnos mér elméletileg sem lesz rekonstruálható.

### **A potenciál gradiens elvezetés tulajdonságai**

Első rétegelektrodos elvezetéseinket a szokásos referenciális erősítővel végeztük. Kórházi műtői körülmények között a mezőpotenciál méréseink sok esetben kiértékelhetetlenül zajosak voltak. Megfigyeltük, hogy a referencia elektród elhelyezése alapvetően befolyásolta a mérési eredményeket. Bizonyos helyekre fektetve a referencia elektródot az elvezetések kevésbé zajosak voltak. Sajnos szisztematikus összefüggést nem találtunk a referencia elhelyezése és a regisztrátum minősége között, ezért figyelmünk a referencia független megoldások felé fordult.

Mivel az általunk használt rétegelektrodok elvezetési pontjai szabályszerűen helyezkednek el egy vonal mentén egymástól azonos távolságban, ezt a topológiai adottságot használtuk fel egy referencia független, nagy zajtoleranciájú rendszer megtervezésére. Egy adott külső referencia ponttól való függetlenséget úgy tudtuk elérni, hogy bipoláris elvezetéseket használtunk. Sorban a rétegelektrod szomszédos elvezető kontaktusai közötti feszültség különbséget mértük a műszererősítővel tízszeres erősítésben. Az erősítés nagyságát precíziós ellenállással (0.05 %-os tolerancia) állítottuk be. Az eszköz tehát a mezőpotenciál első térbeli deriváltját szolgáltatja a kimeneten tízszeres erősítésben, a későbbiekben ezért a potenciál gradiens elvezetés elnevezést használjuk.

A szomszédos kontaktusok a rétegelektrod esetében igen közel helyezkednek el egymáshoz, tipikusan 0.15 mm-re, ellentétben a klasszikus referenciális elvezetéssel, amikor a referencia és aktív elektród közötti távolság sokkal nagyobb, tipikusan a cm-es tartományba esik. A referencia és aktív elektródok között mért távolsággal arányosan nő a köztük mérhető impedancia. A zajokat létrehozó, a szövetben folyó áramok függetlenek a mérőrendszer topológiájától, valamint az adott zajáram nagyobb impedanciákon nagyobb feszültség esést okoz, így távoli referencia esetében a zajfeszültség nagyobb lesz, mint közeli referencia

esetén. Különösen igaz a fenti megállapítás egy olyan zajos környezet esetén, mint a kórházi műtő, vagy az intenzív betegmegfigyelő szoba.

Klasszikus referenciális elvezetések esetében az aktív és referencia elektródok általában nagyon eltérő impedanciájúak. Míg az aktív elektródok kicsi felületűek és nagy impedanciájúak, hogy a mezőpotenciálok mellett az akciós potenciálok is regisztrálhatóak legyenek, addig a referencia elektród nagy felületű így kicsi impedanciájú, hogy stabil referencia feszültséget biztosítson. Az impedancia egyenlőtlenség a referenciális esetben leronthatja közös módusú zajelnyomást, így a zajos lesz az elvezetés.

A rétegelektrodok esetében a szomszédos elvezetési pontok impedanciájának értéke sokkal közelebb van egymáshoz, mint a referenciális elvezetések esetében, így a közös módusú zajelnyomás kevésbé romlik, ennek következtében a kimeneti zaj is alacsonyabb lesz. Összegezve tehát a gradiens előerősítő, különösen zajos környezetben jobb elvezetési minőséget produkál, mint a klasszikus referenciális eszközök.

### **Az adatregisztráló rendszer**

Az előerősítő differenciális jeleit a saját tervezésű főerősítőben (1000) található aktív szűrők osztották mezőpotenciál/EEG (0.1 Hz - 500 Hz) és akciós potenciál/soksejt aktivitás (100 Hz - 5 kHz) tartományra. Ezeket külön-külön két sávban digitalizáltuk, a mezőpotenciál/EEG tartományt nagy felbontású (16 bit) de lassabb (2 kHz/csatorna) analóg-digitális átalakítóval, míg az akciós potenciál/soksejt aktivitás tartományt gyors (20 kHz/csatorna) de kisebb felbontású (12 bit) analóg-digitális átalakítóval. A biztonsági követelmények betartása érdekében a főerősítő fokozat egy galvanikus izolátort is tartalmazott. Nagy kapacitású és gyors számítógépet és saját tervezésű regisztráló szoftvert használunk az adatgyűjtésre. Az adatokat merevlemezen tároltuk a további feldolgozásra.

### **Adatanalízis**

#### **Áramforrás sűrűség elemzés**

Az agykéregben detektálható mezőpotenciálok szummációs jellegű elektromos folyamatok eredményei. Kialakulásukért a megfigyelési helytől távoli idegsejt elemek éppúgy felelősek, mint a közeli generátorok. Minket az intrakortikális folyamatok lokális megjelenése érdekelt leginkább, ezért a távoli hatások eliminálására segítségül hívtuk az áramforrás sűrűség analízist (Mitzdorf, 1985; Nicholson and Freeman, 1975). Az áramforrás

sűrűség analízis megadja a potenciáletteret generáló helyi áram források, illetve áram nyelők tér és időbeli mintázatát. Egy dimenziós, Hamming-ablakkal simított (Rappelsberger et al., 1981) a széleken interpolált (Vaknin et al., 1988) öt pontos áramforrás sűrűség analízist használtunk, mely matematikailag megfelel a mezőpotenciál második téri deriváltjának, illetve esetükben a mezőpotenciál gradiens első téri deriváltjának (Ulbert et al., 2001a). Az áram nyelő a lokális sejtpopulációnak a sejten kívüli térből a sejten belüli térbe irányuló összegzett membránáramát jelzi. A befelé folyó áram egyrészt a membránok szinaptikus depolarizációjából eredhet, mint aktív áramforrás sűrűség komponens, másrészt jelentheti az aktív áram nyelő által meghatározott áramkör passzív záródását. Az áram forrás kifelé irányuló összegzett membránáramot jelez. Fiziológiailag ez egyrészt passzív kiegyenlítődesi áramként értelmezhető, másrészt aktív hiperpolarizációt is jelenthet. Utóbbi lehet szinaptikusan hajtott hiperpolarizáció vagy például nem szinaptikus eredetű utóhiperpolarizáció.

Az áram források és áram nyelők egymáshoz viszonyított latenciájának, rétegek szerinti elhelyezkedésének, az észlelési hely szövettani környezetének és az akciók potenciál (egysejt), valamint a soksejt aktivitás tér és időbeli mintázatának ismerete a legtöbb esetben elegendő arra, hogy az észlelt elektromos jelekből az azokat létrehozó elemi idegi jelenségekre következtessünk.

### **Egysejt és soksejt aktivitás elemzés**

A soksejt aktivitás folyamatos becslésére a felvett adatokat tovább szűrtük digitálisan (300-3000 Hz sáv áteresztő szűrő, 48 db/oktáv meredekség, nulla fázistolás), majd vettük a jel abszolút értékét és egy végső digitális simító szűrést alkalmaztunk (50 Hz alul áteresztő szűrő, 24 db/oktáv meredekség, nulla fázistolás). Ez az analízis hasonló eredményeket szolgáltatott, mint a hagyományos egysejt és soksejt feldolgozó módszerek (Ulbert et al., 2001a).

A áramforrás sűrűség és soksejt analízis módszerek térbeli felbontását is vizsgáltuk, hogy becsléseket tudjunk adni, mekkora nagyságú térrészből tudunk aktív generátorokat kimutatni. Az általunk elvégzett szimulációk eredménye szerint egy aktív generátor szélétől számítva az áramforrás sűrűség értékek körülbelül tized részükre csökkennek 300 mikrométeren belül, míg a mezőpotenciálok ennél kisebb mértékben veszítenek amplitúdójukból a generátortól laterális irányban távolodva. A vertikális irányban még nagyobb a áramforrás sűrűség térbeli esése, így még a szürke állományon belül szinte nullára

csökkenhet az áram források és áram nyelők nagysága (Wang et al., 2005). Irodalmi adatok alapján a soksejt aktivitás térbeli esése az általunk kimutatott csökkenés nagyságrendjébe esik (Grover and Buchwald, 1970; Humphrey, 1968). Összegzőként tehát elmondhatjuk, hogy az általunk használt regisztrációs és analitikus módszerek térbeli érzékenysége a kérgi kolumnák nagyságrendjébe esik, így módszereink megfelelően nagy téri felbontásúak a kérgi mikro-régiók aktivitásának kimutatására.

### **Spektrális analízis**

Komplex Morlet-waveletre alapozott, az egyedi, átlagolatlan jelalakokat figyelembe vevő idő-frekvencia analízist használtunk mind a rétegelektrodos, mind a klinikai elvezetések spektrális elemzésére (Halgren et al., 2002; Kronland-Martinet et al., 1987). A frekvencia tartománybeli skálázást linearizáltuk, így aránylag egyöntetű idő-frekvencia tartománybeli leképezést tudunk elérni, körülbelül 80 ms-os időbeli és 2 Hz-es frekvencia tartománybeli felbontással, 1 Hz-es minimális detektálható frekvenciával (Wang et al., 2005).

Az egyes elektródok közötti fázis kapcsoltságot az irodalomban megtalálható módszerek szerint implementáltuk (Lachaux et al., 1999). Szimulációs eredményeink szerint a felhasznált módszer megfelelően detektálta az egyes elektródok fázis kapcsoltságot az 1 Hz-es tartománytól felfele, és a kapcsoltság kimutatása nagymértékben független volt az egyes jelalakok amplitúdójának nagyságától (Wang et al., 2005).

### **Műtéti eljárások**

A rétegelektrodát a szem felügyelete alatt vezettük be a kéregbe, a hippokampuszba, illetve a szubikulumba, merőlegesen annak felszínére. Krónikus elvezetések esetén műtét után a beteget az intenzív megfigyelő szobában helyeztük el, ahol a szokásos videó-EEG epilepszia monitorozás mellett különböző kognitív feladatokhoz kapcsolódó elektromos tevékenységet és spontán aktivitást vezettünk el. Miután a páciens epilepsziás fókuszát meghatározták, egy második műtetre került sor, melyben a fókuszot eltávolította az idegsebész, a rétegelektrod nyomot tartalmazó agyszövettel együtt. Az intraoperatív elvezetéseknel az előzőleg vizsgált szövetet a mérés után közvetlenül blokkban került eltávolításra. A kimetszett mintát szövettanilag feldolgoztuk, megállapítottuk az elektród szúrt csatornájának helyét, valamint a kérgi rétegek mélységét. Az elektród, valamint a szúrt

csatorna hosszából és a rétegek méreteiből kiszámítottuk az egyes elektród pontok helyzetét az agykéregben.

## **Hisztológia**

A szövet 4-5 mm széles blokkokra vágtuk és immerziósan fixáltuk 4 % paraformaldehidet, 0.1 % glutáraldehidet és 0.2 % pikrinsavat tartalmazó 0.1 M foszfát puffer alapú oldatban. A blokkokból vibrotómmal 60 mikrométer vastag szeleteket vágunk, és egymást követő foszfát pufferes mosások után a metszeteket immunfestettük, illetve párhuzamos metszeteken Nissl-festést végeztünk az elektródnyom rekonstrukciójához.

Az immunfestés során a következő eljárást követtük: a nem kötött fixálót 6x20 perces 0.1 M foszfát pufferrel kimostuk, majd tris pufferelt szalina oldatba helyeztük át a metszeteket. Minden szérumot tris pufferelt szalina oldatban hígítottunk, és az egyes inkubációs lépések között mostuk a metszeteket (3x20 perc). Blokkoló anyagot (5 %-os tejpor és 2 % bovin szérum albumin keveréke) is tettünk a metszetekre. Ezt követte a primer szérumokban történő inkubáció. Poliklonális nyúl-anti-parvalbumin, nyúl-anti-calbindin, nyúl-anti-calretinin primereket használtunk. Ezután biotinilált kecske-anti-nyúl szekunder szérumot tettünk a metszetekre. Ezt követte az avidin-biotin-tormaperoxidáz komplexszel történő inkubáció. A metszeteket kimostuk és 0.05 M koncentrációjú 3,3'-diaminobenzidin tetrahidrokloridban előinkubáltuk 20 percig, majd ehhez 0.01 %-os hidrogénperoxidot adva előhívtuk (Fabo et al., 2005; Ulbert et al., 2004b).

## **A kísérleti személyek összeállítása**

A kutatásban résztvevő személyek gyógyszer rezisztens epilepsziában szenvedtek. A páciensek gyógyításuk érdekében kerültek műtétre, részvételük a kutatásban önkéntes volt. A betegek epilepsziás roham fókuszát a sebészi feltárást megelőző diagnosztikus eljárások nem tudták megfelelően megállapítani, ezért vált szükségessé az epilepsziás fókusz invazív, intrakraniális elektrofiziológiai eszközökkel történő vizsgálata. A kísérleti személyek kiválasztását és a tudományos kutatásról való részletes tájékoztatását az idegsebész és a vezető kutató végezte. A betegek informált beleegyezési nyilatkozatot tettek, széles körűen tájékoztattuk őket a beavatkozásokkal kapcsolatos veszélyekről és előnyökről.

A klinikai vizsgálatok alapján az epilepszia sebészeti munkacsoport döntötte el, milyen sebészeti feltárást szükséges az egyes betegek operációjához, és hogy az alkalmazott

sebészeti technika lehetővé teszi-e az agykérgi rétegelvezetéseket. A sebészeti technikáról való döntés megelőzte a kísérletben való részvétel felmerülésének lehetőségét, attól függetlenül történt, mindenben a beteg gyógyulásának érdekeit tartva szem előtt.

A felhasznált etikai engedélyeket az Egészségügyi Tudományos Tanács, Tudományos és Kutatásetikai Bizottsága jegyezi: „A mikro-mély-elektrodák alkalmazása epilepsia sebészi kezelése során” (242/KO/2001. 6008/6/2001/ETT) és „A humán kortikális elektromos tevékenység komplex in vivo és in vitro vizsgálata agysebészeti műtetre kerülő páciensekben” (368/PI/2012. 20680-4/2012/EKU).

### **A kutatáshoz kapcsolódó kockázatok**

A kísérleteknek három kockázati tényezője van. Az intrakraniális vérzés, a gliózis és az esetleges fertőzés. Mivel az elektrodok a műtét alatt, direkt szemkontaktussal kerültek beültetésre, az idegsebész rögtön megtehetette a szükséges intézkedéseket. A gliózis keletkezésének lehetősége kizárható, mivel a beültetendő terület az eltávolítandó kéregrészre esett.

A rétegelektrod sterilizálása minden tekintetben hasonlóként történt, mint a klinikai elektrodák sterilizálása, ezért a fertőző ágensek műtét közbeni bevitelének kockázata minimális volt. Mivel a rétegelektrod kivezetése és izolációja minden tekintetben hasonlóként történt, mint a klinikai elektrodák kivezetése illetve izolációja, ezért a monitorozás alatti fertőzések kockázata szintén minimális volt.

A rétegelektrod beültetése során jelentkező kockázati tényezők tehát nagyban megegyeztek a konvencionális klinikai elektrodák beültetése következtében jelentkező kockázati tényezőkkel. Ezen kockázatokról a műtét közbeni komplikációkról, azok hatásáról illetve megoldásáról a használt gyógyszerek mellékhatásairól a kezelő orvos és a műtétet vezető sebész a kötelező klinikai és kísérletes protokollon keresztül tájékoztatta a pácienseket.

### **A kutatáshoz kapcsolódó előnyök**

Tapasztalataink szerint az egyik fontos motiváló erő a kutatásban való részvételre a páciensek természetes önzetlensége, a másokon való segíteni akarás volt. Sok, a kutatásba bevont beteg örömként élte meg a lehetőséget, hogy segíthetett más betegeken a saját adatait adományozva, így morális előnyt, hasznot kovácsolt ebből a szituációból. A másik lelki

természetű előny tapasztalataink szerint a kognitív feladatok elvégzéséhez kapcsolódott. Ezekben a vizsgálatokban résztvevő betegek általában magas motivációval végezték a tesztek, sikerélményként élték meg a jól teljesített feladatokat.

A kutatásban résztvevő betegek speciálisan kidolgozott mágneses rezonancia (MR) vizsgálatra kerültek, mely vizsgálatok sokkal részletesebb strukturális képet adtak a páciensek agyáról, mint a standard klinikai gyakorlatban alkalmazott eljárások. Nagy felbontású strukturális MR vizsgálatokkal kívántuk megjeleníteni az esetlegesen standard MR vizsgálatokkal nem észrevehető nagyon kicsi területre kiterjedő agyfejlődési rendellenességeket és egyéb térfoglaló folyamatokat.

### **Kognitív feladatok**

A teljesség igénye nélkül az alábbi típusú kognitív feladatokat végezték a páciensek.

Az egyszerű/választásos reakció idő feladatban a célinger ~60 ms-ig villant fel jobb vagy baloldalon, míg a kísérleti személynek a bal vagy a jobb kezével kellett nyomnia a válaszgombot. Az egyszerű feladatban vagy a jobb, vagy a bal gombot kellett megnyomni, attól függetlenül, melyik oldalon jelent meg a célinger. A választásos feladatban vagy az inger oldalával megegyező, vagy azzal ellentétes kézzel kellett nyomni a gombot.

A késleltetett szómemória feladatban a kísérleti személynek 10 szót kellett memorizálni, ezek szolgáltak célingerként a próbák felében, mely szavakat a másik 50 %-ban meg nem ismételt szavak alkották. Összesen 12-szer ismétlődött véletlenszerűen a feladatok során az előzőleg memorizált 10 szó, melyeket képernyőre vetítettük egyenként ~300 ms ideig, fekete háttér előtt fehér betűkkel. A kísérleti személynek a domináns kezével kellett nyomnia a válaszgombot. Az inger után különböző hang jelezte a jó illetve a rossz választ.

A rímeléses feladatban a kísérleti személynek el kellett döntenie, hogy a bemutatott szó (angol) rímel-e az „AY”-ra. A bemutatott szavak egy része nem rímelt, a másik rész szabályszerűen rímelt (pl. say) a harmadik rész pedig szintén rímelt, de írásmódja rendhagyó volt (pl. weigh).

Az akusztikus kakukktojás feladatban a kísérleti személyek a sűrűn bemutatott hangok (79 %) mellett a ritkán bemutatott (10.5 %) célingerre kellett gombnyomással válaszolnia, míg a hasonló valószínűséggel (10.5 %) bemutatott nem célinger újdonság hangot figyelmen kívül kellett hagynia. Minden egyes újdonság hang magassága és spektrális tartalma unikális volt, kivéve a hang burkoló görbáját, mely megegyezett a standard és célinger (egyébként tiszta, szinuszos) hangok burkolójával.

**EREDMÉNYEK****A hemodinamikai és idegi tevékenység kapcsolata (1)**

Az agyi véráramlás dinamikájának és az agyi elektromos működésnek a kapcsolatát intenzíven kutatják napjainkban is. Funkcionális mágneses rezonancia (fMR) vizsgálatokkal kombinált elektrofiziológiai kísérletekben próbálják meghatározni az agyi véráramlás és az idegi tevékenység összefüggéseit (Logothetis et al., 2001; Logothetis, 2003). Az fMR vizsgálatok segítségével a vér oxigén telítettségétől függő jelet (blood oxygenation level dependent: BOLD) mérik, mely a különbözően oxigenált hemoglobinok koncentrációjától (deoxihemoglobin és oxihemoglobin) az oxigén helyi metabolikus rátájától, a helyi vérvolumentől és a helyi véráramlás nagyságától függ (Buxton et al., 1998). A BOLD választ meghatározó három legfontosabb mérőszám az oxi- és deoxihemoglobin koncentráció valamint az agyi véráramlási sebesség, melyek mérése optikai módszerekkel is lehetséges. Optikai módszereket alkalmazva állatkísérletes modellekben vizsgáltuk a BOLD válasz és az idegi tevékenység kapcsolatát (Devor et al., 2003; Devor et al., 2005; Devor et al., 2007; Devor et al., 2008).

Célunk egy olyan epilepsziás páciensekbe ültethető optikai-elektrofiziológiai regisztráló eszköz (1/1. ábra) és feldolgozó rendszer kifejlesztése volt, mellyel pont spektroszkópiát (1/2. ábra) és lézer-doppler áramlás méréseket tudtunk végezni, egyidejűleg a rétegelvezetésekkel. A spektroszkópia segítségével meghatározhatjuk az oxi- és deoxihemoglobin koncentrációkat, a lézer-doppler mérések segítségével következtetni tudunk a helyi véráramlás sebességére, a rétegelvezetésekkel pedig regisztrálni tudjuk a helyi idegi tevékenységet (Keller et al., 2009).

**A hemodinamikai és rétegelvezetési jelek egyidejű regisztrációja (1)**

A kifejlesztett optóddal (1/4. ábra) készült lézer-doppler áramlás mérések jól mutatták a helyi véráramlási sebesség változását a szív ciklus függvényében, hasonlóan az irodalmi adatokhoz (Basano et al., 2001; Montgomery et al., 1995).

A hemoglobin koncentrációk változását lélegzet visszatartásos feladatban vizsgáltuk és azt találtuk, hogy a lélegzet visszatartása után a deoxihemoglobin koncentráció megnőtt és az oxihemoglobin koncentráció lecsökkent (1/5. ábra), ami szintén megfelel az irodalmi adatoknak (Thomason et al., 2005).

Az elektrofiziológiai és hemodinamiai tevékenység összehasonlításához a klinikai kérgi elektromos ingerlést vettük igénybe, mivel az ingerlés egyébként is az epilepszia kivizsgálási protokoll része, tehát plusz megterhelés nem érte a beteget (1/3. ábra). A beültetett rács elektródokon keresztül bipolárisan ingereltük a kérget rövid (500 ms) és hosszú (5 sec) áram sorozatokkal, 50 Hz-es sorozaton belüli frekvenciával, a sorozatokat 6 sec illetve 8 sec-os időközökben ismételtük (1/6. ábra).

Rövid időtartamú ingerlés után oxihemoglobin növekedést találtunk 2 sec-os csúcs latenciával, valamint együttes deoxihemoglobin csökkenést tapasztaltunk, melynek csúcs latenciája 3 sec volt. A megnövekedett oxigenizáció az ingerlés után 5-6 sec-al tért vissza az alapvonalra. Az áramforrás sűrűség analízis a rövid ingerlés időtartama alatt serkenési folyamatokat, áram nyelőt mutatott az a középső rétegekben, míg a felső rétegekben áram forrás volt látható. Az ingerlést követően, az offset válasz során áram forrásokat, tehát valószínűleg gátlási folyamatokat, kifelé irányuló membrán áramokat regisztráltunk a középső és mély rétegekből (1/6b. ábra).

A hosszú ingerlés erőteljesen átrendezte a hemodinamikai válasz előzőekben tapasztalt szerkezetét. Egyrészt a hosszú ingerrel kiváltott hemoglobin koncentráció változás a rövid ingerhez képest annak tízszeresére nőtt, másrészt az oxi- és deoxihemoglobin koncentráció a válasz kezdeti fázisának kivételével ellenkezően változott. Az áramforrás sűrűség szerkezete kevésbé dinamikus változott, leginkább az offset válasz amplitúdója nőtt meg a rövid ingerléssel összehasonlítva (1/6a. ábra).

Megállapítható tehát, hogy az ingerlés tartama nem lineárisan változtatja meg a hemodinamikai választ, az elektrofiziológiai válasz viszont közel lineárisan változott ingerlés hosszúságának változásával. A hemodinamikai és idegi válaszok kapcsolatának általunk előzőekben állatkísérletekben kimutatott nem-linearitása tehát a fenti paradigmában emberen is kimutatható volt (Devor et al., 2003). Eredményeink arra utalnak, hogy a kidolgozott optikai-elektrofiziológiai regisztráló módszer jól hasznosítható a humán idegi és hemodinamikai kölcsönhatások kutatásában (Keller et al., 2009).

## Az elülső cinguláris kéreg kognitív funkciói (2)

Az elülső cinguláris kéreg három nagy anatómiai-funkcionális kérgi hálózat a motoros, a limbikus és a prefrontális rendszer kereszteződésében áll (Vogt et al., 2004). A motoros rendszerben az elülső cinguláris kéreg - anatómiai összeköttetéseit figyelembe véve - rögtön a szupplementer motoros kéreg előtt helyezkedik el és vetít mind a motoros kéregbe, mind a gerincvelőbe (Dum and Strick, 1993). A limbikus rendszerben az elülső cinguláris kéreg közvetlen kapcsolatban áll a szubikuláris komplexszel, ezen keresztül a hippokampuszal, a hátsó orbitális kéreggel, az elülső thalamikus maggal és az autonóm funkciókkal rendelkező agytörzsi magokkal. Az elülső cinguláris kéreg továbbá erős kétirányú kapcsolatban áll a dorzolaterális prefrontális lebennyel valamint a halántéklebennyel (Barbas, 2000).

A régió aktivitását sokféle kognitív feladathelyzetben kimutatták: olvasási feladatok (Fiez and Petersen, 1998), szógenerálás (Crosson et al., 1999), epizodikus memória előhívás (Nyberg, 1998), munkamemória feladatok (Bunge et al., 2001), érzelmekkel kapcsolatos (Phan et al., 2002) valamint figyelmi feladatok (Cabeza and Nyberg, 2003; Corbetta et al., 1998; Mesulam, 1981). A régió funkcióit vizsgálva kimutatták továbbá, hogy az adott feladatban adható lehetséges válaszok számához szorosan kötődik az aktivitása, felvetve a lehetőségét annak, hogy az elülső cinguláris kéregnek fontos szerepe lehet az adott feladatra való felelet, akció kiválasztásában (Frith et al., 1991; Posner et al., 1988). Ezek a lehetséges ECK funkciók egyrészt a mozgítás megtervezésével, irányítással lehetnek kapcsolatban (Kollias et al., 2001; Picard and Strick, 2001) másrészt olyan szituációk felismerésében és kezelésében vehetnek részt, melyben a lehetséges válaszok ellentmondóak és így hibákhoz vezethetnek (Carter et al., 2000; Kiehl et al., 2000).

Kutatásainkban rétegelektrodokkal vizsgáltuk az idegsejt populációk szinaptikus/transz-membrán áramainak valamint az idegsejt populációk akciók potenciál tevékenységének változásait az elülső cinguláris kérgi régiók (2/1. ábra) egyes rétegeiben különböző kognitív feladathelyzetben: egyszerű választás, késleltetett szó felismerés, rímelés, akusztikus össze nem illési feladat, betű felismerési feladatban (2/2. ábra). A kérgi generátorok tér és időbeli dinamikájának feltárása érdekében arra kerestünk választ, hogy a vizsgált kérgi mikro-régiók részt vesznek-e több kognitív feladat feldolgozásában, továbbá arra, hogy ez a részvétel milyen idegi mechanizmusokra épül, valamint hogy ezek a feldolgozási folyamatok mely kérgi rétegekhez kötöttek.

## Az elülső cinguláris kéreg aktivitása különböző feladatokban (2)

Minden feladat nagymértékű szinaptikus/transz-membrán és soksejt aktivitást váltott ki az elülső cinguláris kérgi területeken, de emellett a vizsgált kérgi mikro-régiók rétegek szerinti differenciált válaszait tártuk fel különös tekintettel a hiba felismerésre, az újdonságra, a feladat nehézségére és az orientációra (2/3. ábra).

A legerősebb választ az inger időpillanata után 300-800 ms-al regisztráltuk, mely rendszerint együtt járt a kéreg felszíni rétegeire lokalizálódó áram forrással és csökkent akciós potenciál aktivitással (2/4a, b. ábra), mely arra utal, hogy a szupragranuláris rétegekben aktív gátlási folyamat indult be a viselkedéses válasz ideje alatt. Ezt a gátlást rendszerint egy áram nyelő követte szintén a szupragranuláris rétegekben az inger után 800-1400 ms-os latenciával (2/4c. ábra), mely tevékenység a gátló válasz utáni visszacsapó serkentéssel magyarázható. A szupragranuláris rétegében észlelt aktív gátlás meglehetősen általános válasz volt több kognitív feladat esetén is, mely gátlást követő visszacsapó serkentés fontos integrációs ablakot nyithat a további ingerfeldolgozásra.

Kimutattuk a szinaptikus/transz-membrán és soksejt mérések segítségével, hogy az egyes vizsgált mikro-régiók több különböző feladat és a feladaton belüli kontraszt hatására is hasonlóan aktiválódnak. Emellett a különböző feladatra adott lokális válaszok között világosan kimutatható különbségeket is tapasztaltunk, tehát nem egy sztereotip, hanem feladatonként árnyalt feldolgozást találtunk az elülső cinguláris mikro-régiókban (2/5. ábra).

Kimutattuk továbbá, hogy az elülső cinguláris kéreg felső rétegeiben a különböző kognitív feladatok (szómémória, kakukktójás feladat) az inger után 500-700 ms-os latenciával modulálják a helyi théta aktivitás teljesítményét (2/6. ábra).

A feladatokhoz kapcsolódó, régiók közötti théta-sávbeli fázis viszonyok kimutatására megvizsgáltuk az elülső cinguláris kéreg és számos iEEG módszerrel egyszerre regisztrált kérgi régió aktivitását. A legtöbb kognitív feladatban szignifikáns théta-sávbeli fázis szinkronizációt tapasztaltunk a 200-700 ms-os latenciákon az elülső cinguláris és temporális, frontális és hippokampális régiók között (2/7. ábra). A théta fázis szinkronizációs adataink arra utalnak, hogy a vizsgált kognitív feladatokban az egyes elülső cinguláris kérgi mikro-régiók aktívan részt vesznek az elosztott, sok lebenyre lokalizálódó idegi hálózat működésében.

Eredményeink azt mutatják, hogy a különböző feladatokra adott kérgi válasz rétegek szerinti eredete átfed egymással a vizsgált milliméter alatti felbontásban. Mivel mind az áramforrás sűrűséget, mind a soksejt aktivitást nagy részben a helyi egy, vagy néhány kérgi

kolumnán belüli idegi tevékenység határozza meg, ez a megfigyelés arra enged következtetni, hogy az egyes kognitív feladat típusok idegi feldolgozásában térben és időben azonos, vagy legalábbis nagyon közeli hálózatok vesznek részt az elülső cinguláris régióban.

### **Az anteroventrális temporális lebeny kognitív funkciói (3)**

A humán anteroventrális temporális lebenyt az inferotemporális, perirhinális és entorhinális kérgék alkotják. Az anteroventrális temporális lebeny kölcsönös összeköttetésben áll a ventrális látórendszerrel, a nyelvi feldolgozási rendszerekkel valamint a hippocampális területekkel. Anatómiai (Felleman and VanEssen, 1991), fiziológiai (Naya et al., 2001) és léziós (Murray and Bussey, 1999) tanulmányok bizonyítják az anteroventrális temporális lebeny fontos szerepét mind a memória, mind a legmagasabb szintű vizuális tárgyfelismerési folyamatokban. A nyelvi feladatokban is szerepe van, hiszen az anteroventrális temporális lebeny atrófiája jellemző például bizonyos típusú szemantikus demenciákra (Hodges et al., 1992), és megnövekedett hemodinamikai aktivitás jellemzi itt a szemantikai feladatokat (Devlin et al., 2002). A memória funkciókban játszott szerepét bizonyítják azok a vizsgálatok is, melyek ismétlési hatásokat mutattak ki a temporális lebenyben (Dale et al., 2000; Dhond et al., 2003; Marinkovic et al., 2003). Az anteroventrális temporális lebeny tehát mintegy integrálja a magas szintű nyelvi és vizuális feldolgozást a memória bevéséssel, és memória visszaidézéssel, így segítheti a hippocampus-kéreg dialógust és a memória függő absztrakciót (Buzsáki, 1996).

Az eddigiekben leggyakrabban használt humán funkcionális vizsgálatok (fMR, EEG, iEEG, ECoG és MEG) sajnos nem rendelkeznek megfelelő tér és időbeli felbontással ahhoz, hogy a mikro-régiók milliméteres nagyságrendjébe eső kognitív feldolgozási lépéseket azonosítsuk, továbbá nem adnak információt a résztvevő elemi idegi mechanizmusok típusáról sem. Megállapíthatatlan például, hogy a makroszkóposan mért hemodinamikai válasz, a potenciál tér vagy mágneses tér változások (fMR, EEG, iEEG, ECoG és MEG) milyen szinaptikus/transz-membrán, folyamatokhoz kötöttek, illetve milyen ezek alatt az akciós potenciálok mintázata. Majomkísérletekben, egysejt vizsgálatokkal ezek a kérdések részben tisztázhatók, viszont a humán szenzoros és kognitív rendszerek a törzsféjlődés során átalakultak, leginkább a nyelv megjelenésének köszönhetően. A frontális kéreg növekedése mellett a temporális területek, különösen az anteroventrális rész expanziója figyelhető meg az emberi evolúció folyamán, így a majomkísérletekből közvetlen következtetéseket a humán szenzoros és kognitív funkciókkal kapcsolatban nem vonhatunk le.

Kutatásaink célja, a kognitív feladatok által kiváltott idegi aktivitás elemi folyamatainak lokalizálása, az akciós potenciálok és a szinaptikus/transz-membrán áramok szintjén az anteroventrális temporális kérgi mikro-régiókban és agykérgi rétegekben. A rétegelektrodos mérésekkel a makroszkópos megfigyeléseknél pontosabb eredményeket kaphatunk az egyes agyi régióknak belüli, illetve az agyi régiók közötti hálózati kapcsolatok tér és időbeli dinamikájáról. A rétegelektrodos mérések eredményeit összevetve a már jól ismert makroszkópos mérési eredményekkel jobban meghatározhatóvá válhatnak az egyes EEG, iEEG, ECoG és MEG mintázathoz tartozó elemi idegi mechanizmusok.

### **Az ismétlés feldolgozása az anteroventrális temporális lebenyben (3)**

Az új és az ismételt, előzőleg már bemutatott szavak által kiváltott idegi aktivitást vizsgáltuk az inferotemporális kéregben (3/1. ábra). A szómemória tesztben a kísérleti személy elsődleges (explicit) feladata volt az ismételt szó felismerése és a rá adott motoros válasz, míg a hosszúság megállapítási és igeragozási tesztekben a szavak ismétlődése, új, vagy előzőleg már bemutatott mivolta rejtett (implicit) volt, nem az ismétlés feldolgozása volt ezekben az esetekben az elsődleges feladat.

Rétegelvezetési mérésekkel kimutattuk, hogy az inferotemporális és perirhinális területeken a korai válasz ~120ms-os latenciával kezdődött az inger bemutatása után mind az újdonság, mind az ismételt szavakra, melynek csúcsa ~170 ms-nál jelentkezett (3/2. ábra). Ezekon a korai latenciákon az áramforrás sűrűség mélységi eloszlása egy középső (III-IV) rétegbeli áram nyelőt mutatott, ami megfelel egy előre csatolt bemenetnek, mely a megnövekedett soksejt aktivitással együtt értelmezve serkentő típusú posztszinaptikus folyamatot jelent (3/3. ábra). A bemeneti serkentés forrása valószínűleg az alacsonyabb rendű vizuális régiók kimeneti rostjai lehetnek, melyek a kéreg középső rétegeiben végződnek. A korai áram nyelőhöz hasonló latenciákon jelentkező akciós potenciál tevékenység növekedés is alátámasztja a megfigyelt áramforrás sűrűség mintázatát: aktív, előre csatolt serkentési folyamatok túlsúlya látható a bemeneti rétegekben a korai válasz esetén. A korai latencia tartományban (0-220 ms) sem az inferotemporális, sem a perirhinális régióban nem tapasztaltunk szignifikáns ismétlési hatást sem az áramforrás sűrűség, sem a soksejt mérésekben.

Kimutattuk továbbá, hogy a legkorábbi ismétlési hatás mind az inferotemporális, mind a perirhinális régióban ~250 ms-latenciával jelentkezett. A legerősebb ismétlési hatás a soksejt aktivitás mély rétegbeli csökkenése volt az új szavak által kiváltott válaszhoz

viszonyítva mindkét régióban. A soksejt tevékenység ismétléshez kapcsolt csökkenésével együtt az ~500 ms-os latencia tartományban a középső rétegbeli kitartott nyelő csökkenése járt együtt (3/3. ábra), ami a helyi serkentési mechanizmusok fokozatos mérséklődésével magyarázható.

Az entorhinális kéregben kimutattuk, hogy a kiváltott válasz ~200 ms-os latenciával jelentkezett, jóval később, mint az inferotemporális és perirhinális régióban. A korai kérgi tevékenység áramforrás profilja szintén jelentős eltérést mutatott. Az entorhinális kéreg esetében mind a felszíni, mind a mély rétegekben áram nyelőket találtunk, melyek különböző mértékben voltak áram forrásokkal körülvéve. A válasz korai szakaszában (0-300 ms) ismétlési hatást sem áramforrás sűrűség, sem soksejt aktivitás mérésekkel nem sikerült kimutatni (3/4. ábra).

A legkorábbi ismétlési hatás az entorhinális kéregben ~300 ms-os latenciával jelentkezett. Kimutattuk, hogy ellentétben az inferotemporális és perirhinális hatásokkal, az entorhinális kéregben az ismételt szavak nagyobb szinaptikus/transz-membrán és soksejt aktivitást váltottak ki mind a felszíni, mind a mély rétegekben. A fokozott sejtüzelés a válasz 300-600 ms-os latencia tartományában együtt járt a felszíni és mély áram nyelők növekedésével, tehát az ismétlésre adott válasz ebben a régióban serkentési folyamatokkal magyarázható (3/4. ábra).

Eredményeink arra utalnak, hogy az anteroventrális temporális lebenyben az ismétlés és az újdonság feldolgozása alapvetően szekvenciális és térben elosztott folyamat, valamint a vizsgált mikro-régiók különféle feldolgozási stratégiát követnek. A korai idegi válaszban az egyes újdonságtartalmában különböző vizuális szavak feldolgozása nem tér el egymástól. A válasz későbbi szakaszában jelenik meg a helyi idegi folyamatokban az újdonság-ismétlés diszkrimináció, mely kérgi régióként különböző idegi mechanizmusokkal jöhet létre.

**Az alvási oszcillációk rétegelemzéses vizsgálata (4, 5, 6)**

A kérgi tevékenységet az agyi elektromos ritmusok szervezik (Buzsaki and Draguhn, 2004), melyek oszcillációk formájában az EEG-ben jelennek meg, mint az agyi aktivitás egyik karakterisztikus vonása. Az epilepszia kezelése során a műtéti beavatkozások lehetőséget adnak az agykérgi hálózatok nagy tér és időbeli felbontású vizsgálatára emberben, így az agyi elektromos oszcillációk forrásainak kérgi rétegek, illetve egyes idegsejtek szintjén való meghatározására (Cash et al., 2009; Csercsa et al., 2010; Hangya et al., 2011; Keller et al., 2009; Keller et al., 2011; Steinvorth et al., 2009; Ulbert et al., 2005; Wittner et al., 2009). A téma érdekességét mutatja, hogy az elmúlt években kutatócsoportunkon kívül több független laboratórium is elkezdte vizsgálni epilepsiás betegeken intrakraniális (ECoG, iEEG) valamint mikroelektrodos elvezetésekkel a lassú oszcilláció tulajdonságait (Andrillon et al., 2011; Botella-Soler et al., 2012; Le Van Quyen et al., 2010; Nir et al., 2011; Valderrama et al., 2012).

Az agyi oszcillációkat frekvencia tartományokba szokás osztani, mely tartományok aránylag jól elválaszthatóak egymástól, más-más funkciót tükröznek a kognitív feldolgozásban, az alvás-ébrenléti állapotokban és az epilepsziában. Különösen a lassú (*delta*: 0-3Hz) és a gyors (*fast ripple*: ~200-500Hz) ritmusok kötődnek a patológiás folyamatokhoz. A fast ripple oszcillációk például jól jelzik temporális lebeny epilepsiás betegeken a patológiás érintettség oldaliságát (Staba et al., 2002b). A delta tartományba eső oszcillációknak is fontos szerepe van az alvásban, illetve az alvás-ébrenlét határon előforduló rohamok kialakulásában például frontális lebeny epilepsiás betegeknél (Scheffer et al., 1995). A lassú oszcillációnak a patológiás eseteken kívül szerepe lehet még az éber és az alvás alatti információ feldolgozásban, a szenzoros és kognitív funkciókban (Cash et al., 2009; Lakatos et al., 2008; Stefanics et al., 2010).

Az alvás létfontosságú élettani folyamat, amit eddig leginkább különféle állatmodellekben vizsgálták (Steriade and Amzica, 1996; Steriade, 2006). A két legfontosabb idegi hálózat, melyben a lassú oszcilláció kifejeződik a kéreg és a thalamusz. Az, hogy milyen szerepet kapnak a thalamokortikális körön belül az egyes hálózati elemek, a különféle kérgi mezők és a thalamikus magvak még nem tisztázott (Crunelli and Hughes, 2010; Timofeev and Chauvette, 2011). A lassú hullámú alvás alatti kérgi tevékenység az egyik legjobban ismert és kutatott alvási EEG jelenség emberben. Ebben az alvási fázisban kialakuló nagy amplitúdójú lassú oszcilláció frekvenciája állatban és hasonlóan emberben 1 Hz környékére tehető (Achermann and Borbely, 1997; Luczak et al., 2007).

Állatmodellekben különféle narkózisban vizsgálták a lassú hullámú kérgi tevékenységet az idegsejtek és az idegi mechanizmusok szintjén (Steriade et al., 1993b). Mind a mai napig ezekből az altatásos állatkísérletekből tudhatjuk meg a legtöbbet a lassú hullámú aktivitás bonyolult idegi mechanizmusairól. A természetes alvás és az egyes altatásos alvásmodellek bizonyos empirikus egyezést mutatnak, ezért a szakirodalomban elfogadott az a vélemény, hogy az alvás alapvető idegi mechanizmusai hasonlóak lehetnek a két esetben. Mivel a hasonlóságok mellett a narkózis indukálta és a természetes alvás között sok különbség is található, ezért napjainkban egyre inkább a természetes alvást magukban foglaló állatmodellek felé fordul a figyelem (Luczak et al., 2007).

Állatkísérletekben, narkózis alatt, sejten belüli elvezetésekkel mérhető a kérgi idegsejtek membrán potenciálja a lassú oszcilláció alatt. Ezek a mérések rámutattak arra, hogy a lassú oszcillációt két állapot váltakozása jellemzi (Steriade and Timofeev, 2003). Az aktív fázisban a membránon nagyszámú serkentő és gátló posztszinaptikus potenciál fluktuációt mérhetünk, a membrán potenciál alapvetően depolarizált és a sejtek akciós potenciálokat generálnak. Mezőpotenciál mérésekben az agykérgi felszíni rétegek pozitív, a mély rétegek negatív amplitúdót mutatnak. A felszíni pozitív (mély negatív) feszültség görbén erőteljes magas frekvenciájú oszcillációkat láthatunk. Az inaktív fázisban sejten belüli mérésekkel erőteljes hiperpolarizációt látunk, valamint a serkentő és gátló posztszinaptikus potenciálok, és az akciós potenciálok teljes hiányát. Mezőpotenciál mérésekben a felszíni rétegek negatív, a mély rétegek pozitív amplitúdót mutatnak, a feszültség görbén magasabb frekvenciájú oszcillációt nem látunk az inaktív fázisban.

Egészséges kísérleti személyeken természetes alvás alatt skalp EEG elvezetésekben vizsgálták a lassú oszcilláció fázis viszonyait, valamint tér és időbeli dinamikáját, melyekben az állatkísérletekhez hasonló aktív és inaktív fázisokat tudtak megkülönböztetni (Massimini et al., 2004; Molle et al., 2002).

Az alvás és a lassú oszcilláció funkcióiról meglehetősen keveset tudunk, de az utóbbi időben három fontos kutatási területen születnek biztató eredmények.

Köztudott, hogy az epilepszia és az alvás szoros kapcsolatban van egymással. Bizonyos típusú epilepsziák például alvásban aktiválódnak és az epilepsziás rohamok is sűrűbben fordulnak elő alvás megvonás után (Halasz, 2012; Steriade, 2003).

A másik fontos funkciója a lassú oszcillációnak a tényekre irányuló emléknymok megszilárdítása (memória konszolidáció) lassú hullámú alvásban, mely hatás egyes körülírt agyi régióban helyileg is jelentkezik (Huber et al., 2004; Vyazovskiy et al., 2008). A memória konszolidáció idegi mechanizmusa valószínűleg sokrétű. Az egyik idegi

mechanizmus az úgynevezett szinaptikus homeosztázis modell, ahol azok a szinaptikus kapcsolatok maradnak meg lassú hullámú alvásban, melyek egy bizonyos súlyt értek, míg a kevés súllyal rendelkező szinapszisok eltűnnek. Az így konszolidálódott szinaptikus kapcsolatok erősebbek és stabilabbak lesznek (Vyazovskiy et al., 2008). Az idegsejtek közötti kapcsolatok megerősítésében másik fontos tényező lehet az éber állapotban kialakult emléknymokhoz kapcsolható agykérgi sejt együttesek alvásban való újra aktiválódása. Állatkísérletekben az alvás alatti sejt együttesek reaktivációja erősíti az emléknymok bevéssődést (Euston et al., 2007), valamint a legújabb eredmények azt mutatják, hogy a lassú oszcilláció hosszú távú plaszticitást is kivált a thalamokortikális rendszerben (Chauvette et al., 2012). Végül a harmadik lehetséges útja a memória konszolidációnak az alvás alatti kéreg-hippokampusz együttműködés lehet, melyben kérgi orsó aktivitás alatt megnyíló hosszú távú plaszticitási ablakban erősödhetnek meg a hippokampuszban tárolt és alvás alatt a kéregbe visszajátszott információk (Molle et al., 2006).

A harmadik lassú oszcilláció funkció a szenzoros és kognitív működések alvás alatti kontrollja, különös tekintettel a lassú oszcillációhoz közvetlenül kapcsolódó K-komplex alvásvédő, illetve ébresztő funkciójára (Colrain, 2005; Halasz, 2005). Az egyik legvitatottabb funkciójú alvási EEG mintázat a K-komplex. Mind a mai napig pro és kontra kísérleti eredmények sokaságát közlik a szakirodalomban a K-komplex alvásvédő valamint ébredési reakciót kiváltó funkciójáról (Amzica and Steriade, 2002; Cash et al., 2009; Dang-Vu et al., 2011; Jahnke et al., 2012).

Az alvás védelmében, illetve az egyed fizikai integritásának védelmében alvás alatt a külvilág ingereit megfelelően kell monitorozni. Ha például minden akusztikus inger ébredési reakciót váltana ki, akkor az egyed alvás megvonásban elpusztulna, míg az ébresztő reakció hiánya adott esetben az egyed életébe kerülhet például egy külső támadás, vagy egyéb, potenciálisan életveszélyes esemény miatt. Bár az ember a táplálkozási lánc csúcsán található, elképzelhető, hogy az evolúció alatt előzőekben kifejlődött ébresztő mechanizmusok még mindig működnek. A K-komplexnek tulajdonított alvásvédő vagy ébresztő szerep megítélésünk szerint kibékíthető egymással, különösen a legújabb kísérleti eredmények tükrében, ahol a ritmosos akusztikus ingerek egyrészt késleltették az elalvást (ébresztő szerep), de ha már a stabil mély alvás kialakult, akkor a ritmosos akusztikus ingerek a lassú oszcillációt erősítették (alvásvédő szerep) (Ngo et al., 2012).

Az alvási oszcillációk vizsgálata emberben eddig nagyrészt skalp EEG és makroszkópos intrakraniális (ECoG, iEEG) elvezetésekre koncentrált, mely mérésekkel az elemi idegi folyamatokat nem lehet elkülöníteni. Az alvási oszcillációkhoz kapcsolódó

elemi idegi folyamatok eredetét eddig állatmodellekben, alacsonyabb rendű emlősökön vizsgálták. Kutatásaink célja a humán alvási oszcillációk kérgi rétegeloszlásának vizsgálata, az alvási lassú oszcilláció és a K-komplex elemi idegi mechanizmusainak leírása volt.

#### **A K-komplex kérgi forrásai (4)**

Epilepsziás betegeken a parietális és frontális területeken (4/1. ábra) vizsgáltuk az alvási oszcillációk kérgi rétegeloszlását elsőként a szakirodalomban (Cash et al., 2009; Csercsa et al., 2010). Részletesen kidolgoztuk a krónikus rétegelektrod beültetés technikai feltételeit és a vizsgálatok forgatókönyvét. Létrehoztunk egy kombinált rétegelektrodos és konvencionális klinikai rács, szalag elektrodos elvezető rendszert, mely segítségével az operáció alatt, illetve krónikusan tudunk elvezetni intrakortikális, valamint szubdurális potenciálokat.

Kimutattuk, hogy az emberi K-komplexek nagyméretű kérgi régiókra terjednek ki (4/1. ábra), és nagy amplitúdójú felszíni negatív komponense az idegsejtek csúcsi dendritikus nyúlványain keletkezik az agykéreg felső rétegeiben (4/2A. ábra). Kimutattuk továbbá, hogy a K-komplex prominens negatív komponense alatt az agyhullámok teljesítménye nagymértékben lecsökken (4/3A3. ábra) és ezzel szinkronban az egyes agysejtek aktivitása is a minimumra esik (4/3A2. ábra). Hipotézisünk szerint az emberi K-komplex meghatározó felszíni negatív komponense nem más, mint az úgynevezett inaktív állapot, ami a lassú oszcilláció egyik fázisa (4/2C. ábra). Az inaktív állapot alatt az agykéreg kiterjedt területei szinte kikapcsolt, inaktív állapotba kerülnek, az agysejtek tevékenysége drasztikusan lecsökken egy rövid időre.

Mivel a K-komplex véletlenül előforduló hangingerek hatására is kiváltható emberben (4/2B. ábra), az így kialakult inaktivitásnak fontos szerepe lehet normális esetben az alvás védelmében, valamint a visszacsapó serkentés hatására az epilepsziás működésekben. Eredményeink egy könnyen megfigyelhető, nem kóros, univerzálisan előforduló emberi EEG jelenséget kötnek össze a sejtmembrán áramok és az idegsejt aktivitás megfigyelésén keresztül a már ismert állatkísérletes mechanizmusokkal. Eredményeinket felhasználva az alvási és epilepsziás EEG jelenségek, mechanisztikus idegrendszeri modellekben széleskörűen értelmezhetővé válhatnak.

### A lassú oszcilláció kérgi forrásai (5)

Rétegelektrodás mérések segítségével leírtuk a nagyagykérgi neuronhálózatok működésének egyes jellemzőit a lassú alvási oszcilláció aktív és inaktív fázisaiban epilepsziás emberben (5/1. ábra), különös tekintettel a sejt tüzelésre, a lokálisan generált áramokra, és az oszcillációs teljesítményre (Cserecsa et al., 2010).

Kimutattuk, hogy az epilepsziás betegekben vizsgált lassú oszcilláció számos hasonlóságot mutat az állatkísérletekben és egészséges emberben észleltekkkel összehasonlítva. Mind az oszcilláció frekvencia tartománya (5/3A, B. ábra), mind az aktív, illetve az inaktív fázisok időbeli és spektrális paraméterei nagy hasonlóságot mutattak (5/3C, D. ábra). Az alapvető hasonlóságokon kívül számos különbséget is találtunk. Kimutattuk, hogy az emberi lassú oszcilláció generálásában a felszínhez közelebb eső szupragranuláris réteg lényegesen nagyobb szerepet vállal, mint a mélyebben található infragranuláris réteg (5/6. ábra). Mind a mezőpotenciál, mind az áramsűrűség eloszlások a szupragranuláris rétegekben voltak maximálisak, ami ellentmond az eddigi állatkísérletes eredményeknek (Chauvette et al., 2010; Sakata and Harris, 2009). Az akciós potenciál tevékenység a harmadik illetve az ötödik rétegben volt a legnagyobb (5/6F. ábra), ami szintén új megfigyelés, hiszen állatban eddig az ötödik rétegben találtak maximális sejt tüzelési intenzitást (Sakata and Harris, 2009). Kimutattuk továbbá, hogy alvás alatt az ember nagyagykérgi neuronjai lényegesen kisebb frekvenciával tüzelnek (5/10. ábra), mint a rágcsálók és macskák kérgi idegsejtjei (Steriade et al., 1993a). Új eredménynek számít továbbá az a megfigyelésünk is, hogy emberben az aktív fázis kezdete az egyes kérgi rétegek között meglehetősen szinkronizáltan zajlik (5/9. ábra), ellentétben az állatkísérletes adatokkal, ahol az infragranuláris rétegeknek van időben vezető szerepe (Chauvette et al., 2010; Sanchez-Vives and McCormick, 2000).

Kutatásaink egyik igen érdekes eredménye a szupragranuláris rétegek kiemelt szerepének feltárása az emberi alvási oszcillációkban (5/7. ábra). Eredményeink azt mutatják, hogy az alvási oszcillációkhoz kötődő ECoG és EEG jelek forrásai a kéreg felső harmadából származnak, míg a mélyebb rétegek elhanyagolható szerepet játszanak az agy felszínén és a skalpon megfigyelhető potenciál mintázatok kialakításában. Ez a megfigyelés valószínűleg több okra vezethető vissza.

A főemlősök evolúciója során az asszociációs területek nagy fejlődésen mentek keresztül mind méretüket, mind kapcsolataik számát tekintve. Az egyik legfontosabb és egyben legnagyobb asszociációs terület a frontális lebenyhez köthető prefrontális mező,

(ahonnan az elvezetések egy része is származik) melynek felépítése főemlősben és emberben nagyfokú különbségeket mutat az alacsonyabb rendű emlősökkel összehasonlítva (Herculano-Houzel et al., 2007). Anatómiai módszerekkel kimutatható, hogy különösen a főemlősök prefrontális területén elhelyezkedő piramis sejtek morfológiája nagyban elüt például a vizuális területen található idegsejtektől, leginkább a dendrit elágazódások és a dendrit tüskék száma nagyobb prefrontálisan (Elston et al., 2006). Az apikális dendritek sűrűsége sokkal nagyobb a szupragranuláris rétegekben, tehát a dendriteken folyó áramok - melyek a felszínen detektálható potenciálok elsődleges generátorai – eloszlása nem egyenletes a kéregben, szupragranuláris túlsúllyal kell rendelkeznie. Mivel a dendritek végzik a kérgi integrációs funkciókat, nagyon valószínű, hogy a magasabb rendű intelligenciáért, az emberre jellemző kognitív képességeikért ez az anatómiai mintázat lehet felelős (Elston, 2003).

A szupragranuláris rétegek kifejezettebb aktivitásával kapcsolatosan a másik érdekes megfigyelésünk a calretinin pozitív (CR+) gátlósejtek egyenlőtlen rétegeloszlása volt (5/2B. ábra). Különösen emberben találtak nagy CR+ sejt sűrűséget szupragranulárisan, patkánnyal összehasonlítva (Gabbott et al., 1997). A CR+ sejtek leginkább másik gátlósejten végződnek a szupragranuláris rétegekben, míg infragranulárisan inkább a piramis sejteket idegzik be (Meskenaite, 1997). A gátlósejt-gátlósejt kapcsolat pozitív visszacsatolásként fogható fel, mely a szupragranuláris oszcillációkat erősítheti, míg a gátlósejt-piramis sejt kapcsolat egy negatív visszacsatolásként fogható fel, mely a kialakuló oszcillációs folyamatokat gátolhatja infragranulárisan.

### **A lassú oszcilláció térbeli terjedésének vizsgálata (6)**

A lassú oszcillációt indító régiók és az oszcillációs hullámok terjedésének tulajdonságait egészséges emberben nagy felbontású skalp EEG elvezetésekben vizsgálták. Ezzel a módszerrel azt találták, hogy a lassú oszcilláció utazó hullámként viselkedik (Massimini et al., 2004). Az epilepsziás páciensek esetében az ECoG elvezetések a skalp EEG vizsgálatoknál jóval nagyobb felbontású képét adják az agykérgi aktivitásnak (6/1. ábra). A lassú oszcilláció térbeli terjedésének jobb megértéséért csoportunk krónikusan beépített szubdurális rács elektródokkal vizsgálta a lassú oszcillációs hullámok terjedési mintázatait (6/2. ábra) nem lineáris módszerek felhasználásával (Hangya et al., 2011).

Az előzőleg egészségesekben skalp EEG regisztrációval leírt haladó hullámú (Massimini et al., 2004) terjedéssel szemben kimutattuk, hogy a lassú oszcilláció terjedése

ebben az ECoG elvezetések mérettartományban (1-6cm) leginkább rövid távolságokra korlátozódik (6/3. ábra), sok esetben ugráló, tehát térben nem folyamatos terjedés mutatható ki. A terjedési mintázatok alapvetően helyi jellegűek, néhány centiméterre terjednek ki és igen sokfélék lehetnek, például rövid távú oda-vissza terjedést és cirkuláris terjedést (6/6. ábra) is gyakran megfigyeltünk (Hangya et al., 2011).

Véleményünk szerint a megfigyelt lokális típusú, komplex ECoG aktivációs minta a helyi funkcionális területek kapcsolatára jellemző, míg az EEG a globális, tehát szinte az egész agyra kiterjedő funkcionális régiók kapcsolatát tükrözheti. Eredményeink egybevágóak azokkal a megfigyelésekkel, melyek szerint a lassú hullámú alvás nem csupán egy globális agyi állapot, hanem összetett térbeli finomszerkezettel rendelkezik (Huber et al., 2004; Vyazovskiy et al., 2011).

### **Az epilepszia hatása az alvási oszcillációkra**

Adataink epilepsziás betegekből származnak, tehát kézenfekvő kérdés az, hogy eredményeink mennyire általánosíthatóak az egészséges populációra nézve. Kutatásaink során kiemelt figyelmet kapott az az erőfeszítés, hogy az esetleges patológiás eseményeket kizárjuk a lassú oszcillációhoz kapcsolódó adatfeldolgozásból (Cash et al., 2009; Csercsa et al., 2010). Kizártuk az analízisből azokat az időszakokat, melyek a rohamot követték, vagy megelőzték legalább egy órával, továbbá azokat az elvezetési helyeket, melyek intenzív interiktális (rohamok közötti) tüskézést, vagy rohamokat mutattak.

Bár rétegelvezetéses mezőpotenciál és akciós potenciál adataink közvetlenül nem hasonlíthatók össze az egészségesben elvezetett skalp EEG-vel, de például a lassú oszcillációs fázisok matematikai leírása során felhasznált egyes paraméterek (előfordulási frekvencia, detekciós frekvencia hisztogram, interdetekciós-intervallum hisztogram, spektrális eloszlás) az egészséges és epilepsziás kísérleti személyek között nagy hasonlóságot mutattak (Achermann and Borbely, 1997; Csercsa et al., 2010; Massimini et al., 2004; Molle et al., 2002). Továbbá, az idegsejtek tüzelési és börszt frekvenciája is a normális intervallumba esett minden kiválogatott sejt esetében (Staba et al., 2002a; Staba et al., 2002c). Egy páciensben találtunk vélhetően patológiás működést két kiválogatott sejtnél. Ezek a sejtek az inaktív állapotban nem szüneteltették a tüzelésüket. Bár ez a megfigyelés nem feltétlenül jelent klinikailag patológiás érintettséget, mégis arra enged következtetni, hogy epilepsziában egyes érintett sejtek nem respektálják a lassú oszcilláció inaktív fázisát. Hasonló megfigyeléssel eddig a szakirodalomban még nem találkoztunk.

A lassú oszcilláció feltételezeten fiziológias forrásait összevetve a patológias jelek forrásaival megállapítottuk, hogy az interiktális kisülések egy részében, a kisülés felszíni potenciál mintázatát meghatározó agykérgi áramforrások a mély rétegekben helyezkednek el, így a fiziológias és patológias funkciók térben is elkülönülhetnek az emberi agykéregben (Csercsa et al., 2010; Ulbert et al., 2004a). Kutatásaink segítségével tehát mód nyílt a kóros és egészséges felszíni potenciál mintázatok elkülönítésére is a hullámalakok elemzése segítségével.

**Az epilepsziás tevékenység rétegelemzéses vizsgálata (7, 8, 9, 10)**

Az epilepszia összetett, sokszor ismeretlen eredetű krónikus agyi működészavar, melyet visszatérő rohamok jellemeznek. Az eddigi elfogadott hipotézisek szerint az epilepszia hátterében az idegsejtek fokozott kisülési és szinkronizációs hajlandósága áll. Az epilepszia valamennyi megjelenési formájára jellemző, hogy az agy meghatározott területein, vagy az egész agyra kiterjedően, rendellenes EEG tevékenység észlelhető.

A betegség széles körben kimutatható anatómiai elváltozásokat is mutat. Temporális lebeny eredetű epilepsziák esetén a hippokampális régió bizonyos sejtcsoportjai kiterjedten pusztulnak, más sejtcsoportokra az anatómiai kapcsolatok újra szerveződése, reorganizációja jellemző (Magloczky et al., 2000; Wittner et al., 2001; Wittner et al., 2002; Wittner et al., 2005). A sejtpusztulás és reorganizáció kezelés hiányában egyre fokozódhat, a beteg mentális képességei hanyatlanak, majd ha a görcstevékenység életfontosságú területeket is érint, a betegek életüket veszthetik (Miller et al., 1994). A fokális epilepsziák nagy része temporális lebeny eredetű betegség (Margerison and Corsellis, 1966) és elsősorban a limbikus rendszer struktúráiban okoznak eltéréseket, ez megmagyarázza, hogy epilepsziás betegek tanulási és kognitív képességei miért szenvednek gyakran károsodást (Wieser, 1988).

Az epilepsziás agy alapvető tulajdonsága a roham jelenség mellett az interiktális (rohamok közötti) tüskézés. Az emberi epilepsziában megfigyelt tüskézés (Pedley, 1984; Penfield and Jasper, 1954) sok azonos vonást mutat az állatkísérletes epilepszia modellekben észlelt paroxizmális depolarizációs eltolódással (Schwartzkroin and Wheal, 1984) melynek kiváltható okai igen sokfélék lehetnek (Connors and Telfeian, 2000; Connors et al., 2001; Swann and Hablitz, 2000). A paroxizmális depolarizációs eltolódás megjelenése állatmodellekben a jól karakterizálható úgynevezett tüske-hullám mintázatokhoz kapcsolódott, mely megjelenésében nagyon hasonló az emberi tüskézéshez (Goldensohn and Purpura, 1963; Steriade and Contreras, 1998). A kezdeti alapvetően serkentéses gyors tüske tranziens lassú hullám követi, melynek okai állatkísérletekben a rekurrens gátlás, utóhiperpolarizáció, diszfacilitáció illetve egyéb  $K^+$  áramok lehetnek (McCormick and Contreras, 2001). A serkentő szinapszisok tüske alatti aktivitásának és a sejtek tüzelésnek a növekedése, valamint a lassú hullám alatti gátlás, mint egymáshoz szorosan kötődő folyamatok alkotják az epileptogenezis egyik fontos lokális, intrakortikális idegi mechanizmusát állatmodellekben (de Curtis and Avanzini, 2001).

Emberben a tüskézés idegi mechanizmusai még tisztázásra szorulnak. Sajnos egyetlen állatmodell sem írja le megfelelően, minden részében árnyaltan a különböző emberi epilepsziákban előforduló interiktális tüske aktivitást, így az állatmodellek eredményeinek általános használata emberi diagnosztikai és gyógyítási célokra meglehetősen kétséges. Az interiktális tüskézés emberben a rohamtevékenységtől független, de egyértelműen patológias tevékenység (Clemens et al., 2005; Gotman, 1980). Bár a roham alatti és rohamok közötti elektromos tevékenység kapcsolata emberben még kevésbé tisztázott, a tüskézéssel kapcsolatos információkat intenzíven használják a klinikumban a roham fókuszának meghatározására (Avoli et al., 2012; Blume et al., 2001; de Curtis and Avanzini, 2001).

Kutatásainkban az interiktális tüskézés eredetét vizsgáltuk különböző típusú epilepsziában szenvedő éber és altatott betegen, különböző kérgi lokalizációkban. A különféle tér és időbeli felbontású elektrofiziológiai és a szövettani technikák segítségével feltártuk azokat a kérgi hálózatokat és idegi mechanizmusokat, melyek az interiktális tüskézés kialakításáért felelősek emberben (Fabo et al., 2008; Keller et al., 2010; Ulbert et al., 2004a; Ulbert et al., 2004b).

### **Az interiktális tüskézés tulajdonságai a hippocampusban (7)**

Altatásos műtét alatt, a hippocampusz eltávolítása előtt vizsgáltuk rétegelektrodos elvezetésekben a gyrus dentatus és a cornu ammonis régiók (CA1) elektromos tevékenységet (7/1. ábra) temporális lebeny epilepsziás betegeken (Ulbert et al., 2004b).

Az altatás ellenére kivétel nélkül minden betegben kimutatható volt tüskéző, vagy oszcillátoros aktivitás a CA1 (7/1B. ábra) és a gyrus dentatus (7/1C. ábra) régiókban. A gyrus dentatusból 25-45Hz-es aktivitást vezettünk el szinte minden esetben, szklerotikus páciensekben pedig különösen nagy amplitúdójú oszcillációkat találtunk. A gyrus dentatus oszcillátoros aktivitására jellemző volt, hogy az áramforrás sűrűség és a soksejt aktivitás a granuláris rétegben gátlási hatásokat mutatott: áram forrás, mely együtt járt a soksejt aktivitás növekedésével, és kicsi széli áram nyelő, hasonlóan alacsony soksejt kisüléssel. Ezek a megfigyelések igazolni látszanak azokat a szövettani eredményeket, melyek szerint hippocampális szklerózisban a szemcsesejtek gátlása fokozódik (Wittner et al., 2001), és ez a változás magas frekvenciájú oszcillációk, és epilepsziás kisülések megjelenésének kedvez.

A laterális temporális lebenyben és a CA1-ben hasonló mintázatú tüskézés volt megfigyelhető, aminek valószínűleg az entorhinális kéreg – hippocampusz – szubikulum – entorhinális kéreg pálya kapcsolat lehet az alapja (7/2. ábra). Az áramforrás sűrűség és

soksejt aktivitás analízis a CA1 régióban serkentési mintázatot mutatott, a serkentési fázisra szinkronizálódó magas frekvenciás akciós potenciál börsztöléssel (7/3. ábra).

Megállapítható tehát, hogy altatás alatt a gyrus dentatus és CA1 régió és a laterális temporális kéreg igen aktív, így az intraoperatív elvezetések alkalmasak lehetnek a temporális epilepszia lokális és hálózati kapcsolatainak vizsgálatára. A gyrus dentatusnak szerepe lehet a kóros oszcillációk fenntartásában, hiszen a helyi reorganizáció (Magloczky et al., 2000; Wittner et al., 2001) megteremtheti ezek feltételeit, mely a gyrus dentatus széles kapcsolati rendszerén keresztül a hippokampális (Henze et al., 2002) és kérgi területekre is hatást gyakorolhat. A gyrus dentatus oszcillátoros aktivitása mintegy előfeszítve, de stabil állapotban tarthatja a kapcsolódó hippokampális struktúrákat, külső ingerek hatására az átmeneti stabilitás felborulhat, utat engedve az epilepsziás folyamatoknak. A perforáns pályán keresztül a gyrus dentatus kapcsolatban áll az agykéreggel is, így akár fiziológias kérgi események is (pl. gamma oszcilláció, orsó) kiválthatják az epilepsziás folyamatokat.

### **Az interiktális tüskézés tulajdonságai a szubikulumban (8)**

Szintén temporális lebeny epilepsziás betegeken vizsgáltuk altatás alatt a szubikuláris (8/1. ábra), valamint a laterális temporális kérgi interiktális tüske tevékenység tulajdonságait (Fabo et al., 2008). A hippokampusz bemeneti és kimeneti pályáinak egy jelentős része a szubikulumban kapcsolódik át, ezért nagy hangsúly kapott a szubikulum esetleges epilepsziát elősegítő szerepének kutatása (Cohen et al., 2002). Állatkísérletes modellekben, illetve in vitro humán elvezetésekben a szubikulum meglehetősen aktívnak mutatkozott, ritmikus interiktális tüskézést produkált, bár alacsonyabb frekvenciával, mint a humán gyrus dentatus (Cohen et al., 2002; Wu et al., 2006).

Kimutattuk, hogy a szubikulum - hasonlóan a korábban in vitro vizsgált szelet-preparátumokhoz - képes interiktális epilepsziás tüskék generálására in vivo körülmények között, altatás alatt is (8/2. ábra). Kimutattuk továbbá, hogy az emberi szubikulum altatásban is képes az interiktális tüskézéshez kapcsolódó, a már korábban leírt, magas frekvenciás, epilepsziára jellemző oszcillációk generálására (8/5. ábra) (Staba et al., 2004; Staba et al., 2007). A szubikuláris tüskék megfigyelése tehát az általunk választott mérési technikával lehetséges, a szubikuláris elektromos aktivitás fuzionálható az anatómiai feldolgozás során megállapított sejtrétegekkel (8/3. ábra). Az általunk választott technikával tehát részletesebben, nagy tér és időbeli felbontásban leírhatók a tüskézés idegi mechanizmusai.

Kimutattuk továbbá, hogy a szubikulum egymástól 6-8mm távolságra elhelyezkedő területei szinkron módon aktiválódnak a tüskék alatt (8/3. ábra). A laterális temporális kérgi és a szubikuláris tüskék megjelenését vizsgálva megállapítottuk, hogy szoros időbeli kapcsolat létezik a két epilepsziás aktivitás között (8/6. ábra). A szubikuláris tüskék egyes esetekben megelőzték a kérgi tüskéket, ami felveti egy elsődleges szubikuláris tüske fókusz jelenlétét is (8/8. ábra).

Az emberi szubikulumban a szakirodalomban először sikerült kimutatni legalább kettő különböző típusú interiktális tüskét (8/4. ábra). Ez a megfigyelés alátámasztani látszik azokat az eredményeinket, melyek éber, nem altatott páciensekben az interiktális tüskék változatos viselkedését írták le nem temporális lebeny epilepsziás betegeken (Keller et al., 2010; Ulbert et al., 2004a). A gyakrabban (~73 %-ban) előforduló kisülést (I típus) a sejt test régióra koncentrált kezdeti serkentő áram nyelők jellemezték, melyek együtt jártak a soksejt aktivitás növekedésével, valamint a piramis sejt réteg megnövekedett széles spektrumú (50-250 Hz) mezőpotenciál gradiens aktivitásával (8/4, 8/5. ábra). A csúcsi dendrit régióban áram forrásokat találtunk, ami valószínűleg passzív, kiegyenlítődesi áramként fogható fel. Ez a rétegeloszlási mintázat arra enged következtetni, hogy a sejt test környékén aktív depolarizációs folyamatok zajlanak, melyet a csúcsi dendritek elektrotónusos hiperpolarizációja egyenlít ki. Hasonló mintázatot már korábban is megfigyeltek állatmodellben a szubikulumban, gyors glutamáterg rekurrens serkentés esetén (Menendez de la Prida and Gal, 2004). A lassú hullám komponens alatt áram forrásokat találtunk a sejt test régióban, mely együtt járt a spektrális teljesítmény és a soksejt aktivitás csökkenésével. Véleményünk szerint, míg a korai hiperpolarizáció valószínűleg aktív szinaptikus (GABA<sub>A</sub>) gátlási komponenst tartalmaz (Cohen et al., 2002), addig a késői hiperpolarizáció egyéb, nem GABA<sub>A</sub> áramokat foglal magában (Alger and Nicoll, 1980; Fernandez de Sevilla et al., 2006). Hasonló aktivációs mintázatot figyeltek meg emberi szubikulumban in vitro körülmények között spontán módon (Cohen et al., 2002), illetve elektromos ingerlés hatására (Huberfeld et al., 2007), ami azt mutatja, hogy a szubikulum epilepsziás aktivitása a spontán belső generálás mellett külső ingerekkel is kiváltható.

A ritkábban előforduló (~27 %) második típusú (II típus) tüske sokkal változékonyabb rétegelvezetési profilt mutatott, mint az első típus, ami arra mutat, hogy ennek a kisülési mintázatnak a generátor mechanizmusai kevésbé stabilak, illetve összetettebbek voltak (8/4, 8/5. ábra). A tüske kisülés kezdeti fázisát egy gyors szomatikus áram forrás jellemezte, mely együtt járt a csúcsi dendritekben észlelt áram nyelővel. Ez a mintázat konzisztens egy csúcsi dendritekre érkező serkentő bemenettel, mely ott kifelé folyó

membrán áramokat kelt, míg az aktív szinaptikus dendritikus serkentés a sejt test régióban passzív kiegyenlítődesi áramokat indít el (Wu and Leung, 2003). A lassú hullám komponens lefutása hasonló volt az I típusú eseményhez, itt is a korai aktív gátlás és a késői nem-szinaptikus áramok szerepe valószínűsíthető. Hasonló mintázatot figyeltek meg a szubikulumban, in vitro állatmodellben a kérgi elektromos ingerlés hatását vizsgálva (Cappaert et al., 2007).

Fontos megjegyezni, hogy az eltérő áramforrás sűrűség profil mellett a II típusú kisülés alacsonyabb soksejt aktivitással és magas frekvenciás oszcillációval is járt, mint az I típusú. A tüske kisülések előfordulásának és frekvencia összetételének vizsgálata fontos diagnosztikai eredményekre vezethet. Az elektromos ingerléssel való kiválthatóság és a magas frekvenciás komponensek eloszlása alapján bizonyos esetekben jól meghatározhatóvá vált az epilepsziás fókuszhelyezkedése (Staba et al., 2004; Staba et al., 2007; Valentin et al., 2002).

A többfajta tüskézés megfigyelése egy mikro-régió belül választ adhat arra a kérdésre, miért is annyira ellentmondásos a tüskézés megítélése klinikai körökben (Avoli et al., 2012; de Curtis and Avanzini, 2001). Kutatásaink a szakirodalomban először egyértelmű bizonyítékokat szolgáltatottak arra a feltételezésre, hogy az interiktális tüskézés korántsem egységes jelenség. A különböző típusú tüskék között igen nagy mechanizmusbeli eltérések lehetnek, amik meghatározhatják ezen események pontos szerepét az epilepsziás folyamatokban.

### **Az interiktális tüskézés tulajdonságai a kéregben (9)**

Kombinált réteglevezetési áramforrás sűrűség, soksejt aktivitás analízis és ECoG módszerekkel vizsgáltuk a kérgi konvexitás interiktális tüskézés mintázatát (9/1. ábra) éber, nem temporális lebeny epilepsziás betegeken. Felszíni ECoG elvezetésekben meghatároztuk az interiktális tüskézés nagy léptékű tér és időbeli eloszlását (9/2. ábra), míg a réteglevezetésekkel (9/3. ábra) regisztráltuk az egyes tüske típusokhoz tartozó mélységi elektromos tevékenységet (Ulbert et al., 2004a).

A felszíni elvezetések tér és időbeli elemzése alapján megkülönböztettünk terjedő és helyben generált tüskéket egy adott rétegelektrodos elvezetési helyen, mely egy adott rácselektrod közvetlen környezetében helyezkedett el (9/2. ábra). A terjedő tüskézés esetében ECoG elvezetésekben kimutattuk, hogy a tüskék terjedési sebessége az 0.05-0.1 m/s-os sebességtartományba esik, mely egyezik bizonyos állatkísérletes adatokkal (Steriade and

Amzica, 1994). Kimutattuk, hogy a rétegelvezetéssel detektálható interiktális tüske-hullám kiséletek egy korai tranziens követő lassú hullámból állnak (9/3. ábra), mely megfigyelés szintén egyezik a szakirodalmi adatokkal (de Curtis and Avanzini, 2001).

Kimutattuk továbbá, hogy a tüske korai tranziense alatt a kéreg meghatározott rétegeinek serkentési folyamata dominál. Egy adott rétegelvezetési helyen csak egy esetben találtunk mind terjedő mind helyben generált tüskét, legtöbbször csak egy fajta tüske volt megfigyelhető. A terjedő tüskék esetében kettő fajta, rétegeloszlásában jól elkülönülő áramforrás sűrűség profilt mutattunk ki. A gyakrabban előforduló *granuláris* mintázat (9/3. ábra) jellemzője a korai IV rétegi serkentő áramok és megnövekedett soksejt aktivitás volt, melyet később a III és V rétegek aktivitása követett. A ritkábban előforduló *szupragranuláris* mintázatra (9/4. ábra) az I-III rétegek kezdeti fokozott serkentési tevékenysége volt a jellemző, mely később beterjedt a mélyebb rétegekbe is (Ulbert et al., 2004a). A *helyben generálódott* tüskék rétegelemzése az V rétegben mutatott ki magas kezdeti serkentő aktivitást, mely később beterjedt a felső rétegekbe (9/5. ábra). Kimutattuk továbbá, hogy a kezdeti serkentő típusú gyors aktivitás után kialakuló lassú hullám együtt jár a szupragranuláris rétegekben tapasztalható elhúzódnó hiperpolarizációs jelenséggel, mely egyes esetekben a soksejt aktivitás csökkenésével is társul.

Eredményeink alapján a következő hipotézist tudjuk felállítani. Az interiktális tüske indítása az V rétegi piramis sejtekhez kötődik, ahonnan a korai aktivitás előre csatoló kapcsolatokon terjed és a IV rétegben okoz helyi serkentést, mely serkentés tovább terjed a felszíni és mély rétegekbe. Az epilepsziás tüske terjedés széli zónájára a felszíni rétegek serkentési folyamatai a jellemzőek. A rétegelvezetések finomabb analizisével tehát elkülöníthetjük az epilepsziás hálózat egyes elemeit, a hálózatban betöltött szerepük szerint, összevetve az elektrofiziológiai adatokat a szövettani vizsgálatokkal, pontosan meghatározhatjuk a generátorok kérgen belüli elhelyezkedését.

### **Az egysejt aktivitás és az interiktális tüskézés kapcsolata (10)**

Az előzőekben ismertetett, tüskézéshez kötődő áramforrás sűrűség és soksejt aktivitás vizsgálatával kimutattuk, hogy a kezdeti tranziens aktivitás összességében megnövekedett sejt tüzeléssel jár. Mivel a soksejt aktivitás elemzése nem diszkriminál az egyes sejtek között, tovább vizsgáltuk az egyes kiválogatott sejtek (10/1. ábra) és a tüske-hullám kapcsolatát (Keller et al., 2010).

Meglepő módon, a kiválogatott egyes sejteknek csak a fele (48 %) mutatott a tüskézéshez kapcsolódó tüzelési ráta változást, a kisülés 500 ms-os környezetében vizsgálva. A kisülés alatt modulációt mutató sejtek 27%-ánál a tüzelési ráta a korai tranziens tüske alatt (a csúcshoz viszonyítva 35 ms-on belül) növekedést mutatott az alapvonalis aktivitáshoz képest (a tüske csúcsa előtti 1000 ms). A lassú hullám alatt a modulált sejtek 50 %-a a tüzelési rátáját lecsökkentette.

A kisülés alatt az egyes modulált sejtek viselkedését időbeli mintázatok alapján (10/3. ábra) próbáltuk leírni és nem kevesebb, mint 15 időbeli mintázatot sikerült megkülönböztetni (10/2. táblázat, 10/6. ábra). A leggyakrabban előforduló modulált egysejt mintázat (36 %) a tüske alatt nem mutatott változást, a hullám alatt viszont csökkent a kisülési ráta. A második leggyakoribb mintázat (15 %) viszont a tüske alatt volt a legaktívabb. Az öt leggyakrabban előforduló mintázat alkotta a modulált tüskék 75 %-át. Több mintázatban megfigyeltük a tüske előtti időpontokban az akciós potenciál aktivitás frekvenciájának szignifikáns változásait, valamint a mezőpotenciálok szinkronizációját, delta sávba eső ritmusosságát is (10/4, 10/5. ábra).

Megállapítható tehát, hogy a tüskézés alatt a sejtek igen heterogén módon viselkedtek, ami ellentmond azoknak a korábbi hipotéziseknek, melyek szerint az interiktális epilepsziás működésre a nagymértékben megnövekedett serkentési folyamatok és a hiperszinkronitás jellemző (Goldensohn and Purpura, 1963; Steriade et al., 1998). Az akciós potenciálok, valamint a mezőpotenciál ritmikus modulációja arra enged következtetni, hogy a tüskézés hátterében a delta sávba eső oszcillációs folyamatok állhatnak. Következtetéseink szerint az interiktális tüskézés mind térben, mind időben igen összetett finomszerkezettel rendelkezik, mely tükrözi a különböző funkciójú és összeköttetésű idegsejt populációk fiziológiásan is meglévő tér és időbeli kapcsolatait.

## ÖSSZEFOGLALÁS

Kutatásaink során kidolgoztuk a humán intrakortikális rétegelvezetések különféle módozatait, melyekkel megbízhatóan tudtuk regisztrálni a kérgi elektromos tevékenységet kognitív feladathelyzetben, lassú hullámú alvásban, illetve epilepsziás események alatt. Kidolgoztuk a hemodinamikai és elektrofiziológiai adatok együttes regisztrálásán alapuló optód technikát, mellyel a vaszkuláris-elektromos csatolás tulajdonságait vizsgáltuk. Kidolgoztuk továbbá az elektrofiziológiai és anatómiai adatok fúziójára alkalmas módszereket, mellyel az idegi aktivitás kérgi rétegek szerinti elhelyezkedését határoztuk meg.

Kognitív feladatokban kimutattuk, hogy a kérgi ingerfeldolgozás többféle stratégiát követhet a vizsgált kérgi területeken. Amíg az elülső cinguláris kéreg esetében kérgi mikro-régiók számos különböző feladat feldolgozásában nagyon hasonló módon kapnak szerepet, addig az anteroventrális temporális lebeny esetében az egyes mikro-régiók ellentétes ingerfeldolgozási stratégiával valósíthatják meg a kognitív célt. Az anteroventrális temporális lebenyben elektrofiziológiai mérésekkel kimutattuk, hogy az ismétlés feldolgozásában mind a gátlási, mind a serkentési folyamatok részt vesznek, térben szeparálva.

Az alvási oszcillációkat elemezve kimutattuk, hogy a K-komplex prominens negatív komponense nem más, mint a lassú alvási oszcilláció inaktív állapota, mely az agyfelszínhez közeli kérgi rétegekben a piramis sejtek csúcsi dendritjein keletkezik. A lassú alvási oszcillációt vizsgálva kimutattuk, hogy megjelenése sok tekintetben hasonló az állatmodellekben regisztrált lassú hullámú aktivitáshoz, bár lényeges eltérések is találhatók. Az emberi lassú oszcillációban, ellentétben az állatmodellekkel, leginkább a szupragranuláris kérgi rétegek vesznek részt, az aktív állapotok szinkronizáltan keletkeznek az egyes kérgi rétegekben és az akciós potenciál aktivitás frekvenciája jóval kisebb, mint állatban. A lassú oszcilláció terjedését vizsgálva ECoG mérésekkel kimutattuk, hogy a skalp EEG mérésekben tapasztalt haladó hullámú terjedéssel ellentétben, számos különféle helyi komplex terjedési mintázat figyelhető meg.

Az epilepsziás tüskézést különböző agyterületeken vizsgáltuk. Kimutattuk, hogy ellentétben az eddigi feltételezésekkel, a tüskézés kevésbé homogén, egy régió akár többféle interiktális kisülést is produkálhat, illetve az egyes sejtek heterogén tüzelési mintázatot mutatnak a kisülések alatt. A rétegelvezetések segítségével elkülönítettük az epilepsziás hálózat egyes elemeit a hálózatban betöltött szerepük szerint. Az interiktális tüskézés tehát igen összetett finomszerkezettel rendelkezik, mely tükrözi a különböző funkciójú és összeköttetésű idegsejt populációk fiziológiásan is meglévő kapcsolatait.

## KÖSZÖNETNYILVÁNÍTÁS

Köszönetemet szeretném kifejezni először is mesteremnek, Karmos Györgynek, aki gyakorlatilag mindenre megtanított, amit egy neurofiziológusnak tudnia kell, és végig támogatott a pályámon mind szakmailag, mind emberileg.

Bodócs László, Charles Schroeder, Gay Heit és Eric Halgren korábbi mentoraimnak, későbbi kollégáimnak köszönöm, hogy hagytak már egyetemista, illetve doktorandusz koromban önállóan gondolkodni, dolgozni és nem adtak olyan feladatot, amit vissza tudtam volna utasítani.

Köszönöm Fabó Dániel, Csercsa Richárd és Dombovári Balázs volt doktorandusz hallgatóimnak a sok segítséget az adatok feldolgozásában.

A kutatási projektben résztvevő számos idegsebésznek és neurológusnak, elsősorban Eröss Lorándnak, Halász Péternek és Sydney Cashnek köszönöm a kivételes együttműködési hajlandóságukat és az intellektuális hozzájárulásukat. Corey Keller, Vajda János, Czirják Sándor, Sólyom András, Rásonyi György, Kelemen Anna, Szűcs Anna, Juhos Vera, Bognár László, Szabó Zerind és Tóth Szabolcs, mint szerzőtársak, szintén fontos szerepet kaptak a kutatásokban, köszönöm az együttműködésüket.

Köszönöm Maglóczky Zsófiának és Freund Tamásnak a bizalmat, a lehetőséget, a tanácsokat és a sok-sok támogatást és segítséget az anatómiai munkában.

Köszönöm Papp Lászlónak a kivételes technikai segítséget, ami nélkül ez a kutatási program nem valósulhatott volna meg ilyen eredményesen.

Mind általában a tudomány, mind a konkrét kutatási program nevében szeretném megköszönni azoknak a betegeknek a segítségét, akik önzetlenül felajánlották részvételüket a kísérletekben.

Wittner Lucának, feleségemnek és két gyermekem édesanyjának köszönöm, hogy végig támogatott mind szakmailag, mind érzelmileg és megértően, zokszó nélkül viselte a hosszú heteket, hónapokat, amikor a kutatással voltam elfoglalva a családi együttlét élvezete helyett.

Végül köszönöm szüleimnek, hogy végig támogattak és soha nem kételkedtek abban az útban, amin járnom kellett.

## IRODALOMJEGYZÉK

- Achermann, P., Borbely, A.A., 1997. Low-frequency (< 1 Hz) oscillations in the human sleep electroencephalogram. *Neuroscience*. 81, 213-22.
- Alger, B.E., Nicoll, R.A., 1980. Epileptiform burst afterhyperpolarization: calcium-dependent potassium potential in hippocampal CA1 pyramidal cells. *Science*. 210, 1122-4.
- Amzica, F., Steriade, M., 2002. The functional significance of K-complexes. *Sleep Med Rev*. 6, 139-49.
- Andrillon, T., et al., 2011. Sleep spindles in humans: insights from intracranial EEG and unit recordings. *J Neurosci*. 31, 17821-34.
- Avoli, M., de Curtis, M., Kohling, R., 2012. Does interictal synchronization influence ictogenesis? *Neuropharmacology*.
- Barbas, H., 2000. Connections underlying the synthesis of cognition, memory, and emotion in primate prefrontal cortices. *Brain Res Bull*. 52, 319-30.
- Basano, L., et al., 2001. Pulsatile electrical impedance response from cerebrally dead adult patients is not a reliable tool for detecting cerebral perfusion changes. *Physiol Meas*. 22, 341-9.
- Blume, W.T., Holloway, G.M., Wiebe, S., 2001. Temporal epileptogenesis: localizing value of scalp and subdural interictal and ictal EEG data. *Epilepsia*. 42, 508-14.
- Botella-Soler, V., et al., 2012. Large-scale cortical dynamics of sleep slow waves. *PLoS One*. 7, e30757.
- Bunge, S.A., et al., 2001. Prefrontal regions involved in keeping information in and out of mind. *Brain*. 124, 2074-86.
- Buxton, R.B., Wong, E.C., Frank, L.R., 1998. Dynamics of blood flow and oxygenation changes during brain activation: the balloon model. *Magnetic Resonance in Medicine*. 39, 855-64.
- Buzsaki, G., 1996. The hippocampo-neocortical dialogue. *Cereb Cortex*. 6, 81-92.
- Buzsaki, G., Draguhn, A., 2004. Neuronal oscillations in cortical networks. *Science*. 304, 1926-9.
- Cabeza, R., Nyberg, L., 2003. Functional neuroimaging of memory. *Neuropsychologia*. 41, 241-4.
- Cappaert, N.L., Wadman, W.J., Witter, M.P., 2007. Spatiotemporal analyses of interactions between entorhinal and CA1 projections to the subiculum in rat brain slices. *Hippocampus*. 17, 909-21.
- Carter, C.S., et al., 2000. Parsing executive processes: strategic vs. evaluative functions of the anterior cingulate cortex. *Proc Natl Acad Sci U S A*. 97, 1944-8.
- Cash, S.S., et al., 2009. The human K-complex represents an isolated cortical down-state. *Science*. 324, 1084-7.
- Chauvette, S., Volgushev, M., Timofeev, I., 2010. Origin of Active States in Local Neocortical Networks during Slow Sleep Oscillation. *Cereb Cortex*.
- Chauvette, S., Seigneur, J., Timofeev, I., 2012. Sleep oscillations in the thalamocortical system induce long-term neuronal plasticity. *Neuron*. 75, 1105-13.
- Clemens, Z., et al., 2005. Factors affecting spiking related to sleep and wake states in temporal lobe epilepsy (TLE). *Seizure*. 14, 52-7.
- Cohen, I., et al., 2002. On the origin of interictal activity in human temporal lobe epilepsy in vitro. *Science*. 298, 1418-21.
- Colrain, I.M., 2005. The K-complex: a 7-decade history. *Sleep*. 28, 255-73.
- Connors, B.W., Telfeian, A.E., 2000. Dynamic properties of cells, synapses, circuits, and seizures in neocortex. *Adv Neurol*. 84, 141-52.
- Connors, B.W., Pinto, D.J., Telfeian, A.E., 2001. Local pathways of seizure propagation in neocortex. *Int Rev Neurobiol*. 45, 527-46.
- Corbetta, M., et al., 1998. A common network of functional areas for attention and eye movements. *Neuron*. 21, 761-73.
- Crosson, B., et al., 1999. Activity in the paracingulate and cingulate sulci during word generation: an fMRI study of functional anatomy. *Cereb Cortex*. 9, 307-16.
- Crunelli, V., Hughes, S.W., 2010. The slow (<1 Hz) rhythm of non-REM sleep: a dialogue between three cardinal oscillators. *Nat Neurosci*. 13, 9-17.
- Csercsa, R., et al., 2010. Laminar analysis of slow wave activity in humans. *Brain*. 133, 2814-29.
- Dale, A.M., et al., 2000. Dynamic statistical parametric mapping: combining fMRI and MEG for high-resolution imaging of cortical activity. *Neuron*. 26, 55-67.
- Dang-Vu, T.T., et al., 2011. Interplay between spontaneous and induced brain activity during human non-rapid eye movement sleep. *Proc Natl Acad Sci U S A*. 108, 15438-43.
- de Curtis, M., Avanzini, G., 2001. Interictal spikes in focal epileptogenesis. *Prog Neurobiol*. 63, 541-67.
- Devlin, J.T., et al., 2002. Is there an anatomical basis for category-specificity? Semantic memory studies in PET and fMRI. *Neuropsychologia*. 40, 54-75.
- Devor, A., et al., 2003. Coupling of total hemoglobin concentration, oxygenation, and neural activity in rat somatosensory cortex. *Neuron*. 39, 353-9.

- Devor, A., et al., 2005. Coupling of the cortical hemodynamic response to cortical and thalamic neuronal activity. *Proc Natl Acad Sci U S A.* 102, 3822-7.
- Devor, A., et al., 2007. Suppressed neuronal activity and concurrent arteriolar vasoconstriction may explain negative blood oxygenation level-dependent signal. *J Neurosci.* 27, 4452-9.
- Devor, A., et al., 2008. Stimulus-induced changes in blood flow and 2-deoxyglucose uptake dissociate in ipsilateral somatosensory cortex. *J Neurosci.* 28, 14347-57.
- Dhond, R.P., et al., 2003. Spatiotemporal maps of past-tense verb inflection. *Neuroimage.* 19, 91-100.
- Dum, R.P., Strick, P.L., 1993. The cingulate motor areas. In: *Neurobiology of cingulate cortex and limbic thalamus.* Vol., B.A. Vogt, M. Gabriel, ed.^eds. Birkhäuser, Boston, pp. 415-441.
- Elston, G.N., 2003. Cortex, cognition and the cell: new insights into the pyramidal neuron and prefrontal function. *Cereb Cortex.* 13, 1124-38.
- Elston, G.N., et al., 2006. Specializations of the granular prefrontal cortex of primates: implications for cognitive processing. *Anat Rec A Discov Mol Cell Evol Biol.* 288, 26-35.
- Euston, D.R., Tatsuno, M., McNaughton, B.L., 2007. Fast-forward playback of recent memory sequences in prefrontal cortex during sleep. *Science.* 318, 1147-50.
- Fabo, D., et al., 2005. Subiculum-temporal cortex interactions during spikes and seizure. *Epilepsia.* 46, 220-220.
- Fabo, D., et al., 2008. Properties of in vivo interictal spike generation in the human subiculum. *Brain.* 131, 485-99.
- Felleman, D.J., VanEssen, D.C., 1991. Distributed hierarchical processing in the primate cerebral cortex. *Cerebral Cortex.* 1, 1-47.
- Fernandez de Sevilla, D., et al., 2006. Calcium-activated afterhyperpolarizations regulate synchronization and timing of epileptiform bursts in hippocampal CA3 pyramidal neurons. *J Neurophysiol.* 96, 3028-41.
- Fiez, J.A., Petersen, S.E., 1998. Neuroimaging studies of word reading. *Proceedings of the National Academy of Sciences of the United States of America.* 95, 914-921.
- Frith, C.D., et al., 1991. Willed action and the prefrontal cortex in man: a study with PET. *Proc R Soc Lond B Biol Sci.* 244, 241-6.
- Gabbott, P.L., Jays, P.R., Bacon, S.J., 1997. Calretinin neurons in human medial prefrontal cortex (areas 24a,b,c, 32', and 25). *J Comp Neurol.* 381, 389-410.
- Goldensohn, E.S., Purpura, D.P., 1963. Intracellular potentials of cortical neurons during focal epileptogenic discharges. *Science.* 139, 840-2.
- Gotman, J., 1980. Quantitative measurements of epileptic spike morphology in the human EEG. *Electroencephalogr Clin Neurophysiol.* 48, 551-7.
- Grover, F.S., Buchwald, J.S., 1970. Correlation of cell size with amplitude of background fast activity in specific brain nuclei. *J Neurophysiol.* 33, 160-171.
- Halasz, P., 2005. K-complex, a reactive EEG graphoelement of NREM sleep: an old chap in a new garment. *Sleep Med Rev.* 9, 391-412.
- Halasz, P., 2012. Sleep and epilepsy. *Handb Clin Neurol.* 107, 305-22.
- Halgren, E., et al., 2002. Rapid distributed fronto-parieto-occipital processing stages during working memory in humans. *Cerebral Cortex.* 12, 710-728.
- Hangya, B., et al., 2011. Complex propagation patterns characterize human cortical activity during slow-wave sleep. *J Neurosci.* 31, 8770-9.
- Henze, D.A., Wittner, L., Buzsaki, G., 2002. Single granule cells reliably discharge targets in the hippocampal CA3 network in vivo. *Nat Neurosci.* 5, 790-5.
- Herculano-Houzel, S., et al., 2007. Cellular scaling rules for primate brains. *Proc Natl Acad Sci U S A.* 104, 3562-7.
- Hodges, J.R., et al., 1992. Semantic dementia. Progressive fluent aphasia with temporal lobe atrophy. *Brain.* 115, 1783-806.
- Huber, R., et al., 2004. Local sleep and learning. *Nature.* 430, 78-81.
- Huberfeld, G., et al., 2007. Perturbed chloride homeostasis and GABAergic signaling in human temporal lobe epilepsy. *J Neurosci.* 27, 9866-73.
- Humphrey, D.R., 1968. Re-analysis of the antidromic cortical response. II. On the contribution of cell discharge and PSPs to the evoked potentials. *Electroencephalogr Clin Neurophysiol.* 25, 421-42.
- Jahnke, K., et al., 2012. To wake or not to wake? The two-sided nature of the human K-complex. *Neuroimage.* 59, 1631-8.
- Keller, C.J., et al., 2009. Intracranial microprobe for evaluating neuro-hemodynamic coupling in unanesthetized human neocortex. *J Neurosci Methods.* 179, 208-18.
- Keller, C.J., et al., 2010. Heterogeneous neuronal firing patterns during interictal epileptiform discharges in the human cortex. *Brain.* 133, 1668-81.
- Keller, C.J., et al., 2011. Intrinsic functional architecture predicts electrically evoked responses in the human brain. *Proc Natl Acad Sci U S A.* 108, 10308-13.

- Kiehl, K.A., Liddle, P.F., Hopfinger, J.B., 2000. Error processing and the rostral anterior cingulate: an event-related fMRI study. *Psychophysiology*. 37, 216-23.
- Kollias, S.S., et al., 2001. Identification of multiple nonprimary motor cortical areas with simple movements. *Brain Res Brain Res Rev*. 36, 185-95.
- Kronland-Martinet, R., Morlet, J., Grossmann, A., 1987. Analysis of sound patterns through wavelet transforms. *International Journal of Pattern Recognition and Artificial Intelligence*. 1, 273-302.
- Lachaux, J.P., et al., 1999. Measuring phase synchrony in brain signals. *Hum Brain Mapp*. 8, 194-208.
- Lakatos, P., et al., 2008. Entrainment of neuronal oscillations as a mechanism of attentional selection. *Science*. 320, 110-3.
- Le Van Quyen, M., et al., 2010. Large-scale microelectrode recordings of high-frequency gamma oscillations in human cortex during sleep. *J Neurosci*. 30, 7770-82.
- Logothetis, N.K., et al., 2001. Neurophysiological investigation of the basis of the fMRI signal. *Nature*. 412, 150-7.
- Logothetis, N.K., 2003. The underpinnings of the BOLD functional magnetic resonance imaging signal. *J Neurosci*. 23, 3963-71.
- Luczak, A., et al., 2007. Sequential structure of neocortical spontaneous activity in vivo. *Proc Natl Acad Sci U S A*. 104, 347-52.
- Maglóczky, Z., et al., 2000. Changes in the distribution and connectivity of interneurons in the epileptic human dentate gyrus. *Neuroscience*. 96, 7-25.
- Margerison, J.H., Corsellis, J.A.N., 1966. Epilepsy and the temporal lobes. *Brain*. 89, 499-530.
- Marinkovic, K., et al., 2003. Spatiotemporal dynamics of modality-specific and supramodal word processing. *Neuron*. 38, 487-97.
- Massimini, M., et al., 2004. The sleep slow oscillation as a traveling wave. *J Neurosci*. 24, 6862-70.
- McCormick, D.A., Contreras, D., 2001. On the cellular and network bases of epileptic seizures. *Annu Rev Physiol*. 63, 815-46.
- Mehta, A.D., Ulbert, I., Schroeder, C.E., 2000a. Intermodal selective attention in monkeys. II: physiological mechanisms of modulation. *Cereb Cortex*. 10, 359-70.
- Mehta, A.D., Ulbert, I., Schroeder, C.E., 2000b. Intermodal selective attention in monkeys. I: distribution and timing of effects across visual areas. *Cereb Cortex*. 10, 343-58.
- Menendez de la Prida, L., Gal, B., 2004. Synaptic contributions to focal and widespread spatiotemporal dynamics in the isolated rat subiculum in vitro. *J Neurosci*. 24, 5525-36.
- Meskenaite, V., 1997. Calretinin-immunoreactive local circuit neurons in area 17 of the cynomolgus monkey, *Macaca fascicularis*. *J Comp Neurol*. 379, 113-32.
- Mesulam, M.M., 1981. A cortical network for directed attention and unilateral neglect. *Annals of Neurology*. 10, 309-25.
- Miller, L., et al., 1994. Amygdalar sclerosis: preoperative indicators and outcome after temporal lobectomy. *J Neurol Neurosurg Psychiatry*. 57, 1099-1105.
- Mitzdorf, U., 1985. Current source-density method and application in cat cerebral cortex: investigation of evoked potentials and EEG phenomena. *Physiol Rev*. 65, 37-100.
- Molle, M., et al., 2002. Grouping of spindle activity during slow oscillations in human non-rapid eye movement sleep. *J Neurosci*. 22, 10941-7.
- Molle, M., et al., 2006. Hippocampal sharp wave-ripples linked to slow oscillations in rat slow-wave sleep. *J Neurophysiol*. 96, 62-70.
- Montgomery, L.D., Montgomery, R.W., Guisado, R., 1995. Rheoencephalographic and electroencephalographic measures of cognitive workload: analytical procedures. *Biol Psychol*. 40, 143-59.
- Murray, E.A., Bussey, T.J., 1999. Perceptual-mnemonic functions of the perirhinal cortex. *Trends in Cognitive Sciences*. 3, 142-151.
- Naya, Y., Yoshida, M., Miyashita, Y., 2001. Backward spreading of memory-retrieval signal in the primate temporal cortex. *Science*. 291, 661-4.
- Ngo, H.V., et al., 2012. Induction of slow oscillations by rhythmic acoustic stimulation. *J Sleep Res*.
- Nicholson, C., Freeman, J.A., 1975. Theory of current source density analysis and determination of the conductivity tensor for anuran cerebellum. *Journal of Neurophysiology*. 38, 356-368.
- Nir, Y., et al., 2011. Regional slow waves and spindles in human sleep. *Neuron*. 70, 153-69.
- Nyberg, L., 1998. Mapping episodic memory. *Behav Brain Res*. 90, 107-14.
- Pedley, T., 1984. Epilepsy and the human electroencephalogram. In: *Pathophysiology of epilepsy*. Vol., P. Schwartzkroin, H. Wheal, ed. Academic Press, London, pp. 1-30.
- Penfield, W., Jasper, H., 1954. *Epilepsy and the functional anatomy of the human brain*, Vol., Little Brown, Boston.

- Phan, K.L., et al., 2002. Functional neuroanatomy of emotion: a meta-analysis of emotion activation studies in PET and fMRI. *Neuroimage*. 16, 331-48.
- Picard, N., Strick, P.L., 2001. Imaging the premotor areas. *Curr Opin Neurobiol*. 11, 663-72.
- Posner, M.I., et al., 1988. Localization of cognitive operations in the human brain. *Science*. 240, 1627-31.
- Rappelsberger, P., Pockberger, H., Petsche, H., 1981. Current source density analysis: methods and application to simultaneously recorded field potentials of the rabbit's visual cortex. *Pflugers Arch*. 389, 159-70.
- Sakata, S., Harris, K.D., 2009. Laminar structure of spontaneous and sensory-evoked population activity in auditory cortex. *Neuron*. 64, 404-18.
- Sanchez-Vives, M.V., McCormick, D.A., 2000. Cellular and network mechanisms of rhythmic recurrent activity in neocortex. *Nat Neurosci*. 3, 1027-34.
- Scheffer, I.E., et al., 1995. Autosomal dominant nocturnal frontal lobe epilepsy. A distinctive clinical disorder. *Brain*. 118 ( Pt 1), 61-73.
- Schwartzkroin, P.A., Wheal, H.V., 1984. *Electrophysiology of Epilepsy*, Vol., Academic, New York.
- Staba, R.J., et al., 2002a. Sleep states differentiate single neuron activity recorded from human epileptic hippocampus, entorhinal cortex, and subiculum. *J Neurosci*. 22, 5694-704.
- Staba, R.J., et al., 2002b. Quantitative analysis of high-frequency oscillations (80-500 Hz) recorded in human epileptic hippocampus and entorhinal cortex. *J Neurophysiol*. 88, 1743-52.
- Staba, R.J., et al., 2002c. Single neuron burst firing in the human hippocampus during sleep. *Hippocampus*. 12, 724-34.
- Staba, R.J., et al., 2004. High-frequency oscillations recorded in human medial temporal lobe during sleep. *Ann Neurol*. 56, 108-15.
- Staba, R.J., et al., 2007. Increased fast ripple to ripple ratios correlate with reduced hippocampal volumes and neuron loss in temporal lobe epilepsy patients. *Epilepsia*. 48, 2130-8.
- Stefanics, G., et al., 2010. Phase entrainment of human delta oscillations can mediate the effects of expectation on reaction speed. *J Neurosci*. 30, 13578-85.
- Steinorth, S., et al., 2009. Human entorhinal gamma and theta oscillations selective for remote autobiographical memory. *Hippocampus*.
- Steriade, M., McCormick, D.A., Sejnowski, T.J., 1993a. Thalamocortical oscillations in the sleeping and aroused brain. *Science*. 262, 679-85.
- Steriade, M., Nunez, A., Amzica, F., 1993b. A novel slow ( 1 Hz) oscillation of neocortical neurons in vivo: depolarizing and hyperpolarizing components. *J Neurosci*. 13, 3252-65.
- Steriade, M., Amzica, F., 1994. Dynamic coupling among neocortical neurons during evoked and spontaneous spike-wave seizure activity. *J Neurophysiol*. 72, 2051-69.
- Steriade, M., Amzica, F., 1996. Intracortical and corticothalamic coherency of fast spontaneous oscillations. *Proc Natl Acad Sci U S A*. 93, 2533-8.
- Steriade, M., et al., 1998. Spike-wave complexes and fast components of cortically generated seizures. II. Extra- and intracellular patterns. *J Neurophysiol*. 80, 1456-79.
- Steriade, M., Contreras, D., 1998. Spike-wave complexes and fast components of cortically generated seizures. I. Role of neocortex and thalamus. *J Neurophysiol*. 80, 1439-55.
- Steriade, M., 2003. *Neuronal substrates of sleep and epilepsy*, Vol., Cambridge University Press, Cambridge.
- Steriade, M., Timofeev, I., 2003. Neuronal plasticity in thalamocortical networks during sleep and waking oscillations. *Neuron*. 37, 563-76.
- Steriade, M., 2006. Grouping of brain rhythms in corticothalamic systems. *Neuroscience*. 137, 1087-106.
- Swann, J.W., Hablitz, J.J., 2000. Cellular abnormalities and synaptic plasticity in seizure disorders of the immature nervous system. *Ment Retard Dev Disabil Res Rev*. 6, 258-67.
- Thomason, M.E., et al., 2005. Breath holding reveals differences in fMRI BOLD signal in children and adults. *Neuroimage*. 25, 824-37.
- Timofeev, I., Chauvette, S., 2011. Thalamocortical oscillations: local control of EEG slow waves. *Current topics in medicinal chemistry*. 11, 2457-2528.
- Ulbert, I., et al., 2001a. Multiple microelectrode-recording system for human intracortical applications. *J Neurosci Methods*. 106, 69-79.
- Ulbert, I., et al., 2001b. Early discrimination of coherent versus incoherent motion by multiunit and synaptic activity in human putative MT+. *Hum Brain Mapp*. 13, 226-38.
- Ulbert, I., et al., 2004a. Laminar analysis of human neocortical interictal spike generation and propagation: current source density and multiunit analysis in vivo. *Epilepsia*. 45 Suppl 4, 48-56.
- Ulbert, I., et al., 2004b. In vivo laminar electrophysiology co-registered with histology in the hippocampus of patients with temporal lobe epilepsy. *Exp Neurol*. 187, 310-8.
- Ulbert, I., et al., 2005. Intracortical activation sequence of spontaneous and evoked spike-wave complexes in humans. *Epilepsia*. 46, 200-200.

- Vaknin, G., DiScenna, P.G., Teyler, T.J., 1988. A method for calculating current source density (CSD) analysis without restoring sites outside the sampling volume. *J. of Neurosci. Methods.* 24, 131-135.
- Valderrama, M., et al., 2012. Human gamma oscillations during slow wave sleep. *PloS one.* 7.
- Valentin, A., et al., 2002. Responses to single pulse electrical stimulation identify epileptogenesis in the human brain in vivo. *Brain.* 125, 1709-18.
- Vogt, B.A., Hof, P.R., Vogt, L.J., 2004. Cingulate Gyrus. In: *The Human Nervous System. Vol., G. Paxinos, J.K. Mai, ed.^eds. Elsevier Academic, San Diego, pp. 915-949.*
- Vyazovskiy, V., et al., 2011. Local sleep in awake rats. *Nature.* 472, 443-450.
- Vyazovskiy, V.V., et al., 2008. Molecular and electrophysiological evidence for net synaptic potentiation in wake and depression in sleep. *Nat Neurosci.* 11, 200-8.
- Wang, C., et al., 2005. Responses of human anterior cingulate cortex microdomains to error detection, conflict monitoring, stimulus-response mapping, familiarity, and orienting. *J Neurosci.* 25, 604-13.
- Wieser, H.G., 1988. Selective amygdalo-hippocampotomy for temporal lobe epilepsy. *Epilepsia.* 29, S100-S113.
- Wittner, L., et al., 2001. Preservation of perisomatic inhibitory input of granule cells in the epileptic human dentate gyrus. *Neuroscience.* 108, 587-600.
- Wittner, L., et al., 2002. Synaptic reorganization of calbindin-positive neurons in the human hippocampal CA1 region in temporal lobe epilepsy. *Neuroscience.* 115, 961-78.
- Wittner, L., et al., 2005. Surviving CA1 pyramidal cells receive intact perisomatic inhibitory input in the human epileptic hippocampus. *Brain.* 128, 138-52.
- Wittner, L., et al., 2009. The epileptic human hippocampal cornu ammonis 2 region generates spontaneous interictal-like activity in vitro. *Brain.* 132, 3032-46.
- Wu, C.P., et al., 2006. Spontaneous rhythmic field potentials of isolated mouse hippocampal-subicular-entorhinal cortices in vitro. *J Physiol.* 576, 457-76.
- Wu, K., Leung, L.S., 2003. Increased dendritic excitability in hippocampal ca1 in vivo in the kainic acid model of temporal lobe epilepsy: a study using current source density analysis. *Neuroscience.* 116, 599-616.

## AZ ÉRTEKEZÉS ALAPJÁUL SZOLGÁLÓ SAJÁT KÖZLEMÉNYEK

1. Keller CJ, Cash SS, Narayanan S, Wang C, Kuzniecky R, Carlson C, Devinsky O, Thesen T, Doyle W, Sassaroli A, Boas DA, **Ulbert I**, Halgren E. Intracranial microprobe for evaluating neuro-hemodynamic coupling in unanesthetized human neocortex. *JOURNAL OF NEUROSCIENCE METHODS* 179:(2) 208-218 (2009) *IF: 2.295*
2. Wang C, **Ulbert I**, Schomer DL, Marinkovic K, Halgren E. Responses of human anterior cingulate cortex microdomains to error detection, conflict monitoring, stimulus-response mapping, familiarity, and orienting. *JOURNAL OF NEUROSCIENCE* 25:(3) pp. 604-613. (2005) *IF: 7.506*
3. Halgren E, Wang C, Schomer DL, Knake S, Marinkovic K, Wu J, **Ulbert I**. Processing stages underlying word recognition in the anteroventral temporal lobe. *NEUROIMAGE* 30:(4) pp. 1401-1413. (2006) *IF: 5.559*
4. Cash SS, Halgren E, Dehghani N, Rossetti AO, Thesen T, Wang C, Devinsky O, Kuzniecky R, Doyle W, Madsen JR, Bromfield E, Eross L, Halasz P, Karmos G, Csercsa R, Wittner L, **Ulbert I**. The human K-complex represents an isolated cortical down-state. *SCIENCE* 324:(5930) pp. 1084-1087. (2009) *IF: 29.747*
5. Csercsa R, Dombovari B, Fabo D, Wittner L, Eross L, Entz L, Solyom A, Rasonyi G, Szucs A, Kelemen A, Jakus R, Juhos V, Grand L, Magony A, Halasz P, Freund TF, Magloczky Z, Cash SS, Papp L, Karmos G, Halgren E, **Ulbert I**. Laminar analysis of slow wave activity in humans. *BRAIN* 133:(Pt 9) pp. 2814-2829. (2010) *IF: 9.230*
6. Hangya B, Tihanyi BT, Entz L, Fabo D, Eross L, Wittner L, Jakus R, Varga V, Freund TF, **Ulbert I**. Complex Propagation Patterns Characterize Human Cortical Activity during Slow-Wave Sleep. *JOURNAL OF NEUROSCIENCE* 31:(24) pp. 8770-8779. (2011) *IF: 7.115*
7. **Ulbert I**, Magloczky Z, Eross L, Czirjak S, Vajda J, Bogнар L, Toth S, Szabo Z, Halasz P, Fabo D, Halgren E, Freund TF, Karmos G. In vivo laminar electrophysiology co-registered with histology in the hippocampus of patients with temporal lobe epilepsy. *EXPERIMENTAL NEUROLOGY* 187:(2) pp. 310-318. (2004) *IF: 3.369*
8. Fabo D, Magloczky Z, Wittner L, Pek A, Eross L, Czirjak S, Vajda J, Solyom A, Rasonyi G, Szucs A, Kelemen A, Juhos V, Grand L, Dombovari B, Halasz P, Freund TF, Halgren E, Karmos G, **Ulbert I**. Properties of in vivo interictal spike generation in the human subiculum. *BRAIN* 131:(Pt 2) pp. 485-499. (2008) *IF: 9.603*
9. **Ulbert I**, Heit G, Madsen J, Karmos G, Halgren E. Laminar analysis of human neocortical interictal spike generation and propagation: current source density and multiunit analysis in vivo. *EPILEPSIA* 45:(Suppl 4) pp. 48-56. (2004) *IF: 3.329*
10. Keller CJ, Truccolo W, Gale JT, Eskandar E, Thesen T, Carlson C, Devinsky O, Kuzniecky R, Doyle WK, Madsen JR, Schomer DL, Mehta AD, Brown EN, Hochberg LR, **Ulbert I**, Halgren E, Cash SS. Heterogeneous neuronal firing patterns during interictal epileptiform discharges in the human cortex. *BRAIN* 133:(Pt 6) pp. 1668-1681. (2010) *IF: 9.230*

Az értekezés alapjául szolgáló közlemények összesített impakt faktora: 86.983

**AZ ÉRTEKEZÉS TÉMÁJÁHOZ KAPCSOLÓDÓ EGYÉB KÖZLEMÉNYEK**

- Chan AM, Baker JM, Eskandar E, Schomer D, **Ulbert I**, Marinkovic K, Cash SS, Halgren E. First-Pass Selectivity for Semantic Categories in Human Anteroventral Temporal Lobe. *JOURNAL OF NEUROSCIENCE*, 2011 Dec 7;31(49):18119-18129.
- Keller CJ, Bickel S, Entz L, **Ulbert I**, Milham MP, Kelly C, Mehta AD. Intrinsic functional architecture predicts electrically evoked responses in the human brain. *PNAS*. 2011 Jun 21;108(25):10308-13.
- Stefanics G, Hangya B, Hernádi I, Winkler I, Lakatos P, **Ulbert I**. Phase entrainment of human delta oscillations can mediate the effects of expectation on reaction speed. *JOURNAL OF NEUROSCIENCE* 2010 Oct 13;30(41):13578-85.
- Steinvorth S, Wang C, **Ulbert I**, Schomer D, Halgren E. Human entorhinal gamma and theta oscillations selective for remote autobiographical memory. *HIPPOCAMPUS* 2010 Jan;20(1):166-73.
- Schachter SC, Gutttag J, Schiff SJ, Schomer DL; Summit Contributors (Ulbert I). Advances in the application of technology to epilepsy: the CIMIT/NIO Epilepsy Innovation Summit. *EPILEPSY & BEHAVIOR* 2009 Sep;16(1):3-46.
- Wittner L, Huberfeld G, Clémenceau S, Eross L, Dezamis E, Entz L, **Ulbert I**, Baulac M, Freund TF, Maglóczky Z, Miles R. The epileptic human hippocampal cornu ammonis 2 region generates spontaneous interictal-like activity in vitro. *BRAIN*. 2009 Nov;132(Pt 11):3032-46.
- Knake S, Wang CM, **Ulbert I**, Schomer DL, Halgren E. Specific increase of human entorhinal population synaptic and neuronal activity during retrieval. *NEUROIMAGE* 37:(2) 618-622 (2007)
- Ulbert I**, Halgren E, Heit G, Karmos G. Multiple microelectrode-recording system for human intracortical applications. *JOURNAL OF NEUROSCIENCE METHODS* 106:(1) 69-79 (2001)
- Ulbert I**, Karmos G, Heit G, Halgren E. Early discrimination of coherent versus incoherent motion by multiunit and synaptic activity in human putative MT+. *HUMAN BRAIN MAPPING* 13:(4) 226-238 (2001)

**A TELJES ÉLETMŰ TUDOMÁNYMETRIAI MUTATÓI**

Eredeti közlemények száma:	57
Idézetek száma:	2342
Független idézetek száma:	1904
Összegzett impakt faktor:	341.46
Hirsch-index:	25

dc\_303\_11

**MELLÉLKETEK**

AZ ÉRTEKEZÉS ALAPJÁUL SZOLGÁLÓ SAJÁT KÖZLEMÉNYEK: 1-10

dc\_303\_11

## **1. Melléklet**



Contents lists available at ScienceDirect

## Journal of Neuroscience Methods

journal homepage: [www.elsevier.com/locate/jneumeth](http://www.elsevier.com/locate/jneumeth)

## Intracranial microprobe for evaluating neuro-hemodynamic coupling in unanesthetized human neocortex

Corey J. Keller<sup>a,c,\*</sup>, Sydney S. Cash<sup>a</sup>, Suresh Narayanan<sup>a</sup>, Chunmao Wang<sup>b</sup>, Ruben Kuzniecky<sup>b</sup>, Chad Carlson<sup>b</sup>, Orrin Devinsky<sup>b</sup>, Thomas Thesen<sup>b</sup>, Werner Doyle<sup>b</sup>, Angelo Sassaroli<sup>c</sup>, David A. Boas<sup>d</sup>, Istvan Ulbert<sup>e,f</sup>, Eric Halgren<sup>g</sup>

<sup>a</sup> Department of Neurology, Massachusetts General Hospital, Boston, MA, USA

<sup>b</sup> Comprehensive Epilepsy Center, New York University Langone Medical Center, New York, NY, USA

<sup>c</sup> Department of Biomedical Engineering, Tufts University, Medford, MA, USA

<sup>d</sup> Athinoula A. Martinos Center for Biomedical Imaging, Harvard Medical School, Charlestown, MA, USA

<sup>e</sup> Institute for Psychology of the Hungarian Academy of Sciences, Budapest, Hungary

<sup>f</sup> Peter Pazmany Catholic University, Department of Information Technology, Budapest, Hungary

<sup>g</sup> Multimodal Imaging Laboratory, Department of Radiology, University of California at San Diego, La Jolla, CA, USA

## ARTICLE INFO

## Article history:

Received 12 November 2008

Received in revised form 27 January 2009

Accepted 29 January 2009

## Keywords:

Microelectrode

BOLD

Oxygenation

Hemodynamics

Neuro-hemodynamic coupling

Breath-hold

Electrocardiogram

Cortical electrical stimulation

## ABSTRACT

Measurement of the blood-oxygen-level dependent (BOLD) response with fMRI has revolutionized cognitive neuroscience and is increasingly important in clinical care. The BOLD response reflects changes in deoxy-hemoglobin concentration, blood volume, and blood flow. These hemodynamic changes ultimately result from neuronal firing and synaptic activity, but the linkage between these domains is complex, poorly understood, and may differ across species, cortical areas, diseases, and cognitive states. We describe here a technique that can measure neural and hemodynamic changes simultaneously from cortical microdomains in waking humans. We utilize a “laminar optode,” a linear array of microelectrodes for electrophysiological measures paired with a micro-optical device for hemodynamic measurements. Optical measurements include laser Doppler to estimate cerebral blood flow as well as point spectroscopy to estimate oxy- and deoxy-hemoglobin concentrations. The microelectrode array records local field potential gradients (PG) and multi-unit activity (MUA) at 24 locations spanning the cortical depth, permitting estimation of population trans-membrane current flows (Current Source Density, CSD) and population cell firing in each cortical lamina. Comparison of the laminar CSD/MUA profile with the origins and terminations of cortical circuits allows activity in specific neuronal circuits to be inferred and then directly compared to hemodynamics. Access is obtained in epileptic patients during diagnostic evaluation for surgical therapy. Validation tests with relatively well-understood manipulations (EKG, breath-holding, cortical electrical stimulation) demonstrate the expected responses. This device can provide a new and robust means for obtaining detailed, quantitative data for defining neurovascular coupling in awake humans.

© 2009 Elsevier B.V. All rights reserved.

### 1. Introduction

In recent years, studying brain activation with non-invasive functional MRI (fMRI) has become an essential tool in the field of

neuroscience. However, the utility of fMRI is limited because it measures hemodynamic responses that have an unknown relationship to the electrophysiological activity that is used for neural information processing. We describe here a method for simultaneous quantitative measurement of both domains at the level of the cortical column in awake humans. These measurements may be used to calculate the transfer function between vascular and electrophysiological changes, and thus allow more precise interpretation of non-invasive hemodynamic results.

fMRI measures the blood-oxygenation-level dependent (BOLD) response. The neural basis of the BOLD signal is the focus of very active studies and has been reviewed previously (Logothetis and Wandell, 2004; Nair, 2005; Logothetis, 2007). The iron in hemoglobin (Hb) strongly affects the spin of nearby protons, but

\* Corresponding author at: Department of Neurology, Massachusetts General Hospital, Boston, MA, USA. Tel.: +1 802 578 6292.

E-mail addresses: [cjkeller@partners.org](mailto:cjkeller@partners.org) (C.J. Keller), [scash@partners.org](mailto:scash@partners.org) (S.S. Cash), [suresh.narayanan@ge.com](mailto:suresh.narayanan@ge.com) (S. Narayanan), [wangch@nidcd.nih.gov](mailto:wangch@nidcd.nih.gov) (C. Wang), [ruben.kuzniecky@med.nyu.edu](mailto:ruben.kuzniecky@med.nyu.edu) (R. Kuzniecky), [ccarlso2@gmail.com](mailto:ccarlso2@gmail.com) (C. Carlson), [od4@nyu.edu](mailto:od4@nyu.edu) (O. Devinsky), [thomas.thesen@med.nyu.edu](mailto:thomas.thesen@med.nyu.edu) (T. Thesen), [wkd1@nyu.edu](mailto:wkd1@nyu.edu) (W. Doyle), [angelo.sassaroli@tufts.edu](mailto:angelo.sassaroli@tufts.edu) (A. Sassaroli), [dboas@nmr.mgh.harvard.edu](mailto:dboas@nmr.mgh.harvard.edu) (D.A. Boas), [ulbert@cogpsyphy.hu](mailto:ulbert@cogpsyphy.hu) (I. Ulbert), [ehalgren@ucsd.edu](mailto:ehalgren@ucsd.edu) (E. Halgren).

not if it is shielded by oxygen, i.e., in oxy-hemoglobin (Hbo). Thus, the BOLD signal ultimately reflects changes in concentration of paramagnetic deoxy-hemoglobin (Hbr) (Ogawa et al., 1990). The concentration of Hbr, Hbo, and total Hb (Hbt) depends on the local cerebral metabolic rate for oxygen (LCMRO<sub>2</sub>), cerebral blood volume (CBV), and the rate of regional cerebral blood flow (rCBF). Thus, the BOLD signal can be precisely modeled from these measures (Buxton et al., 1998). Since changes in rCBF and CBV are thought to be coupled (Grubb et al., 1974), and LCMRO<sub>2</sub>'s effects are reflected in blood oxygenation (Hoge et al., 1999; Mandeville et al., 1999; Waldvogel et al., 2000; Jones et al., 2001), the critical hemodynamic measures are rCBF, Hbr, and Hbo.

It is known that neural activity triggers an increase in LCMRO<sub>2</sub>. Shortly thereafter, an increase in rCBF is observed that overcompensates for the increased LCMRO<sub>2</sub> and as a result Hbr eventually decreases. Although the exact aspect of neural activity that triggers and controls these hemodynamic changes has been extensively studied, the underlying mechanisms involved are still under debate (Hewson-Stoate et al., 2004; Dunn et al., 2005; Logothetis, 2003; Buzsaki et al., 2007). Some studies describe a linear neurovascular coupling (Martindale et al., 2003; Sheth et al., 2003), while others report a non-linear relationship when stimulation parameters are varied over a wider range (Devor et al., 2003; Jones et al., 2004). It has also been reported that the BOLD signal correlates with spiking activity (Rees et al., 2000; Heeger et al., 2000), although the preponderance of evidence supports a correlation with synaptic activity (Logothetis et al., 2001; Galuske et al., 2005; Mukamel et al., 2005). Equally controversial, groups have found that a stimulus-evoked negative BOLD response is a result of neuronal inhibition (Schmuel et al., 2006; Devor et al., 2007), while others support a vascular steal interpretation (Harel et al., 2002). Additionally, the "initial dip" continues to be highly controversial, primarily because this decrease in Hbo and increase in Hbr prior to any change in CBF has been reproducible in several studies (Vanzetta and Grinvald, 1999; Mayhew et al., 2000; Jones et al., 2001) while others have found no evidence of its presence (Lindauer et al., 2001). In order to further understand the "initial dip" which will strengthen fMRI studies on human brain function, the basic physiology of neurovascular coupling must be addressed (Buxton, 2001).

Based on the complexity of these relationships, with critical parameters that may vary between species and components of cognitive activation that differ in anatomical location, latency, and behavioral correlates, it is essential that the inter-relations of neuronal activity and hemodynamics be measured directly in humans during cognition.

Hemodynamic responses to neuronal activation appear to be controlled at the level of a vascular unit, where rCBF is regulated by changing the contraction of smooth muscles in arteriole walls. Anatomically, a vascular unit supplies one or a few cortical columns. While individual measurement of all  $\sim 10^5$  neurons and  $\sim 10^9$  synapses within this volume is clearly beyond current technology, effective population measures based on microelectrode arrays have been developed. The different populations of cortical neurons, as well as their inputs from different areas, tend to be segregated into layers (Felleman and VanEssen, 1991). Firing by these different populations can be estimated with microelectrode arrays sampling multi-unit activity (MUA) in different cortical layers, and trans-membrane neuronal current flows associated with activation of these different synaptic inputs can be estimated from the second spatial derivative of the field potentials recorded by the same contacts (Current Source Density, CSD, Nicholson and Freeman, 1975; Ulbert et al., 2001a,b; Einevoll et al., 2007). Quantification of trans-membrane current is of particular interest since restoring ionic balance is the largest single process consuming energy in the brain (Attwell and Iadecola, 2002). In addition, MUA measurement allows interpretation of CSD currents as excitatory or inhibitory.

Cortical point spectroscopy allows recording of local hemoglobin concentration changes by utilizing absorption and scattering properties of Hbo and Hbr in tissues (Dunn et al., 2005). While hemodynamic concentration changes are a critical component of the BOLD response, blood flow is also involved and is not monitored by spectroscopy. Therefore, simultaneous blood flow measurements will be acquired using the laser Doppler flowmetry (LDF) technique, which permits regional cerebral blood flow measurements from changes in the flux of red blood cells in microvasculature (Bonner and Nossal, 1981). Measuring simultaneous local blood flow and oxygenation will provide a further understanding of the complex relationship between hemodynamics, metabolic activity, and the BOLD response.

It is with this motivation that we present a novel device that allows for robust semi-chronic intracranial recordings of the human neocortex that incorporates simultaneous neuronal and optical measurements at the level of the cortical microcolumn. A multicontact microelectrode array inserted perpendicularly to the neocortex records PG and MUA while an optical emitter/detector pair senses blood flow and oxygenation. Design of this device is described and preliminary results are presented from *in vivo* responses of EKG, breath-holding, and cortical stimulation.

## 2. Materials and methods

### 2.1. Microelectrode design

Construction and use of the laminar microelectrode have been described previously (Ulbert et al., 2001a,b). Briefly, 24 platinum iridium (90/10%) contacts 40  $\mu\text{m}$  in diameter are equally spaced at 150  $\mu\text{m}$  centers to span the 3.6 mm width of the gyral grey matter (Fig. 1a, b). The microelectrode array is embedded in a polyimide-epoxy substrate with total outer diameter of 350  $\mu\text{m}$ . A thin square made of silicone with surface area of  $\sim 1\text{ cm}^2$  is attached at the top of the microelectrode, and surface tension between the surface square and the cortical surface assists in securing the microprobe in position. Output leads are embedded in silicone and attached to a 26-pole ribbon cable connector. Intercontact impedance is  $1\text{ M}\Omega \pm 10\%$  at 100 Hz and thermal noise is 7.5  $\mu\text{V}$  in EEG range and 20  $\mu\text{V}$  in MUA range.

### 2.2. Optical microprobe design

The optical component of the device consists of an emitter and detector fiber optic unit embedded in the silicone sheet and is able to probe activity in the microcolumns surrounding the microelectrode. Both fiber bundles (F2 core/8250 cladding, 50  $\mu\text{m}$  diameter, 300 fibers, 1 mm total diameter, FiberOptix Technology, Pomfret, CT) run parallel to the cortical surface. Fiber bundle diameter was chosen to be 1 mm, small enough to not hinder clinical recordings when placed directly below the subdural electrode grid but able to carry significant light power. In order to re-direct light so the emitter and detector are parallel to the cortical surface, dichroic prisms (PN #716603, Westchester Technologies, Peekskill, NY) were assembled at the termination of the fibers. The prisms are cut at a 45° angle and silvered in order to direct the light downward from the emitter or upward to the detector (Fig. 1a,b). Dichroic prisms lay above the cortex while the microelectrode array penetrates the pia and is oriented normal to the cortical surface. In order to develop a probe with the safety and resolution necessary to meet the above requirements, each component of the microprobe including wavelength range, optical fiber size, and emitter-detector separation distance was considered.

When spectroscopy is used for Hbr and Hbt measurements from the scalp, the main design limitation is photon penetration, and thus infrared wavelengths from 650 to 900 nm are used. However,

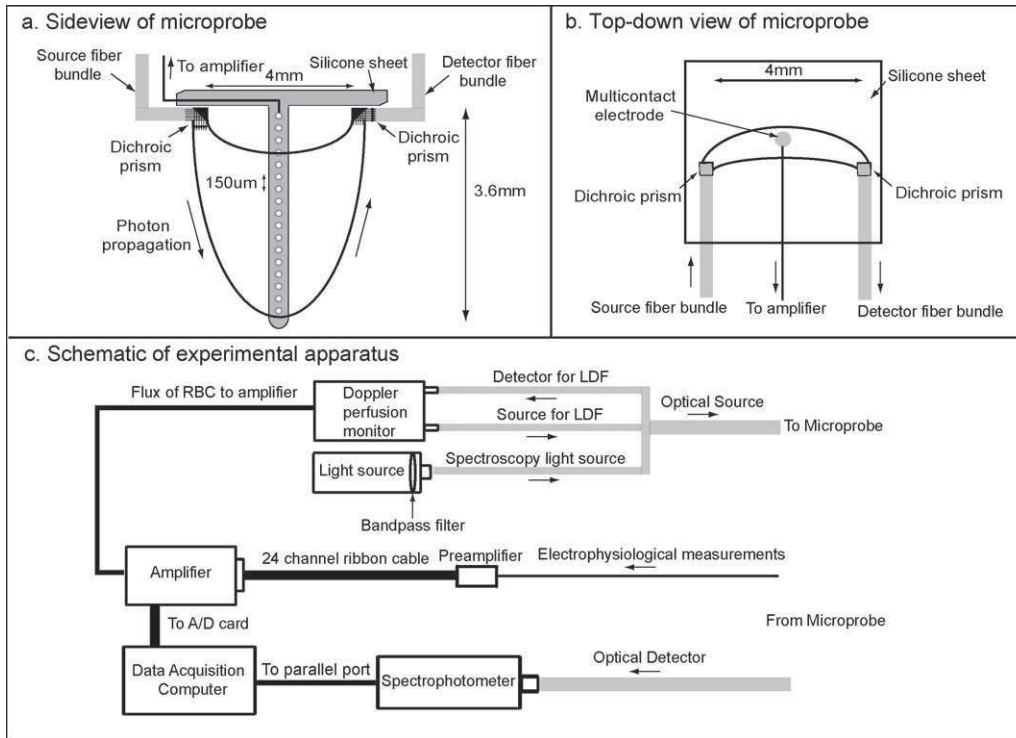


**Fig. 1.** Schematic of the laminar optode and experimental apparatus. (a, b) Side and top-down views of device. The laminar optode consists of a 3.6 mm long 24-contact shaft that spans the cortical grey matter at the gyral crown. In addition, an emitter-detector pair probes the tissue surrounding the shaft. The path of light can be modeled by a banana-shaped curve. (c) Schematic of experimental apparatus. Grey lines indicate fiber bundles. Light for Doppler and spectroscopy measurements mix and are transmitted to the cortex. Scattered light for both modalities as well as amplified and filtered electrophysiological measurements are simultaneously transmitted to the acquisition computer.

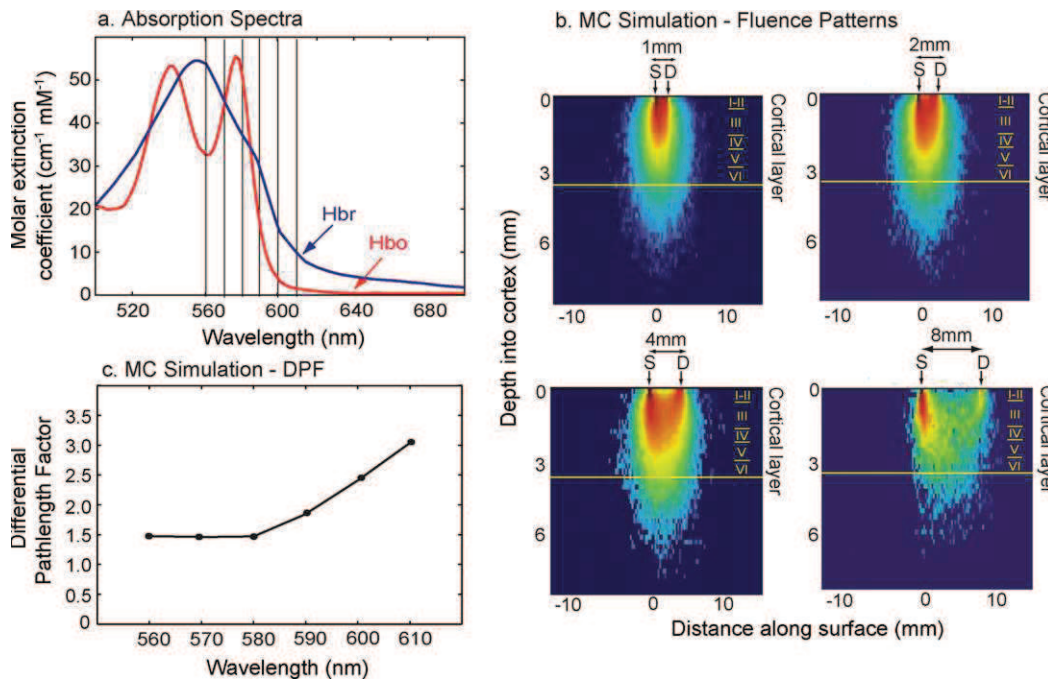


**Fig. 2.** Calculation of absorption spectra, photon propagation, and the differential path length factor. These model calculations were used to guide the choices of wavelength range, sensor separations, and spectroscopic calculations. (a) Absorption coefficients for oxy- and deoxy-hemoglobin for the visible light range offers higher absorption and greater variability to calculate hemodynamic concentrations compared to the near-infrared region above 700 nm. Vertical lines denote bandpass filters used for spectroscopy calculations. (b) Simulated normalized fluence patterns for 1, 2, 4 and 8 mm separations. At a separation distance of 4 mm, measurement of light absorption is sufficient to sample the entire depth of the cortex without undue lateral spread. (c) The differential path length factor for wavelengths in the visible light range accounts for absorption and scattering changes due to wavelength property differences.

optical probes directly implanted in the target organ are not limited by the distance of wavelength penetration (Obrig et al., 2003). Wavelengths in the visible light range, specifically 560 to 610 nm, offer an increased sensitivity to hemodynamic changes compared to the near-infrared range due to high absorption coefficients in this region (Fig. 2a). In addition, less than 10% of scattering is due to chromophores other than hemoglobin and water. This spectral range also has the advantage of including wavelengths highly selective for Hbt and Hbr. Specifically, within this range, isobestic points (525, 545, 570, and 583 nm) are sensitive to Hbt changes while 610 nm is sensitive to Hbr changes (Haglund and Hochman, 2004).

In order to determine the emitter-detector separation distance that will sample the six layers of the neocortex without undue lateral spread, the algorithm established by Kohl et al. (2000) was applied to conduct Monte Carlo simulations and determine the fluence patterns in this spectral range. Monte Carlo simulations calculate the direction and path length of each photon reaching the detector within its acceptance angle and the fluence through each voxel in the semi-infinite geometry used. For the simulation, a single emitter was placed on the pial surface with four detectors in a linear array 1, 2, 4, and 8 mm from the emitter. The cortex was modeled as a semi-infinite homogeneous tissue with uniform scattering coefficient  $\mu_s = 10 \text{ mm}^{-1}$ , absorption coefficient  $\mu_a = 0.1 \text{ mm}^{-1}$ , and an anisotropic factor of  $g = 0.9$ . Twenty-five million photons were used for this simulation. The fluence of the detected photons was calculated as

$$\phi(t) = \frac{1}{N_{\text{photons}}(t)} \sum_{i=1}^{N_{\text{photons}}(t)} \prod_{j=1}^{N_{\text{regions}}} e^{(-\mu_a \cdot l_{i,j})} \quad (1)$$

where  $\Phi(t)$  is the measured photon fluence at detector  $j$ ,  $N_{\text{photons}}$  is the number of photons injected into the medium,  $e^{(-\mu_a \cdot l_{i,j})}$  corrects for the effects of absorption in each region where  $l_{i,j}$  is the path length of photon  $i$  through region  $j$ , and  $N_{\text{regions}}$  is the number of regions through which the photons migrate (Boas et al., 2002; Custo et al., 2006). The depth profile of sampling, as indicated by the normalized fluence patterns (Fig. 2b), increases from one to two to four mm separation before deteriorating somewhat at 8 mm. These Monte Carlo simulations revealed that the measurements of light absorption sufficient to sample the entire depth of the cortex without undue lateral spread and relatively uniform layer sampling are possible with an emitter-detector separation of 4 mm.

The mean penetration depth ( $z$ ) of photons can also be calculated for various emitter-detector separations and is defined as

$$z = \frac{\sqrt{d/\mu_{\text{eff}}}}{2} \text{ where } \mu_{\text{eff}} = \sqrt{3\mu_a\mu'_s} \text{ and } \mu'_s = \mu_s(1-g) \quad (2)$$

where  $d$  is the emitter-detector separation,  $\mu_{\text{eff}}$  is the effective attenuation coefficient,  $\mu'_s$  is the reduced scattering coefficient calculated to be  $1 \text{ mm}^{-1}$ , and  $g$  is the anisotropy factor (Patterson et al., 1995). The mean penetration depth for 1, 2, 4, and 8 mm emitter-detector separations were calculated to be 1.2, 1.7, 2.4, and 3.4 mm, respectively. At a mean penetration depth of 2.4 mm with a 4 mm emitter-detector separation, the majority of photons will transverse layer IV–V where pyramidal cell bodies reside. In addition, cortical layers above and below are also sufficiently sampled. Therefore, based on the fluence patterns and mean penetration depth calculations, a 4 mm separation distance was chosen for this device.

### 2.3. Data acquisition system and analysis

An overview of the recording apparatus and analysis approach will be described here, followed by specific details in later sections concerned with different measurement modalities and validation tests. The schematic diagram of the experimental setup is shown in Fig. 1c. Briefly, two light sources used for blood flow and hemody-

amic measurements are mixed and sent into the cortex. Reflected light is analyzed with a photomultiplier for hemodynamic changes and a perfusion monitor for blood flow recordings. Simultaneous electrophysiological information is transmitted from the micro-electrode into the amplifier where it is isolated and filtered into low (PG, 0.5–500 Hz) and high (MUA, 500 Hz–20 kHz) frequency signals. All information is transmitted to the data acquisition computer using a custom-written Labview program (National Instruments, Inc.). Additionally, isolation boxes allow safe synchronization of the microprobe measurements with clinical recordings.

Data management and a stepwise approach are necessary when recording simultaneously with multiple modalities. The dynamics of population neuronal input and output in different cortical layers are first estimated from current source density and multi-unit activity, respectively. Simultaneous hemodynamic parameters including rCBF, Hbo, Hbr, and Hbt in the same tissue are then calculated from the optical measures. Finally, electrophysiological and hemodynamic parameters are related.

### 2.4. Estimation of population trans-membrane current flows in different cortical layers

Population synaptic activity as well as slow voltage-gated active channels directly produce trans-membrane current flows (Murakami et al., 2002) which were estimated using current source density (CSD) analysis (Freeman and Nicholson, 1975). Assuming that the currents are radially symmetric around the laminar electrode trajectory, CSD is calculated as the second spatial derivative of field potentials (0.5–30 Hz) after applying a 5-point Hamming filter (Ulbert et al., 2001a,b). CSD analysis assumes that conductivity is uniform and isotropic in the tissue immediately surrounding the probe (Mitzdorf, 1985). This assumption has been tested in the hippocampus where deviations from the homogeneous approximation were found to be too small to influence the spatial distribution of sources and sinks (Holsheimer, 1987). Variable electrode spacing or potential amplification could produce spurious CSD signals but these effects were evaluated experimentally in our system and found to be less than 5% (Ulbert et al., 2001a,b). CSD analysis will miss trans-membrane currents if they do result in a net radial extracellular current, as might happen if they are produced by synapses on a spherically symmetrical dendritic domain. CSD will also fail to detect currents that flow over distances that are small relative to the spatial sampling density. Modeling and experimental measures indicate that the center-to-center contact spacing of  $150 \mu\text{m}$  used in the current study is adequate to sample laminar CSD in macaque primary visual cortex (Schroeder et al., 1998; Tenke et al., 2003). The limiting factor was the dendritic domains of stellate cells in thalamorecipient layer IVc. Cortex is thicker in humans, and the sampled areas are not known to have a thin but important sublayer comparable to IVc. Nonetheless, it is likely that the CSD analysis reported here is relatively insensitive to synaptic activity on layer IV stellate cells. Explicit models accounting for the effects of the differences in conductivity above and below the cortical grey matter, as well as the limited radial extent of the sink, have been described (Peterson et al., 2006; Einevoll et al., 2007). Finally, current sources or sinks can be missed if the laminar probe does not sample the entire cortical depth.

### 2.5. Laser Doppler flowmetry

LDF was carried out using the MoorLab Server (MoorLAB Server, Devon, UK). LDF has excellent temporal resolution and allows continuous recording of red blood cell changes in microvasculature. It is based on the principle that low power coherent light (780 nm) is scattered by moving red blood cells and the backscattered light is frequency broadened (Bonner and Nossal, 1981). This light coupled

with scattered light from tissue is high pass filtered (700 nm cutoff) and subsequently collected by a photodetector at 40 Hz, digitized, and processed to produce a measure of the flux of red blood cells, correlated with rCBF.

## 2.6. Cortical point spectroscopy

Light from a halogen light source (HL-2000, Tungsten Halogen Light Source, Ocean Optics, Dunedin, FL) is sent into the cortex and reflected light is gathered and sent to a photomultiplier (S2000, Ocean Optics, Dunedin, Florida) where it is split into 360 frequency bands 0.5 nm wide. Counts are integrated at adjustable frame rates from 10 to 20 Hz. The recording frequency was set based on the signal-to-noise ratio of the recording and was determined to be acceptable at 1000 counts. At this frequency range the cardiac pulse and low frequency hemodynamic responses can be monitored, and the onset of response to stimulation can be sufficiently measured.

The Modified Beer Lambert Law relates the changes in reflection spectra of the tissue with concentration changes in the chromophores in the tissue:

$$\Delta A(\lambda) = \log_{10} \left( \frac{R_0}{R} \right) = \sum_i (\varepsilon_i(\lambda) \Delta c_i) \text{DPF}(\lambda) \quad (3)$$

where  $\Delta A(\lambda)$  is the attenuation at a given wavelength,  $\varepsilon_i$  is extinction coefficient of the  $i$ th chromophore,  $\Delta c_i$  is the change in concentration of the  $i$ th chromophore, DPF is the differential path-length factor, and  $R_0$  and  $R$  are the initial reflectance and reflectance at time  $t$ , respectively, for a given wavelength  $\lambda$ . Extinction coefficients used for Hbr and Hbo were previously established (Wray et al., 1988).

A Monte Carlo simulation was conducted to determine the DPF (Sassaroli et al., 2006), necessary to accurately calculate chromophore concentration changes in (3). The DPF accounts for the different optical path lengths through the tissue due to the different absorption and scattering at varying wavelengths. MIE theory calculates the angular probability distribution (phase function) of the single scattering event due to a spherical particle suspended in a homogeneous medium. Baseline scattering properties were  $\mu_s = 10 \text{ mm}^{-1}$  and  $g = 0.9$ , and the emitter-detector separation of 4 mm determined from the fluence maps (Fig. 2b) were used. The Monte Carlo simulation output of the DPF as a function of wavelength can be found in Fig. 2c.

Estimation of hemodynamic variables from spectroscopic measurements using wavelengths in the range of 500–650 nm is not as established as when using the near-infrared range where 690 and 830 nm are frequently chosen. Reasons for recording in the visible spectra are described earlier. In order to minimize possible errors in our hemodynamic calculations, a least squares approach was implemented as described previously (Dunn et al., 2005). Six wavelengths with 10 nm separations from 560 to 610 nm were used for this linear regression (Fig. 2a). By measuring the reflectance spectra ( $R_0/R$ ) from these wavelengths, we can identify the change in Hbr and Hbo over time. This can be written in a matrix format as

$$y(\lambda, t) = \begin{bmatrix} \Delta A(\lambda_1) \\ \Delta A(\lambda_2) \\ \vdots \\ \vdots \end{bmatrix} = \begin{bmatrix} \varepsilon_{\text{Hb}}^{\lambda_1} & \varepsilon_{\text{HbO}}^{\lambda_1} \\ \varepsilon_{\text{Hb}}^{\lambda_2} & \varepsilon_{\text{HbO}}^{\lambda_2} \\ \vdots & \vdots \\ \vdots & \vdots \end{bmatrix} \begin{bmatrix} \Delta c_{\text{Hb}}^{t_1} & \Delta c_{\text{Hb}}^{t_2} & \cdots \\ \Delta c_{\text{HbO}}^{t_1} & \Delta c_{\text{HbO}}^{t_2} & \cdots \end{bmatrix} = F(\lambda)x(t) \quad (4)$$

The Hbr and Hbo time course can be computed from the equation as a minimum norm solution given by

$$\begin{bmatrix} \Delta c_{\text{Hb}}^{t_1} & \Delta c_{\text{Hb}}^{t_2} & \cdots \\ \Delta c_{\text{HbO}}^{t_1} & \Delta c_{\text{HbO}}^{t_2} & \cdots \end{bmatrix} = x(t) = (F^T F)^{-1} F^T y(\lambda, t) \quad (5)$$

This algorithm permits accurate hemodynamic estimates to be calculated from measurements in less commonly utilized spectral ranges.

## 2.7. Breath-hold experimental paradigm

Prior to the breath-hold challenge, patients were informed of the details of the experiment and asked to avoid head movement during the task. At the beginning of each of three 150 s cycles patients were asked to breathe normally until visual and auditory cues prompted a 30 s breath-hold. Each cycle was separated by 120 s of normal breathing to allow physiological parameters to return to baseline. Hemodynamic measurements were acquired via the data acquisition system. End-tidal  $\text{CO}_2$  ( $\text{PET}_{\text{CO}_2}$ ) was sampled from a leak-free mask and analyzed (CardioPulmonary Technologies, Sussex, WI) to validate the breath-hold.

## 2.8. Electrical stimulation

The subdural grid electrodes are commonly stimulated with low level electrical currents as part of the clinical protocol in order to reproduce elements of the clinical manifestations of the seizure, or to map regions of eloquent cortex (Ojemann, 1991). Individual clinical grid contacts (4 mm diameter disk, Adtech Medical Inc.) were stimulated with varying duration and amplitude well below the safety threshold: stimuli were isolated, charge balanced, biphasic, and constant current, with a charge density per phase below  $50 \mu\text{C}/\text{cm}^2$  (Lesser et al., 1987). Simultaneous electrical activity, blood flow, and oxygenation were measured with the microprobe during stimulation.

## 2.9. Surgical procedure

Patients with intractable epilepsy returning after a Phase 1 scalp EEG monitoring session undergo a craniotomy under general anesthesia followed by subdural grid electrode placement. The cortical area to be sampled was based on prior scalp EEG initial monitoring, ictal behavior, and other non-invasive tests (MRI, SPECT, PET). The laminar optode is first cleaned by dipping into EtOH for 30 s followed by 0.9% NaCl for 60 s and activated by applying +6V against an Ag/AgCl electrode for 30 s in saline, thereby removing debris from electrode sites. It is then cleaned in saline for 10 min to achieve stabilization of the double layer after which it is sterilized prior to implantation in a high temperature gas chamber (minimum 5 h, 130–180 °F) with a post sterilization settling time of 6 h (Ulbert et al., 2001a,b). During implantation, it is inserted normal to the cortical surface directly beneath the subdural grid, allowing surface tension to secure the microprobe in place. The location of the insertion is determined by the clinical team without regard for the research agenda and is targeted to a section of cortex which is expected to be resected at the time the patient returns to the OR for removal of epileptogenic cortex. The two optical fiber bundles and the output lead of the microelectrode are secured by stitching the leads to the edge of the bone. Although the fibers used were reasonably robust and able to handle the rigors of the clinical environment, great care is taken to minimize attenuation by not bending the fibers when securing in place. Post-operatively, glass fibers at the extracranial termination of fiber bundles are exposed, two component medical grade epoxy is applied (Epotek, Billerica, MA), and custom connectors

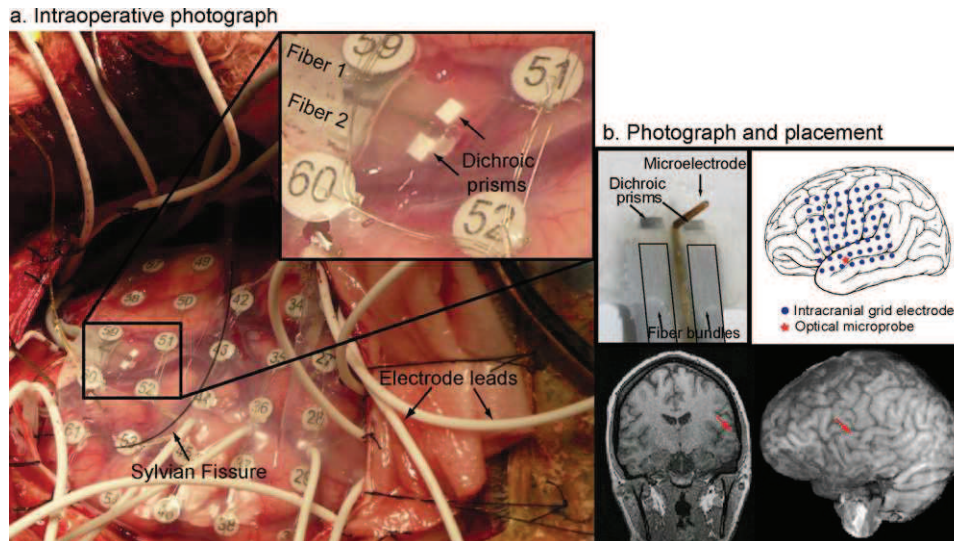


**Fig. 3.** (a) Intraoperative photograph of clinical grid electrodes and laminar optode. Subdural electrode arrays were placed to confirm the hypothesized seizure focus and locate epileptogenic tissue in relation to essential cortex, thus directing surgical treatment. The laminar optode device consists of a multicontact microelectrode coupled with emitter and detector fiber optic bundles that terminate at dichroic prisms. The microelectrode is inserted perpendicularly to the cortical surface to span the cortical grey matter layers. The dichroic mirrors at the termination of the fiber optic bundles lay beneath the grid electrodes on top of the pia. This microprobe was inserted into the left superior temporal gyrus in a patient with frontotemporal epilepsy. (b) From top-left clockwise: Photomicrograph of device, subdural grid electrodes and microprobe placement on standard brain, location on coronal view of MRI, location on 3D rendering of MRI.

attach the microprobe to the light guide assay. Semi-chronic spontaneous recordings span the duration of hospital admittance which ranges from 5 to 10 days. At the time of resection, cortical tissue surrounding the electrode can be removed *en bloc* and sent to pathology for staining with luxol fast blue, Bielschowsky, and hematoxylin and eosin in order to identify cortical laminae using standard criteria.

### 2.10. Patients and potential risks

Four patients (two females, ages 24–36) with long-standing pharmacoresistant complex partial seizures participated after fully informed consent according to NIH guidelines as monitored by the local Institutional Review Board. Simultaneous scalp, macroelectrode, and microelectrode cortical recordings were made over the course of clinical monitoring for spontaneous seizures. Patients were all right handed with intelligence and personality in the normal range. The decision to implant, the electrode targets, and the duration of implantation were made entirely on clinical grounds without reference to this experiment. The patients were informed that participation in the experiment would not alter their clinical treatment in any way, and that they may withdraw at any time without jeopardizing their clinical care.

Minor risks associated with the microprobe implantation include intracranial hemorrhaging of a blood vessel and gliosis. Neurosurgeons trained in microelectrode placement techniques avoid placement in close proximity to blood vessels. In addition, strict adherence to sterilization protocol minimizes risk of infection. In any case, the microarray is placed in tissue that the patient's epileptologist anticipates will be removed in the definitive surgery.

Measures were taken to ensure that human tissue exposure to light is well within safety standards to avoid tissue damage. The fluence due to all wavelengths in the spectral range 500–650 nm was calculated to be  $0.058 \text{ W/cm}^2$ . Coupled with the peak power density due to laser Doppler measurements,  $0.002 \text{ W/cm}^2$ , the total optical fluence at the cortex is  $0.060 \text{ W/cm}^2$ , well below the maximum per-

missible exposure of  $0.2 \text{ W/cm}^2$  for each wavelength in this range from a continuous wave laser for times larger than 10 s (see ANSI Standard Z136.1-1993).

## 3. Results

To date, this device has been successfully implanted in four patients with intractable epilepsy who are undergoing placement of subdural grid electrodes for clinical purposes. When implanted, the microprobe is positioned directly beneath the subdural grid and surface tension secures the optical fiber bundles and microprobe in place (Fig. 3a). EEG recordings from clinical contacts surrounding the microprobe were not compromised by the introduction of the device. The hemodynamic responses synchronized with both the electrocardiogram and a breath-holding task will be described as means to validate the technique. In addition, neural activity and hemodynamic changes recorded during cortical stimulation will be discussed.

### 3.1. Electrocardiogram and cerebral blood flow

The pulsatile cerebrovascular response, synchronized to the EKG, is a strong and reliable signal that has been used to validate various novel non-invasive and invasive hemodynamic measurement techniques (Montgomery et al., 1995; Basano et al., 2001; Zhang and Levine, 2006; Kucwicz et al., 2007). In each of these studies, an increase in rCBF was observed after each cardiac pulse, with a latency of 100–200 ms measured from the R-peak of the QRS wave to the initial increase in rCBF. Across these studies, the percent change in blood flow is often not consistent and in some cases not reported.

In order to determine the validity of the LDF measurements *in vivo*, simultaneous EKG and rCBF were monitored. Representative data from a continuous recording with the laminar optode can be found in Fig. 4a. An increase in rCBF ranging from 8 to 20% can be observed after each ventricular depolarization. An average (Fig. 4b) of 500 EKG pulses elucidates a 12% peak increase in blood flow, as well as a latency of 150 ms between the R-peak and rCBF increase,

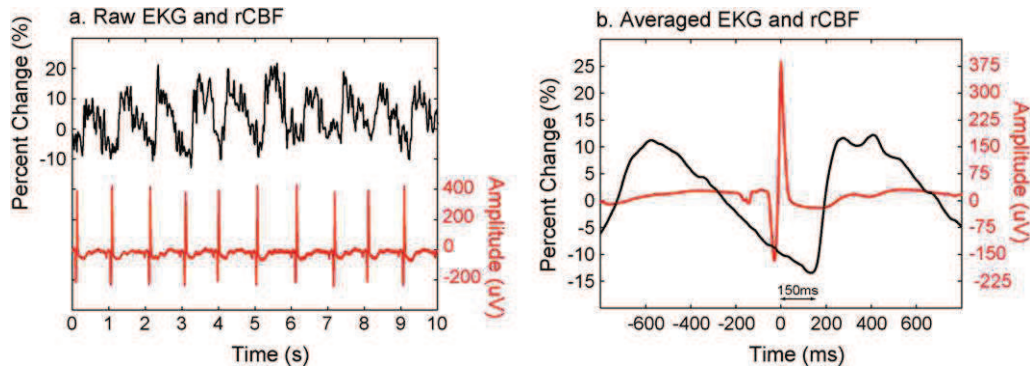


**Fig. 4.** (a) Representative data of continuous recording of electrocardiogram (EKG) and regional cerebral blood flow (rCBF) using laser Doppler flowmetry (LDF) with the laminar optode. Percent signal change of rCBF is on the left axis and EKG amplitude on the right. An 8–20% increase in rCBF is evident following ventricular depolarization. (b) EKG with percent change of rCBF averaged over 500 cardiac pulses demonstrates a 12% increase in rCBF peaking 150 ms after the R-peak in the QRS wave.

consistent with previous studies (Montgomery et al., 1995; Basano et al., 2001).

### 3.2. Breath-holding

Breath-holding is a simple cerebrovascular challenge commonly employed to validate fMRI and spectroscopy studies (Kastrup et al., 1999). Breath-holding induces a hypercapnic state, i.e., an elevated partial pressure of arterial carbon dioxide. Carbon dioxide acts as a vasodilator, producing a global increase in cerebral blood flow (Xie et al., 2005). During a breath-hold task, increases are commonly observed in the BOLD signal (Wise et al., 2007; Thomason et al., 2005), the FAIR signal (Flow-sensitive Alternating Inversion Recovery) relating rCBF values (Kastrup et al., 1999; MacIntosh et al., 2003), and Hbr and Hbt with near-infrared spectroscopy (NIRS, Safonova et al., 2003; MacIntosh et al., 2003).

One patient performed a breath-holding task consisting of three cycles of alternating normocapnic and hypercapnic events. Hemodynamic concentrations from the microprobe were recorded during the breath-hold challenge with simultaneous end-tidal  $\text{CO}_2$  measurements ( $\text{PET}_{\text{CO}_2}$ ) to corroborate results. Each cycle consisted of a 30 s breath-hold followed by 120 s of normal breathing, providing sufficient time for physiological components to return to baseline. Average hemodynamic concentration changes and  $\text{PET}_{\text{CO}_2}$  changes are shown in Fig. 5. Transparent colored curves indicate one standard deviation above and below average values. Dotted lines represent the start and end of the breath-hold while the grey area after the dotted lines indicates the latency before physiological change. As expected, increases in Hbr and Hbt and a decrease in Hbo were observed beginning approximately 5 s after breath-hold onset. These changes progressively increased until peaking 5 s after breath-hold termination and eventually settling back to normal physiological baseline values after a slight hyperoxygenation period.  $\text{PET}_{\text{CO}_2}$  values remained at 0% for the duration of the breath-hold and increased following the event, confirming that it was sufficient to elevate vascular  $\text{CO}_2$  levels. The direction, timing, size, and coupling of these measures are consistent with the well-known neurovascular changes during hypercapnia and are discussed later.

### 3.3. Cortical electrical stimulation

Direct cortical electrical stimulation is commonly employed in patients with intractable epilepsy undergoing surgery in order to localize functional brain areas (Ojemann, 1991). If cortical stimulation results in a behavioral deficit then the stimulated cortex is inferred to contribute to the tested behavior (Halgren et al., 1985). Cortical stimulation may also produce sensory or motor activity by stimulation of sensory or motor cortices, or complex

mental phenomena by stimulation of limbic cortex (Halgren et al., 1978a,b). The clinician will vary stimulation amplitude, duration, and inter-stimulus interval in order to probe the functional contribution of the stimulated cortex. Although this technique assumes that cortical stimulation operates by disrupting cortical function, its underlying mechanism is largely unknown. Hypotheses include electrophysiological mechanisms (disruption of synaptic activity, Nathan et al., 1993), neurochemical mechanisms (neurotransmitter depletion, Haycock et al., 1987), and neurovascular mechanisms (transient focal ischemia with a prolonged increase of Hbr, Suh et al., 2005).

Stimulation was performed for purely clinical purposes without any reference to possible scientific interpretation. Consequently, there was no systematic control for the possible confounding effects of site and stimulation parameters. Shown here are representative effects of stimulation between a cortical site adjacent to the laminar optodes, one proximal to the laminar optode recording with a longer stimulation period and one distal with a shorter stimulation period, to demonstrate the potential of this technique to measure changes in cortical processing and hemodynamics during different stimulation patterns.

The effects of short (500 ms) and long (5000 ms) duration stimulation trains on neural activity and hemodynamics are shown in Fig. 6. Single trial hemodynamics and CSD from both types of

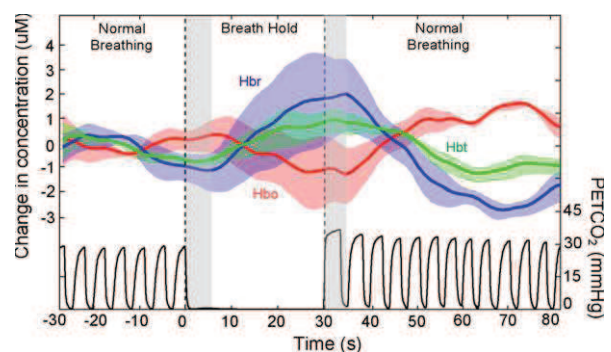


**Fig. 5.** Cerebral hemodynamics and  $\text{PET}_{\text{CO}_2}$  measured during a breath-hold challenge in one patient. Each of three cycles consisted of 30 s of breath-holding followed by 120 s of normal breathing. The plot shows the average hemodynamics and  $\text{PET}_{\text{CO}_2}$  values 30 s prior to until 80 s after stimulus onset. Hemodynamic parameters are measured in  $\mu\text{M}$  and  $\text{PET}_{\text{CO}_2}$  in mmHg. The colored transparent areas indicate one standard deviation above and below the averaged colored plot. Dotted lines represent the onset and termination of the breath-hold and the grey area after the dotted lines show the time latency before physiological change. Hbr and Hbt increased 5 s following onset of event, peaked 5 s after event, and gradually returned to baseline values.  $\text{PET}_{\text{CO}_2}$  values remained at 0 mmHg for the breath-hold duration and increased following breath-hold, confirming that the event was sufficiently long to elevate vascular  $\text{CO}_2$  levels.

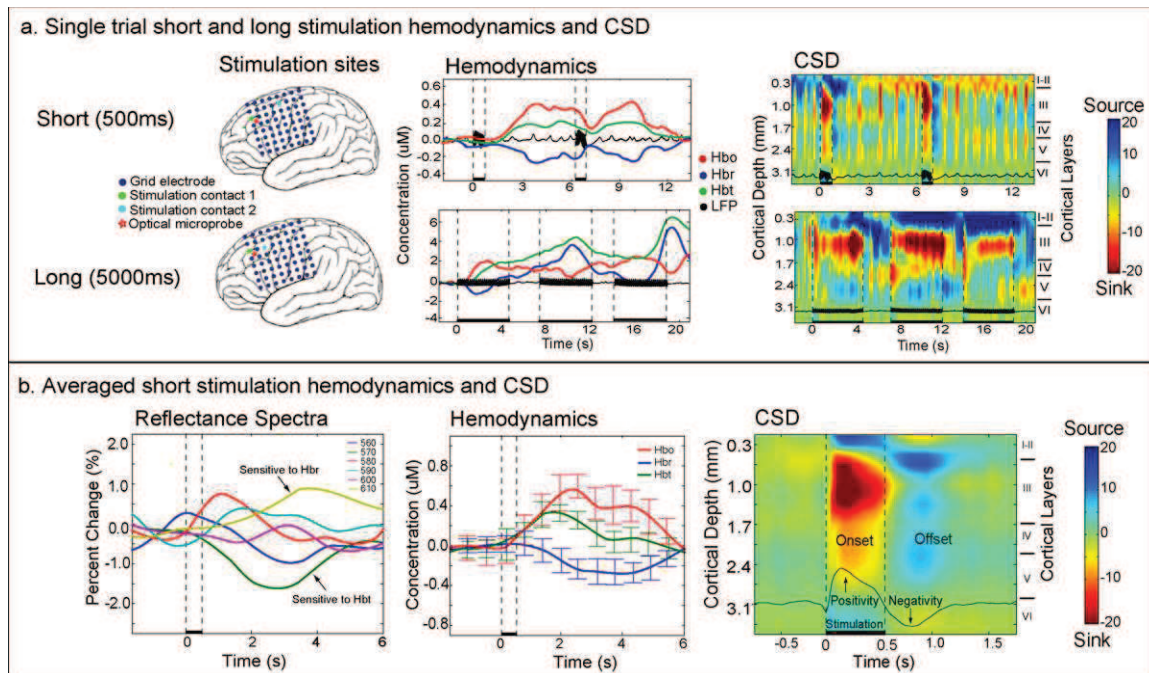


**Fig. 6.** Neural activity and hemodynamic changes recorded during cortical stimulation for functional mapping, in response to short (500 ms) and long (5000 ms) 50 Hz pulse trains. Pulses were symmetric and biphasic with 0.3 ms per phase. Pulses were applied between the contact immediately anterior to the laminar optode, and another grid location either ~4 cm or ~2 cm posterior for the short and long stimulation trains, respectively. Current source density (CSD) measures the trans-membrane current and identifies current sources (blue) and sinks (red) in cortical layers (scale is in z-score). Black dotted lines and bars represent the stimulus duration. (a) Single trial hemodynamics and CSD. Template brain maps indicate reference and stimulated intracranial grid electrodes and optical microprobe locations. Single trial hemodynamic changes demonstrate that while a short stimulus induces the expected increased oxygenation (presumably secondary to increased blood flow as suggested by increased total hemoglobin), longer stimulation causes increased deoxy-hemoglobin, with each stimulation accentuating the response. Single trial CSD plots show clear onset and offset response for short and long stimulus, while the long stimulus train is not as stereotyped. (b) Averaged reflectance spectra, hemodynamics, and CSD plots with the overlaid filtered local field potential of the superficial-most electrode. Following stimulation, reflectance increases at 610 nm and decreases at 570 nm, corresponding to an increase in Hbo and Hbt and a decrease in Hbr. Averaged CSD shows mirrored onset and offset source/sink pairs with a superficial positivity during the onset and negativity during the offset response. Multi-unit activity was recorded in this patient; however, due to the artifact during the stimulation phase, interpretation both during and directly following the stimulation was difficult and is not reported. A low-pass 30 Hz temporal filter minimized stimulus artifact in the CSD plots, and dotted black lines and black bars both denote the stimulation duration. Color CSD plots are observed in z-scores and error bars denote one standard deviation above and below the average. (For interpretation of the references to color in this figure legend, the reader is referred to the web version of the article.)

stimulation (Fig. 6a) as well as averaged reflectance spectra, hemodynamics, and CSD plots with overlaid local field potentials from the most superficial microelectrode contact from short stimulations (Fig. 6b) are shown. Multi-unit activity was recorded in this patient; however, due to the artifact during the stimulation phase, interpretation both during and directly following the stimulation was difficult and is not reported.

For the short stimulation, single trial hemodynamics show a local hyperoxidation peaking 3–4 s following stimulation with Hbo increasing  $\sim 0.4 \mu\text{M}$ , Hbr decreasing  $\sim 0.2 \mu\text{M}$ , and Hbt increasing  $\sim 0.2 \mu\text{M}$  (Fig. 6a). The corresponding CSD plot shows a stereotyped activity to the short stimulation with current sink/source pairs (sources in layers I–II, VI; sinks in III–V) during the stimulation (Fig. 6a). Averaged reflectance spectra, hemodynamics, and CSD plots for short stimulations are shown in Fig. 6b. The reflectance spectra used to calculate the associated hemodynamics show an increase in reflectance at 610 nm (sensitive to Hbr) and a decrease at 570 nm (sensitive to Hbt) following stimulation. Averaged hemodynamics demonstrate this local hyperoxidation following stimulation. Averaged CSD plots show a superficial positivity with current sink/source pairs (sources in I–II, VI; sinks in III–V) during the stimulation onset response and mirrored surface negativity with sink/source pairs (sources in III–V; sinks in I–II, VI) during the offset response (Fig. 6b).

Single trial hemodynamics to long stimulation trains shows strong contrasts to those of the short stimulation (Fig. 6a). Although, as would be expected, the initial hemodynamic responses to short

or long trains are similar when they are preceded by a rest period, as the stimulation continues the initially decreased Hbr returns to zero and increases above baseline, indicating that the increased Hbt is no longer able to decrease Hbr concentration, and indeed is unable to keep pace with metabolic demand by this criterion. When a second long train follows shortly after the first, Hbr increases more, and an even larger increase is present to a third train in short succession. Hbt increases progressively, so Hbo never falls below baseline. The long stimulation condition causes hemodynamic changes that are 10 fold higher in amplitude than short stimulus pulses. These results further corroborate the hypothesis set forth by Suh et al. (2005) where increased stimulation amplitude results in increased Hbr. However, this response is not likely to be accompanied by ischemia as the concentration of oxygenated hemoglobin remains high.

The corresponding CSD plot shows similar sink/source pairs as in the shorter stimulation (sources in I–II, VI; sinks in III–V). However, following the initial onset response, the surface source deepens, the middle layered sink decreases in amplitude, and a new smaller amplitude current sink/source pair appears (source in IV–V, sink in VI) and continues for the duration of each stimulation. The offset response to the first stimulation in the train shows current sink/source pairs (sources in III, V; sinks in I–II, IV) which contrast the short stimulation offset response (Fig. 6b). Hemodynamic responses to long stimulations could not be averaged across stimulation trains, because they may take 40 s to return to baseline (see above), and clinical considerations dictated shorter delays between stimulus trains.

## 4. Discussion

### 4.1. Summary

Electrophysiological activities and cerebrovascular control processes are both extremely complicated. Despite the extensive use in clinical and research arenas, fMRI is not completely understood. fMRI is used mainly to study high level cognition in unanesthetized humans, while animals are preferred when studying low level sensory processes or anesthetized brains because electrophysiology may be measured directly. Thus, although the basic mechanisms of neurovascular coupling will need to be worked out in animal studies, studies in unanesthetized humans performing cognitive tasks will be important to validate these mechanisms and quantify their parameters in order to strongly interpret most fMRI experiments. The technique described here provides a means to measure the critical electrophysiological and hemodynamic variables simultaneously from the same small cortical volume, semi-chronically, with high spatial and temporal resolution in unanesthetized humans performing cognitive tasks.

The electrophysiological methodology (Ulbert et al., 2001a,b) has been validated in previously published experiments in humans during cognitive tasks (Ulbert et al., 2001a,b; Knake et al., 2007; Wang et al., 2005) and epilepsy (Ulbert et al., 2004). The validation efforts presented here thus concentrate on the spectroscopic and Doppler measures using evoking circumstances whose effects on hemodynamics are relatively well understood.

#### 4.1.1. Electrocardiogram and cerebral blood flow

We have validated our laser Doppler flowmetry technique by observing its relationship to the heartbeat as measured by the simultaneously recorded EKG. As predicted, the heartbeat strongly modulated the rCBF inferred from laser Doppler, with the main rCBF peak occurring 150 ms following the R-peak in the QRS wave of the EKG, consistent with prior estimates of the vascular delay from the heart to the brain (Montgomery et al., 1995; Basano et al., 2001; Kucewicz et al., 2007). While latency time periods have been relatively consistent across studies, the direction and absolute size of the peak change from baseline is highly variable due to a number of reasons including measurement modality and location. Our device is placed in cortical grey matter relatively distant from arteries and veins, so measurements reported are most likely rCBF changes in capillaries, venules, and arterioles coursing nearby. As a result, it is unlikely that local recording of rCBF changes in microvasculature in humans have been reported and the 12% observed increase may in fact be a new finding.

#### 4.1.2. Breath-holding

Breath-holding increases arterial CO<sub>2</sub>, which in turn is known to produce vasodilation. The increased Hbt shown using point spectroscopy with the current technique is consistent with this vasodilation. In addition, the current data shows that this vasodilation is not sufficient to prevent a decrease in Hbo. The magnitude and direction of change during the breath-hold is relatively consistent with previous studies where an increase in both Hbr and Hbt on the order of a few  $\mu$ M has been observed (MacIntosh et al., 2003; Safonova et al., 2003). Although the direction of the hemodynamic change is consistent, the latency between event onset and the physiological change is less so. Wise et al. (2007) report a 5 s delay while MacIntosh et al. (2003) report a 20 s delay before hemodynamic changes. Kastrup et al. (1999) demonstrated that this discrepancy in latency can be explained by whether breath-holding is preceded by inspiration versus expiration. The dynamic changes reported here have an initial latency ( $\sim$ 5 s) between both the onset and termination of breath-holding to physiological changes, consistent with previous studies in humans (Safonova et al., 2003; Wise

et al., 2007). Because we did not explicitly tell patients to inspire or expire directly before the hypercapnic event, this could account for the large variation between trials in this time period.

#### 4.1.3. Cortical electrical stimulation

We recorded from the laminar optode during clinical cortical mapping using electrical stimulation of subdural electrodes. To our knowledge, these are the first measurements of neural processing and hemodynamics at the level of the cortical microcolumn during functional mapping at the patient's bedside. Preliminary results show differing neural and hemodynamic responses to short and longer stimulation. Both stimuli exhibit large initial current sink/source pairs, and the short stimuli exhibit an offset response that mirrors the stimulation onset. Unfortunately, multi-unit recordings were not available to inform interpretation of these current source/sink patterns as excitatory or inhibitory. However, comparison with unpublished laminar MUA and CSD recordings collected during controlled single-pulse electrical stimulation indicates that this layer III source in the offset response of the averaged short stimuli corresponds to neuronal inhibition consisting of outward (hyperpolarizing) current, decreased neuronal firing, and decreased high gamma power (Entz et al., 2007). Based on this preliminary data, the superficial positivity and presumably active current sink in middle cortical layers during the stimulation phase may describe cortical excitation and contribute to the increase in hyperoxygenation observed. In addition, the superficial negativity and passive current source observed during the offset response may describe cortical inhibition and have an inhibitory effect on the hemodynamic response.

An increase in Hbo and decrease in Hbr was observed peaking 3–4 s following the short stimulation train, while an increase in Hbr was observed following the long stimulation train. Although these stimulations also differed in the separation of the active stimulation electrode contacts, we hypothesize the differences between short and long stimulation trains result from the increased metabolic demand induced by the sustained stimulation. The hemodynamic changes could underlie some of the apparent cortical deficits induced by intense clinical stimulation (cf. Suh et al., 2005). However, due to the clinical nature of the functional mapping, the stimulation amplitude, duration, SOA, and contact spacing were confounded, and so these conclusions remain to be verified in a more controlled setting.

#### 4.2. Potential applications

Semi-chronically implanting this device into the human neocortex for up to ten days has both basic science and clinical implications. Unlike intraoperative recordings of intrinsic signals or non-invasive imaging such as PET/fMRI, data can be collected in a relatively natural setting by the bedside of the patient. A variety of cortical states can be monitored including spontaneous recordings to study cortical oscillations, sleep studies, epileptiform discharges, functional motor and language mapping, as well as a variety of visual, auditory, and somatosensory tasks. Analyzing the neurovascular response from each of these recordings will enable us to obtain quantitative results of coupling in each of these cortical areas and disease states, essential as this relationship is not necessarily constant across modalities. Once this model is established, identical cognitive tasks and spontaneous recordings will be performed with fMRI and MEG, and a transfer function between this relationship at the local level recorded with the laminar optode and the global level can be determined. This model will allow non-invasive imaging conclusions to be made about cortical processing at the level of the microcolumn and not inferred as it is currently. In addition, we hope to shed light on the controversial topics of BOLD correlation to synaptic or spiking activity, stimulus-evoked negative

BOLD response, and the elusive “initial dip.” We believe that this device can answer many of these fundamental questions that will strengthen fMRI interpretations.

The clinical significance and utility of this type of device is also substantial. Besides creating a model for interpreting non-invasive results such as pre-operative fMRI motor and language mapping, MEG source localization, and PET/SPECT used to localize regions indicative of epileptic cortex, we can develop a better understanding of functional mapping. Cortical stimulation involves many of the contacts on a subdural electrode grid, and by detecting the electrophysiological and neurovascular changes with the microprobe we can record measurements from different locations in the cortex. Therefore, when the patient undergoes motor and language mapping, we can develop a spatiotemporal model of electrophysiological, hemodynamic, and behavioral responses in order to further explore the mechanisms involved in the response to cortical stimulation.

In addition, this device may provide an essential insight into the controversy surrounding the onset and termination of seizures. It is generally accepted that epileptic seizures are associated with an increase in cerebral blood flow due to the abnormal firing rate of neurons (Penfield and Jasper, 1954). Studies have shown that generalized tonic-clonic seizures are associated with an approximate 20% increase in rCBF following seizure onset and a return to baseline levels after the seizure is resolved (Blumenfeld et al., 2003; Nersesyan et al., 2004). Nersesyan et al. (2004) further reports that spike-wave discharges in rats elicit an increase in focal neuronal activity and blood flow, while generalized tonic-clonic seizures are associated with more widespread blood flow increases. Recently, Zhao et al. (2007) were able to capture spontaneous electrographic seizures intraoperatively in the human motor cortex. They report an increase in Hbr and rCBF nearly 20 s preceding seizure onset. In addition, they found that blood flow was not sufficient to meet metabolic demand during the seizure. This device has recorded hemodynamics and electrophysiological signals during several ictal events to gain insight into the mechanisms involved in the onset, evolution, and termination of seizures.

#### 4.3. Limitations

Although this device allows semi-chronic recording of intracortical electrophysiology and hemodynamics in a relatively natural setting with high spatial and temporal resolution, there are also several limitations of these recordings. First, the sampling area is limited to cortical columns proximal to the device. This problem could be partially resolved by placing multiple (up to four) devices into the cortex in order to sample from multiple cortical areas simultaneously. Second, accurate labeling of the cortical layers as well as evaluation of cortical pathology requires histology from the resected tissue. However, histology requires not only en bloc resection of the tissue surrounding the laminar optode, but also cooperation from medical staff which may not always be available. Lacking histology, the cortical layers can only be approximated and CSD interpretation is difficult. While histology was not performed in these patients, in other patients in which a similar device was implanted, histological examination showed relatively well-preserved tissue suggesting that the electrode pushes aside a column of tissue equal to its cross-section, thus minimizing the damage it imposes (Ulbert et al., 2001a,b). The total fluence of the optical components is well within safety standards for humans, and thus they are not likely to cause any additional damage (see Section 2.5). Finally, the microprobe is only placed in locations that are likely to be removed in the definitive surgery, and this would not include locations where removal would produce blindness, plegia, or aphasia. Consequently, it is unlikely that measurements with this device will be obtained in primary motor, sensory, or language cor-

tices. However, the device can probe neurovascular coupling during important cognitive functions performed by association cortices lying outside of these highly eloquent areas.

#### 5. Conclusions

We have developed a device that records detailed electrophysiological parameters in each cortical layer as well as blood flow and oxygenation of cortical microdomains in the unanaesthetized human cortex. EKG with simultaneous blood flow measurements and a breath-holding challenge confirm the validity of the recording techniques. In addition, preliminary results from electrophysiology and hemodynamic responses from cortical stimulation suggest differing responses from short and long stimulation. This device can provide insight into neurovascular coupling during cognitive tasks as well as clinical events such as functional mapping, sleep disorders, and seizures. In the near future we will be able to develop a quantitative model to interpret non-invasive results and apply this model to clinical events to gain a better understanding and lead to more effective treatments and therapies.

#### Acknowledgements

We would like to thank Andrew Dykstra, Alex Chan, Justine Cormier, and Nima Dehghani for excellent critique of this manuscript and László Papp for excellent technical support. This research is funded by NIH grants RO1-NS44623 and NS18741.

#### References

- Attwell D, Iadecola C. The neural basis of functional brain imaging signals. *Trends Neurosci* 2002;25:621–5.
- Basano L, Ottonello P, Nobili F, Vitali P, Pallavicini FB, Ricca B, et al. Pulsatile electrical impedance response from cerebrally dead adult patients is not a reliable tool for detecting cerebral perfusion changes. *Physiol Meas* 2001;22:341–9.
- Blumenfeld H, Westerveld M, Ostroff RB, Vanderhill SD, Freeman J, Necochea A, et al. Selective frontal, parietal, and temporal networks in generalized seizures. *Neuroimage* 2003;19:1556–66.
- Boas DA, Culver JP, Stott JJ, Dunn AK. Three Dimensional Monte Carlo code for Photon migration through complex heterogeneous media including the adult human head. *Opt Express* 2002;10:159–64.
- Buxton R. The elusive initial dip. *Neuroimage* 2001;13:953–8.
- Buxton RB, Wong EC, Frank LR. Dynamics of blood flow and oxygenation changes during brain activation: the balloon model. *Magn Reson Med* 1998;39:855–64.
- Buzsaki G, Kaila K, Raichle M. Inhibition and brain work. *Neuron* 2007;56:771–83.
- Bonner R, Nossal R. Model for laser Doppler measurements of blood flow in tissue. *Appl Opt* 1981;20:2097–107.
- Custo A, Wells WM, Barnett AH, Hillman EMC, Boas DA. Effective scattering coefficient of the cerebral spinal fluid in adult head models for diffuse optical imaging. *Appl Opt* 2006;45:4747–55.
- Devor A, Dunn AK, Andermann ML, Ulbert I, Boas DA, Dale AM. Coupling of total hemoglobin concentration, oxygenation, and neural activity in rat somatosensory cortex. *Neuron* 2003;39:353–9.
- Devor A, Tian P, Nishimura N, Teng IC, Hillman EM, Narayanan SN, et al. Suppressed neuronal activity and concurrent arteriolar vasoconstriction may explain negative blood oxygenation level-dependent signal. *J Neurosci* 2007;27:4452–9.
- Dunn AK, Devor A, Dale AM, Boas DA. Spatial extent of oxygen metabolism and hemodynamic changes during functional activation of the rat somatosensory cortex. *Neuroimage* 2005;27:279–90.
- Einevoll GT, Pettersen KH, Devor A, Ulbert I, Halgren E, Dale AM. Laminar population analysis: estimating firing rates and evoked synaptic activity from multielectrode recordings in rat barrel cortex. *J Neurophysiol* 2007;97:2174–90.
- Entz L, Fabo D, Eross L, Halasz P, Wittner L, Karmos G, Halgren E, Ulbert I. Inhibitory effects of cortical electrical stimulation in epileptic patients. *Society for Neuroscience*, Nov 2007.
- Felleman DJ, VanEssen DC. Distributed hierarchical processing in the primate cerebral cortex. *Cereb Cortex* 1991;1:1–47.
- Freeman JA, Nicholson C. Experimental optimization of current source-density technique for anuran cerebellum. *J Neurophysiol* 1975;38:369–82.
- Grubb Jr RL, Raichle ME, Eichling JO, Ter-Pogossian MM. The effects of changes in PaCO<sub>2</sub> on cerebral blood volume, blood flow, and vascular mean transit time. *Stroke* 1974;5:630–9.
- Haglund MM, Hochman DW. Optical imaging of epileptiform activity in human neocortex. *Epilepsia* 2004;45:43–7.
- Halgren E, Walter RD, Cherlow DG. Mental phenomena evoked by electrical stimulation of the human hippocampal formation and amygdale. *Brain* 1978a;101:83–117.

- Halgren E, Wilson CL, Stapleton JM. Human medial temporal-lobe stimulation disrupts both formation and retrieval of recent memories. *Brain Cogn* 1978b;4:287–95.
- Haycock JW, Levy WB, Cotman CW. Stimulation dependent depression of neurotransmitter release in the brain:[Ca] dependence. *Brain Res* 1987;155:192–5.
- Heeger DJ, Huk AC, Geisler WS, Albrecht DG. Spikes versus BOLD: what does neuroimaging tell us about neuronal activity? *Nat Neurosci* 2000;3:631–3.
- Holsheimer J. Electrical conductivity of the hippocampal CA1 layers and application to current-source-density analysis. *Exp Brain Res* 1987;67:402–10.
- Jones M, Berwick J, Johnston D, Mayhew J. Concurrent optical imaging spectroscopy and laser-Doppler flowmetry: the relationship between blood flow, oxygenation, and volume in rodent barrel cortex. *NeuroImage* 2001;13:1002–15.
- Jones M, Hewson-Stoate N, Martindale J, Redgrave P, Mayhew J. Nonlinear coupling of neural activity and CBF in rodent barrel cortex. *NeuroImage* 2004;22:956–65.
- Kastrup A, Ti T, Glover GH, Moseley ME. Cerebral blood flow-related signal changes during breath-holding. *Am J Neuroradiol* 1999;20:1233–8.
- Knake S, Wang CM, Ulbert I, Schomer DL, Halgren E. Specific increase of human entorhinal population synaptic and neuronal activity during retrieval. *Neuroimage* 2007;37:618–22.
- Kohl M, Lindauer U, Royl G, Kuhl M, Gold L, Villringer A, et al. Physical model for the spectroscopic analysis of cortical intrinsic optical signals. *Phys Med Biol* 2000;45:3749–64.
- Kucewicz JC, Dunmire B, Leotta DF, Panagiotides H, Paun M, Beach KW. Functional tissue pulsatility imaging of the brain during visual stimulation. *Ultrasound Med Biol* 2007;33:681–90.
- Lesser RP, Luders H, Klem G, Dinner DS, Morris HH, Hahn JF, et al. Extraoperative cortical functional localization in patients with epilepsy. *J Clin Neurophysiol* 1987;4:27–53.
- Lindauer U, Royl G, Leithner C, Kuhl M, Gethmann GL, Kohl-Bareis M, et al. No evidence for early decrease in blood oxygenation in rat whisker cortex in response to functional activation. *Neuroimage* 2001;13:986–99.
- Logothetis NK, Pauls J, Augath M, Trinath T, Oeltermann A. Neurophysiological investigation of the basis of the fMRI signal. *Nature* 2001;412:150–7.
- Logothetis NK, Wandell BA. Interpreting the BOLD signal. *Ann Rev Physiol* 2004;66:735–69.
- Logothetis NK. The ins and outs of fMRI signals. *Nat Neurosci* 2007;10:1230–2.
- Logothetis NK. The underpinning of the BOLD functional magnetic resonance imaging signal. *J Neurosci* 2003;23:3963–71.
- MacIntosh BJ, Klassen LM, Menon RS. Transient hemodynamics during a breath hold challenge in a two part functional imaging study with simultaneous near-infrared spectroscopy in adult humans. *NeuroImage* 2003;20:1246–52.
- Mandeville JB, Marota JJ, Ayata C, Moskowitz MA, Weisskoff RM, Rosen BR. MRI measurement of the temporal evolution of relative CMRO(2) during rat forepaw stimulation. *Magn Reson Med* 1999;42:944–51.
- Martindale J, Mayhew J, Berwick J, Jones M, Martin C, Johnston D, et al. The hemodynamic impulse response to a single neural event. *J Cereb Blood Flow Metab* 2003;23:546–55.
- Mayhew J, Johnston D, Berwick J, Jones M, Coffey P, Zheng Y. Spectroscopic analysis of neural activity in brain: increased oxygen consumption following activation of barrel cortex. *Neuroimage* 2000;12:664–75.
- Mitzdorf U. Current source-density method and application in cat cerebral cortex: investigation of evoked potentials and EEG phenomena. *Physiol Rev* 1985;65:37–100.
- Montgomery LD, Montgomery RW, Guisado R. Rheoencephalographic and electroencephalographic measures of cognitive workload: analytical procedures. *Biol Psychol* 1995;40:143–59.
- Mukamel R, Gelbard H, Arieli A, Hasson U, Fried I, Malach R. Coupling between neuronal firing, field potentials, and fMRI in human auditory cortex. *Science* 2005;309:951–4.
- Murakami S, Zhang T, Hirose A, Okada YC. Physiological origins of evoked magnetic fields and extracellular field potentials produced by guinea-pig CA3 hippocampal slices. *J Physiol* 2002;544:237–51.
- Nair DG. About being BOLD. *Brain Res Rev* 2005;50:229–43.
- Nathan SS, Sinha SR, Gordon B, Lesser RP, Thakor NV. Determination of current density generated by electrical stimulation of the human cerebral cortex. *Electroencephalogr Clin Neurophysiol* 1993;86(3):193–292.
- Nicholson C, Freeman JA. Theory of current source-density analysis and determination of conductivity tensor for anuran cerebellum. *J Neurophysiol* 1975;38:356–68.
- Nersesyian H, Herman P, Erdogan E, Hyder F, Blumenfeld H. Relative changes in cerebral blood flow and neuronal activity in local microdomains during generalized seizures. *J Cereb Blood Flow Metab* 2004;24:1057–68.
- Ogawa S, Lee TM, Kay AR, Tank DW. Brain magnetic resonance imaging with contrast dependent on blood oxygenation. *Proc Natl Acad Sci USA* 1990;87:9868–72.
- Ojemann GA. Cortical organization of language. *J Neurosci* 1991;11:2281–7.
- Patterson MS, Andersson-Engels S, Wilson BC, Osei EK. Absorption spectroscopy in tissue-simulating materials: a theoretical and experimental study of photon paths. *Appl Opt* 1995;34:22–30.
- Peterson KH, Devor A, Ulbert I, Dale AM, Einevoll GT. Current-source density estimation based on inversion of electrostatic forward solution: Effects of finite extent of neuronal activity and conductivity discontinuities. *J Neurosci Methods* 2006;154:116–23.
- Rees G, Friston K, Koch C. A direct quantitative relationship between the functional properties of human and macaque V5. *Nat Neurosci* 2000;3:716–23.
- Sassaroli A, Martelli F, Fantini S. Perturbation theory for the diffusion equation by use of the moments of the generalized temporal point spread function. II. Continuous wave results. *JOSA A* 2006;23:2119–31.
- Safonova LP, Michalos A, Wolf U, Choi JH, Wolf M, Mantulin WW, et al. Diminished cerebral circulatory autoregulation in obstructive sleep apnea investigated by near-infrared spectroscopy. *Sleep Res Online* 2003;5:123–32.
- Schmuel A, Augath M, Oeltermann A, Logothetis NK. Negative functional MRI response correlates with decreases in neuronal activity in monkey visual area V1. *Nat Neurosci* 2006;9:569–77.
- Schroeder CE, Mehta AD, Givre SJ. A spatiotemporal profile of visual system activation revealed by current source density analysis in the awake macaque. *Cereb Cortex* 1998;8:575–92.
- Suh M, Bahar S, Mehta AD, Schwartz TH. Temporal dependence in uncoupling of blood volume and oxygenation during interictal epileptiform events in rat neocortex. *J Neurosci* 2005;25:68–77.
- Thomason ME, Burrows BE, Gabrieli JDE, Glover GH. Breath holding reveals differences in fMRI BOLD signal in children and adults. *NeuroImage* 2005;25:824–37.
- Ulbert I, Karmos G, Heit G, Halgren E. Early discrimination of coherent versus incoherent motion by multiunit and synaptic activity in human putative MT+. *Hum Brain Mapp* 2001a;13:226–38.
- Ulbert I, Halgren E, Heit G, Karmos G. Multiple microelectrode-recording system for human intracortical applications. *J Neurosci Methods* 2001b;106:69–79.
- Ulbert I, Heit G, Madsen J, Karmos G, Halgren E. Laminar analysis of human neocortical interictal spike generation and propagation: current source density and multiunit analysis in vivo. *Epilepsia* 2004;45:48–56.
- Vanzetta I, Grinvald A. Increased cortical oxidative metabolism due to sensory stimulation: implications for functional brain imaging. *Science* 1999;286:1555–8.
- Waldvogel D, van Gelderen P, Muellbacher W, Ziemann U, Immisch I, Hallett M. The relative metabolic demand of inhibition and excitation. *Nature* 2000;406:995–8.
- Wang C, Ulbert I, Ives JR, Schomer DL, Blume H, Marinkovic K, et al. Responses of human anterior cingulate cortex microdomains to error detection, conflict monitoring, stimulus-response mapping, familiarity, and orienting. *J Neurosci* 2005;25:604–13.
- Wise RG, Pattinson KTS, Bulte DP, Chiarelli PA, Mayhew SD, Balanos GM, et al. Dynamic forcing of end-tidal carbon dioxide and oxygen applied to functional magnetic resonance imaging. *J Cereb Blood Flow Metab* 2007;27:1521–32.
- Wray S, Cope M, Delpy DT, Wyatt JS, Reynolds EO. Characterization of the near infrared absorption spectra of cytochrome aa3 and haemoglobin for the non-invasive monitoring of cerebral oxygenation. *Biochim Biophys Acta* 1988;933:184092.
- Xie A, Skatrud JB, Khayat R, Dempsey JA, Morgan B, Russell D. Cerebrovascular response to carbon dioxide in patients with congestive heart failure. *Am J Resp Crit Care Med* 2005;172:371–8.
- Zhang R, Levine BD. Autonomic ganglionic blockade does not prevent reduction in cerebral blood flow velocity during orthostasis in humans. *Stroke* 2006;38:1238–44.
- Zhao M, Suh M, Ma M, Perry C, Geneslaw A, Schwartz TH. Decreases in focal perfusion and hemoglobin oxygenation precede seizure onset in spontaneous human lesional epilepsy. *Epilepsia* 2007;48:2059–67.

dc\_303\_11

## **2. Melléklet**

# Responses of Human Anterior Cingulate Cortex Microdomains to Error Detection, Conflict Monitoring, Stimulus–Response Mapping, Familiarity, and Orienting

Chunmao Wang,<sup>1,2</sup> Istvan Ulbert,<sup>2,5</sup> Donald L. Schomer,<sup>3</sup> Ksenija Marinkovic,<sup>2</sup> and Eric Halgren<sup>2,4</sup>

<sup>1</sup>Comprehensive Epilepsy Center, New York University School of Medicine, New York, New York 10016, <sup>2</sup>Massachusetts General Hospital/Massachusetts Institute of Technology/Harvard Medical School Martinos Center for Biomedical Imaging, Charlestown, Massachusetts 02129, <sup>3</sup>Department of Neurology, Beth Israel Deaconess Medical Center, Harvard Medical School, Boston, Massachusetts 02215, <sup>4</sup>Institut National de la Santé et de la Recherche Médicale, Marseille 13009, France, and <sup>5</sup>Institute for Psychology, Hungarian Academy of Sciences, Budapest 1068, Hungary

Human anterior cingulate cortex (ACC) activity modulation has been observed in numerous tasks, consistent with a wide variety of functions. However, previous recordings have not had sufficient spatial resolution to determine whether microdomains (approximately one to two columns) are involved in multiple tasks, how activity is distributed across cortical layers, or indeed whether modulation reflected neuronal excitation, inhibition, or both. In this study, linear arrays of 24 microelectrodes were used to estimate population synaptic currents and neuronal firing in different layers of ACC during simple/choice reaction time, delayed word recognition, rhyming, auditory oddball, and cued conditional letter-discrimination tasks. Responses to all tasks, with differential responses to errors, familiarity, difficulty, and orienting, were recorded in single microdomains. The strongest responses occurred ~300–800 ms after stimulus onset and were usually a current source with inhibited firing, strongly suggesting active inhibition in superficial layers during the behavioral response period. This was usually followed by a sink from ~800 to 1400 ms, consistent with postresponse rebound activation. Transient phase locking of task-related theta activity in superficial cingulate layers suggested extended interactions with medial and lateral frontal and temporal sites. These data suggest that each anterior cingulate microdomain participates in a multilobar cortical network after behavioral responses in a variety of tasks.

**Key words:** intracranial EEG; current source density; unit firing; attention; memory, theta

## Introduction

The anterior cingulate cortex (ACC) lies at the crossroads of three vast anatomic-functional systems: motor, limbic, and prefrontal (Vogt et al., 2004). In the motor system, the ACC lies immediately inferior to the supplementary motor cortex and projects to motor cortex as well as the spinal cord (Dum and Strick, 1993). In the limbic system, the ACC is directly related to the subicular complex (and thus hippocampus), posterior orbital cortex (area 32), and the anterior thalamic nucleus, as well as brainstem nuclei concerned with autonomic control. Finally, the ACC has strong bidirectional connections with the dorsolateral prefrontal and temporal cortices (Barbas, 2000; Vogt et al., 2004).

Consistent with these connections, functional magnetic resonance imaging (fMRI) and positron emission tomography (PET) have found ACC hemodynamic activation in a wide variety of tasks involving reading (Fiez and Petersen, 1998), word generation

(Crosson et al., 1999), episodic recall (Nyberg, 1998; Cabeza et al., 2003), working memory (Bunge et al., 2001), emotion (Phan et al., 2002), and attention (Mesulam, 1981; Corbetta et al., 1998; Cabeza et al., 2003). ACC activation is related to the number of possible responses in a task, suggesting that it may contribute to response choice or “selection-for-action” (Posner et al., 1988; Petersen et al., 1989; Frith et al., 1991). This may reflect a basic contribution to motor control (Kollias et al., 2001; Picard and Strick, 2001) or a role in detecting situations that requires strategic intervention because of conflicting potential responses that may lead to errors (Carter et al., 2000; Kiehl et al., 2000).

Some authors emphasize the juxtaposition of different functions, especially emotional and cognitive as the key to ACC function (Duncan and Owen, 2000; Allman et al., 2001; Paus, 2001), whereas others emphasize the anatomical segregation of different functions (Peterson et al., 1999). For example, cognitive activation in ACC has been located anterior to the anterior commissure line of Talairach and posterior to the anterior limit of the corpus callosum, with emotional activation in more anteroinferior ACC (Bush et al., 2000). Motor areas may be above and behind the cognitive division (Dum and Strick, 2002), visuospatial areas in posterior cingulate, and memory-related areas inferior to posterior cingulate in retrosplenial cortex (Vogt et al., 2004).

As an alternative to anatomical segregation, some functions

Received Oct. 6, 2004; revised Nov. 19, 2004; accepted Nov. 26, 2004.

This work was supported by National Institutes of Health Grants NS18741 and NS44623. We thank G. Karmos, G. Heit, B. Rosen, J. R. Ives, and M. Glessner for their contributions to this research. This paper is dedicated to the memory of Howard Blume.

Correspondence should be addressed to Eric Halgren, Martinos Center for Biomedical Imaging, Six 13th Street, Charlestown, MA 02129. E-mail: halgren@nmr.mgh.harvard.edu.

DOI:10.1523/JNEUROSCI.4151-04.2005

Copyright © 2005 Society for Neuroscience 0270-6474/05/250604-10\$15.00/0

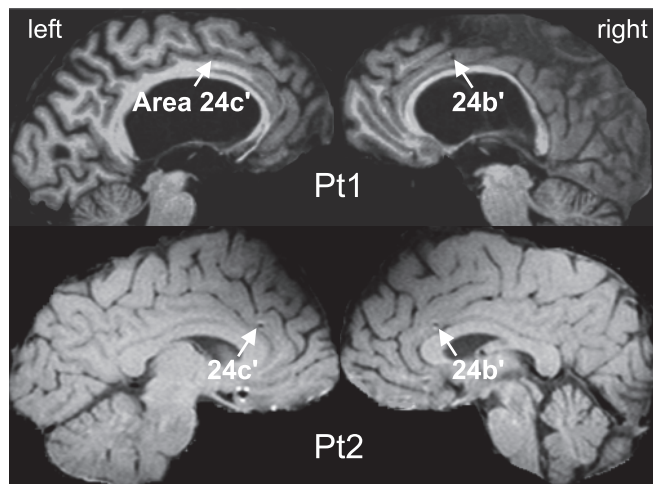


**Figure 1.** Locations of laminar probes in MRIs taken with the electrodes *in situ*. Laminar probes are indicated by dark MRI artifacts (arrowheads; artifacts are larger than the actual electrodes). All contacts appear to lie in Brodmann's area 24' (Vogt et al., 2004). Note the dilation of the third ventricle in Pt1 attributable to compensated aqueductal stenosis.

may reflect different levels of neuronal processing related to the same integrative function. For example, the ACC may contribute to both orienting–monitoring and response–choice but at different phases of the response or trial. This would imply that there is also a temporal segregation of ACC function.

It is difficult to distinguish between these hypotheses using noninvasive imaging methods because of their limited spatial resolution (Dale and Halgren, 2001). Furthermore, noninvasive methods lack the physiological resolution to distinguish excitation from inhibition (EEG and magnetoencephalography) or are hemodynamic, which has an unknown relationship to neuronal activity. Intracranial measures have greater spatial accuracy but typically record from all cortical layers in a region that contains many cortical columns. The current study used simultaneous recordings from an array of microelectrodes to characterize synaptic activity and neuronal firing in relatively small populations of ACC neurons. These data demonstrate that multiple responses related to novelty, memory, set, errors, and the difficulty of stimulus–response mapping are colocalized at a submillimeter level. Surprisingly, inhibition in superficial cortical layers appeared to be a common response by the ACC to cognitive stimuli. Relative excitation after the inhibition may provide a window when the ACC contributes to wider cortical processing.

## Materials and Methods

**Patients and electrodes.** Patients with complex partial seizures resistant to all appropriate medications were considered for surgical removal of their epileptogenic focus. When extensive noninvasive diagnostic tests were unable to unambiguously locate the focus, intracranial recordings from potential seizure onset sites were recommended. Patient 1 (Pt1) was a 35-year-old right-handed male; patient 2 (Pt2) was a 55-year-old right-handed female. Their intelligence and personality were in the normal range. Both gave fully informed consent according to National Institutes of Health guidelines to add a linear array of microcontacts to the tips of their clinical macroelectrodes. Each laminar probe was ~3.5 mm long with a row of 24 40- $\mu$ m-diameter contacts separated by 110  $\mu$ m (Ulbert et al., 2001a). The choice of patients and sites to implant, as well as the duration of implantation, were made on completely clinical grounds. Successful recordings were obtained bilaterally from area 24' of the ACC in both patients (Fig. 1). Electrode positions were slightly more posterior in patient 1, rendering it possible that one or both could lie in the anterior

cingulate motor area. However, there were no systematic response differences noted between patients. Seizure origin in Pt1 was multifocal in the right hemisphere including the hippocampus and orbitofrontal cortex and in Pt2 was in the left temporal lobe remote from the ACC; the ACC recordings reported here did not display interictal spikes during waking and were made at least 24 h after the most recent seizure.

**Recordings.** Differential recordings were made from 23 pairs of successive contacts. After wideband (DC, 10,000 Hz) preamplification (gain, 10 $\times$ ; common mode rejection ratio, 90 db; input impedance, 10<sup>12</sup>  $\Omega$ ), the signal was split into field potentials (filtered at 0.2–500 Hz; gain, 1000 $\times$ ; digitized at 2000 Hz; 16 bit) and action potentials (filtered at 200–5000 Hz; gain, 1000 $\times$ ; digitized at 20,000 Hz; 12 bit) and stored continuously with stimulus markers. Population transmembrane current flows were estimated using linear current source density (CSD) analysis (Nicholson and Freeman, 1975; Ulbert et al., 2001b), calculated using the second spatial derivative of local field potentials (LFP). Population action potentials [multiunit activity (MUA)] were estimated by rectifying the bandpass filtered data [zero phase shift, 300–3000 Hz; 48 db/octave (oct)] and then low-pass filtering the result (zero phase shift, 30 Hz; 12 db/oct).

**Spatial resolution.** A simulation was performed to evaluate how steeply LFP and CSD decline with distance from the neural generator (see supplemental material I, available at [www.jneurosci.org](http://www.jneurosci.org)). CSD amplitude in this simulation declines 10-fold at ~300  $\mu$ m from the cortical column, whereas potential decreases at a slower slope. This falloff is in the direction parallel to the cortical surface; the falloff is more rapid in the orthogonal direction, actually reaching zero while still within the cortex. Theoretical and empirical studies in animals indicate that MUA should decline with distance at least as rapidly as a result of the short duration, asynchrony, and spatial distribution of action potential fields (Humphrey, 1968; Grover and Buchwald, 1970). In summary, CSD and MUA estimate the activity of neurons in a volume approximately corresponding to that of a cortical column.

**Spectral analysis.** For time-frequency spectral measures, the single trial signal for each channel was convolved with complex Morlet's wavelets (Kronland-Martinet et al., 1987; Halgren et al., 2002). Relatively constant temporal and frequency resolution across target frequencies was obtained by adjusting the wavelet widths according to the target frequency. The wavelet widths increase linearly from 1 to 6.5 as frequency increases from 1 to 13 Hz, resulting in a constant temporal resolution of 80 ms and frequency resolution of 2 Hz. Tests with simulated data confirmed that the methods used here accurately measure spectral power patterns, even at frequencies as low as 1 Hz (see supplemental material II, available at [www.jneurosci.org](http://www.jneurosci.org)).

In addition to the microarray recordings in ACC, recordings from clinical macrocontacts were available in multiple temporal and frontal sites in Pt2. The macrocontacts consisted of 1.3-mm-diameter cylinders, each 1.5 mm long and separated from the next contact by 3.5 mm. Our initial results showed that event-related spectral activity is mainly in the theta range and is generated in the superficial ACC layers. Thus, we focused our calculations on the theta and adjacent bands and calculated the phase locking between the superficial ACC contacts and simultaneous macrorecordings. This measure is sensitive to the similarity of the timing of activity in a particular frequency range between two structures, regardless of their amplitudes (Lachaux et al., 1999). Our simulation confirmed that the method accurately detects the phase-locking period, even at frequencies as low as 1 Hz (see supplemental material II, available at [www.jneurosci.org](http://www.jneurosci.org)). Potential gradients from both microrecordings and macrorecordings were used for these calculations. Statistical significance of the difference between conditions for a particular recording channel, latency, and measure (CSD, MUA, or spectral power) was assessed using a *t* test of values from individual trials. Significant deviations of responses from baseline were assessed using one-sample *t* tests of values from each trial. Threshold was set at  $p < 0.01$  (two-tailed). Time-frequency maps of spectral power or phase-locking factor are displayed as z-scores relative to the mean and variance of the same measure in the prestimulus period. Baseline measures were calculated separately for each frequency and channel.

**Cognitive tasks.** To probe ACC activity during different functions, we used the following five tasks (Fig. 2): (1) simple/choice reaction time

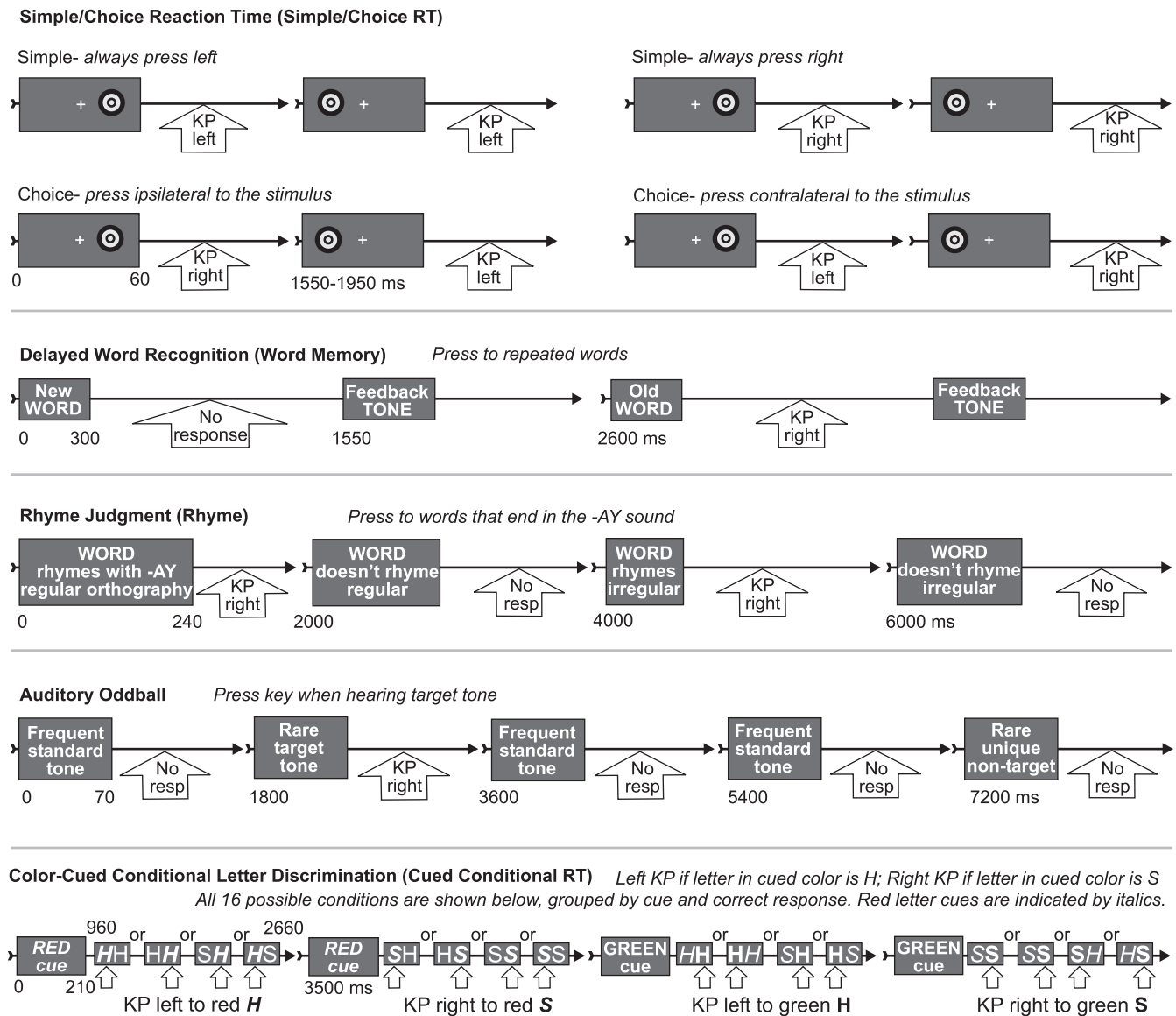


**Figure 2.** Five cognitive tasks and conditions compared in the present study. Time lines show the sequence of events in typical trials. KP, Key press. Please see Materials and Methods for additional explanation.

(simple/choice RT): targets flashed for 60 ms in the left or right visual field, and subjects responded with the left or right hand under two simple instructions (press always left or always right, regardless of stimulus laterality) and two choice instructions (press always ipsilateral or always contralateral to the stimulus). There were 196 trials for each of these four instructions. Stimulus onset asynchrony (SOA) was randomized from 1550 to 1950 ms. (2) Delayed word recognition (word memory): the subject memorizes 10 words that subsequently served as recognition targets on one-half of the trials randomized with unrepeated words. Words were visually presented for 300 ms in white font on a black background. There were 240 items in the test section; one-half of them were unrepeated, and one-half were 10 target words repeated 12 times randomly. Subjects were required to press a key with their dominant hand within 1200 ms after presentation of a repeating word. At 1550 ms post-stimulus, a 55 ms sawtooth feedback tone was presented indicating whether the response (or lack thereof) had been correct (1000 Hz) or wrong (200 Hz) (Halgren et al., 1994). (3) Rhyme judgment (rhyme): the subject was requested to press a key to each word rhyming “AY” in a set of 240 words. Words differed in whether they rhymed with the target and whether they had regular orthography (e.g., “say”) or irregular (e.g., “weigh”). Words were presented for 240 ms, and SOA was 2000 ms. (4)

Auditory oddball: subjects pressed a key to rarely occurring target tones (76; 10.5%) embedded in a series of frequently occurring standard tones (571; 79%) and nontarget novel tones (76; 10.5%) requiring no response. All stimuli were 70 ms in duration, presented every 1.8 s. Each nontarget novel sound was a unique sound differing in pitch and harmonics but with the same amplitude envelope as the pure tones serving as frequent and targets (Marinkovic et al., 2001). (5) Color-cued conditional letter discrimination (cued conditional RT): subjects were presented with a color cue for 210 ms (“red” or “green”). After a delay of 750 ms, two letters (HH, SS, SH, or HS) in two colors were presented for 1700 ms. If the letter in the cued color was an H, then the subject made a left-handed keypress; if the letter in the cued color was an S, then the subject made a right-handed keypress (Gehring and Knight, 2000). The 16 permitted combinations of cues and imperative stimuli with the correct responses are shown in Figure 3, bottom panel. There were a total of 533 trials. Total SOA was 3500 ms. Only Pt2 was tested on task 5.

Adequate performance was found in most tasks for both subjects (Table 1). When available, error rates were lower than 7% except for Pt1 on the rhyme judgment task (37.5% errors). Mean reaction times ranged from 449 to 912 ms.

**Table 1. Behavioral results**

	Simple/choice RT	Word memory	Auditory oddball	Rhyme	Cued conditional RT
Pt1					
RT	N/A	N/A	659 (151)	912 (288)	N/G
ER	N/A	3.75%	6.58%	37.50%	N/G
Pt2					
RT	449 (76)	784 (96)	N/A	819 (129)	N/A
ER	1.65%	4.17%	N/A	0.42%	N/A

For RT, SDs are in parentheses. ER, Error rate; N/A, not available as a result of technical problems; N/G, task not given to that patient.

## Results

Extensive task-related activity was found in all sites and tasks. Activity was measured as CSD, which is the transmembrane current density. EPSCs produce current sinks at the active synapses, with passive sources as current returns (Nicholson and Freeman, 1975). At the membrane potentials typical of waking neocortex (Destexhe et al., 2003), IPSCs should produce current sources at the active synapses, with passive sinks as current returns. If simultaneous MUA increases during a current sink, then it probably represents an EPSC. Conversely, if MUA decreases during a current source, then it probably represents active inhibition, an IPSC.

In all four recording sites, the strongest CSD responses occurred from ~300 to 800 ms after stimulus onset and were located in superficial layers. In Pt1 left ACC and Pt2 both left and right ACC, this response was a current source, followed from ~800 to 1400 ms by a current sink. In both locations with MUA recordings, superficial cell firing decreased during the local source, suggesting active inhibition. Pt1 right ACC and Pt2 left ACC also generated task-related theta activity in superficial layers. Theta in Pt2 showed a task-related transient increase in phase locking to distant cortical sites.

CSD recordings from two patients during multiple tasks are shown in Figure 3. Recordings in Figure 3*a* show a large source (upward deflection) that is evoked from ~300 to 800 ms after stimulus onset by visual targets (in a simple/choice reaction time task), words (in declarative memory and rhyming tasks), and brief sounds (in an auditory oddball task). The currents are significantly larger to stimuli that provoked wrong responses in the simple/choice RT task, as well as to feedback tones indicating a wrong response in the word memory task. The currents are larger to rare stimuli in the auditory oddball task and to old (i.e., repeated) words in the word memory task. The currents are larger when the response requires a choice in the simple/choice RT task, or the word orthography is irregular in the rhyming task. All responses exhibit similar morphologies and time courses and were recorded at the same microcontact. They show that the same ACC microdomain can respond in very similar ways to quite different tasks and stimuli, with differential responses to errors (either indicated by feedback or not), to rare events (presumably evoking orienting responses), to repeated words, and to difficulty (in stimulus–response mapping or orthographic–phonological decoding).

Biophysically, the source in the top panel could be attributable to active inhibitory synapses or could represent a passive current return to excitatory synapses located elsewhere. In Figure 3*b*, simultaneous MUA and CSD recordings from patient 2 allows the net local level of excitation to be estimated. A source is again observed across multiple tasks. The technical quality of the recordings is not as good, and relatively little task related modula-

tion occurs between conditions. However, MUA significantly decreases during the CSD source in the auditory oddball, word memory, and rhyming tasks, suggesting that the source may represent active inhibition.

In Figure 3*a*, the cortical layer in which the source is located is hard to determine, because the laminar probe was in the sulcus (i.e., was not perpendicular to cortical surface). In Figure 3*b*, the source was recorded in the most medial contacts of the laminar probe, suggesting upper layers, but the technical quality of the recording was not adequate to confirm this suggestion.

Both the superficial location of the source and the association of the source with decreased MUA are confirmed in recordings from the left ACC of Pt2, as shown in Figure 4. The MRI indicated that the probe penetrated the crown of the gyrus perpendicular to its surface. At the top, CSD sources (blue) and sinks (red) over the cortical depth are plotted as contours versus time. At the bottom are plotted CSD and local MUA waveforms from a medial laminar contact near the cortical surface. A repeated observation across most tasks and conditions is a superficial sink from ~200 to 800 ms poststimulus, displayed as a blue area in the contour plots and an upward deflection in the CSD waveforms. The source is accompanied by a sink in deeper layers (red area in contour plots) with approximately the same time course. Simultaneous MUA is inhibited in all tasks and conditions, again with a similar time course. In most cases, the superficial source inverts to a strong sink after ~800 ms. Note that the sources in both Pt1 left ACC (Fig. 3*a*) and Pt2 right ACC (Fig. 3*b*) also invert to sinks after ~800 ms. These recordings also confirm the responsiveness of ACC microdomains to multiple tasks and the modulation of this response by different condition contrasts, including difficulty in stimulus–response mapping, word repetition, and cue consistency. Thus, across these three ACC microdomains, and across multiple tasks and conditions, a superficial CSD source with decreased MUA indicate active inhibitory postsynaptic currents.

The fourth recording location (Pt1 right ACC) (Fig. 5) also shows a strong CSD response across multiple tasks with large differentiations across task conditions. Again, the response is larger to choice than simple RT, to wrong than correct trials in that task, to repeated than nonrepeated words, and to rare auditory stimuli. The CSD contour has a different pattern than that seen in the other sites described above: rather than a source in the superficial layers, there is a sink. This sink is also different in beginning ~100–200 ms later than the source seen in the other three sites. In most cases, the initial activity was a smaller sink in middle layers, beginning shortly after 100 ms. This pattern and timing is more typical of what has been observed in laminar recordings from temporal and prefrontal neocortical sites (E. Halgren, C. Wang, I. Ulbert, S. Knake, K. Marinkovic, J. Wu, J. Madsen, and D. Schomer, unpublished observations). This observation may indicate that only some ACC microdomains show the superficial inhibitory pattern that appears to characterize the recordings described above. Alternatively, this microcontact array may not have penetrated to the cortical surface. In that case, a slightly deeper penetration may have recorded a superficial source indicating inhibition as in the other sites.

The CSD responses described above were based on averaging the CSD with respect to stimulus onset. This method eliminates activity that is not phase locked to stimulus onset. Because the ACC generates theta activity in animals, and it has been proposed that the ERN is actually averaged theta activity in humans (Luu et al., 2003), we examined the ongoing CSD and noted strong oscillations in the theta range in Pt1 right ACC and Pt2 left ACC (Fig. 6). Aver-

aging the CSD on the peaks of these oscillations revealed an average frequency of  $\sim 4$ – $5$  Hz (Fig. 6*a1,b1*). In both cases, theta was generated mainly in superficial layers (Fig. 6*a2,b2*). Theta power was related to the stimulus, increasing after the stimulus and showing significantly different responses to old versus new words and to rare versus frequent auditory stimuli (Fig. 6*a3*). Theta did not have any strong or obvious effect on the MUA in the period between tasks (Fig. 6*b3*). When averaged during the peri-stimulus epoch, theta was associated with MUA decrease (Fig. 6*b3*) but without a theta-range periodicity, suggesting that this decrease was unrelated to the theta but rather was attributable to other aspects of the response (compare Fig. 4).

The consistency of the phase of theta band activity was estimated between the ACC and a sample of temporal and frontal lobe sites using potential gradient measurements (Fig. 7). Phase locking significantly increased in a task-related manner, including a consistent increase from  $\sim 200$  to 700 ms after the stimulus. Additional peaks between  $\sim 500$  and  $\sim 1000$  ms were also observed. These transient increases in the similarity of the local field potential were found between both right and left ACC and sites in temporal neocortex (near the superior temporal sulcus), the frontal neocortex (including inferior, middle, and superior frontal gyri and the orbital gyrus), as well as mesial temporal hippocampal and parahippocampal leads. The increases were apparent both when comparing ACC to ipsilateral cortical as well as contralateral cortical sites. No consistent increases in ACC spectral power or ACC-neocortical phase locking were observed outside of the theta band.

In summary, the most common response was a current source and MUA decrease in ACC superficial layers from  $\sim 300$  to 800 ms after onset, followed by a current sink. Theta rhythm was also found in superficial layers. These responses were observed across a variety of tasks, occurred during different phases of tasks, such as cue, stimulus, and feedback, and modulated across multiple task conditions. These responses were recorded in very small regions, corresponding to parts of one or two cortical columns.

## Discussion

### Multiple cognitive correlates in single ACC microdomains

A clear finding of this study was that synaptic currents and neuronal firing recorded at individual ACC locations responded to multiple tasks and contrasts within tasks. These responses reflected activity within  $\sim 300$   $\mu\text{m}$  from the recording site, as a result of the small

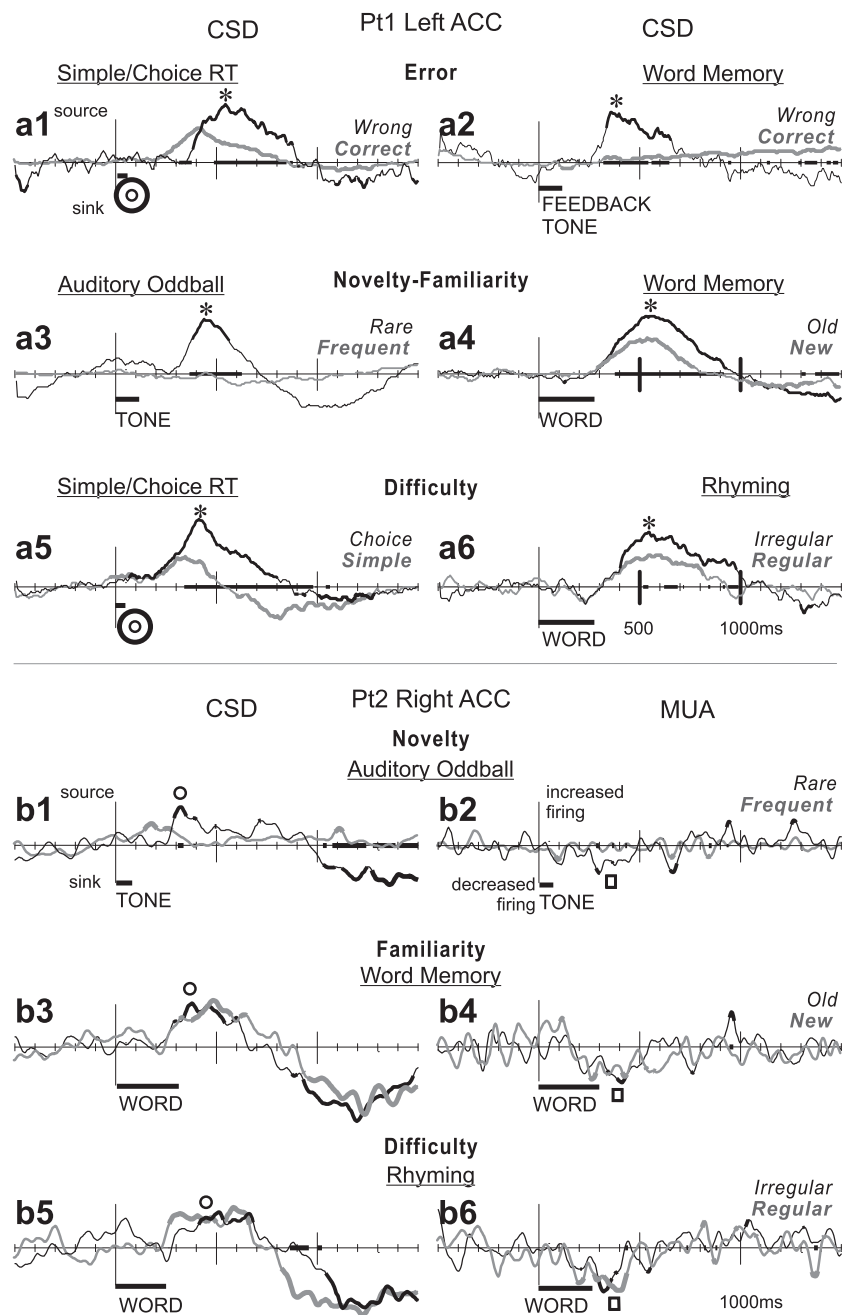


**Figure 3.** Possible IPSC indicated by a large CSD source with decreased MUA across multiple tasks. *a*, CSD waveforms recorded from the left ACC of Pt1. A large current source (\*) was evoked from  $\sim 300$  to 800 ms in simple/choice RT (*a1, a5*), word recognition memory (*a2, a4*), auditory oddball (*a3*), and rhyming (*a6*). Source currents were larger after wrong (compared with correct) responses (*a1*) and after a feedback tone indicating wrong responses (*a2*), suggesting modulation by errors; to rare than frequent tones (*a3*) and to old rather than new words (*a4*), suggesting modulation by novelty–familiarity; to stimuli that required a differential choice response [compared with a constant simple response (*a5*)] or an evaluation of irregular orthography [as opposed to regular orthography (*a6*)], suggesting a relationship to difficulty, perhaps in stimulus–response mapping. *b*, CSD (left) and simultaneous MUA (right) waveforms recorded from the right ACC of Pt2. Again, a current source (○) was evoked from  $\sim 300$  to 700 ms in a variety of tasks involving auditory discrimination (*b1*), word recognition memory (*b3*), or rhyming (*b5*), although differentiation between task conditions is not as clear. Simultaneous MUA recordings show a decrease during these tasks (□) from  $\sim 200$  to 500 ms (*b2, b4, b6*). Task names are underlined; condition names are in italics. Dark gray bars below x-axes indicate stimulus presentation periods. The x-axis is thickened when the two conditions are significantly different from each other; CSD and MUA waveforms are thickened when significantly different from zero (two-tailed  $p < 0.01$ ).

size and close spacing of the recording contacts and the CSD/MUA analytic methods used. Comparably high spatial resolution has also been reported for ultrahigh field (7 T) fMRI in animals (Yang et al., 1998). However, in the usual hemodynamic studies,

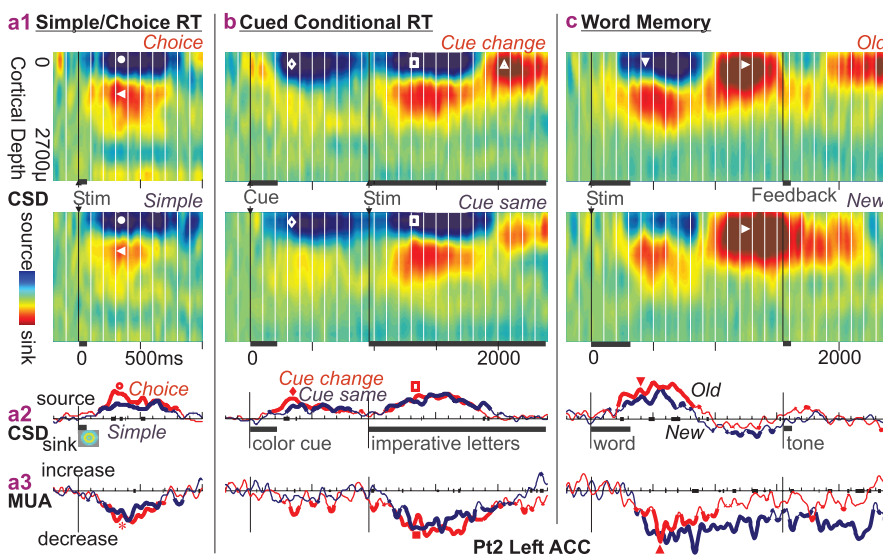


**Figure 4.** Possible IPSCs in superficial cortical layers across multiple cognitive tasks; Pt2 left ACC. *a*, CSD and MUA during simple and choice responses to lateralized visual stimuli. *a1*, Contour plots of CSD over time and cortical depth show sustained superficial sources (blue region with ●, where positive current leaves the cell) with deeper sinks (red region with ▲, where positive current enters the cell). *a2*, The same data are plotted as a waveform from a superficial contact, showing a larger source (○) to choice than simple RT. *a3*, MUA decreases (\*) during the sources shown in *a1* and *a2*, indicating that they are likely IPSCs. *b*, A cued conditional letter discrimination task evokes again a strong superficial source (◇) that is slightly larger when the cue is different from the preceding trial (◆). The source evoked by the imperative stimulus (□) is accompanied by decreased MUA (■) and is followed by a superficial sink (△). *c*, A similar pattern of superficial source (▼) followed by a sink (►) and MUA inhibition (▲) is evoked by words in a memory task, with a larger source to the repeated (old) words. Note that to visualize all of the responses, the vertical scale in the left column has been compressed twofold. Thickening of the CSD and MUA waveforms indicates that they are significantly different from zero; thickening of the x-axis indicates that the two conditions are significantly different from each other (two-tailed  $p < 0.01$ ).

spatial resolution is limited by voxel size and spatial smoothing to a volume  $\sim 1000\times$  larger than that of CSD/MUA. Spatial resolution of hemodynamic measures is also limited by diffusion, vascular control unit size, and downstream vascular effects. Noninvasive electromagnetic measures have worse spatial resolution, especially for extended sources, caused by uncertainties inherent in source estimation (Dale and Halgren, 2001). Depth EEG measurements have less uncertainty but are still limited by the large contact size ( $\sim 1 \text{ mm}^2$ ), intercontact distance ( $\sim 3\text{--}5 \text{ mm}$ ), and use of LFP, which, unlike CSD, can volume conduct for centimeters (Goff et al., 1978).

The current results thus establish that within the very small sampling volumes of CSD/MUA, ACC synaptic and neuronal activity can show multiple cognitive correlates. Conversely, it is still likely that there is relative specialization of different ACC areas for different functions; other ACC microdomains would presumably also respond to multiple tasks but may have a distinct profile. Indeed, although the sites had similar responses in that they all responded to multiple tasks and differentially to multiple condition contrasts, with sustained synaptic activity in superficial cortical layers, they also had clear differences in their degrees and distribution of task modulation. More studies are needed to determine the topography and individuality of these responses.

In any case, these findings clearly support the exploration of functional models in which the ACC calculates its contribution to behavior by integrating multiple types and domains of information within individual cortical columns and/or between nearby columns. That is, within the range of tasks sampled, these data favor solutions

to the multiplicity of ACC activation that posit broad participation through a global function rather than multiple more restricted contributions that are topographically segregated.

The actual tasks and situations evoking ACC responses and differential responses would be consistent with a variety of different formulations for ACC function. Perhaps most consistent with the largest number of observations would be the detection of situations in which there is a larger possibility of error (“conflict monitoring”), which might be expected also to evoke an orienting response (Table 2). However, the activation of a structure in a particular task does not imply that it is essential for performance of that task, nor even that it makes a significant contribution to the task. Given the involvement of the ACC in multiple anatomical systems, it is also possible that some activation reflects a collateral involvement that is only tangentially related to the intended behavioral manipulation. Furthermore, the current study had no effective probe of ACC neuronal output, because most ACC efferents arise from deep layers where we did not record MUA (Barbas, 2000).

#### ACC generation of error-related brain potentials

A negative scalp potential termed “N2” occurs just before the response in conflict situations, and an “error-related negativity” (ERN) peaks  $\sim 120 \text{ ms}$  after initiation of an incorrect response during speeded tasks (Gehring et al., 1993; Dehaene et al., 1994). The association of similar situations with ACC hemodynamic activation, as well as their general scalp topography (Holroyd et al., 1998; Scheffers and Coles, 2000), have led some to suggest that N2 and ERN are generated in ACC (Falkenstein et al., 2000; van Veen and Carter, 2002). Less ambiguous localization has been obtained from direct intracranial ACC recordings showing LFP during incorrect responses (Halgren et al., 2002). The current study provides additional confirmation that ACC generates ERPs during the same period as the N2 and ERN, with similar task correlates. However, more study is needed, including simultaneous scalp and laminar recordings during key tasks and detailed biophysical modeling to conclude that the scalp-recorded N2 and ERN are generated, in whole or in part, in ACC.

In other studies, ACC has been identified as one of the principal cortical structures generating potentials correlated with the orienting response (Baudena et al., 1995). The P3a, elicited by novel stimuli, evokes an involuntary reorientation of attention as well as a constellation of autonomic features including a prominent electrodermal response (Marinkovic et al., 2001). Such features may be mediated by ACC projections directly to brainstem autonomic efferent structures, and ACC stimulation can provoke autonomic and general changes in cortical tonus (Devinsky et al., 1995). Neuroimaging studies also found ACC activation in orientation or autonomic control, in particular to rare stimuli in

oddball tasks (Braver et al., 2001; Downar et al., 2001; Kiehl et al., 2001). The current study provides additional evidence for a role of the ACC in integrating cortical with autonomic aspects of phasic arousal to cognitive stimuli.

### ACC generation of theta

Task-related theta activity was visible in the spontaneous CSD in the ACC of both patients. The theta rhythm is a dominant EEG feature of limbic structures including the hippocampal formation and cingulate gyrus (Leung and Borst, 1987) in most mammals, where it occurs during nonautomatic movements (Vanderwolf, 1969) and orienting (Grastyan et al., 1966). It also entrains location-specific unit activity in rats (O'Keefe and Nadel, 1978), a property that has been hypothesized to aid in memory retrieval (McNaughton, 1998). The task correlates of the mammalian theta thus resemble in several respects those associated with ACC hemodynamic activation (reviewed above) as well as those found in the current study to differentially evoke human ACC synaptic and unit activity.

Theta in the human scalp EEG has also been related to memory processes (Bastiaansen and Hagoort, 2003). The scalp topography of a prominent "frontal midline theta" during working memory tasks is consistent with generation in ACC (Gevins et al., 1997; Ishii et al., 1999), and scalp theta power is correlated across subjects with ACC glucose metabolic rate (measured with PET) (Pizzagalli et al., 2003). Subdural grid recordings have found task-related theta in numerous locations over the cortical convexity (Raghavachari et al., 2001). A single case report recorded spontaneous theta activity in the vicinity of ACC (Uchida et al., 2003). The current findings provide more direct and unambiguous support for task-related theta generation in the human ACC. Furthermore, the task-related increase in phase locking observed here indicates that the ACC theta forms part of a larger network involving widespread cortical locations in the temporal, frontal, and possibly other areas, consistent with the widespread coactivation of ACC with other areas observed with fMRI (Kiehl et al., 2000, 2001).

It is interesting to contrast the current results with depth recordings from the fusiform gyrus during the same word memory task as used in the current study and a similar task using faces. As in the current study, stimuli evoked an event-related increase in spectral power (Klopp et al., 1999). However, unlike the current study, the increase was wide-band (from 5 to 45 Hz) rather than restricted to the theta range,

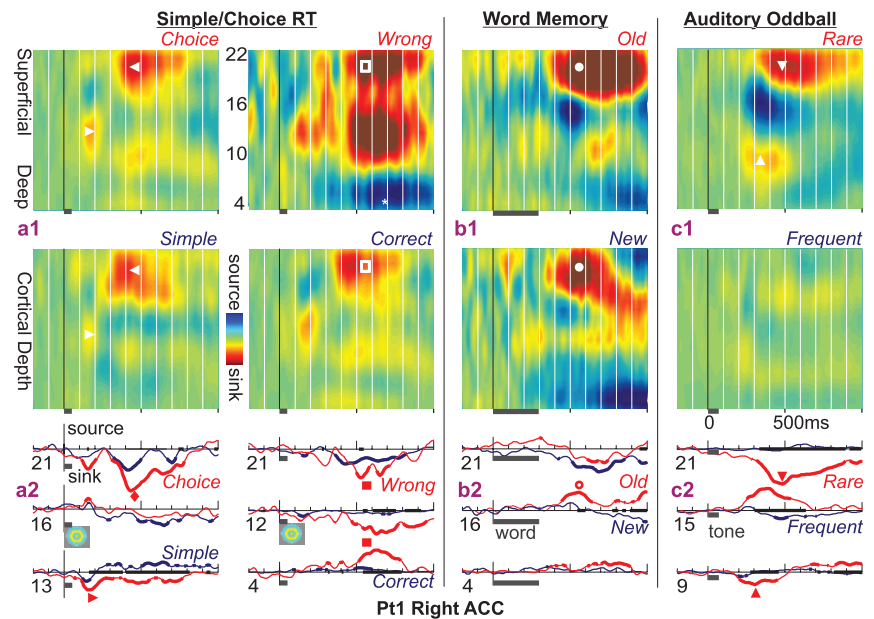


**Figure 5.** CSD sinks in cognitive tasks. CSD contours (above) and waveforms (below) in the right ACC of Pt1, where, unlike other sites, the CSD was dominated by sinks rather than sources. *a1*, CSD contours recorded as the subject makes simple and choice responses to lateralized visual stimuli. The earliest response seen in this site is a small sink in middle layers between 100 and 200 ms (▶), followed by a larger sink in superficial layers from ~350 to 800 ms (◀). The response to choice responses is larger than to simple responses. A larger difference is seen when the trials with incorrect responses are segregated from those with correct responses (◻). The deep source (\*) may be a passive return current. *a2*, CSD waveforms from selected channels in the different conditions show the larger sinks to choice (◆) and wrong (◼) trials. *b1*, A superficial sink (●) is also evoked by words in a declarative memory task from ~350 to 1000 ms, with a larger response to repeated words. *b2*, Traces from selected channels again show that differential responses (○) are present in multiple layers of ACC. *c1, c2*, Current sinks initially in middle layers (▲) then more superficially (▼) from ~300 to 1000 ms are again prominently evoked, in this case by rare tones. Note that to visualize all of the responses, the vertical scale in the left column has been compressed two times in the second and third columns and four times in the right column. CSD waveforms are thickened when significantly different from zero; the x-axis is thickened when the two conditions are significantly different from each other (two-tailed  $p < 0.01$ ).

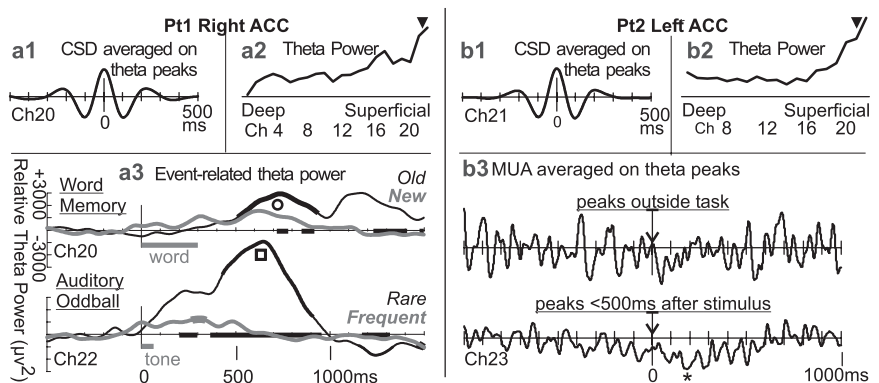


**Figure 6.** Task-related theta rhythm generated in superficial cortical layers of ACC of two patients. *a1, b1*, When averaged on the peak of the single sweep LFP, the CSD theta showed a period of ~200 ms in both patients. *a2, b2*, Theta power (4–7 Hz) was calculated on single-sweep CSD from –512 ms before to 1536 ms after stimulus onset in simple/choice RT. In both patients, theta power was concentrated in superficial cortical layers (▼). *a3*, Event-related theta power was calculated from individual trial CSD recorded in the superficial layers of the right ACC in Pt1 and then averaged. It showed a strong task-related increase peaking at ~700 ms after words (○), especially when repeated words, and after tones (◻), especially when infrequent. The x-axis is thickened when the two conditions are significantly different from each other; the waveforms are thickened when significantly different from zero (two-tailed  $p < 0.01$ ). *b3*, MUA recorded in the superficial layers of Pt2 left ACC was averaged with respect to peaks of the local theta rhythm. No relationship is apparent during the period between tasks, but a decreased firing is apparent with respect to theta occurring immediately after the stimulus (\*).

was specific for faces rather than occurring to a variety of stimuli, was early and brief (150–210 ms) rather than later and extended (~200–1000 ms), and was followed by a profound decrease in spectral power rather than being a monophasic increase. In con-

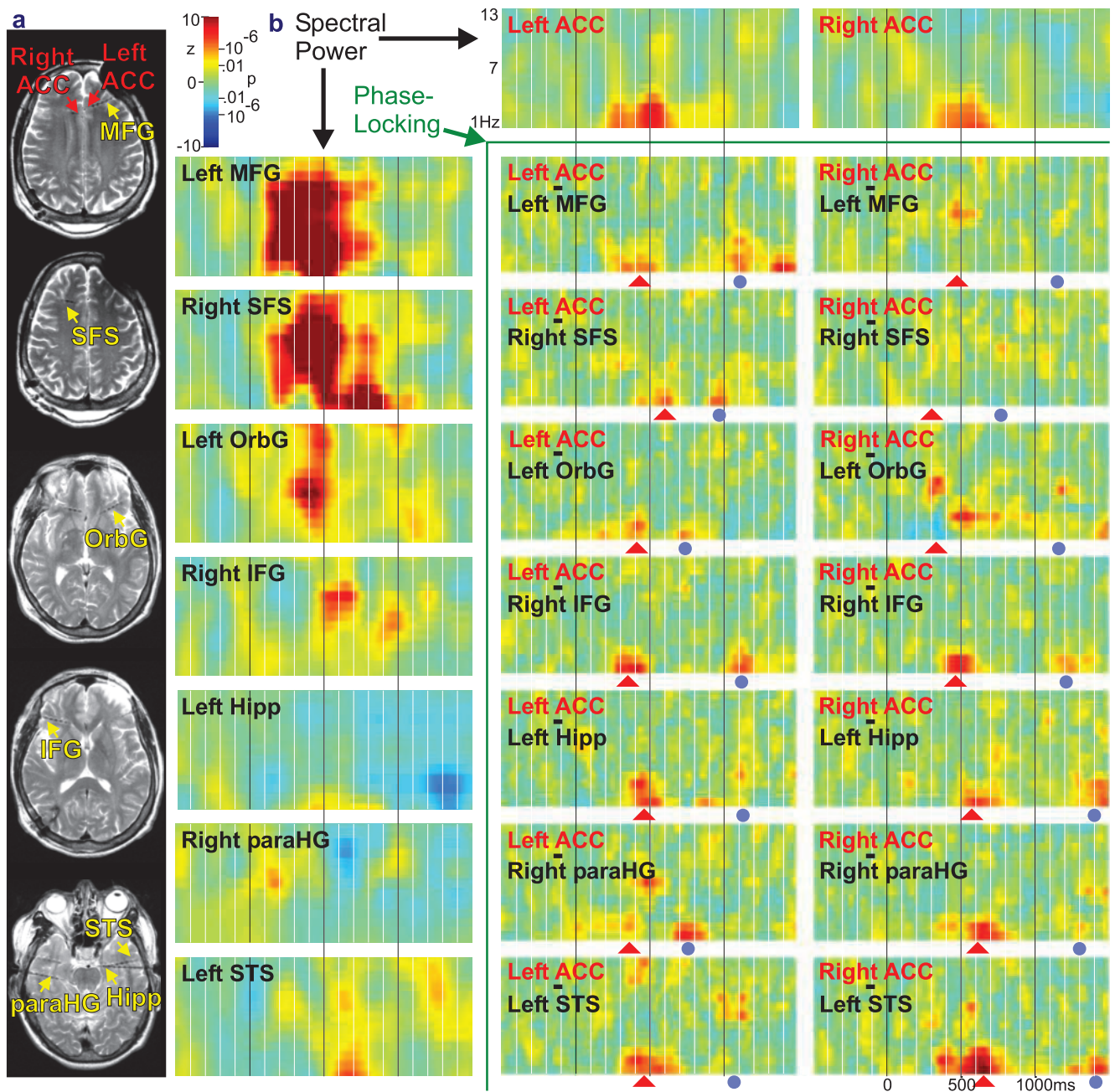


**Figure 7.** Single trial spectral analysis of ACC interaction with other cortical sites. *a*, The locations of micro laminar contacts in ACC (labeled in red) and macro contacts in the frontal and temporal lobes (labeled in yellow) seen in MRI obtained with the probes in place. The defect over the left frontal area is an artifact caused by an external connector. IFG, Inferior frontal gyrus; MFG, middle frontal gyrus; SFS, superior frontal sulcus; OrbG, orbital gyrus; Hipp, hippocampus; STS, superior temporal sulcus; paraHG, parahippocampal gyrus. *b*, Interactions were calculated between micro and macro contacts. Each colored box plots  $z$ -scores comparing spectral measures for each frequency (from 1 to 13 Hz;  $y$ -axis) and each latency ( $-500$ – $1500$  ms;  $x$ -axis) for every trial to those calculated in the baseline period. Spectral power during the rhyme task is plotted in the boxes on the top row and left column; phase locking is plotted in the boxes at bottom right (other tasks gave similar results). Across sites, the most consistent event-related spectral changes were in the theta and gamma bands. Task-related increases in phase locking in these bands between both ACC and multiple frontotemporal sites occurred most reliably between 200 and 700 ms after stimulus onset (indicated by  $\blacktriangle$ ). A second, less consistent burst of phase locking occurred at  $\sim 1000$  ms (indicated by  $\bullet$ ). The correspondence of the  $z$ -scores to probabilities in the normal distribution are shown on the scale.

trast to the fusiform gyrus but similar to the current results, prefrontal sites showed only a late low-frequency (5–12 Hz) spectral power increase to both faces and words. Again, similar to the current study, faces evoked a phasic increase in coherence between the fusiform gyrus and multiple neocortical sites in the temporal, parietal, and frontal lobes (Klopp et al., 2000). However, unlike the current study, the coherence increase was brief and confined to the higher-frequency bands. Based on this limited sample, one may speculate that the increased gamma-

frequency power and coherence that has been hypothesized to promote binding of sensory elements into a percept is characteristic of sensory cortices, whereas high-level association may synchronize through theta range activity (von Stein and Sarnthein, 2000).

#### Inhibition in superficial layers

The most consistent task-related neuronal response observed here is a current source with unit firing decrease indicating IPSCs

**Table 2. Consistency of putative ACC functions with observed CSD/MUA responses**

Evoking tasks	Comparison conditions	Phase of task	Effectiveness in evoking responses	Putative function					
				Error detection	Conflict monitoring	Orienting response	Memory	Motor control	Stimulus–response mapping
Simple/ choice RT	Correct/ wrong	Stimulus	**	**	*	*		**	
Word memory	Correct/ wrong	Feedback	**	**	*	**			
Simple/ choice RT	Choice/ simple	Stimulus	**		**	*		**	**
Auditory oddball	Rare/ frequent	Stimulus	**		*	**			*
Word memory	New/ old	Stimulus	*		*	*	**	*	
Cued conditional RT	Cue change/ cue same	Cue	*		*	*			**
Rhyme	Irregular/ regular	Stimulus	*		*	*			*

The number of asterisks indicates the relative strength.

in superficial ACC layers. One possible source for this inhibition could be local GABAergic interneurons, whose neuropil (as indicated by parvalbumin and calbindin labeling) is most dense in layer III of ACC (Nimchinsky et al., 1997). A second possible source is cholinergic fibers from the Ch4 cell group in the nucleus basalis of Meynert that project mainly to superficial ACC in primates and humans (Geula and Mesulam, 1989; Lewis, 1991; Selden et al., 1998). This is the same system as the medial septum/diagonal band of Broca, whose cholinergic and GABAergic projections to multiple limbic and neocortical sites produce the theta rhythm (Bland and Oddie, 1998). The proximal cause of the hippocampal theta in rats appears to be  $Cl^-$ -mediated IPSCs (Leung, 1998). Although the local neuronal mechanisms of the ACC theta are less clear, AMPA infusion into the nucleus basalis results in decreased cingulate glucose metabolism, suggesting that these basal forebrain influences may be mainly inhibitory (Browne et al., 1998). Consistent with this interpretation, in the current recordings, the theta rhythm originated mostly from ACC superficial layers, and during task performance appeared to be associated with decreased firing. However, the overall effect of cholinergic or theta modulation is a change in the mode of information processing, which extends beyond simple inhibition.

It is unlikely that ACC inhibition is attributable directly to input from dorsolateral prefrontal or other isocortex, which project to the deep layers of ACC (Barbas, 2000). However, such input could occur indirectly via projections to ACC interneurons and/or to basal forebrain modulatory structures. One would predict such projections, because ACC superficial inhibition distinguishes between error and correct trials, and the ERN does not make such distinctions in patients with prefrontal lesions (Gehring and Knight, 2000).

In conclusion, the current results are most consistent with modulation of superficial ACC layers across a wide variety of tasks and situations. This modulation may arise in the basal forebrain, under the control of prefrontal and other areas, and be mediated by local interneurons. It starts well before the behavioral response and continues for several hundred milliseconds. It is larger when the task is difficult or an error has been made. We hypothesize that this modulatory influence gates ACC output during behavior. Although firing from the ACC output layers was not recorded, evidence for ACC-neocortical interaction during this period was found in a transient increase in the phase locking of their synaptic activity in the theta range. Inhibition in cortical pyramidal cells is commonly followed by activation of a nonspecific cation channel that is suppressed by normal waking levels of depolarization (Destexhe et al., 2003). In the present recordings, the superficial source is followed by a superficial sink, suggesting that rebound from superficial inhibition could prime the ACC to deal with the consequences of action in the postresponse period.

## References

- Allman JM, Hakeem A, Erwin JM, Nimchinsky E, Hof P (2001) The anterior cingulate cortex. The evolution of an interface between emotion and cognition. *Ann NY Acad Sci* 935:107–117.
- Barbas H (2000) Connections underlying the synthesis of cognition, memory, and emotion in primate prefrontal cortices. *Brain Res Bull* 52:319–330.
- Bastiaansen M, Hagoort P (2003) Event-induced theta responses as a window on the dynamics of memory. *Cortex* 39:967–992.
- Baudena P, Heit G, Clarke JM, Halgren E (1995) Intracerebral potentials to rare target and distractor auditory and visual stimuli: 3. Frontal cortex. *Electroencephalogr Clin Neurophysiol* 94:251–264.
- Bland BH, Oddie SD (1998) Anatomical, electrophysiological and pharmacological studies of ascending brainstem hippocampal synchronizing pathways. *Neurosci Biobehav Rev* 22:259–273.
- Braver TS, Barch DM, Gray JR, Molfese DL, Snyder A (2001) Anterior cingulate cortex and response conflict: effects of frequency, inhibition and errors. *Cereb Cortex* 11:825–836.
- Browne SE, Muir JL, Robbins TW, Page KJ, Everitt BJ, McCulloch J (1998) The cerebral metabolic effects of manipulating glutamatergic systems within the basal forebrain in conscious rats. *Eur J Neurosci* 10:649–663.
- Bunge SA, Ochsner KN, Desmond JE, Glover GH, Gabrieli JD (2001) Prefrontal regions involved in keeping information in and out of mind. *Brain* 124:2074–2086.
- Bush G, Luu P, Posner MI (2000) Cognitive and emotional influences in anterior cingulate cortex. *Trends Cogn Sci* 4:215–222.
- Cabeza R, Dolcos F, Prince SE, Rice HJ, Weissman DH, Nyberg L (2003) Attention-related activity during episodic memory retrieval: a cross-function fMRI study. *Neuropsychologia* 41:390–399.
- Carter CS, Macdonald AM, Botvinick M, Ross LL, Stenger VA, Noll D, Cohen JD (2000) Parsing executive processes: strategic vs. evaluative functions of the anterior cingulate cortex. *Proc Natl Acad Sci USA* 97:1944–1948.
- Corbetta M, Akbudak E, Conturo TE, Snyder AZ, Ollinger JM, Drury HA, Linenweber MR, Petersen SE, Raichle ME, Van Essen DC, Shulman GL (1998) A common network of functional areas for attention and eye movements. *Neuron* 21:761–773.
- Crosson B, Sadek JR, Bobholz JA, Gokcay D, Mohr CM, Leonard CM, Maron L, Auerbach EJ, Browd SR, Freeman AJ, Briggs RW (1999) Activity in the paracingulate and cingulate sulci during word generation: an fMRI study of functional anatomy. *Cereb Cortex* 9:307–316.
- Dale AM, Halgren E (2001) Spatiotemporal mapping of brain activity by integration of multiple imaging modalities. *Curr Opin Neurobiol* 11:202–208.
- Dehaene S, Posner MI, Tucker DM (1994) Localization of a neural system for error detection and compensation. *Psychol Sci* 5:303–305.
- Destexhe A, Rudolph M, Pare D (2003) The high-conductance state of neocortical neurons in vivo. *Nat Rev Neurosci* 4:739–751.
- Devinsky O, Morrell MJ, Vogt BA (1995) Contributions of anterior cingulate cortex to behavior. *Brain* 118:279–306.
- Downar J, Crawley AP, Mikulis DJ, Davis KD (2001) The effect of task relevance on the cortical response to changes in visual and auditory stimuli: an event-related fMRI study. *NeuroImage* 14:1256–1267.
- Dum RP, Strick PL (1993) The cingulate motor areas. In: *Neurobiology of cingulate cortex and limbic thalamus* (Vogt BA, Gabriel M, eds), pp 415–441. Boston: Birkhäuser.

- Dum RP, Strick PL (2002) Motor areas in the frontal lobe of the primate. *Physiol Behav* 77:677–682.
- Duncan J, Owen AM (2000) Common regions of the human frontal lobe recruited by diverse cognitive demands. *Trends Neurosci* 23:475–483.
- Falkenstein M, Hoormann J, Christ S, Hohnsbein J (2000) ERP components on reaction errors and their functional significance: a tutorial. *Biol Psychol* 51:87–107.
- Fiez JA, Petersen SE (1998) Neuroimaging studies of word reading. *Proc Natl Acad Sci USA* 95:914–921.
- Frith CD, Friston K, Liddle PF, Frackowiak RS (1991) Willed action and the prefrontal cortex in man: a study with PET. *Proc R Soc Lond B Biol Sci* 244:241–246.
- Gehring WJ, Knight RT (2000) Prefrontal-cingulate interactions in action monitoring. *Nat Neurosci* 3:516–520.
- Gehring WJ, Goss B, Coles MGH, Meyer DE, Donchin E (1993) A neural system for error detection and compensation. *Psychol Sci* 4:385–390.
- Geula C, Mesulam MM (1989) Cortical cholinergic fibers in aging and Alzheimer's disease: a morphometric study. *Neuroscience* 33:469–481.
- Gevins A, Smith ME, McEvoy L, Yu D (1997) High-resolution EEG mapping of cortical activation related to working memory: effects of task difficulty, type of processing, and practice. *Cereb Cortex* 7:374–385.
- Goff WR, Allison T, Vaughan Jr HG (1978) The functional neuroanatomy of event related potentials. In: *Event-related brain potentials in man* (Callaway E, Tueting P, Koslow SH, eds), pp 1–79. New York: Academic.
- Grastyan E, Karmos G, Vereczkey L, Kellenyi L (1966) The hippocampal electrical correlates of the homeostatic regulation of motivation. *Electroencephalogr Clin Neurophysiol* 21:34–53.
- Grover FS, Buchwald JS (1970) Correlation of cell size with amplitude of background fast activity in specific brain nuclei. *J Neurophysiol* 33:160–171.
- Halgren E, Baudena P, Heit G, Clarke JM, Marinkovic K (1994) Spatio-temporal stages in face and word processing. I. Depth-recorded potentials in the human occipital, temporal and parietal lobes. *J Physiol (Paris)* 88:1–50.
- Halgren E, Boujon C, Clarke J, Wang C, Chauvel P (2002) Rapid distributed fronto-parieto-occipital processing stages during working memory in humans. *Cereb Cortex* 12:710–728.
- Holroyd C, Dien J, Coles M (1998) Error-related scalp potentials elicited by hand and foot movements: evidence for an output-independent error-processing system in humans. *Neurosci Lett* 242:65–68.
- Humphrey DR (1968) Re-analysis of the antidromic cortical response. II. On the contribution of cell discharge and PSPs to the evoked potentials. *Electroencephalogr Clin Neurophysiol* 25:421–442.
- Ishii R, Shinosaki K, Ukai S, Inouye T, Ishihara T, Yoshimine T, Hirabuki N, Asada H, Kihara T, Robinson SE, Takeda M (1999) Medial prefrontal cortex generates frontal midline theta rhythm. *NeuroReport* 10:675–679.
- Kiehl KA, Liddle PF, Hopfinger JB (2000) Error processing and the rostral anterior cingulate: an event-related fMRI study. *Psychophysiology* 37:216–223.
- Kiehl KA, Laurens KR, Duty TL, Forster BB, Liddle PF (2001) Neural sources involved in auditory target detection and novelty processing: an event-related fMRI study. *Psychophysiology* 38:133–142.
- Klopp J, Marinkovic K, Chauvel P, Nenov V, Halgren E (2000) Early widespread cortical distribution of coherent fusiform face activity. *Hum Brain Mapp* 11:286–293.
- Klopp JC, Halgren E, Marinkovic K, Nenov VI (1999) Face-selective event-related spectral changes in the human fusiform gyrus. *Clin Neurophysiol* 110:677–683.
- Kollias SS, Alkadhi H, Jaermann T, Crelier G, Hepp-Reymond MC (2001) Identification of multiple nonprimary motor cortical areas with simple movements. *Brain Res Brain Res Rev* 36:185–195.
- Kronland-Martinet R, Morlet J, Grossmann A (1987) Analysis of sound patterns through wavelet transforms. *Intern J Pattern Recognit Artif Intell* 1:273–302.
- Lachaux JP, Rodriguez E, Martinerie J, Varela FJ (1999) Measuring phase synchrony in brain signals. *Hum Brain Mapp* 8:194–208.
- Leung LS (1998) Generation of theta and gamma rhythms in the hippocampus. *Neurosci Biobehav Rev* 22:275–290.
- Leung LW, Borst JG (1987) Electrical activity of the cingulate cortex. I. Generating mechanisms and relations to behavior. *Brain Res* 407:68–80.
- Lewis DA (1991) Distribution of choline acetyltransferase-immunoreactive axons in monkey frontal cortex. *Neuroscience* 40:363–374.
- Luu P, Tucker DM, Derryberry D, Reed M, Poulsen C (2003) Electrophysiological responses to errors and feedback in the process of action regulation. *Psychol Sci* 14:47–53.
- Marinkovic K, Halgren E, Maltzman I (2001) Arousal-related P3a to novel auditory stimuli is abolished by a moderately low alcohol dose. *Alcohol Alcohol* 36:529–539.
- McNaughton BL (1998) The neurophysiology of reminiscence. *Neurobiol Learn Mem* 70:252–267.
- Mesulam MM (1981) A cortical network for directed attention and unilateral neglect. *Ann Neurol* 10:309–325.
- Nicholson C, Freeman JA (1975) Theory of current source density analysis and determination of the conductivity tensor for anuran cerebellum. *J Neurophysiol* 38:356–368.
- Nimchinsky EA, Vogt BA, Morrison JH, Hof PR (1997) Neurofilament and calcium-binding proteins in the human cingulate cortex. *J Comp Neurol* 384:597–620.
- Nyberg L (1998) Mapping episodic memory. *Behav Brain Res* 90:107–114.
- O'Keefe J, Nadel L (1978) *The hippocampus as a cognitive map*. Oxford: Clarendon.
- Paus T (2001) Primate anterior cingulate cortex: where motor control, drive and cognition interface. *Nat Rev Neurosci* 2:417–424.
- Petersen SE, Fox PT, Posner MI, Raichle ME, Mintun MA (1989) Positron emission tomographic studies of the processing of single words. *J Cogn Neurosci* 1:153–170.
- Peterson BS, Skudlarski P, Gatenby JC, Zhang H, Anderson AW, Gore JC (1999) An fMRI study of Stroop word-color interference: evidence for cingulate subregions subserving multiple distributed attentional systems. *Biol Psychiatry* 45:1237–1258.
- Phan KL, Wager T, Taylor SF, Liberzon I (2002) Functional neuroanatomy of emotion: a meta-analysis of emotion activation studies in PET and fMRI. *NeuroImage* 16:331–348.
- Picard N, Strick PL (2001) Imaging the premotor areas. *Curr Opin Neurobiol* 11:663–672.
- Pizzagalli DA, Oakes TR, Davidson RJ (2003) Coupling of theta activity and glucose metabolism in the human rostral anterior cingulate cortex: an EEG/PET study of normal and depressed subjects. *Psychophysiology* 40:939–949.
- Posner MI, Petersen SE, Fox PT, Raichle ME (1988) Localization of cognitive operations in the human brain. *Science* 240:1627–1631.
- Raghavachari S, Kahana MJ, Rizzuto DS, Caplan JB, Kirschen MP, Bourgeois B, Madsen JR, Lisman JE (2001) Gating of human theta oscillations by a working memory task. *J Neurosci* 21:3175–3183.
- Scheffers MK, Coles MG (2000) Performance monitoring in a confusing world: error-related brain activity, judgments of response accuracy, and types of errors. *J Exp Psychol Hum Percept Perform* 26:141–151.
- Selden NR, Gitelman DR, Salamon-Murayama N, Parrish TB, Mesulam MM (1998) Trajectories of cholinergic pathways within the cerebral hemispheres of the human brain. *Brain* 121:2249–2257.
- Uchida S, Maehara T, Hirai N, Kawai K, Shimizu H (2003) Theta oscillation in the anterior cingulate and beta-1 oscillation in the medial temporal cortices: a human case report. *J Clin Neurosci* 10:371–374.
- Ulbert I, Halgren E, Heit G, Karmos G (2001a) Multiple microelectrode-recording system for human intracortical applications. *J Neurosci Methods* 106:69–79.
- Ulbert I, Karmos G, Heit G, Halgren E (2001b) Early discrimination of coherent versus incoherent motion by multiunit and synaptic activity in human putative MT+. *Hum Brain Mapp* 13:226–238.
- Vanderwolf CH (1969) Hippocampal electrical activity and voluntary movement in the rat. *Electroencephalogr Clin Neurophysiol* 26:407–410.
- van Veen V, Carter CS (2002) The anterior cingulate as a conflict monitor: fMRI and ERP studies. *Physiol Behav* 77:477–482.
- Vogt BA, Hof PR, Vogt LJ (2004) Cingulate gyrus. In: *The human nervous system*, Ed 2 (Paxinos G, Mai JK, eds), pp 915–949. San Diego: Elsevier Academic.
- von Stein A, Sarnthein J (2000) Different frequencies for different scales of cortical integration: from local gamma to long range alpha/theta synchronization. *Int J Psychophysiol* 38:301–313.
- Yang X, Renken R, Hyder F, Siddeek M, Greer CA, Shepherd GM, Shulman RG (1998) Dynamic mapping at the laminar level of odor-elicited responses in rat olfactory bulb by functional MRI. *Proc Natl Acad Sci USA* 95:7715–7720.

dc\_303\_11

### **3. Melléklet**



## Processing stages underlying word recognition in the anteroventral temporal lobe

Eric Halgren,<sup>a,\*</sup> Chunmao Wang,<sup>b</sup> Donald L. Schomer,<sup>c</sup> Susanne Knake,<sup>d</sup>  
 Ksenija Marinkovic,<sup>e</sup> Julian Wu,<sup>f</sup> and Istvan Ulbert<sup>e,g</sup>

<sup>a</sup>Multimodal Imaging Laboratory, Department of Radiology, University of California at San Diego, La Jolla, CA 92093-0841, USA

<sup>b</sup>Comprehensive Epilepsy Center, Department of Neurology, New York University Medical School, New York, NY 10016, USA

<sup>c</sup>Department of Neurology, Beth Israel Deaconess Medical Center, Harvard Medical School, Boston, MA 02129, USA

<sup>d</sup>Department of Neurology, Philipps-University, Marburg, Germany

<sup>e</sup>Martinos Center, Massachusetts General Hospital, Harvard Medical School, Charlestown, MA 02129, USA

<sup>f</sup>Department of Surgery, Beth Israel Deaconess Medical Center, Harvard Medical School, Boston, MA 02129, USA

<sup>g</sup>Institute for Psychology, Hungarian Academy of Sciences, Budapest, Hungary

Received 3 June 2005; revised 16 October 2005; accepted 31 October 2005

Available online 17 February 2006

The anteroventral temporal lobe integrates visual, lexical, semantic and mnemonic aspects of word processing, through its reciprocal connections with the ventral visual stream, language areas, and the hippocampal formation. We used linear microelectrode arrays to probe population synaptic currents and neuronal firing in different cortical layers of the anteroventral temporal lobe, during semantic judgments with implicit priming and overt word recognition. Since different extrinsic and associative inputs preferentially target different cortical layers, this method can help reveal the sequence and nature of local processing stages at a higher resolution than was previously possible.

The initial response in inferotemporal and perirhinal cortices is a brief current sink beginning at ~120 ms and peaking at ~170 ms. Localization of this initial sink to middle layers suggests that it represents feedforward input from lower visual areas, and simultaneously increased firing implies that it represents excitatory synaptic currents. Until ~800 ms, the main focus of transmembrane current sinks alternates between middle and superficial layers, with the superficial focus becoming increasingly dominant after ~550 ms. Since superficial layers are the target of local and feedback associative inputs, this suggests an alternation in predominant synaptic input between feedforward and feedback modes. Word repetition does not affect the initial perirhinal and inferotemporal middle layer sink but does decrease later activity. Entorhinal activity begins later (~200 ms),

with greater apparent excitatory post-synaptic currents and multiunit activity in neocortically projecting than hippocampal-projecting layers. In contrast to perirhinal and entorhinal responses, entorhinal responses are larger to repeated words during memory retrieval.

These results identify a sequence of physiological activation, beginning with a sharp activation from lower level visual areas carrying specific information to middle layers. This is followed by feedback and associative interactions involving upper cortical layers, which are abbreviated to repeated words. Following bottom-up and associative stages, top-down recollective processes may be driven by entorhinal cortex. Word processing involves a systematic sequence of fast feedforward information transfer from visual areas to anteroventral temporal cortex followed by prolonged interactions of this feedforward information with local associations and feedback mnemonic information from the medial temporal lobe.

© 2005 Elsevier Inc. All rights reserved.

*Keywords:* Entorhinal; Humans; Inferotemporal; Memory; Perirhinal

---

*Abbreviations:* AC, association cortex; avTL, anteroventral temporal lobe; CSD, current source density; EEG, electroencephalogram; EPSC, excitatory post-synaptic current; ER, entorhinal; fMRI, functional magnetic resonance imaging; HC, hippocampal formation; IPSC, inhibitory post-synaptic current; IT, inferotemporal; MEG, magnetoencephalogram; MUA, multiunit activity; PET, positron emission tomography; PR, perirhinal.

\* Corresponding author. UCSD, La Jolla, CA 92093-0841, USA. Fax: +1 858 534 1078.

E-mail address: ehalgren@ucsd.edu (E. Halgren).

Available online on ScienceDirect ([www.sciencedirect.com](http://www.sciencedirect.com)).

### Introduction

The human anteroventral temporal lobe (avTL), comprised of inferotemporal (IT), perirhinal (PR), and entorhinal (ER) cortices, works with the hippocampal formation (HC) to perform an essential role in declarative memory (Squire et al., 2004). These structures are interconnected: the superficial layers of ER are the main source of afferents to HC (via the perforant path), and the deep layers of ER are the main recipient of HC output (via the trisynaptic pathway and subicular complex) (Insausti and Amaral, 2004). Superficial ER receives input from, and deep ER projects to, widespread association cortex (AC). These projections include both direct connections, as well as relays via PR and IT. Basic

physiological studies in rodents find that each step in this long multistage feedback loop between AC and HC, via IT, PR, and ER, is excitatory (Biella et al., 2002a).

In addition to its crucial role in memory, anatomical (Felleman and VanEssen, 1991), physiological (Naya et al., 2001), and lesion (Murray and Bussey, 1999) evidence in primates strongly indicates that the avTL can also be viewed as the highest level of the ventral visual object processing stream. A role in language processing is implied by the avTL atrophy that characterizes semantic dementia (Hodges et al., 1992) and the avTL hemodynamic activation evoked by semantic processing (Devlin et al., 2002). In primates, the avTL is reciprocally connected with cortical areas that may be homologous to Wernicke's and Broca's areas (Insausti and Amaral, 2004).

As the ventral object processing stream proceeds in the anterior and medial directions, stimulus characteristics evoking cellular responses in macaques become more complex and abstract and ultimately appear to be associative. This increasing complexity lies on an unbroken continuum of visual processing with the more posterior visual areas. In contrast, the vivid memories evoked by avTL hyperactivation (Halgren et al., 1978b), as well as its crucial anatomical position relaying hippocampal formation output to association cortex, suggest a countercurrent return of information during memory retrieval from more medial structures (Buzsaki, 1996; Halgren, 1984; Merker, 2004; Qin et al., 1997).

These characteristics suggest a sequential evolution of neural information flow in the feedforward and then feedback directions. An overview of the spatiotemporal processing pattern that these pathways engage during verbal tasks can be found in the event-related potentials (ERPs) recorded locally by electrodes implanted for clinical purposes in epileptics. These studies typically find a more posterior peak at ~200 ms possibly associated with word-form processing and a later more anterior peak at ~400 ms that is related to semantic manipulations, termed the N400 (Halgren et al., 1994; McCarthy et al., 1995; Smith et al., 1986). Event-related magnetoencephalographic (MEG) responses in normal subjects, with similar latency and repetition effects, appear to arise in the same location (Dale et al., 2000; Dhond et al., 2003; Marinkovic et al., 2003), and the cognitive correlates of the N400 have been confirmed and extended in normal subjects using scalp-recorded ERPs (Kutas and Federmeier, 2000).

One interpretation of these studies is that an initial wave of activity passes quickly through the avTL and then is followed by sustained activity in all areas, continuing until well past the behavioral response (Dale et al., 2000; Halgren et al., 1994). However, the spatial resolution of ERP/MEG or even intracranial macroelectrode recordings is insufficient to determine if widespread extended areas are truly active during this entire period or if different areas are active at different latencies, but they are too close to be resolved. Similarly, these techniques lack the physiological resolution to distinguish synaptic inhibition from excitation, so simultaneous activity could actually represent inhibition in some areas and excitation in others. Finally, although ERPs and MEG are the direct instantaneous result of transmembrane currents caused directly or indirectly by synaptic activity, the presynaptic cell at the origin of that synaptic activity is difficult to infer, although this is crucial for functional interpretation.

These issues have been partially addressed in macaques, where the latencies and durations of unit responses in ventral visual stream areas imply their sequential then simultaneous activation, and the delayed onset of distinctive unit responses to certain visual stimulus distinctions suggests that some processing may require

feedback interactions (Lamme and Roelfsema, 2000). However, others argue that macaque data support extraction of high-level information already in the first pass (VanRullen and Thorpe, 2002). In any case, the relation of unit responses in macaques to field potentials in humans is unknown, due not only to differences in the physiological measures, but also to the lack of language in macaques and to the substantial expansion of avTL areas in evolution.

The current study used a novel technique in humans that is capable of localizing transmembrane currents and multiunit activity not only to particular cortical areas, but also to different layers in those areas. Since feedforward and feedback information flow tends to involve different cortical layers (Barbas and Rempel-Clower, 1997; Felleman and VanEssen, 1991), these data lead to hypotheses regarding the sequence of network interactions between and within these areas and their relationship to more macroscopic measures. Recordings were made during overt word recognition as well as during implicit repetition during semantic tasks. The initial wave of activity through IT and PR appeared to reflect feedforward EPSCs in middle cortical layers and was followed by apparent EPSCs that may represent feedback and/or associative processes. Consistent with non-invasive recordings, only the later stages in IT and PR showed repetition suppression. In contrast, ER showed repetition enhancement. These results suggest a spatiotemporal sequence of information processing supporting word processing, with repetition inducing facilitated processing in lateral structures and explicit recollection in medial.

## Materials and methods

### *Subjects and probes*

Three patients with long-standing pharmaco-resistant complex partial seizures participated after fully informed consent according to NIH guidelines as monitored by the local Institutional Review Board. Participants were implanted with depth electrodes (Fig. 1) in order to localize their seizure focus and thus direct surgical treatment (patient 1: male, 30 years old; pt. 2 female, 35 years old; pt. 3 male, 35 years old; all right-handed, with normal intelligence and personality). Clinical electrodes were modified to be smaller diameter (350  $\mu\text{m}$ ) in a 5 mm segment at their tips, containing 24 90%Pt–10%Ir contacts, each 40  $\mu\text{m}$  in diameter and separated by 110  $\mu\text{m}$  (Ulbert et al., 2001a). Simultaneous recordings from macrocontacts on the clinical electrodes were obtained in Pt3. The macrocontacts consisted of 1.3 mm diameter cylinders, each 1.5 mm long and separated from the next contact by 3.5 mm. MRIs taken with the probes in place (Fig. 1) show the tip to lie: in patient 1 in anteroventral IT; in patient 2 in PR; and in patient 3 in ER (Insausti and Amaral, 2004). Laminar contacts in gray matter, white matter, and CSF have characteristic activity patterns, permitting resolution of their entry and exit points. The recorded macrocontacts in patient 3 were located in the crown of the inferior temporal gyrus (probable IT) on the left and fundus of the collateral sulcus (in or near PR) on the right. Structural MRI and/or histological examination of the surgical specimen were normal except for right hippocampal sclerosis in pt. 3. Seizure onset was found to lie outside of the locations reported here: right frontal in patients 1 and 2; right amygdala in patient 3. The decision to implant the electrode targets and the duration of implantation were made entirely on clinical grounds without reference to this experiment.

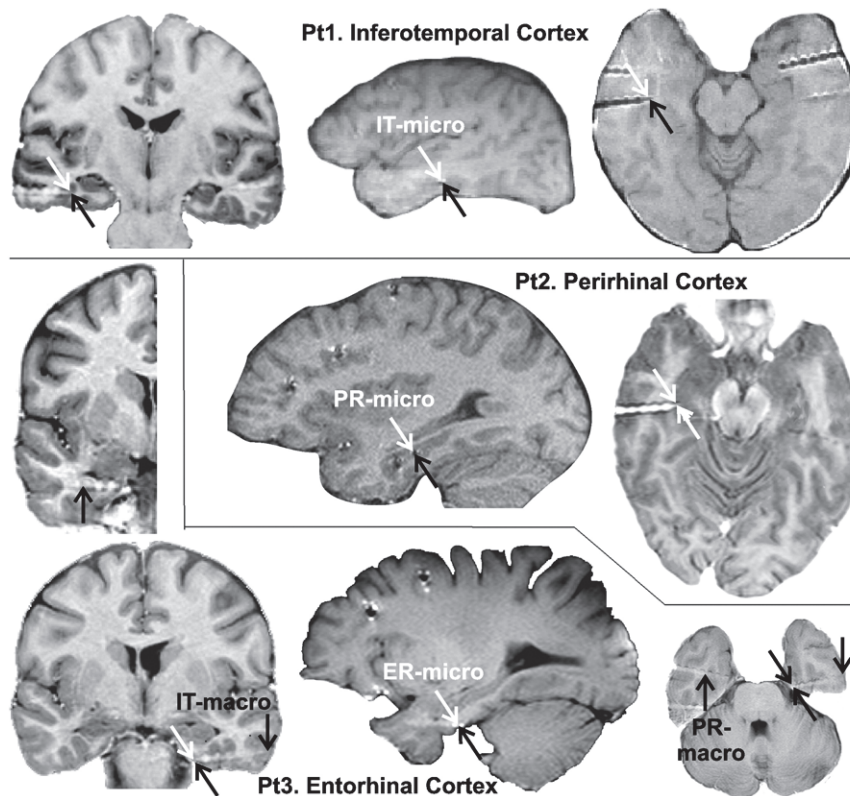


Fig. 1. Locations of recording sites in MRIs taken with the electrodes in situ. Laminar probes are indicated by oblique arrows and macroelectrode contacts by vertical arrows. The white MRI artifacts lateral to the probes are due to the clinical contacts (larger than the actual electrodes). Patient 1, inferotemporal cortex (IT): laminar tip in the lateral aspect of the right fusiform g., medial bank of lateral occipito-temporal s. (coordinates 38 lateral, 22 posterior, 11 down) (Talairach and Tournoux, 1988). Patient 2, perirhinal cortex (PR): laminar tip in the lateral aspect of the right parahippocampal g., medial bank of collateral s. (coordinates 31, -22, -16). Patient 3, entorhinal cortex (ER): laminar tip in the medial aspect of the left parahippocampal g. (coordinates -23, -17, -25). The left macroelectrode (↓) is in the crown of the inferior temporal gyrus (probable IT) and the right macrorecording (↑) is in the fundus of the collateral sulcus, in or near PR. Some MRIs are displayed with inverted contrast to maximize electrode visibility.

### Recordings and analysis

Differential recordings were made from 23 pairs of successive contacts, at 2 kHz (16 bit) sampling rate for CSD and 20 kHz (12 bit) for MUA, and stored continuously with stimulus markers. Population transmembrane current flows were estimated using CSD analysis (Nicholson and Freeman, 1975), calculated as the second spatial derivative of field potentials (0.5–30 Hz) after applying a 5-point Hamming filter (Ulbert et al., 2001a). Although the transmembrane currents localized with CSD are generally interpreted as due to transsynaptic currents (Mitzdorf, 1985), voltage-gated currents may also contribute (Murakami et al., 2002). One-dimensional CSD analysis assumes that the cortical transmembrane currents are radially symmetrical around the electrode track. While cortical currents are thought to be primarily perpendicular to the local surface (Mitzdorf, 1985), neurons in layer II of ER are arranged in islands, ~200  $\mu\text{M}$  in diameter, separated by cell-free zones (Insausti and Amaral, 2004). These islands could result in the unpaired sources and sinks seen in CSD from superficial ER (see Fig. 4). CSD analysis also assumes that conductivity is uniform and isotropic in the tissue immediately surrounding the probe. This assumption has been tested in the HC where deviations from the homogeneous approximation were found to be too small to influence the spatial distribution of sources and sinks (Holsheimer, 1987). Variable electrode spacing or potential amplification could produce

spurious CSD signals, but these effects were evaluated experimentally in our system and found to be less than 5% (Ulbert et al., 2001a). CSD analysis will miss transmembrane currents if they do result in a net radial extracellular current, as might happen if they are produced by synapses on spherically symmetrical dendritic domains. CSD will also fail to detect currents that flow over distances that are small relative to the spatial sampling density. Modeling and experimental measures indicate that the center-to-center contact spacing of 150  $\mu\text{M}$  used in the current study is adequate to sample laminar CSD in macaque primary visual cortex (Schroeder et al., 1998; Tenke et al., 1993). The limiting factor was the dendritic domains of stellate cells in thalamorecipient layer IVc. Cortex is thicker in humans, and the sampled areas are not known to have a thin but important sublayer comparable to IVc. Nonetheless, it is likely that the CSD analysis reported here is relatively insensitive to synaptic activity on layer IV stellate cells. Finally, current sources or sinks can be missed if the laminar probe does not sample the entire cortical depth. This provides another possible explanation for the unpaired sinks and sources noted in ER.

Population neuronal firing (MUA) was estimated by rectifying high frequency activity (300–3000 Hz) and smoothing with a 50 Hz low pass filter (Ulbert et al., 2001a). MUA was not recorded in pt. 1 due to interference from the clinical telemetry system. Statistical significance of the difference between conditions for a particular recording channel, latency, and measure (CSD, MUA, or

spectral power), was assessed using a *t* test of values from individual trials. Significant deviations of responses from baseline were assessed using 1-sample *t* tests of values from each trial. Threshold was set at  $P < 0.01$  (2-tailed).

### Tasks

Subjects viewed single words presented on a computer monitor in Geneva font as white letters on a black background in the central ~5% of visual angle. Stimulus exposure was 240 ms, and stimulus onset asynchrony was 2400 ms unless otherwise noted. The monitor was controlled, and keyboard response accuracy and latency were monitored, by MacProbe software (Hunt, 1994). Subjects remained in their hospital room under videotelemetry during the recordings.

All subjects performed the Word Recognition task to probe explicit recognition and the Size Judgment task to probe implicit word priming:

#### Word recognition (all patients)

Initially, the subjects were instructed to memorize 10 words, each presented 3 times. These words were then presented 12 times each, randomly intermixed with 120 novel words. Any given word repeated after an average delay of ~50 s and ~20 intervening stimuli. Subjects were instructed to press a key with their dominant hand within 1200 ms after presentation of a repeating word. At 1360 ms post-stimulus, a 55 ms feedback tone indicated whether the response (or lack thereof) had been correct (1000 Hz) or wrong (200 Hz). In an identical task, large potentials were recorded in the ventral temporal lobe using depth electrodes in epileptic patients (Halgren et al., 1994; Smith et al., 1986).

#### Size judgment (all patients)

Subjects pressed a key if the object or animal that the word represents is usually more than one foot in its longest dimension. The 160 words that were presented only once ('new') were randomly intermixed with 10 'old' words that each repeated 16 times. Prior to the beginning of the recordings, these ten words were each presented 6 times for familiarization with the task. MEG and fMRI show avTL activation and strong repetition effects in the identical task (Dale et al., 2000; Marinkovic et al., 2003).

#### Supplemental tasks

Individual patients also performed other supplemental tasks, and these results are shown when they help explicate the responses to the Word Recognition and/or Size Judgment tasks.

Abstractness Judgment/Delayed Retrieval (patient 2) tests explicit retrieval, like Word Recognition, but with a longer delay and less repetition. The subject initially made Abstractness Judgments on 480 visually presented words, without being aware that she would later be tested for recognition. Word presentation was 700 ms. Following a 20–30 min break, the subject underwent a Delayed Retrieval test phase, where she was shown 960 words, including the 480 previously shown ("Old"). She responded with her left hand, first to indicate whether the presented word was "New" or "Old" and then to rate her confidence in her response as "High" or "Low". An unpublished MEG study by Dhond et al. inferred strong avTL activation in this task.

During the Learning phase of the Learn/Retrieve task (patient 3), 80 words were presented for study, for 300 ms each, at 2000 SOA. During Retrieval, the initial 80 words were presented again,

randomly intermixed with 80 novel words, and the subject responded to each indicating if it was novel or repeated. This task is modeled after one that has been reported to elicit medial temporal activation with fMRI (Weiss et al., 2004).

Verb Conjugation (patient 1) tests incidental word repetition, as does Size Judgment. The subject was shown 80 new (presented only once) regular verbs, 80 new irregular verbs, 5 old regular verbs (repeated 16 times each), and 5 old irregular verbs, for a total of 320 trials. Regular/irregular and new/old trials were fully crossed and randomly intermixed. Verbs were presented in the infinitive form; the subject silently generated the past tense form and lifted his left index finger if it ended in "-ED". MEG sources were inferred in the avTL in a study using the same task in normal subjects (Dhond et al., 2003).

Visuomotor (patient 3) probed simple sensorimotor processes. Targets were flashed for 60 ms in the left or right visual field in random order at ~8° of visual angle eccentricity, and the subject responded with the left or right hand under two 'Simple' instructions (press always left or right regardless of stimulus laterality) and two 'Choice' instructions (press contralateral or ipsilateral to the stimulus). Stimulus and response lateralities were thus balanced between Simple Reactions and Choice Reactions. There were 197 trials for each of these four sections. Time out for producing a key press was 1230 ms. Stimulus onset asynchrony was randomized from 1550 to 1950 ms.

#### Behavioral performance

The purpose of the behavioral tasks in the current study was not to probe the limits of behavioral performance but to elicit synchronized neuronal responses that contribute to the semantic processing or recognition of words and to observe how those responses are modulated when the word is repeated. For these reasons, each 'old' word in the main behavioral tasks was repeated 12 or 16 times during the recordings, and each had been repeated 3 or 6 times prior to the recordings. This degree of repetition assures excellent performance in all subjects with at least average intelligence and memory, as was the case for those participating in this study. Specifically, during Word Recognition, pt. 2 pressed correctly to 111 of 120 repeating words with a reaction time of  $762 \pm 204$  ms (mean  $\pm$  SD) and correctly withheld pressing to all 120 new words; pt. 3 pressed correctly to 117 of 120 repeating words with a reaction time of  $850 \pm 121$  ms and correctly withheld pressing to 119 of 120 new words. Behavioral results from pt. 1 were not available. Similar results were obtained in larger groups of epileptic patients drawn from the same population, as well as a demographically similar control group (Smith et al., 1986). Due to technical problems, behavioral results are not available for the Size Judgment task. However, in the identical task, a group of young normal subjects responded correctly to 92% of the trials at a latency of  $960 \pm 123$  ms to new words and  $760 \pm 81$  ms to old words ( $d' = 2.64$  and  $3.96$  for new and old words, respectively), demonstrating strong behavioral priming (Marinkovic et al., 2003).

As noted above, supplemental tasks were also administered to individual patients (clinical exigencies prevented recording during these tasks in all subjects). During Abstractness Judgment/Delayed Retrieval, patient 2 responded to 82% of the input trials correctly at a latency of  $1131 \pm 329$  ms and to 65% of the recognition trials correctly at a latency of  $2669 \pm 1611$  ms to hits and  $1993 \pm 1800$  ms to correct rejects. This is similar in accuracy but slower than a group of normal subjects who on the same task responded correctly to 86%

of the input trials at a latency of  $1104 \pm 128$  ms and correctly to 65% of the recognition trials at a latency of  $1104 \pm 104$  ms to hits and  $1274 \pm 117$  ms to correct rejects (Dhond et al., unpublished). Behavioral results are not available for the single subjects who performed Learn/Retrieve and Verb Conjugation. However, in the identical Verb Conjugation task, a group of young normal subjects responded correctly to 96% of the trials at a latency of  $954 \pm 114$  ms to new words and  $841 \pm 112$  ms to old words, demonstrating strong behavioral priming (Dhond et al., 2003). In the Visuomotor task, patient 3 responded to 97% of the Simple trials correctly at a latency of  $325 \pm 15$  ms and to 98% of the Choice trials correctly at a latency of  $739 \pm 98$  ms. In summary, the patients performed in the normal range consistent with their cognitive status. The main tasks, Word Recognition and Size Judgment, utilize multiple repetitions of a group of 10 old words to strongly distinguish their behavioral and neural responses from those evoked by randomly intermingled new words that are each presented only once.

## Results

### Inferotemporal cortex (IT)

#### Current source density (CSD) recordings of synaptic responses to words

CSD was calculated from the linear array of closely spaced microelectrode contacts in order to estimate the time course of synaptic activity in different cortical layers. In Fig. 2, upper panel,

the CSD recorded in three tasks is shown in color maps of cortical depth versus time after stimulus onset. Red indicates current sinks, locations where the local transmembrane current flows into the cells, as happens at excitatory synapses. Blue indicates current sources, where the current flows out of the cell. In the lower panel of Fig. 2, waveforms from the middle and superficial cortical layers are shown.

The columns of Fig. 2 show the responses during three tasks. In all tasks, subjects viewed words and made a key-press to the target category, which occurred on 50% of the trials. In all tasks, half of the words were new, occurring only once in the task and the other half were old from a small set of repeating words. Responses are compared between an overt Word Recognition task and Size Judgment or Verb Conjugation tasks where repetition is incidental. Separate color maps and waveforms are shown for new and old stimuli, for each of the three tasks.

#### Initial middle layer sink

In all tasks and to new and old words, activation begins with a sharp sink in putative layer IV, arising abruptly from the baseline (marked with a in the contour plot and waveforms in Fig. 2). This sink peaks at  $\sim 180$  ms and is accompanied by a source in layer II/III (a', Fig. 2). A *t* test found that the responses significantly ( $P < 0.01$ ) deviated from baseline by  $\sim 120$  ms after stimulus onset. In upper layer IV, to old words, this sink inverts in  $\sim 100$  ms to a source. However, to new words, the sink is prolonged (b, Fig. 2), but it continues to be associated with a source in layers II/III (b', Fig. 2). The prolonged sink in layer IV to new words results in a

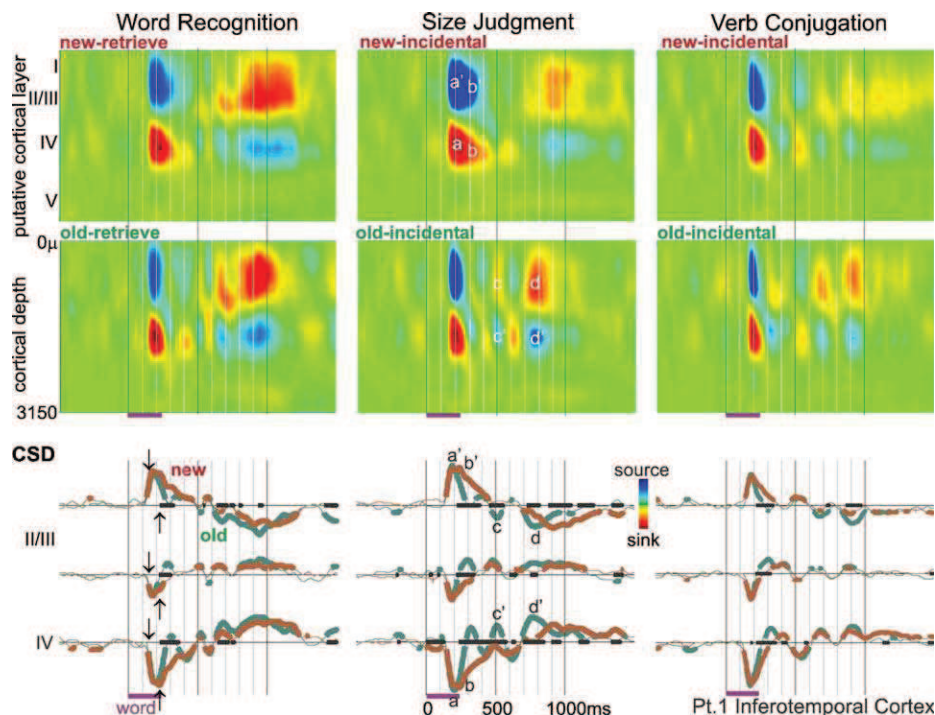


Fig. 2. Inferotemporal population synaptic activity evoked by words in memory tasks. Responses to Word Recognition, Size Judgment, and Verb Conjugation are arranged in columns. Averaged CSD color maps (upper two rows) show an initial transmembrane current sink in putative layer IV (red area, a), with a return source in more superficial layers (blue area, a'). These sinks and sources are longer duration to new words (b, b'). The sink may invert to a source, and vice versa, several times from  $\sim 300$  to  $800$  ms (c, c'), culminating in a sustained superficial sink (d) and middle layer source (d'). The same phenomena can be seen in the averaged CSD waveforms from selected superficial and middle layers in the lower 3 rows. Purple bars below *x* axes indicate word presentation periods. The *x* axis is thickened when new and old words evoke significantly different activity; CSD waveforms are thickened when significantly different from zero (2-tailed  $P < 0.01$ ). The synaptic response begins at  $\sim 120$  ms ( $\downarrow$ ), but differential activity to word repetition does not begin until  $\sim 220$  ms after stimulus onset ( $\uparrow$ ).

divergence in the response to new versus old words at  $\sim 220$  ms after stimulus onset ( $P < 0.01$ ). Thus, evoked activity was identical to new and old words for the initial  $\sim 100$  ms.

#### Later responses

In putative layer IV, the initial sink is followed by alternating sources and sinks until  $\sim 800$  ms (e.g., c, Fig. 2). These middle layer sources and sinks are matched by upper layer sinks and sources (e.g., c', Fig. 2). Examination of the waveforms and color maps to old words reveals three peaks in the putative layer IV current sink, at  $\sim 200$ , 400, and 600 ms, with variable merging of these peaks into a single sustained sink to new words. These variable alternating sources and sinks culminate in a prominent sustained sink in superficial cortical layers in all tasks to new and old words, generally from  $\sim 700$  to 1200 ms after stimulus onset (d, Fig. 2). It is accompanied by a source in middle cortical layers (d', Fig. 2).

#### Perirhinal cortex (PR)

##### Simultaneous synaptic (CSD) and cellular (MUA, multiunit activity) responses to words

CSD and MUA responses in PR during the overt recognition and incidental repetition tasks are illustrated in Fig. 3. Similar

patterns are evoked by all tasks. As in IT, synaptic activity in PR begins with a sink in putative layer IV at  $\sim 120$  ms. The initial sharp component of this sink peaks at  $\sim 150$  ms, lasts  $\sim 100$  ms, and is accompanied by a sharp source in more superficial layers. This initial sharp sink is usually continued with a smaller sustained sink in putative layer IV until  $\sim 500$ – $700$  ms. Sinks are also present in superficial layers at longer latencies. This is especially clear during Size Judgment, where the superficial sink peaks at  $\sim 600$  ms.

MUA, recorded simultaneously with CSD in PR, was most prominent in deeper layers, where it showed a monotonic increase from  $\sim 130$  ms to  $\sim 700$ – $1200$  ms. MUA in putative layer IV showed a sharp increase simultaneous with the local initial sink then a smaller prolonged response peaking at  $\sim 400$  ms.

When CSD current sinks are generated by excitatory post-synaptic currents (EPSCs), they generally are accompanied by passive return current sources (Nicholson and Freeman, 1975). Conversely, at the normal depolarized state of cortical neurons (Destexhe et al., 2003), inhibitory post-synaptic currents (IPSCs) could produce active current sources, and they would be accompanied by a passive current sink. Thus, the initial pattern of sources and sinks shown in Fig. 2 could represent either an

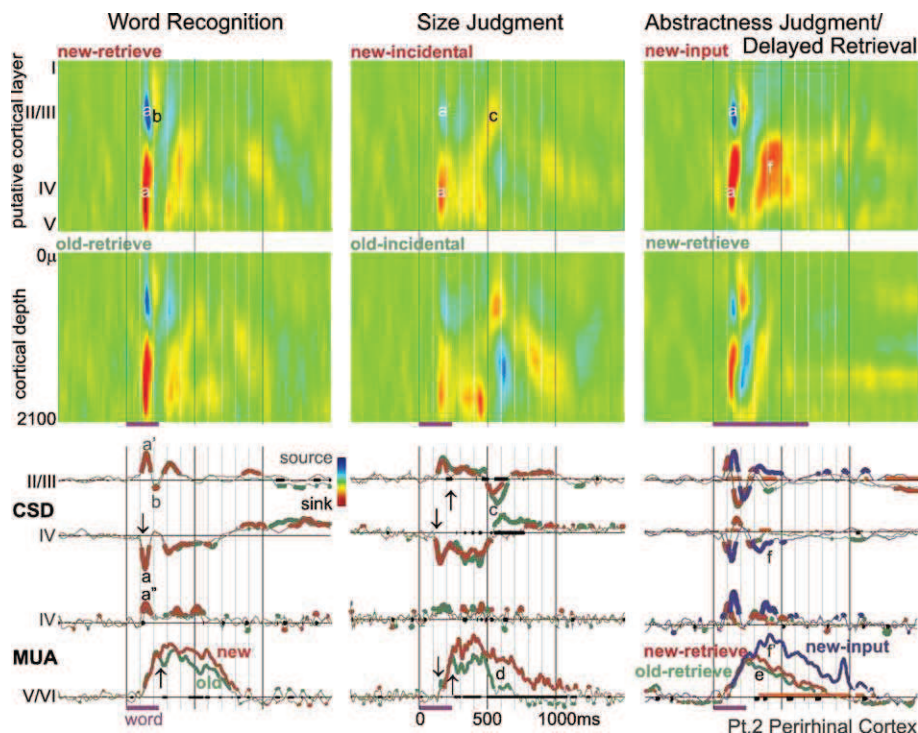


Fig. 3. Perirhinal activity during memory tasks. Words evoke an initial sharp middle layer transmembrane current sink (a) and superficial source (a'), seen in the CSD color maps (upper two rows) and waveforms (middle two rows). The sink likely represents a population EPSC since it is associated with increased population firing (lower two rows), especially in the middle layer (a'). This is followed by a sink in superficial layers (b) and then a variable activity including a very late superficial sink during Size Judgments (c). Population firing and synaptic activity begins at  $\sim 120$  ms ( $\downarrow$ ), but differential activity to word repetition does not begin until  $\sim 220$  ms after stimulus onset ( $\uparrow$ ) when new words evoke stronger sustained firing in deep layers until 800–1100 ms (d). Similar patterns are observed regardless of whether word repetition is explicit (Word Recognition, first column) or implicit (Size Judgment, second column). The third column also shows an explicit word recognition task, but with a single word presentation during Abstractness Judgments and an  $\sim 1$  h delay before Delayed Retrieval. In Word Recognition and Size Judgment, old words are seen several times with delays of  $\sim 1$  min. Although the repetition effect is smaller and later in Delayed Retrieval, it is still present (e). Note that, compared to new words during the output period, new words during the input task evoke a larger middle layer sink (f) and more population firing (f'). The x axis is thickened when responses to new and old words are significantly different from each other; CSD and MUA waveforms are thickened when they are significantly different from zero (2-tailed  $P < 0.01$ ). The thick orange baseline indicates significant differences between responses evoked by new words at input versus retrieval.

EPSC in putative layer IV or an IPSC in putative layers II/III. This ambiguity is not present in the recordings shown in Fig. 3, where the simultaneous MUA strongly increases from baseline, implying that the current sinks represent EPSCs rather than passive current returns.

*Decreased responses to repeated words, across different delays, number of repetitions, and task instructions*

PR was also similar to IT in demonstrating decreased activity to repeated words (Fig. 3). These effects were not apparent in the traces and did not become significant until ~220 ms, i.e., ~100 ms after response onset. In PR, the most striking effect of repetition was a decrease in MUA in deep layers. This effect, as well as a decrease in putative layer IV synaptic currents, was significant even after a single repetition of a word, ~1 h after the initial presentation (DR, Fig. 3). No differences between subsequently remembered versus not remembered words were found.

Again, as for IT, the effects of repetition in PR were similar regardless of whether they were targets in a recognition task or repetition was incidental in a size judgment task (Fig. 3). In both MUA and CSD measures, the effects of repetition in the incidental memory condition were larger and more sustained than in the explicit recognition task, even though they used similar stimuli (words), exposures, delays, and repetitions and were performed on the same day. It is possible that this observation is due to greater depth of processing during the semantic task. In any case, this effect shows that an overt memory task is not necessary in order for repetition suppression to be observed in PR.

Furthermore, the task of explicit retrieval does not specifically drive PR activity, as shown by a comparison of responses during Abstractness Judgment, to those during Delayed Recognition of the same words an hour later (Fig. 3). Larger synaptic and unit responses are observed during the input semantic task, as compared to explicit retrieval, when comparing only novel words in both conditions.

*Origin of the long latency repetition effect*

The clearest repetition effects were noted during Size Judgment, which thus offers the clearest opportunity for examining the relationship of synaptic and neuronal activities in producing repetition effects. The sustained long duration MUA increase to new words in deep layers is associated with a simultaneous sink in middle and deep layers (Fig. 3). This sink greatly decreases (and may even invert to a source) for old words at ~500 ms, at the same time that the MUA also becomes markedly smaller to old words, suggesting that the later part of the repetition effect is associated with a decreased excitatory drive to the lower cortical layers.

To summarize, the response in PR appears to have three phases: (1) an initial biphasic response from ~120 to 220 ms that is not modulated by repetition, consisting of a layer IV sink–source (mirrored by superficial and deep source–sink sequences), and associated with a brief layer IV MUA increase; (2) a sustained layer IV sink from ~250 to 500 ms accompanied by a sustained plateau of deep layer MUA, both of which are moderately changed by repetition; and (3) a deep sink and MUA to new words from ~500 to 1100 ms, and relatively little or even opposite activity to old words (the last phase is most clear during Size Judgment).

*Entorhinal cortex (ER)*

*Overall pattern of synaptic and unit responses in deep and superficial layers*

In all tasks, the initial synaptic activities in ER are CSD sinks in superficial (II/III) as well as deep (V/VI) layers (Fig. 4). Both sinks usually start before 200 ms, and the deeper sink is typically smaller and slightly earlier. Both sinks are sustained until ~500 ms (range ~400–800). The deep sink is surrounded by weaker sources, whereas the return source for the superficial sink is presumably in more superficial layers that were not sampled in these recordings. Both deep and superficial sinks are followed by sources in the same layers, beginning at 400–800 ms after the stimulus (depending upon the task and condition) and continuing in the overt word recognition tasks until more than 1500 ms after stimulus onset. The deep source was in all cases surrounded by sinks; the sink corresponding to the superficial source again appeared to be absent due to inadequate sampling.

Distinct patterns of MUA activity were noted in deep versus superficial layers, most clearly during Word Recognition. In putative layers II/III, the time-course (peak, duration and shape) of the MUA closely resembles that of the local current sink, implying that it represents a population of EPSC. However, in putative layers V/VI, while the initial peaks of the MUA and the local sink correspond, overall, the MUA response is much more prolonged (>1500 ms) than the local sink (~700 ms). The deep MUA may be related to the prolonged sink in intermediate depths that occurs in most tasks. This intermediate level sink begins at ~400–800 ms and continues for ~500–1000 ms, depending on the task and condition.

*Increased synaptic and unit responses to repeated words*

As in IT and PR, CSD and MUA in ER are indistinguishable between new and old words for the initial ~100 ms of the response. However, unlike the pattern described above in IT and PR, in ER, old words consistently evoked more synaptic and unit activity than did new words following this initial period. The increased activity in Word Recognition consisted of a later and larger peak of neuronal firing in both superficial layers (peak at ~300 ms to new and at ~350 ms to old words) and in deep layers (peak ~300 ms to new, ~700 ms to old words). The MUA response duration was also longer to old as compared to new words, ending ~100 ms later in superficial layers (at ~700 ms) and >1000 ms later in deep layers (after 1600 ms). The sinks in both superficial and deep layers were also larger, peaked later, and lasted longer to old compared to new words, as did the subsequent sources in both layers. These differences appeared to be true in all three tasks examining word repetition effects (with the caveat that good MUA recordings were only obtained in the Word Recognition task). The fact that there is a larger response to the old words both in the Word Recognition task (where the old stimuli are targets) and in Learn/Retrieve (where both new and old stimuli are targets) means that targetness is not the critical factor in evoking the greater response to olds. The response during Size Judgment to implicit repetition was markedly less than that to explicit repetition, unlike what has been described above for the same comparison in IT and PR.

*Larger responses during retrieval than during learning*

In addition to the larger response to old stimuli, activity in ER was distinguished by the larger response overall in tasks that

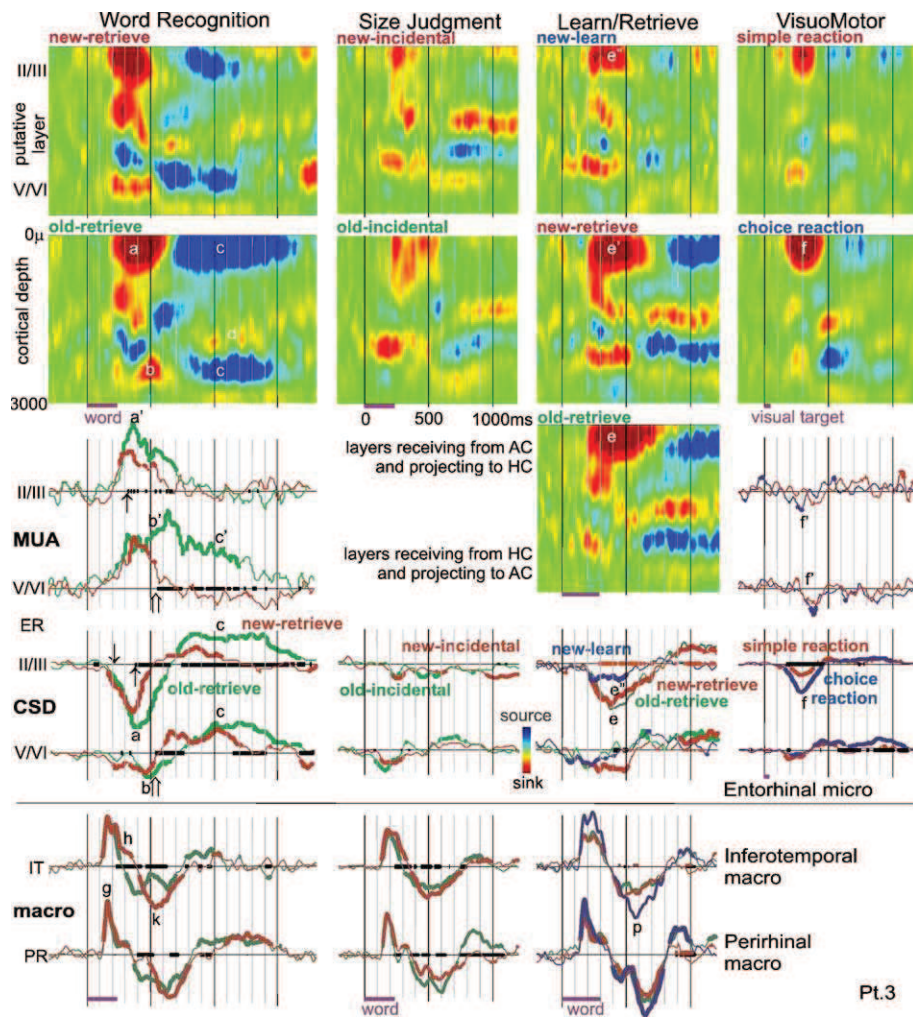


Fig. 4. Entorhinal population synaptic activity and neuronal firing. CSD color maps (upper rows) show the spatiotemporal patterns of population synaptic activity across four tasks (arrayed in columns). Waveforms below CSD maps show simultaneous MUA, CSD, and macroelectrode recordings (third through fifth rows). The most prominent early activity during explicit Word Recognition is a superficial sink starting at  $\sim 200$  ms (l) and peaking at  $\sim 370$  ms (a) with strongly increased firing in superficial and deep layers (a'). Sinks in deeper layers (b) with accompanying MUA (b') also occur during this time. Both deep and superficial sinks are followed by sources in the same layers (c), beginning at  $\sim 700$  ms after the stimulus and continuing for  $\sim 900$  ms. The deep source is surrounded by sinks (e.g., d). Population firing in deep layers continues at a high level during this period (c'), whereas that in superficial layers returns to baseline. All components of the response are larger to old as compared to new words, with the CSD and MUA responses diverging in superficial layers at  $\sim 300$ – $400$  ms ( $\uparrow$ ) and in deep layers at  $\sim 500$ – $600$  ms ( $\uparrow$ ). A broadly similar but substantially weaker spatiotemporal pattern is seen to implicit word repetition during Size Judgments (second column). In Learn/Retrieve (third column), subjects were explicitly asked to memorize the words during Learn and then were presented with forced-choice explicit recognition. In addition to showing a larger synaptic response to old (e) as compared to new (e') words during Retrieval, the response is larger to new words during Retrieval (e') as opposed to new words during Learn (e''). In the fourth column, choice VisuoMotor reactions evoke a similar superficial sink (f) as in Word Recognition, but with less than half the amplitude or duration (a). The difference in neuronal firing is more striking, with VisuoMotor reactions evoking a decrease in firing (f'), whereas Word Recognition evokes a sustained increase (a', b', c'). Bipolar potential recordings from macroelectrodes in left IT and right PR show distinct spatiotemporal patterns that resemble the IT and PR laminar recordings, beginning with a sharp initial peak before 200 ms (g) followed by two components from  $\sim 240$  to 620 ms (h, k) that distinguish new and old words. In contrast to the ER laminar recordings, IT and PR potential gradients are largest during Learning (p). The x axis is thickened when two conditions evoke significantly different activity (black lines for new versus old words, or choice versus simple reactions; orange lines for new-learn vs. new-retrieve in Learn/Retrieve); CSD and MUA waveforms are thickened when each is significantly different from zero (2-tailed  $P < 0.01$ ). MUA responses are only shown for Word Recognition and VisuoMotor tasks because they were given on the first day of testing when the MUA recordings were higher quality. Macroelectrode recordings were not obtained for the VisuoMotor task.

required the overt retrieval of recently stored representations. This is illustrated in the Learn/Retrieve task, where the current sink evoked during learning is much smaller than that evoked during retrieval. This smaller response remains after controlling for repetition, i.e., when comparing new words during learning with new words presented during recognition testing (Fig. 4).

#### *Weak but differential responses during choice reactions*

The memory tests given in the current study all presented words visually and required a key press response. The possible effects of these stimulus–response aspects of the testing situation on ER activity were probed with a test that lacked words or word repetition but possessed the other formal properties of the memory

tasks. In VisuoMotor, the subject makes a key press response depending on the properties of a simple visual stimulus. In some blocks, the responses are always the same (Simple) and in others the laterality of the response depends on the laterality of the stimulus (Choice). Choice-related unit responses were previously noted in this region in humans (Halgren, 1991; Halgren et al., 1978a; Heit et al., 1990), and animal studies suggest that the HC may be crucial for rapidly learning arbitrary sensorimotor mappings (Dybvik and Bland, 2004; Wise and Murray, 1999).

The overall pattern of synaptic activity evoked by VisuoMotor was similar to that evoked by the memory tasks (Fig. 4, compare CSD contour maps in the first and fourth columns), and the synaptic response in superficial layers was about twice as large when a choice reaction was being made, as opposed to a simple reaction. However, the CSD response was about three-fold smaller during visuomotor Choice reactions, and the duration of the response was shorter than during recognition judgments. Furthermore, the MUA response to VisuoMotor was a brief decrease relative to baseline, whereas the MUA response during Word Recognition was a prolonged increase. These data suggest that some aspects of making a choice may weakly engage ER.

#### *IT and PR recordings show repetition suppression simultaneous with ER repetition enhancement*

The laminar responses recorded in IT and PR were consistent with recordings from intracranial macroelectrodes in similar locations during the same tasks, both in the timing of the different field potential components and in the suppression of the major component peaking at ~400 ms by word repetition (Halgren et al., 1994; Smith et al., 1986). Generators with similar latencies, locations, and repetition correlates have also been inferred from MEG in the same tasks (Dale et al., 2000; Marinkovic et al., 2003). Repetition suppression is also commonly found in macaque unit recordings from IT and PR (Miller and Desimone, 1994; Xiang and Brown, 1998). In contrast to the repetition suppression of IT and PR CSD/MUA, the repetition enhancement of ER CSD/MUA was not expected from previous recordings. Since only a single ventral temporal area was recorded with laminar probes in each subject, this raises the possibility that ER repetition enhancement could reflect an idiosyncratic response of the subject rather than a characteristic property of ER.

In order to evaluate this possibility, bipolar macroelectrode recordings were obtained in or near left IT and right PR simultaneously with laminar recordings from ER in patient 3 (electrode sites shown in Fig. 1, recordings in Fig. 4). The potential gradients inverted both medially and laterally at the adjacent contact pairs, strongly implying local generation. These areas showed typical ventral temporal IT or PR responses, with an initial sharp component peaking prior to 200 ms that is identical to new and old words. This is followed by a large peak that resolves more quickly to old words, with the new/old difference visible as an inflection beginning at ~240 ms. Furthermore, a larger macro-IT and PR response is seen during Learn than Retrieve segments of a memory task. Thus, in their latency, repetition suppression, and response during Learning, the IT and PR macrorecordings in pt. 3 resemble previously reported IT macrorecordings in large numbers of subjects, as well as the IT and PR laminar recordings in pts. 1 and 2, but they contrast with the simultaneous ER laminar recordings in pt. 3. Thus, the repetition enhancements and long latencies seen in the laminar ER recordings do not appear to be due

to a patient-specific abnormal response. Nonetheless, further replication of this finding is needed.

## Discussion

The current study provides a high resolution window into the functional activity in avTL during memory and related tasks. Multiple stages of cortical response were present in all three structures examined, the inferotemporal (IT) and perirhinal (PR) cortices laterally and the entorhinal (ER) cortex medially. These stages followed the pathways of inter-areal and intracolumnar cortico-cortical projections previously established in animal studies. Repetition suppression in IT and PR, with repetition enhancement in ER, suggests that the former may be more involved in incidental priming embedded in semantic processing, whereas the later is more involved in active retrieval.

#### *Intracolumnar and intercolumnar circuitry of word processing*

Synaptic activity in IT and PR begins at ~120 ms with a sink in putative layer IV, lasting ~100 ms and accompanied by a sharp source in more superficial layers. This initial sink, peaking before 200 ms, is usually followed by a sustained sink in putative layer IV until ~500 ms or more and then by a sink in more superficial layers peaking at ~600–900 ms. In PR, the sinks are associated with an initial increase in neuronal firing in layer IV and a sustained increase in neuronal firing in layer V. This spatiotemporal pattern of current sinks and increased firing is consistent with an initial phasic layer IV EPSC followed by long-lasting EPSCs first predominantly in layer IV and then layers II/III. The initial phasic EPSCs may be mainly in the dendrites of layer IV granule cells, with later sustained EPSCs involving the superficial dendritic domains of layer V/VI pyramidal cells.

This basic pattern of an initial layer IV sink followed by a sink in more superficial cortical layers has been repeatedly observed in response to visual, somatosensory, and auditory input in animals (Barth and Di, 1990; Schroeder et al., 1998), suggesting engagement of a canonical cortical circuit. Anatomically, layer IV receives input from thalamic relay nuclei or ('lower') areas closer to primary cortex (Barbas and Rempel-Clower, 1997; Felleman and VanEssen, 1991). Layer IV cells project locally to other layer IV cells as well as to layer II/III cells, which in turn project to layer V/VI. The layer II/III pyramids project onward to higher cortical areas, and layer V/VI pyramids project back to the superficial layers of lower cortical areas. Superficial layers also receive local recurrent collaterals. Intracellular (Shao and Burkhalter, 1999; Thomson and Bannister, 2003) and voltage-sensitive dye (Petersen and Sakmann, 2001) recordings in cortical slices confirm that these intra- and intercolumnar projections are excitatory and effective, as do limited recordings in vivo (Mignard and Malpeli, 1991). In vitro studies of the rat visual cortex show that feedforward projections are characterized by sharp excitation followed by immediate inhibitory feedback, whereas feedback is characterized by polysynaptic weaker but more sustained excitation that may be capable of overcoming simultaneous sustained inhibition, especially when feedforward and feedback paths are simultaneously active (Shao and Burkhalter, 1999). This 'countercurrent' pattern of convergent feedforward excitation carrying stimulus-specific information, and feedback excitation carrying contextual information, has been

proposed as a general organizing principle of cortical function (Merker, 2004).

Specific studies of the avTL in animals tend to confirm the general plan of cortical connectivity noted above (Lavenex et al., 2004). Laminar recordings in PR (BA36) to neocortical stimulation in the isolated guinea pig brain show an initial middle layer current sink followed by a superficial layer sink (together with middle layer source). Intracellular recordings show that the initial sink is due to monosynaptic EPSPs, and the later is due to polysynaptic EPSPs (Biella et al., 2001). Conversely, PR (BA36) projects widely to layer I in IT (Lavenex et al., 2002) and also within itself (Suzuki and Amaral, 1994). These studies suggest that the initial middle layer sink noted in the current study represents excitatory input from lower cortical areas; the following middle layer sink represents a period when the predominant excitatory input is feedforward, and the final superficial layer sink a period when top-down and local association afferents predominate.

The delay for the sink to rise from middle to upper cortical layers was as long as ~500 ms in the current study, whereas, in human interictal spikes, it is ~20 ms (Ulbert et al., 2004). Comparable delays have been found in animal sensory areas (Barth and Di, 1990; Schroeder et al., 1998) and human V2 (personal observation). Closer examination of the period between the initial layer IV sink and late layer II/III sink reveals that, although a sustained layer IV sink may predominate (especially to new words that need to be processed deeply), in other circumstances, an alternating series of sinks in middle and superficial layers may be revealed. Thus, the dominance of feedforward, feedback, and associative interactions may alternate in a manner that is sensitive to the contextual familiarity of the stimulus.

Compared to IT and PR, where a single sink appeared to dominate cortical activity at any given post-stimulus time, two or even three sinks were often simultaneously present in ER. This may reflect the fact that the superficial and deep layers of ER have quite distinct anatomical connectivity, are separated by a cell-free 'lamina dissecans,' and may be somewhat isolated physiologically from each other. The superficial ER layers receive input from PR and IT, and the duration of activity in superficial ER observed here is similar to that noted in these lateral areas. Furthermore, animal studies suggest that convergent and/or sustained activation may be necessary to evoke ER activity from PR and IT (Biella et al., 2002a) and that the presence of activity in deep layers of PR indicates that it has become sufficiently active to evoke an ER response (Kajiwara et al., 2003). In the current study, activity was simultaneously present in PR and IT, and the deep layers of PR showed strong sustained MUA, both suggesting that the lateral activation was sufficient to activate ER. Superficial ER also receives extensive projections from other parts of ER in rodents (Biella et al., 2002b). Activity in superficial ER is projected to the hippocampal formation and, after relaying through ~2–5 substructures, returns to deep ER. The much prolonged unit responses in deep ER may reflect the complexity, variety, and synaptic depth of this long positive feedback route.

Long neocortical–hippocampal feedback loops are crucial to memory models that posit formation of specific connections in the hippocampal formation associating the novel constellation of elements in an episodic event, with these connections helping to guide the retrieval of that constellation at a later time (Buzsaki, 1996; Halgren, 1984; Qin et al., 1997). The high-fidelity correspondence of the connections to the event and their ability to accurately guide event retrieval are critically dependent on the

passage of information between association cortices and HC, which must occur primarily through EC, PR, and IT. The current results show that the successive links in this multistage system are co-activated despite the difficulties found in model systems to produce such co-activation alluded to above. A comparison of the known laminar termination of connections between these areas with the laminar dynamics of apparent EPSPs suggests that these areas are participating in alternating feedforward/feedback interactions during encoding/retrieval, with the initial feedforward projection gradually evolving to a dominance of feedback projections. Memory effects only occurred during this interactive period. It is possible that the human in vivo ventral temporal lobe physiological interactions are highly selective and information-specific in a manner that cannot be replicated with electrical stimulation in anesthetized animals or in vitro.

#### *Linking synaptic processing at the quasi-columnar level to macroscopic activity measures*

The local and distant ERPs and MEG produced by a cortical column can be directly estimated from its laminar CSD pattern. Specifically, in IT and PR, the initial sharp sink in layer IV combined with a source in layers II/III would be expected to produce a surface positive local field potential peaking shortly before 200 ms, whereas the late source in layer IV combined with a sink in layers II/III would be expected to produce a surface negative potential peaking at ~600 ms. The intermediate period, dominated by a middle layer sink but with superimposed alternating sink/source patterns in middle/superficial layers, would be expected to produce a predominantly positive surface potential but with multiple peaks, including one at ~400 ms. Thus, the typical CSD pattern observed in IT and PR would be expected to produce an initial surface-positive peak at ~200 ms, a more variable positive peak at ~400 ms, and a negative peak at ~600 ms.

Consistent with the CSD pattern described above, intracranial depth electrode macrorecordings from the human avTL during the Word Recognition task typically record potentials peaking at ~200, ~400, and ~600 ms (Halgren et al., 1994; Smith et al., 1986). The peak at ~400 ms has similar task correlates and latency to the scalp-recorded N400, associated with cognitive contextual integration of words and similar stimuli. While the avTL-N400 occasionally polarity inverts across the collateral sulcus, it is largest, most reliable, and invariably negative in anterior locations immediately above the ventral surface of the anterior temporal lobe (Halgren et al., 1994; Smith et al., 1986). In contrast, when recorded in a similar task by intracranial subdural strips immediately below this surface, the corresponding potential is positive (McCarthy et al., 1995). This gross surface-positive/depth-negative field distribution inferred from intracranial recordings is consistent with the layer IV sink and layer II/III source in the ventral surface of the temporal lobe.

Major sources of the magnetic counterpart of the N400 ('N400m') have been inferred to lie in the avTL from non-invasive magnetic recordings in response to words in the same tasks as were used in the current study (Dale et al., 2000; Dhond et al., 2003; Marinkovic et al., 2003). The orientation of the inferred N400m generator is consistent with an equivalent current dipole in the temporal lobe with intracellular positive current flowing toward the neck. This would result from a layer IV sink and layer II/III source in the ventral surface of the temporal lobe, as recorded here with

CSD. Thus, recordings during the same task using non-invasive MEG, intracranial macroelectrodes, and laminar microelectrode arrays provide a consistent multi-resolution view of the N400 during semantic processing.

Intracranial as well as non-invasive recordings have also identified activity in the avTL at ~200 ms. In some limited locations, this may be specific for words or other visual categories, and the polarity of the activity is less regular (Allison et al., 1999; Halgren et al., 1994). Intracranial recordings also identify a peak following the avTL-N400, peaking at ~600 ms, that has been associated with the scalp late positive component or P3b (Halgren et al., 1994; McCarthy et al., 1995; Smith et al., 1986). The avTL-200 tends to be located more posteriorly in the ventral temporal lobe and the avTL-600 more anteriorly; however, activity over this entire range can be recorded over the entire extent of the ventral temporal lobe (Halgren et al., 1994). Similarly, peaks at ~200 and 400 ms followed by a peak of opposite polarity at ~600 ms have been inferred over the entire avTL using fMRI-biased MEG recordings during Size Judgment (see Fig. 8 of Dale et al., 2000). However, since cortical electromagnetic fields from different sources can superimpose in MEG and intracranial macro-EEG recordings, these previous results are consistent with the different temporal components of the cortical response to words being located in different cortical regions.

Both CSD and MUA decline steeply with distance. Our simulations indicate that CSD amplitude declines ten-fold in ~250  $\mu\text{m}$  (Wang et al., 2005). Theoretical and empirical studies in animals indicate that MUA should decline with distance at least as rapidly (Grover and Buchwald, 1970). Thus, the current study demonstrates for the first time that multiple processing stages over hundreds of milliseconds are generated within the same IT, PR, and EC cortical microdomains roughly corresponding to that of a cortical column.

Both anatomically constrained MEG and intracranial EEG recordings find that other structures, especially the ventrolateral prefrontal cortex, are also active during this entire time period. Taken together with the global view provided by non-invasive studies, these results suggest that words are processed through repeated activation cycles in an extended neural network that involves each of many cortical columns over sustained and cognitively varied processing stages.

#### *Repetition and retrieval effects*

Word repetition decreased the size and duration of the layer IV sink in IT and of the layer V multiunit activity in PR. Repetition suppression of the layer IV sink is consistent with it corresponding to the N400 which shows strong repetition suppression as recorded with MEG (Dale et al., 2000; Marinkovic et al., 2003) or intracranial EEG (Halgren et al., 1994; Smith et al., 1986). Decreased firing confirms similar results in macaques (Miller and Desimone, 1994; Xiang and Brown, 1998) and is consistent with the decreased hemodynamic activity evoked by repeated words in this area in humans (Buckner et al., 2000). The repetition effect was present regardless of whether repetition was task-relevant and, in fact, was largest when repetition was implicit, presumably because in such tasks encoding was relatively deep. Overall, the synaptic and cellular responses in these lateral avTL areas were largest to new words when they were deeply processed.

The repetition-induced decrease in IT and PR reported here was not present in the initial ~100 ms of the response. This is similar to

the findings of MEG in the same tasks where activity spreads to widespread frontal, temporal, and parietal areas before the repetition effects begin, more or less simultaneously, across the entire network (Dale et al., 2000; Marinkovic et al., 2003). The repetition effect seems to arise out of a sustained polysynaptic interaction of an extended trans-cortical network rather than focal plasticity in a small specific antecedent cell group. In this study, the sustained but not the phasic CSD/MUA responses to words show the repetition and semantic effects that have been seen with fMRI in the same area. In contrast, it is the phasic rather than the sustained MUA/CSD response that correlates best with the fMRI response in the human visual motion area MT+ (Ulbert et al., 2001b). These data would suggest that the relationship between synaptic currents, action potentials, and hemodynamics may vary between tasks and location.

The initial layer IV sink is ~50–100 ms in duration before it is cut off with an apparent IPSC. This initial sink probably mainly reflects glutaminergic activation of kainate receptors; the sink is too brief to dislodge the  $\text{Mg}^{++}$  ions blocking *N*-methyl-D-aspartate receptors. Thus, the initial rapid feedforward projection of activity through the visual and semantic systems may be excluded from plasticity. As a consequence, this first pass activity may not change with repetition, unlike the later components reflecting neural networks involved in sustained activity.

In striking contrast to IT and PR, putative EPSCs and neuronal firing in both superficial and deep layers of ER strongly increased to repeated stimuli. While this increase was present in tasks utilizing both implicit and explicit repetition, it was strongest in overt recognition memory tasks. Although this observation was only made in one subject and so needs further replication, within that subject, simultaneously recorded IT and PR macroelectrodes showed typical repetition suppression. When tested within a given task and after controlling for repetition, the ER synaptic and cellular response was larger during the retrieval phase, suggesting a role for ER in intentional retrieval. Increased ER firing to repeats has been observed in monkeys when the repeated stimuli are also the behavioral targets (Suzuki et al., 1997). Some hemodynamic studies have found specific medial temporal activation during intentional recall and experiential recognition over implicit repetition, and lesion studies have found a specific deficit after medial temporal lesions in the same circumstances (Yonelinas et al., 2001, 2002), but both findings are inconsistent (Squire et al., 2004). A variety of evidences in animals have led to the suggestion that familiarity/recognition depends on the repetition-induced decreases in cell firing in more lateral neocortical segments of the ventral temporal lobe, whereas conscious retrieval and recollection depend on medial structures and especially the HC (Brown and Aggleton, 2001).

The finding of selective ER activation during intentional retrieval is consistent with the observation that powerful feelings of familiarity (*déjà vu*) as well as intense reminiscences of previous events can be evoked by electrical stimulation of the human avTL (Bancaud et al., 1994; Halgren et al., 1978b) and perhaps especially ER (Bartolomei et al., 2004). These phenomena imply an active role of ER in shifting the mode of cerebral processing from one of identifying external stimuli to one of retrieving internal representations. In organizational analyses of the cerebral cortex, the hippocampal formation and ER stand at the top of a hierarchy extending down into all modalities (Felleman and VanEssen, 1991). Organization of the retrieval effort may include suppression of external input and attention to imagination (Lepage et al., 2000).

Conceivably, this shift in the leading source of information for defining mental contents would be implemented neurally as a shift in the relative excitation of medial as opposed to lateral avTL, between memory input and output, as was observed here.

*Neocortical–hippocampal interaction during retrieval through the ventral temporal lobe*

Anatomically and physiologically, IT is the most anterior part of visual association cortex. PR has many characteristics of IT and also more strongly interacts with medial limbic cortex, suggesting that it contributes to both visual associations and recognition memory. Repetition probes both aspects of this transition/intersection between visual association of the object stream and memory cortex; the facilitated processing of repeated stimuli provides an implicit marker allowing recognition of familiarity. As visual processing involves increasingly complex and novel constellations of items, processing plasticity blends into associative memory, first as association of visual objects and eventually as supramodal arbitrary associations. In contrast to this continuum on a stimulus level from priming to association, there is a discontinuity on a process level from facilitated processing to active retrieval.

Recognition involves a variety of processes, ranging from implicit (more rapid processing due to previous access of the same neural representation) to explicit (re-instatement of an entire experience within the context of the previous stream of consciousness). The current study demonstrates that all three structures are active and interactive during both input and output from memory and in both semantic and mnemonic tasks. Although all areas are highly differentiated, they are also highly integrated in a series of chained interlocking feedforward/feedback loops. There appears to be a division of labor across time, with activity at different latencies being associated with different aspects of memory. While all components are present in all structures, they are differentially distributed, suggesting that the same network is used across the memory situation, with different organizations emerging to support different aspects.

The first of these spatiotemporal multi-structure components is associated with the scalp-recorded N200. This stage rapidly forwards information through the cortical hierarchy, into layer IV, up to supragranular pyramids and on to the next stage, encoding the stimulus but not evaluating it. The following N400 through the neocortex may support priming. Intentional retrieval requires specialized late top–down physiological processes originating in the medial temporal lobe.

### Acknowledgments

We thank Howard Blume, Gary Heit, John R. Ives, Larry Gruber, George Karmos, Suresh Narayanan, and Katherine Reid. Supported by NIH NS18741 and NS44623. Please address communications to Eric Halgren, ehlgren@ucsd.edu.

### References

Allison, T., Puce, A., Spencer, D.D., McCarthy, G., 1999. Electrophysiological studies of human face perception. I: potentials generated in occipitotemporal cortex by face and non-face stimuli. *Cereb. Cortex* 9, 415–430.

Bancaud, J., Brunet-Bourgin, F., Chauvel, P., Halgren, E., 1994. Anatomical origin of déjà vu and vivid ‘memories’ in human temporal lobe epilepsy. *Brain* 117, 71–90.

Barbas, H., Rempel-Clower, N., 1997. Cortical structure predicts the pattern of corticocortical connections. *Cereb. Cortex* 7, 635–646.

Barth, D.S., Di, S., 1990. Three-dimensional analysis of auditory-evoked potentials in rat neocortex. *J. Neurophysiol.* 64, 1527–1536.

Bartolomei, F., Barbeau, E., Gavaret, M., Guye, M., McGonigal, A., Regis, J., Chauvel, P., 2004. Cortical stimulation study of the role of rhinal cortex in déjà vu and reminiscence of memories. *Neurology* 63, 858–864.

Biella, G., Uva, L., de Curtis, M., 2001. Network activity evoked by neocortical stimulation in area 36 of the guinea pig perirhinal cortex. *J. Neurophysiol.* 86, 164–172.

Biella, G., Uva, L., de Curtis, M., 2002. Propagation of neuronal activity along the neocortical–perirhinal–entorhinal pathway in the guinea pig. *J. Neurosci.* 22, 9972–9979.

Biella, G., Uva, L., Hofmann, U.G., de Curtis, M., 2002. Associative interactions within the superficial layers of the entorhinal cortex of the guinea pig. *J. Neurophysiol.* 88, 1159–1165.

Brown, M.W., Aggleton, J.P., 2001. Recognition memory: what are the roles of the perirhinal cortex and hippocampus? *Nat. Rev., Neurosci.* 2, 51–61.

Buckner, R.L., Koutstaal, W., Schacter, D.L., Rosen, B.R., 2000. Functional MRI evidence for a role of frontal and inferior temporal cortex in amodal components of priming. *Brain* 123, 620–640.

Buzsáki, G., 1996. The hippocampo-neocortical dialogue. *Cereb. Cortex* 6, 81–92.

Dale, A.M., Liu, A.K., Fischl, B.R., Buckner, R.L., Belliveau, J.W., Lewine, J.D., Halgren, E., 2000. Dynamic statistical parametric mapping: combining fMRI and MEG for high-resolution imaging of cortical activity. *Neuron* 26, 55–67.

Destexhe, A., Rudolph, M., Pare, D., 2003. The high-conductance state of neocortical neurons in vivo. *Nat. Rev., Neurosci.* 4, 739–751.

Devlin, J.T., Russell, R.P., Davis, M.H., Price, C.J., Moss, H.E., Fadili, M.J., Tyler, L.K., 2002. Is there an anatomical basis for category-specificity? Semantic memory studies in PET and fMRI. *Neuropsychologia* 40, 54–75.

Dhond, R.P., Marinkovic, K., Dale, A.M., Witzel, T., Halgren, E., 2003. Spatiotemporal maps of past-tense verb inflection. *NeuroImage* 19, 91–100.

Dyppvik, A.T., Bland, B.H., 2004. Functional connectivity between the red nucleus and the hippocampus supports the role of hippocampal formation in sensorimotor integration. *J. Neurophysiol.* 92, 2040–2050.

Felleman, D.J., VanEssen, D.C., 1991. Distributed hierarchical processing in the primate cerebral cortex. *Cereb. Cortex* 1, 1–47.

Grover, F.S., Buchwald, J.S., 1970. Correlation of cell size with amplitude of background fast activity in specific brain nuclei. *J. Neurophysiol.* 33, 160–171.

Halgren, E., 1984. Human hippocampal and amygdala recordings and stimulation: evidence for a neural model of recent memory. In: Squire, L., Butters, N. (Eds.), *The Neuropsychology of Memory*. Guilford, New York, pp. 165–181.

Halgren, E., 1991. Firing of human hippocampal units in relation to voluntary movements. *Hippocampus* 1, 153–161.

Halgren, E., Babb, T.L., Crandall, P.H., 1978. Activity of human hippocampal formation and amygdala neurons during memory testing. *Electroencephalogr. Clin. Neurophysiol.* 45, 585–601.

Halgren, E., Walter, R.D., Cherlow, D.G., Crandall, P.H., 1978. Mental phenomena evoked by electrical stimulation of the human hippocampal formation and amygdala. *Brain* 101, 83–117.

Halgren, E., Baudena, P., Heit, G., Clarke, J.M., Marinkovic, K., 1994. Spatio-temporal stages in face and word processing. 1. Depth-recorded potentials in the human occipital, temporal and parietal lobes. *J. Physiol. (Paris)* 88, 1–50.

Heit, G., Smith, M.E., Halgren, E., 1990. Neuronal activity in the

- human medial temporal lobe during recognition memory. *Brain* 113, 1093–1112.
- Hodges, J.R., Patterson, K., Oxbury, S., Funnell, E., 1992. Semantic dementia. Progressive fluent aphasia with temporal lobe atrophy. *Brain* 115, 1783–1806.
- Holsheimer, J., 1987. Electrical conductivity of the hippocampal CA1 layers and application to current-source-density analysis. *Exp. Brain Res.* 67, 402–410.
- Hunt, S.M.J., 1994. MacProbe: a Macintosh-based experimenter's workstation for the cognitive sciences. *Behav. Res. Meth. Instrum. Comput.* 26, 345–351.
- Insausti, A.M., Amaral, D.G., 2004. Hippocampal formation. In: Paxinos, G., Mai, J.K. (Eds.), *The Human Nervous System*. Elsevier Academic, San Diego, pp. 871–914.
- Kajiwar, R., Takashima, I., Mimura, Y., Witter, M.P., Iijima, T., 2003. Amygdala input promotes spread of excitatory neural activity from perirhinal cortex to the entorhinal–hippocampal circuit. *J. Neurophysiol.* 89, 2176–2184.
- Kutas, M., Federmeier, K.D., 2000. Electrophysiology reveals semantic memory use in language comprehension. *Trends Cogn. Sci.* 4, 463–470.
- Lamme, V.A., Roelfsema, P.R., 2000. The distinct modes of vision offered by feedforward and recurrent processing. *Trends Neurosci.* 23, 571–579.
- Lavenex, P., Suzuki, W.A., Amaral, D.G., 2002. Perirhinal and parahippocampal cortices of the macaque monkey: projections to the neocortex. *J. Comp. Neurol.* 447, 394–420.
- Lavenex, P., Suzuki, W.A., Amaral, D.G., 2004. Perirhinal and parahippocampal cortices of the macaque monkey: intrinsic projections and interconnections. *J. Comp. Neurol.* 472, 371–394.
- Lepage, M., Ghaffar, O., Nyberg, L., Tulving, E., 2000. Prefrontal cortex and episodic memory retrieval mode. *Proc. Natl. Acad. Sci. U. S. A.* 97, 506–511.
- Marinkovic, K., Dhond, R.P., Dale, A.M., Glessner, M., Carr, V., Halgren, E., 2003. Spatiotemporal dynamics of modality-specific and supramodal word processing. *Neuron* 38, 487–497.
- McCarthy, G., Nobre, A.C., Bentin, S., Spencer, D.D., 1995. Language-related field potentials in the anterior–medial temporal lobe: I. Intracranial distribution and neural generators. *J. Neurosci.* 15, 1080–1089.
- Merker, B., 2004. Cortex, countercurrent context, and dimensional integration of lifetime memory. *Cortex* 40, 559–576.
- Mignard, M., Malpeli, J.G., 1991. Paths of information flow through visual cortex. *Science* 251, 1249–1251.
- Miller, E.K., Desimone, R., 1994. Parallel neuronal mechanisms for short-term memory. *Science* 263, 520–522.
- Mitzdorf, U., 1985. Current source-density method and application in cat cerebral cortex: investigation of evoked potentials and EEG phenomena. *Physiol. Rev.* 65, 37–100.
- Murakami, S., Zhang, T., Hirose, A., Okada, Y.C., 2002. Physiological origins of evoked magnetic fields and extracellular field potentials produced by guinea-pig CA3 hippocampal slices. *J. Physiol.* 544, 237–251.
- Murray, E.A., Bussey, T.J., 1999. Perceptual-mnemonic functions of the perirhinal cortex. *Trends Cogn. Sci.* 3, 142–151.
- Naya, Y., Yoshida, M., Miyashita, Y., 2001. Backward spreading of memory-retrieval signal in the primate temporal cortex. *Science* 291, 661–664.
- Nicholson, C., Freeman, J.A., 1975. Theory of current source density analysis and determination of the conductivity tensor for anuran cerebellum. *J. Neurophysiol.* 38, 356–368.
- Petersen, C.C., Sakmann, B., 2001. Functionally independent columns of rat somatosensory barrel cortex revealed with voltage-sensitive dye imaging. *J. Neurosci.* 21, 8435–8446.
- Qin, Y.L., McNaughton, B.L., Skaggs, W.E., Barnes, C.A., 1997. Memory reprocessing in corticocortical and hippocampocortical neuronal ensembles. *Philos. Trans. R. Soc. Lond., B Biol. Sci.* 352, 1525–1533.
- Schroeder, C.E., Mehta, A.D., Givre, S.J., 1998. A spatiotemporal profile of visual system activation revealed by current source density analysis in the awake macaque. *Cereb. Cortex* 8, 575–592.
- Shao, Z., Burkhalter, A., 1999. Role of GABAB receptor-mediated inhibition in reciprocal interareal pathways of rat visual cortex. *J. Neurophysiol.* 81, 1014–1024.
- Smith, M.E., Stapleton, J.M., Halgren, E., 1986. Human medial temporal lobe potentials evoked in memory and language tasks. *Electroencephalogr. Clin. Neurophysiol.* 63, 145–159.
- Squire, L.R., Stark, C.E., Clark, R.E., 2004. The medial temporal lobe. *Annu. Rev. Neurosci.* 27, 279–306.
- Suzuki, W.A., Amaral, D.G., 1994. Topographical organization of the reciprocal connections between the monkey entorhinal cortex and the perirhinal and parahippocampal cortices. *J. Neurosci.* 14, 1856–1877.
- Suzuki, W.A., Miller, E.K., Desimone, R., 1997. Object and place memory in the macaque entorhinal cortex. *J. Neurophysiol.* 78, 1062–1081.
- Talairach, J., Tournoux, P., 1988. *Co-Planar Stereotaxic Atlas Of The Human Brain*. Thieme Medical Publishers, New York.
- Tenke, C.E., Schroeder, C.E., Arezzo, J.C., Vaughan Jr., H.G., 1993. Interpretation of high-resolution current source density profiles: a simulation of sublaminal contributions to the visual evoked potential. *Exp. Brain Res.* 94, 183–192.
- Thomson, A.M., Bannister, A.P., 2003. Interlaminar connections in the neocortex. *Cereb. Cortex* 13, 5–14.
- Ulbert, I., Halgren, E., Heit, G., Karmos, G., 2001. Multiple microelectrode-recording system for human intracortical applications. *J. Neurosci. Methods* 106, 69–79.
- Ulbert, I., Karmos, G., Heit, G., Halgren, E., 2001. Early discrimination of coherent vs incoherent motion by multiunit and synaptic activity in human putative MT+. *Hum. Brain Mapp.* 13, 226–238.
- Ulbert, I., Heit, G., Madsen, J., Karmos, G., Halgren, E., 2004. Laminar analysis of human neocortical interictal spike generation and propagation: current source density and multiunit analysis in vivo. *Epilepsia* 45 (Suppl. 4), 48–56.
- VanRullen, R., Thorpe, S.J., 2002. Surfing a spike wave down the ventral stream. *Vision Res.* 42, 2593–2615.
- Wang, C., Ulbert, I., Schomer, D.L., Marinkovic, K., Halgren, E., 2005. Responses of human anterior cingulate cortex microdomains to error detection, conflict monitoring, stimulus-response mapping, familiarity, and orienting. *J. Neurosci.* 25, 604–613.
- Weiss, A.P., Zalesak, M., DeWitt, I., Goff, D., Kunkel, L., Heckers, S., 2004. Impaired hippocampal function during the detection of novel words in schizophrenia. *Biol. Psychiatry* 55, 668–675.
- Wise, S.P., Murray, E.A., 1999. Role of the hippocampal system in conditional motor learning: mapping antecedents to action. *Hippocampus* 9, 101–117.
- Xiang, J.Z., Brown, M.W., 1998. Differential neuronal encoding of novelty, familiarity and recency in regions of the anterior temporal lobe. *Neuropharmacology* 37, 657–676.
- Yonelinas, A.P., Hopfinger, J.B., Buonocore, M.H., Kroll, N.E., Baynes, K., 2001. Hippocampal, parahippocampal and occipital–temporal contributions to associative and item recognition memory: an fMRI study. *NeuroReport* 12, 359–363.
- Yonelinas, A.P., Kroll, N.E., Quamme, J.R., Lazzara, M.M., Sauve, M.J., Widaman, K.F., Knight, R.T., 2002. Effects of extensive temporal lobe damage or mild hypoxia on recollection and familiarity. *Nat. Neurosci.* 5, 1236–1241.

dc\_303\_11

#### **4. Melléklet**

ficed to establish place preference in the absence of other reward. These results establish a causal role in behavioral conditioning for defined spiking modes in a specific cell type; of course, even a single cell type can release multiple neurotransmitters and neuromodulators (for example, VTA DA neurons primarily release DA but can also release other neurotransmitters such as glutamate) and will exert effects through multiple distinct downstream cell types. Indeed, the optogenetic approach, integrated with electrophysiological, behavioral, and electrochemical readout methods, opens the door to exploring the causal, temporally precise, and behaviorally relevant interactions of DA neurons with other neuromodulatory circuits (22–25), including monoaminergic and opioid circuits important in neuropsychiatric illnesses (26–28). In the process of identifying candidate interacting neurotransmitter systems, downstream neural circuit effectors (29), and subcellular biochemical mechanisms on time scales appropriate to behavior and relevant circuit dynamics, it will be important to continue to leverage the specificity and temporal precision of optogenetic control (30).

#### References and Notes

- R. A. Wise, *Nat. Rev. Neurosci.* **5**, 483 (2004).
- B. J. Everitt, T. W. Robbins, *Nat. Neurosci.* **8**, 1481 (2005).
- T. E. Robinson, K. C. Berridge, *Brain Res. Brain Res. Rev.* **18**, 247 (1993).
- G. F. Koob, M. Le Moal, *Science* **278**, 52 (1997).
- W. Schultz, *Annu. Rev. Neurosci.* **30**, 259 (2007).
- M. A. Ungless, P. J. Magill, J. P. Bolam, *Science* **303**, 2040 (2004).
- F. Zhang, Larry C. Katz Memorial Lecture presented at the Cold Spring Harbor Laboratory Meeting on Neuronal Circuits, Cold Spring Harbor, NY, 13 to 16 March 2008.
- D. Atasoy, Y. Aponte, H. H. Su, S. M. Sternson, *J. Neurosci.* **28**, 7025 (2008).
- E. S. Boyden, F. Zhang, E. Bamberg, G. Nagel, K. Deisseroth, *Nat. Neurosci.* **8**, 1263 (2005).
- G. Nagel *et al.*, *Proc. Natl. Acad. Sci. U.S.A.* **100**, 13940 (2003).
- Materials and methods are available as supporting material on Science Online.
- A. Bjorklund, S. B. Dunnett, *Trends Neurosci.* **30**, 194 (2007).
- Q. S. Liu, L. Pu, M. M. Poo, *Nature* **437**, 1027 (2005).
- S. Robinson, D. M. Smith, S. J. Mizumori, R. D. Palmiter, *Proc. Natl. Acad. Sci. U.S.A.* **101**, 13329 (2004).
- A. R. Adamantidis, F. Zhang, A. M. Aravanis, K. Deisseroth, L. de Lecea, *Nature* **450**, 420 (2007).
- P. E. Phillips, G. D. Stuber, M. L. Heien, R. M. Wightman, R. M. Carelli, *Nature* **422**, 614 (2003).
- G. D. Stuber *et al.*, *Science* **321**, 1690 (2008).
- T. M. Tzschenke, *Addict. Biol.* **12**, 227 (2007).
- C. M. Cannon, R. D. Palmiter, *J. Neurosci.* **23**, 10827 (2003).
- A. A. Grace, S. B. Floresco, Y. Goto, D. J. Lodge, *Trends Neurosci.* **30**, 220 (2007).
- T. S. Hnasko, B. N. Sotak, R. D. Palmiter, *J. Neurosci.* **27**, 12484 (2007).
- P. W. Kalivas, *Am. J. Addict.* **16**, 71 (2007).
- M. R. Picciotto, W. A. Corrigan, *J. Neurosci.* **22**, 3338 (2002).
- J. A. Dani, D. Bertrand, *Annu. Rev. Pharmacol. Toxicol.* **47**, 699 (2007).
- G. C. Harris, G. Aston-Jones, *Neuropsychopharmacology* **28**, 865 (2003).
- E. J. Nestler, W. A. Carlezon Jr., *Biol. Psychiatry* **59**, 1151 (2006).
- J. Williams, P. Dayan, *J. Child Adolesc. Psychopharmacol.* **15**, 160 (2005).
- A. M. Graybiel, *Annu. Rev. Neurosci.* **31**, 359 (2008).
- W. Shen, M. Flajolet, P. Greengard, D. J. Surmeier, *Science* **321**, 848 (2008).
- F. Zhang *et al.*, *Nature* **446**, 633 (2007).
- We thank M. Wightman, P. Phillips, and the entire Deisseroth laboratory for their support. All reagents and protocols are freely distributed and supported by the authors ([www.optogenetics.org](http://www.optogenetics.org)); because these tools are not protected by patents, Stanford University has applied for a patent to ensure perpetual free distribution to the international academic nonprofit community. H.C.T. is supported by a Stanford Graduate Fellowship. F.Z. and G.D.S. are supported by NIH National Research Service award. A.R.A. is supported by the Fonds National de la Recherche Scientifique, NARSAD, and the Fondation Leon Fredericq. L.d.L. is supported by National Institute on Drug Abuse (NIDA), Defense Advanced Research Projects Agency, and NARSAD. K.D. is supported by NSF; National Institute of Mental Health; NIDA; and the McKnight, Coulter, Snyder, Albert Yu and Mary Bechmann, and Keck foundations.

#### Supporting Online Material

[www.sciencemag.org/cgi/content/full/1168878/DC1](http://www.sciencemag.org/cgi/content/full/1168878/DC1)

Materials and Methods

Figs. S1 to S7

References

24 November 2008; accepted 7 April 2009

Published online 23 April 2009;

10.1126/science.1168878

Include this information when citing this paper.

## The Human K-Complex Represents an Isolated Cortical Down-State

Sydney S. Cash,<sup>1\*†</sup> Eric Halgren,<sup>2\*</sup> Nima Dehghani,<sup>2</sup> Andrea O. Rossetti,<sup>5</sup> Thomas Thesen,<sup>3</sup> ChunMao Wang,<sup>3</sup> Orrin Devinsky,<sup>3</sup> Ruben Kuzniecky,<sup>3</sup> Werner Doyle,<sup>3</sup> Joseph R. Madsen,<sup>4</sup> Edward Bromfield,<sup>5</sup> Loránd Eröss,<sup>6</sup> Péter Halász,<sup>7,9</sup> George Karmos,<sup>8,9</sup> Richárd Csercsa,<sup>8</sup> Lucia Wittner,<sup>6,8</sup> István Ulbert<sup>6,8,9\*</sup>

The electroencephalogram (EEG) is a mainstay of clinical neurology and is tightly correlated with brain function, but the specific currents generating human EEG elements remain poorly specified because of a lack of microphysiological recordings. The largest event in healthy human EEGs is the K-complex (KC), which occurs in slow-wave sleep. Here, we show that KCs are generated in widespread cortical areas by outward dendritic currents in the middle and upper cortical layers, accompanied by decreased broadband EEG power and decreased neuronal firing, which demonstrate a steep decline in network activity. Thus, KCs are isolated “down-states,” a fundamental cortico-thalamic processing mode already characterized in animals. This correspondence is compatible with proposed contributions of the KC to sleep preservation and memory consolidation.

**A**lthough the electroencephalogram (EEG) is known to directly and instantaneously reflect synaptic and active transmembrane neuronal currents, the specific channels, synapses, and circuits that generate particular EEG elements in humans remain poorly specified. Much of the EEG is composed of repeated wave forms with characteristic morphologies, durations, amplitudes, frequency content, evoking events, and background states (1). The largest of these EEG “graphoelements” is the KC, characterized by a short surface-positive transient followed by a

slower, larger surface-negative complex with peaks at 350 and 550 ms, and then a final positivity peaking near 900 ms, followed sometimes by 10- to 14-Hz “spindles” (2–4). KCs occur in non-rapid-eye-movement (non-REM) sleep, especially stage 2. Deeper sleep (stages 3 to 4) is characterized by slow waves, demonstrated in extensive animal studies to consist of a “slow oscillation” between periods of intense firing by both excitatory and inhibitory cortical neurons (termed “up-states”) and periods of neuronal silence (“down-states”) (5–9). Using micro- and

macro-electrode arrays placed in patients undergoing evaluation for epilepsy (10), we demonstrate that the microphysiological characteristics of human KCs appear identical to those of down-states recorded in the same patients.

Typical KCs were recorded in eight patients (11). KCs were either spontaneous or evoked by a weak auditory stimulus. Within a given patient, the basic KC wave forms were similar regardless of whether they were recorded at the scalp or intracranially (Fig. 1A). In all cases, the wave form was dominated by a large deflection occurring ~500 to 600 ms after the onset of a stimulus, or after the onset of the initial deflection for spontaneous KCs. Characteristic KC wave forms were recorded by subdural electrodes placed on all cortical lobes, demonstrating widespread

<sup>1</sup>Department of Neurology, Epilepsy Division, Massachusetts General Hospital, Harvard Medical School, Boston, MA 02114, USA.

<sup>2</sup>Departments of Radiology, Neurosciences, and Psychiatry, University of California at San Diego, San Diego, CA 92093, USA.

<sup>3</sup>Comprehensive Epilepsy Center, New York University School of Medicine, New York, NY 10016, USA.

<sup>4</sup>The Children’s Hospital, Boston, MA 02115, USA.

<sup>5</sup>Brigham and Women’s Hospital, Boston, MA 02115, USA.

<sup>6</sup>National Institute of Neurosurgery, H-1145 Budapest, Hungary.

<sup>7</sup>National Institute of Psychiatry and Neurology, Epilepsy Center, H-1145 Budapest, Hungary.

<sup>8</sup>Institute for Psychology, Hungarian Academy of Sciences, H-1394 Budapest, Hungary.

<sup>9</sup>Péter Pázmány Catholic University, Department of Information Technology, H-1083 Budapest, Hungary.

\*These authors contributed equally to this work.

†To whom correspondence should be addressed. E-mail: scash@partners.org

generation (Fig. 1B). In all scalp and most intracranial sites, this deflection was surface-negative. Different KCs recorded in the same patient varied in their relative size and timing across cortical locations (Fig. 1C). That is, KCs were not completely synchronous across the cortical surface, nor were the direction or duration of the transcortical delays constant across different KCs.

Potential gradients across cortical layers during KCs were recorded during these same events by using linear arrays of microelectrodes in temporal, frontal, and parietal sites (Fig. 1A). In all cases, KCs seen on the scalp electrodes were also observed on microelectrodes of the array and vice versa. Spontaneous and evoked KCs were recorded in four patients. They showed similar wave-form characteristics and distribution (Figs. 1D and 2), with the maximal negative response present on the same recording channel. No significant differences were found in the peak amplitude or area under the curve during this peak between spontaneous and evoked KCs (*t* test and Kolmogorov-Smirnov test; powered  $\geq 0.80$  to detect a 20% difference at  $P < 0.05$ ).

Current source density calculated from these data showed a consistent pattern for both spontaneously occurring and triggered KCs. During the surface-negative slow deflection, there was a current sink in the channels closest to the cortical surface, whereas a substantial source was present in middle channels  $\sim 450$  to  $600 \mu\text{m}$  below the sink. This pattern, observed in all

subjects, likely corresponds to a passive sink centered in layer I and an active source centered in layer III (Figs. 2, A and B, and 3A1). Successful recordings of multiunit neuronal firing were obtained in four subjects, all of whom showed decreased firing during the surface-negative slow deflection of either spontaneous or evoked KCs (Figs. 2, A and B, and 3A2). The pattern of sinks and sources and the decreased neuronal firing changes described here indicate hyperpolarizing current flow in layer III during the large surface-negative deflection.

Analysis of the spectral content of both spontaneous and evoked events consistently demonstrated a broadband decrease in the activity during the surface-negative event in multiple cortical layers when we used microelectrodes and in multiple locations with subdural macroelectrodes (Fig. 3). This was particularly pronounced for higher-frequency (gamma) activity from 20 to 100 Hz; low-frequency components—representing the wave form itself—were often maintained. High frequencies could remain depressed past resolution of the negative deflection. In six subjects, higher-frequency power briefly increased at KC onset. However, in no case was the surface-negative slow event preceded by rhythmic modulations of current or gamma power.

This study provides strong evidence that KCs are induced cortical down-states. First, our recordings demonstrate that KCs are generated in widespread cortical locations. Previous extra-

cranial EEG (12), magnetoencephalogram (MEG) (13), and intracranial EEG recordings (14, 15) have not provided unambiguous localization of KC generators because of difficulties in localizing widely distributed sources. Local KC generation near the electrode contact is highly likely in our recordings from the cortical surface and is certain when steep gradients are recorded at  $150\text{-}\mu\text{m}$  intervals with microelectrode arrays. Widespread intracortical generation of KCs is consistent with the generation of down-states in lower mammals, which arise in distributed cortico-cortical networks (16).

The current study also demonstrates that KCs in humans are associated with strong and consistent decreases in gamma and multiunit activity, similar to those observed in animals during the down-state and indicating widespread decreases in cortical activity (5, 6, 8, 9, 17). Direct confirmation of identical microphysiology was obtained in our subjects by comparing KC and slow-oscillation down-states recorded within the same sleep session and by the same microelectrode arrays (Fig. 2). Even at the  $150\text{-}\mu\text{m}$  resolution of these recordings, the two conditions evoke identical laminar distributions of transmembrane currents (correlation coefficient at the peak of the deflection was 0.95 between spontaneous KC and slow waves and 0.96 between evoked KC and slow waves, with  $P < 10^{-12}$  for both). The indices of network synaptic activity (gamma power) and of population firing (multiunit activity) were both decreased during the KC in all cortical layers, but especially in the supragranular layers, as is characteristic of the slow-oscillation down-state (Fig. 3). Finally, although various inhibitory processes in the cortex have a wide range of durations, from less than 20 ms to several seconds, the KC and slow-oscillation down-states both last  $\sim 400$  ms.

Although the data thus strongly support the proposal of Amzica and Steriade (7) that the KC reflects a cortical down-state, it does not support their corollary proposal that the KC is always part of an underlying oscillation (18). Rather, our evidence indicates that, at both the intracortical and epicortical levels, isolated KCs are the rule rather than the exception during stage 2 sleep. This is consistent with numerous observations over the past 70 years (2–4). Also consistent with these previous studies, but in contrast with Amzica and Steriade (7), we found the major component of KCs to be surface-negative.

The down-state is characterized by hyperpolarizing potassium currents, as well as low synaptic activity (6). The lack of a local up-state preceding the KC may pose difficulties for the proposal that an activity-dependent accumulation of calcium or adenosine diphosphate (ADP) triggers a potassium current and, thus, the down-state (19–21). Our findings, as well as recent evidence that the onset of the down-state is more synchronous than that of the up-state (16), suggest the need for additional synchronizing mecha-

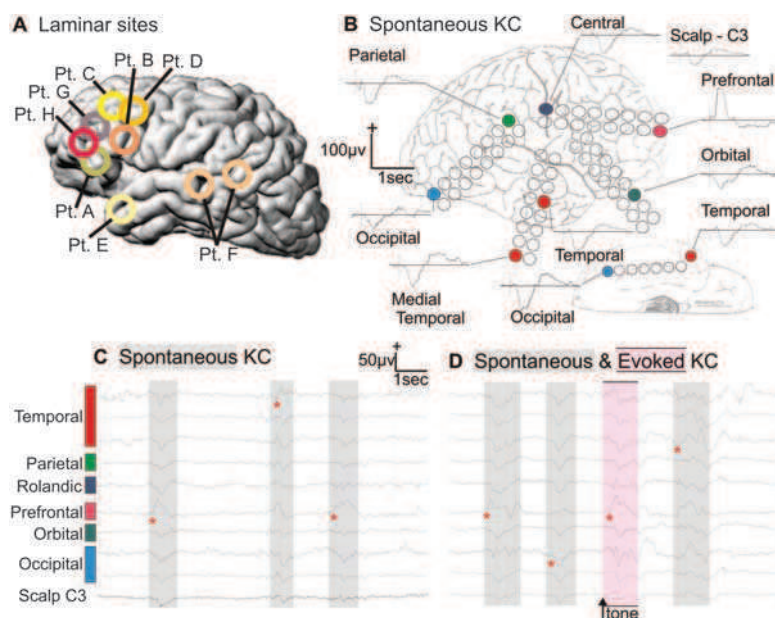


**Fig. 1.** Spontaneous and evoked KCs recorded simultaneously from the surface of all cortical lobes. (A) Approximate locations of microelectrode arrays in the eight patients (Pt.) studied. (B) Averaged spontaneous KCs recorded with grid electrodes in multiple cortical locations and from the scalp (subject E). Unaveraged spontaneous (C and D) and evoked (D) KCs from the same electrodes. Red asterisks show earliest deflection during the KCs and demonstrate the variability in onset and spread. Sleep stages and KCs were identified during natural sleep with standard criteria (27). KCs were evoked with occasional tones. Subdural electrode arrays were placed to confirm the hypothesized seizure focus and to locate epileptogenic tissue in relation to essential cortex, so as to direct surgical treatment.

**Fig. 2.** Population transmembrane currents and neuronal firing in different cortical layers during single evoked (A) and spontaneous (B) KC in stage 2 sleep, and (C) during the slow oscillation in stage 3 to 4 sleep. Evoked and spontaneous KC and the slow-oscillation down-state are all characterized by outward currents (sources) in cortical layers II to III (blue arrows), paired with inward currents (sinks) near the cortical surface (red arrows), and decreased neuronal firing (black arrows). Unlike the KC, the slow-oscillation down-state is embedded in rhythmic alternation with up-states consisting of layer II/III sinks (\*), layer I sources (\*), and increased firing.

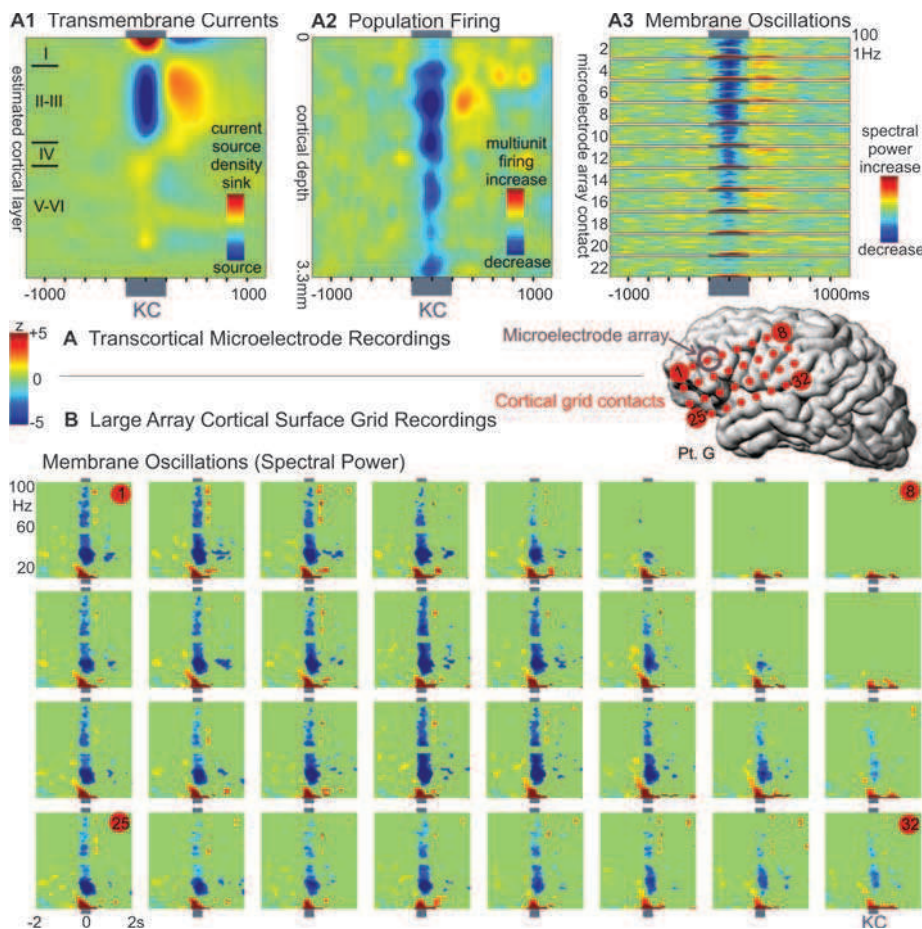
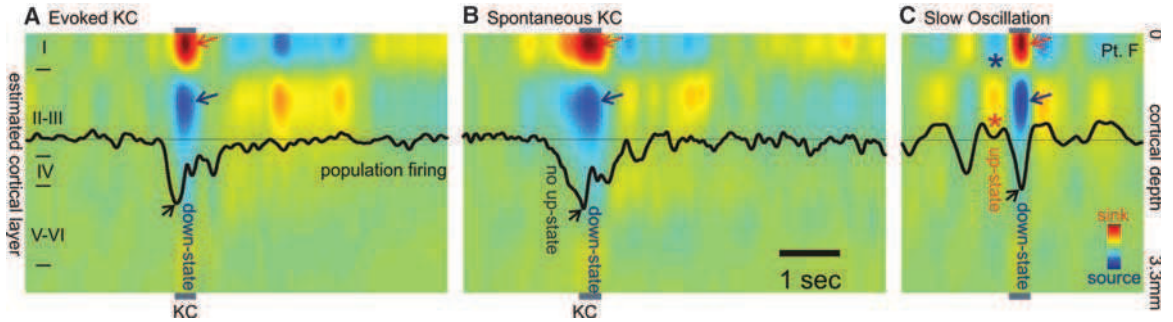


**Fig. 3.** Decrement in population firing and high-frequency membrane oscillations during KC. (A) Microelectrode array recordings of (A1) averaged spontaneous KCs show a layer III source, (A2) decreased neuronal firing, and (A3) membrane oscillations (higher-frequency spectral power), in all layers, especially upper layers. (B) Simultaneous recordings in the same patient from a large grid array of electrodes on the cortical surface also show a decrease in high-frequency spectral power during KC. Plots are set to the same threshold to show significant ( $P < 0.01$ ) spectral power changes compared with a period of 1500 to 250 ms before the KC.

nisms, for instance, cortico-thalamo-cortical interactions, as have been shown for the sleep spindle (22). For example, in the tone-evoked KC, initial medial geniculate and auditory cortex activation could trigger a local down-state that spreads via thalamo-cortical and cortico-cortical connections.

KCs would then occur spontaneously because of a similar mechanism, only with the sensory stimulus occult to the investigator (e.g., gastric), or because of a spontaneous burst of cortical activity. Thus, the KC down-state may follow an up-state, but only in the initiating zone.

Our finding that successive KCs arise in variable cortical locations (Fig. 1D), which confirmed scalp recordings (12) and computational models (19), is consistent with this interpretation.

Sleep is thought to perform essential restorative and mnemonic functions (23). Maintaining sleep is therefore crucial, but so is awakening in the face of danger. Our finding that the KC represents an isolated down-state supports the theory that it suppresses cortical activity and, thus, arousal in response to stimuli that are judged by the sleeping brain not to be dangerous (3, 4). Increasing evidence supports a strong contribution to memory consolidation of stage 2 sleep, characterized by KC and spindles (24). The cortical down-state may provide a period when the near absence of neural activity induces a blanket suppression of synaptic strengths, balancing the synaptic enhancement occurring during waking and up-states and thus preserving the signal-to-noise ratio in network representations (25). In addition, during the recovery from the down-state, cortical firing “reboots” in a systematic order, which allows the potential for engrams encoded in dynamic assemblies of neuronal firing to be repeatedly practiced and thus consolidated (26). The current study ties a universal, normal, prominent, easily-observed EEG phenomenon to its underlying substrate of membrane currents and neuronal circuits through direct observation and homology with animal studies. This allows previous observations relating human sleep EEG to memory and sensory arousal to be interpreted within mechanistic neural models.

#### References and Notes

1. G. Buzsáki, *Rhythms of the Brain* (Oxford Univ. Press, Oxford, 2006).
2. A. L. Loomis, E. N. Harvey, G. Hobart, *J. Neurophysiol.* **13** (suppl.), 231 (1938).
3. I. M. Colrain, *Sleep* **28**, 255 (2005).
4. P. Halasz, *Sleep Med. Rev.* **9**, 391 (2005).
5. M. Steriade, F. Amzica, A. Nunez, *J. Neurophysiol.* **70**, 1385 (1993).
6. D. Contreras, I. Timofeev, M. Steriade, *J. Physiol.* **494**, 251 (1996).
7. F. Amzica, M. Steriade, *Neuroscience* **82**, 671 (1998).
8. M. V. Sanchez-Vives, D. A. McCormick, *Nat. Neurosci.* **3**, 1027 (2000).
9. I. Timofeev, F. Grenier, M. Steriade, *Proc. Natl. Acad. Sci. U.S.A.* **98**, 1924 (2001).

10. I. Ulbert, E. Halgren, G. Heit, G. Karmos, *J. Neurosci. Methods* **106**, 69 (2001).
11. Materials and methods are available as supporting material on Science Online.
12. M. Massimini, R. Huber, F. Ferrarelli, S. Hill, G. Tononi, *J. Neurosci.* **24**, 6862 (2004).
13. J. Numminen, J. P. Makela, R. Hari, *Electroencephalogr. Clin. Neurophysiol.* **99**, 544 (1996).
14. M. Velasco *et al.*, *Clin. Neurophysiol.* **113**, 25 (2002).
15. R. A. Wennberg, A. M. Lozano, *Clin. Neurophysiol.* **114**, 1403 (2003).
16. M. Volgushev, S. Chauvette, M. Mukovski, I. Timofeev, *J. Neurosci.* **26**, 5665 (2006).
17. M. Mukovski, S. Chauvette, I. Timofeev, M. Volgushev, *Cereb. Cortex* **17**, 400 (2007).
18. F. Amzica, M. Steriade, *Neurology* **49**, 952 (1997).
19. M. Bazhenov, I. Timofeev, M. Steriade, T. J. Sejnowski, *J. Neurosci.* **22**, 8691 (2002).
20. A. Compte, M. V. Sanchez-Vives, D. A. McCormick, X. J. Wang, *J. Neurophysiol.* **89**, 2707 (2003).
21. M. O. Cunningham *et al.*, *Proc. Natl. Acad. Sci. U.S.A.* **103**, 5597 (2006).
22. D. Contreras, A. Destexhe, T. J. Sejnowski, M. Steriade, *Science* **274**, 771 (1996).
23. J. A. Hobson, E. F. Pace-Schott, *Nat. Rev. Neurosci.* **3**, 679 (2002).
24. R. Stickgold, *Nature* **437**, 1272 (2005).
25. G. Tononi, C. Cirelli, *Sleep Med. Rev.* **10**, 49 (2006).
26. S. Ribeiro *et al.*, *PLoS Biol.* **2**, E24 (2004).
27. A. Rechtschaffen, A. Kales, *A Manual of Standardized Terminology, Techniques and Scoring System for Sleep Stages of Human Subjects*. (U.S. Government Printing Office, Washington, DC, 1968).
28. Supported by National Institute of Neurological Disorders and Stroke (NIH) grants NS18741 and NS44623 to E.H. and Neuroprobes IST-027017, OTKA49122, ETT135/2006, János Szentágotthai Knowledge Center RET 05/2004 grants to L.U. We thank L. Papp for technical support; and L. Grand, A. Magony, B. Dombóvári, and D. Fabó for support in data analysis and recording. The authors dedicate this work to the memory of Edward Bromfield, who passed away on 10 May 2009.

#### Supporting Online Material

www.sciencemag.org/cgi/content/full/324/5930/1084/DC1  
Materials and Methods  
Fig. S1  
Table S1  
References

11 December 2008; accepted 20 March 2009  
10.1126/science.1169626

# Crystal Structure of the Nuclear Export Receptor CRM1 in Complex with Snurportin1 and RanGTP

Thomas Monecke,<sup>1\*</sup> Thomas Güttler,<sup>2\*</sup> Piotr Neumann,<sup>1</sup> Achim Dickmanns,<sup>1</sup> Dirk Görlich,<sup>2†</sup> Ralf Ficner<sup>1</sup>

CRM1 mediates nuclear export of numerous unrelated cargoes, which may carry a short leucine-rich nuclear export signal or export signatures that include folded domains. How CRM1 recognizes such a variety of cargoes has been unknown up to this point. Here we present the crystal structure of the SPN1-CRM1-RanGTP export complex at 2.5 angstrom resolution (where SPN1 is snurportin1 and RanGTP is guanosine 5' triphosphate-bound Ran). SPN1 is a nuclear import adapter for cytoplasmically assembled, m<sub>3</sub>G-capped spliceosomal U snRNPs (small nuclear ribonucleoproteins). The structure shows how CRM1 can specifically return the cargo-free form of SPN1 to the cytoplasm. The extensive contact area includes five hydrophobic residues at the SPN1 amino terminus that dock into a hydrophobic cleft of CRM1, as well as numerous hydrophilic contacts of CRM1 to m<sub>3</sub>G cap-binding domain and carboxyl-terminal residues of SPN1. The structure suggests that RanGTP promotes cargo-binding to CRM1 solely through long-range conformational changes in the exportin.

Nuclear transport proceeds through nuclear pore complexes (NPCs) and supplies cell nuclei with proteins and the cytoplasm with nuclear products such as ribosomes and tRNAs. Most nuclear transport pathways are mediated by importin  $\beta$ -type nuclear transport receptors, which include nuclear export receptors (exportins), as well as importins (1, 2). These receptors bind cargoes directly or through adapter molecules, shuttle constantly between the nucleus and cytoplasm, and use the chemical potential of the nucleocytoplasmic RanGTP-gradient to act as unidirectional cargo pumps (where GTP is guanosine 5' triphosphate and RanGTP is GTP-bound Ran) (3).

Exportins recruit cargo at high RanGTP levels in the nucleus, traverse NPCs as ternary cargo-exportin-RanGTP complexes, and release their cargo upon GTP hydrolysis into the cytoplasm. CRM1 (exportin1/Xpo1p) (4, 5) and CAS (Cse1p/exportin2) (6) are the prototypical exportins. Whereas CAS is specialized to retrieve the nuclear import adapter importin  $\alpha$  back to the cytoplasm (6), CRM1 exports a very broad range of substrates from nuclei (4, 5, 7–11), including ribosomes and many regulatory proteins. It also depletes translation factors from nuclei and is essential for the replication of viruses such as HIV.

CRM1 has a dual function during biogenesis of spliceosomal U small nuclear ribonucleoproteins (snRNPs). It exports m<sup>7</sup>G-capped U small nuclear RNAs to the cytoplasm (4, 12), where they recruit Sm-core proteins and receive a 2,2,7-trimethyl (m<sub>3</sub>G) cap structure. The import adapter snurportin 1 (SPN1) and importin  $\beta$  then transport the mature m<sub>3</sub>G-capped U snRNPs into nuclei (13). To mediate another import cycle, SPN1 is returned to the cytoplasm by CRM1 (14).

Many CRM1 cargoes harbor a leucine-rich nuclear export signal (NES) that typically includes four characteristically spaced hydrophobic residues (7). Examples are the HIV-Rev protein (15) or the protein kinase A inhibitor (PKI) (16). In other cases, however, CRM1 recognizes not just a short peptide, but instead a large portion of the export cargo; here, SPN1 is the prototypical example (14). CRM1 binds SPN1 tighter than other export substrates, apparently because CRM1 must displace the imported U snRNP from SPN1 before export may occur.

The cytoplasmic dissociation of CRM1 from SPN1 is essential for multi-round import of U snRNPs. Hydrolysis of the Ran-bound GTP alone is insufficient to fully disrupt the interaction (Fig. 1, A to C) (14), but importin  $\beta$  can displace CRM1 from SPN1 (Fig. 1A). Thus, either the binding sites of SPN1 for CRM1 and importin  $\beta$  overlap, or importin  $\beta$  forces SPN1 into a conformation that is incompatible with CRM1 binding.

Two functional domains in SPN1 have been described: (i) the m<sub>3</sub>G cap-binding domain (SPN<sup>97–300</sup>) (17) and (ii) the N-terminal importin  $\beta$ -binding (IBB) domain (SPN<sup>1–65</sup>) (14, 18, 19), which confers binding to and import by importin  $\beta$  (20). A multiple alignment of SPN1 from various species revealed another conserved region that precedes the IBB domain and includes the hydrophobic residues Leu<sup>4</sup>, Leu<sup>8</sup>, Phe<sup>12</sup>, and Val<sup>14</sup>. Mutating any of those residues to serine or deleting Met<sup>1</sup> strongly impaired the interaction with CRM1, in particular at higher salt concentrations (Fig. 1B and fig. S1). Even though the SPN1 N terminus (with its conserved hydrophobic residues) resembles a classical NES, there are clear differences: foremost that CRM1 binds the isolated SPN1 N terminus (SPN<sup>1–21</sup>) considerably weaker than, for instance, the PKI-NES (Fig. 1C). In the context of full-length SPN1, however, this difference is more than compensated by the contribution of the m<sub>3</sub>G cap-binding domain to the CRM1 interaction.

We then assembled, purified, and crystallized an export complex containing full-length human SPN1<sup>1–360</sup>, full-length mouse CRM1<sup>1–1071</sup>, and GTP-RanQ69L<sup>1–180</sup>, a C-terminally truncated and GTPase-deficient form of human Ran (21).

<sup>1</sup>Abteilung für Molekulare Strukturbiologie, Institut für Mikrobiologie und Genetik, GZMB, Georg-August-Universität Göttingen, Justus-von-Liebig-Weg 11, 37077 Göttingen, Germany. <sup>2</sup>Abteilung Zelluläre Logistik, Max-Planck-Institut für Biophysikalische Chemie, Am Fassberg 11, 37077 Göttingen, Germany.

\*These authors contributed equally to this work.

†To whom correspondence should be addressed. E-mail: goerlich@mpibpc.mpg.de

dc\_303\_11

## 5. Melléklet

## OCCASIONAL PAPER

# Laminar analysis of slow wave activity in humans

Richárd Csercsa,<sup>1</sup> Balázs Dombovári,<sup>1,2</sup> Dániel Fabó,<sup>1,3</sup> Lucia Wittner,<sup>1,3,4</sup> Loránd Eröss,<sup>3</sup> László Entz,<sup>1,3</sup> András Sólyom,<sup>3</sup> György Rásonyi,<sup>3</sup> Anna Szűcs,<sup>3</sup> Anna Kelemen,<sup>3</sup> Rita Jakus,<sup>3</sup> Vera Juhos,<sup>5</sup> László Grand,<sup>1,2</sup> Andor Magony,<sup>1,6</sup> Péter Halász,<sup>2</sup> Tamás F. Freund,<sup>4</sup> Zsófia Maglóczky,<sup>4</sup> Sydney S. Cash,<sup>7</sup> László Papp,<sup>8</sup> György Karmos,<sup>1,2</sup> Eric Halgren<sup>9</sup> and István Ulbert<sup>1,2,3</sup>

1 Institute for Psychology, Hungarian Academy of Sciences, Budapest, Hungary

2 Pázmány Péter Catholic University, Faculty of Information Technology, Budapest, Hungary

3 National Institute of Neuroscience, Budapest, Hungary

4 Institute of Experimental Medicine, Hungarian Academy of Sciences, Budapest, Hungary

5 Department of Neurology, Szent István Hospital, Budapest, Hungary

6 School of Clinical and Experimental Medicine, University of Birmingham, Birmingham, UK

7 Department of Neurology, Massachusetts General Hospital, Boston, MA, USA

8 Neuronelektrod Kft, Budapest, Hungary

9 Departments of Radiology, Neuroscience and Psychiatry, University of California, San Diego, La Jolla, CA, USA

Correspondence to: István Ulbert,  
MTA PKI,  
Szondi u. 83-85,  
Budapest, 1068, Hungary  
E-mail: ulbert@cogpsyphy.hu

Brain electrical activity is largely composed of oscillations at characteristic frequencies. These rhythms are hierarchically organized and are thought to perform important pathological and physiological functions. The slow wave is a fundamental cortical rhythm that emerges in deep non-rapid eye movement sleep. In animals, the slow wave modulates delta, theta, spindle, alpha, beta, gamma and ripple oscillations, thus orchestrating brain electrical rhythms in sleep. While slow wave activity can enhance epileptic manifestations, it is also thought to underlie essential restorative processes and facilitate the consolidation of declarative memories. Animal studies show that slow wave activity is composed of rhythmically recurring phases of widespread, increased cortical cellular and synaptic activity, referred to as active- or up-state, followed by cellular and synaptic inactivation, referred to as silent- or down-state. However, its neural mechanisms in humans are poorly understood, since the traditional intracellular techniques used in animals are inappropriate for investigating the cellular and synaptic/transmembrane events in humans. To elucidate the intracortical neuronal mechanisms of slow wave activity in humans, novel, laminar multichannel microelectrodes were chronically implanted into the cortex of patients with drug-resistant focal epilepsy undergoing cortical mapping for seizure focus localization. Intracortical laminar local field potential gradient, multiple-unit and single-unit activities were recorded during slow wave sleep, related to simultaneous electrocorticography, and analysed with current source density and spectral methods. We found that slow wave activity in humans reflects a rhythmic oscillation between widespread cortical activation and silence. Cortical activation was demonstrated as increased wideband (0.3–200 Hz) spectral power including virtually all bands of cortical oscillations, increased multiple- and single-unit activity and powerful inward transmembrane currents, mainly localized to the supragranular layers. Neuronal firing in the up-state was sparse and the average discharge rate of single cells was less than expected from animal studies. Action potentials at up-state onset were synchronized within  $\pm 10$  ms across all cortical layers, suggesting that any layer could initiate firing at up-state onset. These findings provide strong direct experimental evidence that slow wave activity in humans is characterized by hyperpolarizing currents associated

Received January 25, 2010. Revised and Accepted May 13, 2010. . Advance Access publication July 22, 2010

© The Author (2010). Published by Oxford University Press on behalf of the Guarantors of Brain. All rights reserved.

For Permissions, please email: journals.permissions@oxfordjournals.org

with suppressed cell firing, alternating with high levels of oscillatory synaptic/transmembrane activity associated with increased cell firing. Our results emphasize the major involvement of supragranular layers in the genesis of slow wave activity.

**Keywords:** current source density; unit activity; laminar recording; slow wave activity; sleep

**Abbreviations:** CSD = current source density; ECoG = electrocorticogram; LFP = local field potential; REM = rapid eye movement

## Introduction

Brain rhythms, a prominent characteristic of EEG discovered in its initial recordings by Berger (1929), are thought to organize cortical activity (Buzsaki and Draguhn, 2004). Especially prominent in sleep (Loomis *et al.*, 1937), microphysiological studies of their neural basis have until now relied on animal models (Steriade, 2006). Presurgical diagnostic procedures in epilepsy may allow the experimenter to open an invasive window on the brain and record local field and action potentials in order to investigate the fine scale generators of electrical brain oscillations (Worrell *et al.*, 2004, 2008; Jirsch *et al.*, 2006; Clemens *et al.*, 2007; Urrestarazu *et al.*, 2007; Axmacher *et al.*, 2008; Fabo *et al.*, 2008; Cash *et al.*, 2009; Jacobs *et al.*, 2009; Schevon *et al.*, 2009; Crepon *et al.*, 2010). Traditionally, cortical oscillations have been divided into distinct bands, with more or less distinct roles in, for example, vigilance states, various cognitive functions and pathology. Most importantly, the slow (delta) and especially the very fast rhythms (ripple and fast ripple) have been found with fine scale intracranial observations to influence pathological excitability effectively, and may serve as a basic substrate underlying paroxysmal activity (Bragin *et al.*, 2002; Worrell *et al.*, 2004, 2008; Jirsch *et al.*, 2006; Urrestarazu *et al.*, 2007; Fabo *et al.*, 2008; Jacobs *et al.*, 2009; Schevon *et al.*, 2009; Crepon *et al.*, 2010). More generally, during normal cortical function, oscillations are hierarchically organized and this oscillatory hierarchy can effectively control neuronal excitability and stimulus processing (Lakatos *et al.*, 2005; Steriade, 2006). Low-frequency oscillations seem to play an important role in cognitive functions even in the awake state (Lakatos *et al.*, 2008; Schroeder and Lakatos, 2009), despite the fact that under other circumstances, slow rhythms are usually good signatures of compromised cerebral functions (Ebersole and Pedley, 2003) and sleep (Achermann and Borbely, 1997). In this work, we attempt to link the slow- and higher-frequency cortical oscillations to gain a better insight into the intricate mechanisms of human cortical electrical activity, and show the organizing principles that may govern the structure of human cortical electrical rhythms in sleep.

A fundamental mode of cortical activity in mammals is the predominance of slow (<1 Hz) oscillations during the deepest stage of non-rapid eye movement (REM) sleep (Achermann and Borbely, 1997; Steriade *et al.*, 2001; Timofeev *et al.*, 2001; Luczak *et al.*, 2007). In humans, this stage (the third and deepest stage of non-REM sleep; N3, also called slow wave sleep) is reached when 20% or more of an epoch consists of slow wave activity (0.5–2 Hz) in the frontal EEG, having peak-to-peak amplitudes larger than 75  $\mu$ V, and accompanied by the behavioural signs of sleep (Iber *et al.*, 2007). Intracellular recordings in cats during natural slow wave sleep have revealed that slow oscillations are

composed of rhythmically recurring phases of increased cellular and synaptic activity (up-states) followed by hyperpolarization and cellular silence (down-states) (Steriade and Timofeev, 2003). In human slow wave sleep, the surface positive slow wave activity half-wave (up-state) contains increased alpha and beta power compared with the surface negative slow wave activity half-wave (down-state), suggesting that their basic neurophysiology may be similar to animal findings (Molle *et al.*, 2002; Massimini *et al.*, 2004). While the slow oscillation in animals is limited to below 1 Hz (Steriade *et al.*, 1993b), the recent American Academy of Sleep Medicine guidelines suggest the 0.5–2 Hz range for slow wave activity in humans (Iber *et al.*, 2007).

Studies into the neural mechanisms of slow waves have been motivated by reports that they underlie restorative sleep functions and serve memory consolidation (Huber *et al.*, 2004; Marshall *et al.*, 2006; Vyazovskiy *et al.*, 2008) via ensemble reactivation (Born *et al.*, 2006; Euston *et al.*, 2007) and synaptic strength normalization (Vyazovskiy *et al.*, 2008). Slow oscillation can be induced artificially by various anaesthetics *in vivo* (Steriade *et al.*, 1993b; Volgushev *et al.*, 2006; Luczak *et al.*, 2007) and ionic environments *in vitro* (Sanchez-Vives and McCormick, 2000; Shu *et al.*, 2003; Haider *et al.*, 2006). Slow oscillations are generated in cortico-cortical networks, since they survive thalamectomy (Steriade *et al.*, 1993a), but not the disruption of cortico-cortical connections (Amzica and Steriade, 1995). However, recent data suggest a complex thalamocortical interplay in slow oscillation generation (Crunelli and Hughes, 2010). Fine scale laminar analysis of neuronal firing activity revealed that artificial slow oscillations in slice preparations are the earliest and most prominent in the infragranular layers, where they are initiated, and spread toward the superficial layers with a long  $\sim$ 100 ms inter-laminar delay (Sanchez-Vives and McCormick, 2000). Subthreshold membrane potential fluctuations giving rise to local field potentials (LFPs) clearly precede neuronal firing at up-state onset; thus, firing may be the consequence rather than the cause of up-state initiation (Chauvette *et al.*, 2010). Current source density (CSD) analysis of the low-frequency (<1 Hz) components of the artificial, anaesthesia-induced slow oscillations (Steriade and Amzica, 1996) localized the most prominent up-state-related sinks to the middle and deepest cortical layers (most probably layers III and VI). In contrast, the fast (30–40 Hz) components were more distributed, composed of ‘alternating microsinks and microsources’ along the whole cortical depth (Steriade and Amzica, 1996). In another publication the same authors reported a massive up-state-related sink in layers II–III, besides weaker ones in the deeper layers during spontaneous and evoked K-complexes (Amzica and Steriade, 1998). In still another cat study, the maximal up-state-related sink in natural sleep was located in the

middle and deep layers (Chauvette *et al.*, 2010). The laminar distribution of the major up-state-related sink in the rat primary auditory cortex was variable (Sakata and Harris, 2009). On average across animals, the maximal up-state-related sink was located in middle and deep layers (most probably layers III–V) in natural sleep, whereas it was located in superficial layers (most probably layers II and III) under urethane anaesthesia (Sakata and Harris, 2009). In intact animals the up-state onset-related initial firing, intracellular membrane potential and LFP changes could be detected in any layer in a probabilistic manner, with a short inter-laminar delay (~10 ms); however, on average, the earliest activity was found in the infragranular layers (Sakata and Harris, 2009; Chauvette *et al.*, 2010). Although the cellular and synaptic/transmembrane mechanisms of slow waves during natural sleep are thus under intense investigation in animals, these mechanisms have not previously been studied in humans.

Here we show the basic correspondence between the surface positive phase of the slow wave in humans and the up-state described in animals. Besides spindle and beta band oscillations (Molle *et al.*, 2002), we found that the up-state in humans strongly groups action potentials, alpha, gamma (30–150 Hz) and ripple oscillations (100–200 Hz), which have been implicated in attention, memory and epilepsy (Grenier *et al.*, 2003; Molle *et al.*, 2004; Jensen *et al.*, 2007). Despite these basic similarities, we found that the neural mechanisms of natural slow wave activity in humans show several differences compared with previous studies in animals. Specifically, the cortical synaptic/transmembrane generators of the slow wave activity slow (<2 Hz) components, as well as the associated high-frequency (10–200 Hz) oscillations, were all strongly and consistently localized in the supragranular layers, in partial contrast to previous proposals based on studies in animals (Steriade and Amzica, 1996; Sakata and Harris, 2009; Chauvette *et al.*, 2010). In addition, we found that, as measured by cellular discharges, the onset of the up-state was rather synchronous across cortical layers, as in intact animals (Sakata and Harris, 2009; Chauvette *et al.*, 2010) but unlike in slices from ferrets, where long inter-laminar firing delays at up-state onset were found (Sanchez-Vives and McCormick, 2000). Furthermore, the average firing rate of human cortical neurons in the up-state was a fraction of what has generally been observed in animal studies (Steriade *et al.*, 2001; Isomura *et al.*, 2006; Luczak *et al.*, 2007). We consider the experimental, cytoarchitectonic, pathological and phylogenetic aspects that may have contributed to these important differences between the slow waves in humans versus lower mammals.

## Materials and methods

### Patients and electrodes

Five patients with intractable epilepsy underwent chronic clinical subdural grid and strip electrode implantation (Fig. 1) as a standard procedure for localization of the seizure focus and eloquent areas. Fully informed consent was obtained from each subject under the auspices of the Hungarian Medical Scientific Council and local ethical committee, National Institute of Neuroscience, Budapest, Hungary according

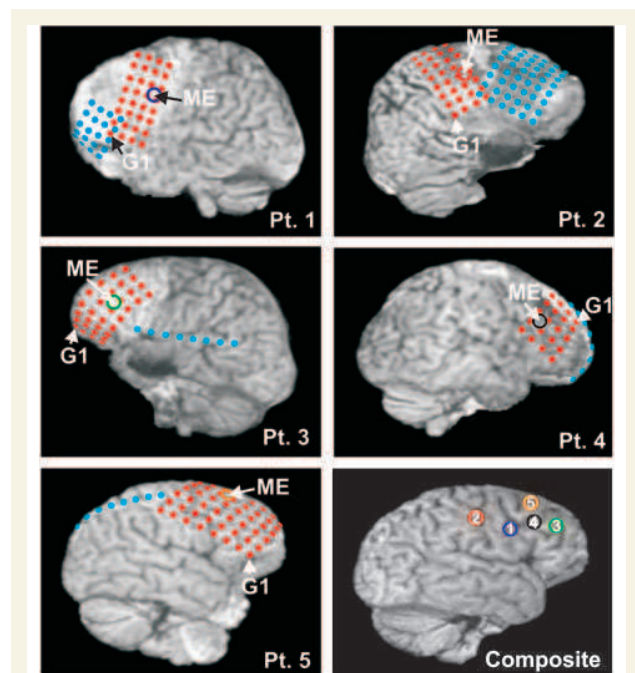
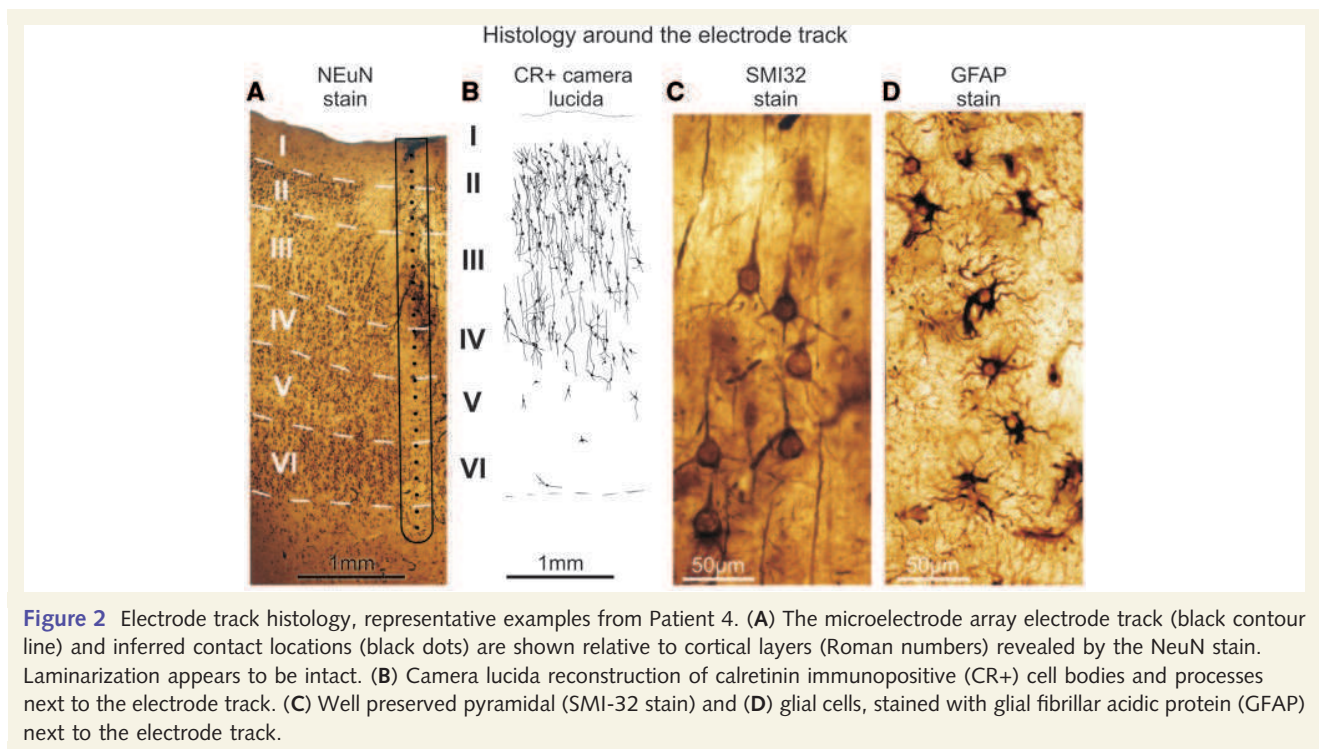


**Figure 1** Grid, strip and multichannel microelectrode array (ME) locations in all patients. Locations are superimposed on 3D reconstructions of MRIs taken with the electrodes in place, aided by intraoperative navigation and photographs. Grid and strip electrode contacts are depicted in red and blue colours; the first grid contact is marked with G1. Microelectrode array locations of Patient (Pt) 1 (blue), left Brodmann area (BA) 9; Patient 2 (red), right BA 2; Patient 3 (green), left BA 46; Patient 4 (black), right BA 9; Patient 5 (orange), right BA 8 are marked with circles.

to the World Medical Association Declaration of Helsinki. Conventional clinical subdural electrocorticography (ECoG) electrode strips and grids were implanted to cover the frontal, temporal and parietal gyri. In addition to the surface electrodes, a 350  $\mu\text{m}$  diameter, 24-contact experimental laminar multichannel microelectrode array was implanted perpendicular to the cortical surface, underneath the clinical grids (Ulbert *et al.*, 2001a, b, 2004a; Cash *et al.*, 2009; Keller *et al.*, 2009). The 40  $\mu\text{m}$  diameter Platinum/Iridium contacts were spaced evenly at 150  $\mu\text{m}$  providing LFP recordings from a vertical, 3.5 mm long cortical track, spanning from layer I to layer VI. A silicone sheet attached to the top of the microelectrode array shank prevented the first contact from sliding more than 100  $\mu\text{m}$  below the pial surface (Ulbert *et al.*, 2001a). In each case, the explanted microelectrode array was visually inspected under a microscope for structural damage, and we did not find any alteration, indicating intact structure throughout the recordings. The location and duration of the clinical electrode implantation were determined entirely by clinical considerations, and the microelectrode array was placed in cortex that was likely to be removed at the definitive surgery.

### Histology

The positions of the electrodes were confirmed by intraoperative navigation, co-localization of intraoperative photographs, pre- and post-operative magnetic resonance scans and 3D magnetic resonance reconstructions (Fig. 1). Photographs were also taken during the



resective surgery to confirm that the surface electrodes did not shift during monitoring. The brain tissue containing the electrode track in Patients 4 and 5 was removed *en bloc* for further anatomical analysis (Ulbert *et al.*, 2004b; Fabo *et al.*, 2008). It was cut into 2–5 mm blocks and immersed into a fixative containing 4% paraformaldehyde, 0.1% glutaraldehyde and 0.2% picric acid in 0.1 M phosphate buffer (pH 7.4). The fixative was changed every hour to a fresh solution during constant agitation for 6 h, and then the blocks were post-fixed in the same fixative overnight. Vibratome sections (60 µm thick) were cut from the blocks and photographs were taken from the electrode tracks. Following washing in phosphate buffer, sections were immersed in 30% sucrose for 1–2 days and then frozen three times over liquid nitrogen. Endogenous peroxidase was blocked by 1% H<sub>2</sub>O<sub>2</sub> in phosphate buffer for 10 min. Sections containing the electrode track were processed for immunostaining against the neuron marker NeuN (Fig. 2A), calretinin (Fig. 2B, reconstructed from camera lucida), SMI-32 (Fig. 2C) and glial fibrillar acidic protein (Fig. 2D) to stain every neuron, a subset of interneurons, pyramidal cells and glia, respectively. Phosphate buffer was used for all the washes (3 × 3–10 min between each step) and dilution of the antisera. Non-specific immunostaining was blocked by 5% milk powder and 2% bovine serum albumin. Monoclonal mouse antibodies against NeuN (1:3000, Chemicon, Temecula, CA, USA), SMI-32 (1:3000, Covance, Princeton, NJ, USA), glial fibrillar acidic protein (1:2000, Novocastra, Newcastle, upon Tyne, UK) and calretinin (1:5000, SWANT, Bellinzona, Switzerland) were used for 2 days at 4°C. Specificity of the antibodies has been thoroughly tested by the manufacturers. For visualization of immunopositive elements, biotinylated anti-mouse immunoglobulin G (1:300, Vector) was applied as secondary antiserum followed by avidin-biotinylated horseradish peroxidase complex (ABC; 1:300, Vector). The immunoperoxidase reaction was developed by 3,3'-diaminobenzidine tetrahydrochloride (DAB; Sigma), as a chromogen. Sections were then osmicated (0.25% OsO<sub>4</sub> in phosphate buffer,

30 min) and dehydrated in ethanol (1% uranyl acetate was added at the 70% ethanol stage for 30 min) and mounted in Durcupan (ACM, Fluka). Layers of the neocortex were outlined using all of the above stains and a shrinkage correction factor published earlier (Turner *et al.*, 1995; Wittner *et al.*, 2006).

Cell counting was performed in Patients 4 and 5 using camera lucida drawing (Fig. 2B) of calretinin immunopositive cells (two sections per patient). The normalized (between 0 and 1) calretinin immunopositive cell density laminar depth profile (number of cells over unit area of cortex) was calculated in each consecutive 150 µm wide and variable length (1–3 mm) horizontal cortical stripes to match the depth structure of the electrophysiology measurements.

## Recordings

After electrode placement, the patients were transferred to the intensive monitoring unit for 5–7 days, where continuous 24 h video-EEG observation took place in order to localize the seizure focus. ECoG from clinical strip and grid electrodes (32–92 channels, mastoid reference) was recorded concurrently with patient video using the standard hospital system (band-pass: 0.1–200 Hz, acquisition rate: 400–5000 Hz/16 bit). Video-EEG data for the duration of monitoring were stored on hard disks for later analysis. The spatial LFP gradient, the voltage difference between consecutive laminar electrode contacts, was provided by a special preamplifier placed inside the head bandage of the patient (Ulbert *et al.*, 2001a). For simplicity, throughout the text the spatial potential gradient is expressed in microvolts rather than the formally correct microvolt per inter-contact distance (150 µm). This reference-independent measurement method was proven to be effective in minimizing the motion-related and electro-magnetic artefacts (Ulbert *et al.*, 2001a). The LFP gradient was split into the EEG range (0.1–300 Hz) and single- and multiple-unit activity frequency range (300–5000 Hz) by analogue band-pass filtering at the level of a

custom-made main amplifier (Ulbert *et al.*, 2001a). An EEG range signal was sampled at 2 kHz/16 bit; the multiple-unit activity range was sampled at 20 kHz/12 bit and stored on a hard drive.

## Slow wave activity detection

We have analysed the LFP gradient, multiple-unit activity, single-unit activity and ECoG data acquired from each patient during one to three nocturnal recording sessions. Since the sleep of the patients was fragmented due to medical care and distress from the hospitalization and head wound, we cannot provide standard hypnograms that are usually obtained from healthy subjects without a recent craniotomy. Craniotomies may also distort the scalp distribution of the EEG due to the lack of bone and excessive fluid accumulation below the scalp; furthermore, if scalp electrodes are placed close to the frontal craniotomy wounds, they may induce infection, and therefore we avoided placing more than two frontal scalp EEG electrodes. Partial sleep staging was performed based on readings of the available scalp EEG and ECoG electrodes by expert neurologists. In this study, we have analysed electrophysiological data obtained only from the deepest stage of non-REM sleep (N3, or slow wave sleep) (Iber *et al.*, 2007). Behavioural sleep was confirmed by the video recording, while slow wave sleep was electrographically identified in accordance with the recent American Academy of Sleep Medicine guidelines (Iber *et al.*, 2007). Slow wave sleep periods were identified when 20% or more of an epoch consisted of slow wave activity (waves in the 0.5–2 Hz frequency range with peak-to-peak amplitude larger than 75  $\mu\text{V}$ , measured over the frontal regions) (Iber *et al.*, 2007). Data containing interictal spikes (within 1 min) and seizures (within 60 min) were excluded from the study to avoid epileptic contamination.

In addition to spectral (Fig. 3A) and autocorrelation analyses (Fig. 3B), slow wave activity cycle detection was based on phase and amplitude information, extracted from the narrow-band filtered (0.3–3 Hz, 24 dB/octave, zero phase shift) layer II LFP gradient (Fig. 4A) and ECoG (Fig. 4B) data. Instantaneous phase of the filtered signal was calculated by the Hilbert transformation. In our implementation, a single slow wave activity cycle was defined between  $-180^\circ$  and  $+180^\circ$  phase. The  $-180^\circ$  phase value corresponded to the trough of the negative half-wave (down-state) preceding the  $0^\circ$  phase, which corresponded to the peak of the positive half-wave (up-state) and finally the  $+180^\circ$  phase corresponded to the following negative half-wave trough (down-state). At each  $+180^\circ$  crossing, the phase was wrapped  $-360^\circ$  for better visualization. To avoid the detection of higher-frequency (e.g. theta) oscillations, waves with shorter than 500 ms cycle lengths (corresponding to higher than 2 Hz frequency) were excluded from the analysis. Waves with non-monotonic phase runs were also excluded, since phase inversions may indicate higher frequency contamination. In addition to phase constraints, valid slow wave activity cycles had to fulfil the following amplitude criteria: the up-state peak amplitude had to be more positive than  $+50 \mu\text{V}$ , and the preceding or following down-state trough amplitude had to be more negative than  $-50 \mu\text{V}$ . The slow wave activity detection algorithm parameters were tuned and carefully validated by expert electroencephalographers. Similar algorithmic parameters were used for all of the patients. To facilitate comparison of our results with previous animal studies, the threshold level was set to  $+50 \mu\text{V}$  on the filtered (0.3–3 Hz, 24 dB/octave, zero phase shift) upper layer III LFP gradient, and the wave triggered (up-state locked) averages were calculated on the unfiltered LFP gradient and multiple-unit activity (Supplementary Fig. 10).

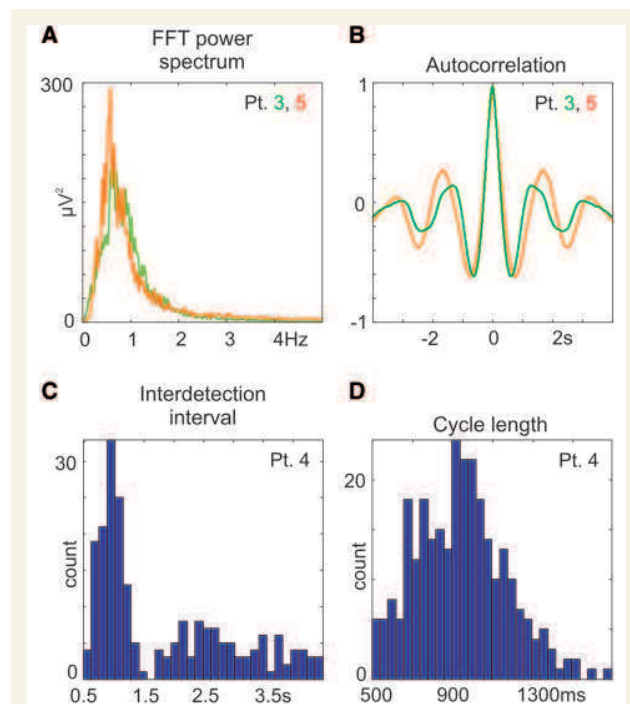


**Figure 3** Spectral and temporal properties of slow wave activity cycles. (A) Representative examples of the fast Fourier transformation power spectrum and (B) autocorrelation of supra-granular LFP gradient in Patients 3 and 5. For additional fast Fourier transformation and autocorrelations see Supplementary Fig. 5G and H. (C) Representative examples of interdetection interval histograms (y-axis: counts, x-axis: time between up-state detections, 166 ms bin) and (D) cycle length histogram (y-axis: counts, x-axis: valid cycle lengths, 33 ms bin) in Patient 4. For additional data see Supplementary Figs 3 and 4.

To quantify and compare slow wave activity parameters with other studies, the frequency of slow wave activity occurrence (detected valid cycles per minute), the interdetection interval histogram (Fig. 3C) and the cycle length histogram (Fig. 3D) were calculated (Massimini *et al.*, 2004). The single sweep (Fig. 4C and D) and averaged (Fig. 5A) time-frequency content of the slow wave activity signal was also computed using wavelet transforms (Delorme and Makeig, 2004). In addition, we attempted to describe the laminar distribution of the slow wave activity in more detail using the LFP gradient fast Fourier transformation power spectrum depth profile (Fig. 5B), the pairwise linear coherence between each LFP gradient trace in the slow wave activity (0.3–3 Hz) frequency range (Fig. 5C) and the depth profile of the LFP gradient autocorrelation (Fig. 5D).

## Current source density analysis

CSD analysis identifies synaptic/transmembrane generators of LFP in laminated neural structures (Freeman and Nicholson, 1975; Nicholson and Freeman, 1975). The negative of the second spatial derivative of the LFP closely approximates the macroscopic current density over a unity cell membrane area. Since the LFP gradient (Fig. 6A) is the first spatial derivative of LFP, one additional spatial derivation yielded the CSD (Fig. 6C) for the EEG range (0.1–300 Hz) data. Inhomogeneous conductivity and electrode spacing were not taken into account

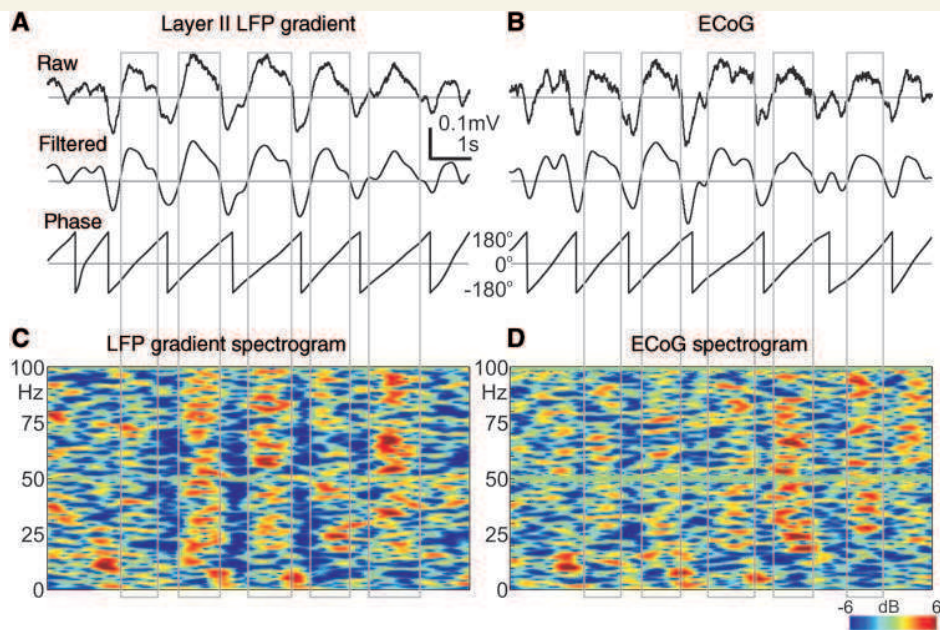


**Figure 4** Similarity between LFP gradient recorded with a microelectrode array within the cortex and ECoG recorded from macrocontacts subdurally. (A) Upper: 'raw' traces of single sweeps containing slow wave activity; broadband (0.1–300 Hz) LFP gradient from layer II. Middle: 'filtered' traces after band-pass (0.3–3 Hz) filtering. Lower: 'phase' traces showing the instantaneous phase of the 'filtered' trace above derived by the Hilbert transform. Grey rectangles indicate automatically detected up-states (surface positive half-waves). Patient 4. (B) Same as (A), but recorded from neighbouring ECoG contacts. (C) Colour map of LFP gradient and (D) ECoG spectral power during the slow wave activity shown in (A) and (B). x-axis: time, y-axis: frequency, z-axis: colour coded relative spectral power in dB, compared with the mean of the entire interval in each frequency band (relative spectrogram). For more examples of single sweep traces, see Supplementary Figs 1 and 2.

(both were substituted by the dimensionless number 1 in the calculations); high spatial frequency noise and boundary effects were reduced by Hamming-window smoothing and interpolation (Ulbert *et al.*, 2001a), and thus CSD was expressed in microvolts. It was shown previously (Ulbert *et al.*, 2001a, b, 2004a, b; Wang *et al.*, 2005; Halgren *et al.*, 2006; Knake *et al.*, 2007; Fabo *et al.*, 2008; Cash *et al.*, 2009; Steinorth *et al.*, 2009; Wittner *et al.*, 2009) that our recording and analysis techniques can reliably detect CSD activity in each layer of the human cortex and hippocampus.

## Statistical analysis of electrophysiology and histology

ANOVA with Tukey's honestly significant difference test were applied to the normalized values (LFP gradient and CSD: between  $-1$  and  $+1$ ; multiple-unit activity, gamma band LFP gradient and CSD: between  $0$  and  $1$ ). Normalized values were grouped by layers (I–VI), and the grand average (across all patients) of LFP gradient, multiple-unit activity, CSD, gamma band (30–150 Hz) LFP gradient and gamma band CSD power depth profile at the up-state peak were tested to determine statistically significant differences ( $P < 0.01$ ) between electrophysiological activations in different layers of the cortex (Fig. 6E–H). Results are depicted on box-whisker plots [small box = mean; big box = standard error (SE); whisker = standard deviation (SD)]. For detailed statistical data, see Supplementary Fig. 9.

In Patients 4 and 5 (with available histology), the averaged, normalized calretinin immunopositive cell density (Fig. 8A) and averaged, normalized electrophysiology depth profiles (consecutive values at

each cortical depth) were constructed. Average depth profiles of the LFP gradient (Fig. 8B) and CSD (Fig. 8C) at the peak of the up-state were normalized between  $-1$  and  $+1$ , while average depth profiles of multiple-unit activity (Fig. 8D) and spectral measures (Fig. 8E and F) (gamma band LFP gradient and CSD) at the peak of the up-state were normalized between  $0$  and  $1$ . The calretinin immunopositive cell density depth profile was normalized between  $0$  and  $1$ . SE is marked by whisker in this case. The normalized cell density and electrophysiology measures were compared using the Pearson  $r$  correlation method with  $P < 0.01$  significance level criterion.

## Single- and multiple-unit activity analysis

A continuous estimate of population neuronal firing rate was calculated from the multiple-unit activity range (300–5000 Hz) data. The signal was further filtered (500–5000 Hz, zero phase shift, 48 dB/octave), rectified and decimated at 2 kHz, applying a 0.5 ms sliding average rectangular window, followed by a final, smoothing low-pass filter (20 Hz, 12 dB/octave) (Fig. 6B). Putative single units (Fig. 10B, Supplementary Fig. 7) were analysed by conventional threshold detection and clustering methods using Dataview and Klustawin (Heitler, 2006) and custom-made MATLAB software. Putative single units from Patients 1, 4 and 5 were included in the analyses, which were recorded stably for at least 600–1000 s in slow wave sleep. In Patient 2, multiple-unit activity was not recorded for technical reasons, while Patient 3 showed no discriminable single units. After threshold recognition (mean  $\pm 3$ –5 SD) (Csicsvari *et al.*, 1998) at a given channel,

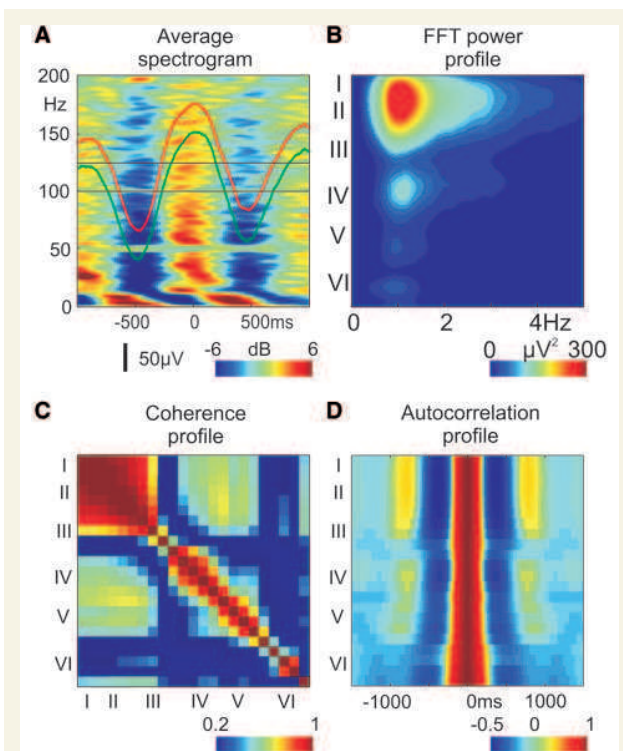


**Figure 5** Spectro-temporal and spatial properties of slow wave activity, representative data from Patient 3. **(A)** Increased broadband spectral activity during up-states: up-state locked, averaged, relative spectrogram of layer II LFP gradient (x-axis: time, y-axis: frequency, z-axis: colour-coded averaged relative spectral power in dB). For the neighbouring ECoG, the averaged relative spectrogram is depicted in Supplementary Fig. 5A. Red (LFP gradient) and green (ECoG) traces show the average potentials. **(B)** Depth distribution profile of the LFP gradient fast Fourier transformation power spectrum (EEG range: 0.1–300 Hz data, no additional digital filtering was used, x-axis: frequency, y-axis: cortical depth, with corresponding layers, z-axis: colour-coded fast Fourier transformation power). For more power spectrum examples, see Supplementary Fig. 5B. **(C)** Depth distribution profile of pairwise coherence of LFP gradient channels in different cortical layers. x-axis: cortical depth, with corresponding layers, y-axis: cortical depth, with corresponding layers, z-axis: colour-coded pairwise coherence of the band-pass (0.3–3 Hz) LFP gradient. For more pairwise coherence examples, see Supplementary Fig. 5C. **(D)** Depth distribution profile of LFP gradient autocorrelation. x-axis: time, y-axis: cortical depth, with corresponding layers, z-axis: colour-coded autocorrelation of the LFP gradient. For more laminar autocorrelation examples, see Supplementary Fig. 5D.

three representative amplitude values were assigned to each unclustered spike waveform. These triplets were projected into 3D space and a competitive expectation-maximization based algorithm (Harris *et al.*, 2000) was used for cluster cutting (Heitler, 2006). If the autocorrelation of the resulting clusters contained spikes within the 2 ms refractory interval, it was reclustered. If reclustered did not yield a clean refractory period, the cell was regarded as multiple units and omitted from the single cell analysis. Given the gradient recording, spikes at

neighbouring traces appeared as mirror images, thus from adjacent channels (150  $\mu\text{m}$  apart) only one channel (the one that yielded the better signal to noise ratio) was included in the analysis. To reveal double detection, the cross-correlogram was constructed (Staba *et al.*, 2002b) for next to adjacent (300  $\mu\text{m}$  apart) pairs of putative single cells. No coincident interactions [99% confidence limit at 0 ms (Staba *et al.*, 2002b)] were found. A spike train was determined as a burst, if at least three consecutive spikes occurred within a maximum 20 ms long interval, which was preceded and followed by at least 20 ms long intervals with neuronal silence (Staba *et al.*, 2002a).

Phase dependence of single cell firing rate (Fig. 10C) was computed for 30° phase bins; the total number of firing in a given bin was divided by the total time that the cortex spent in that phase bin (thus producing a phase histogram). The Rayleigh test ( $P < 0.01$ ) was used to judge if the resulting circular distribution was significantly different from the uniform distribution.

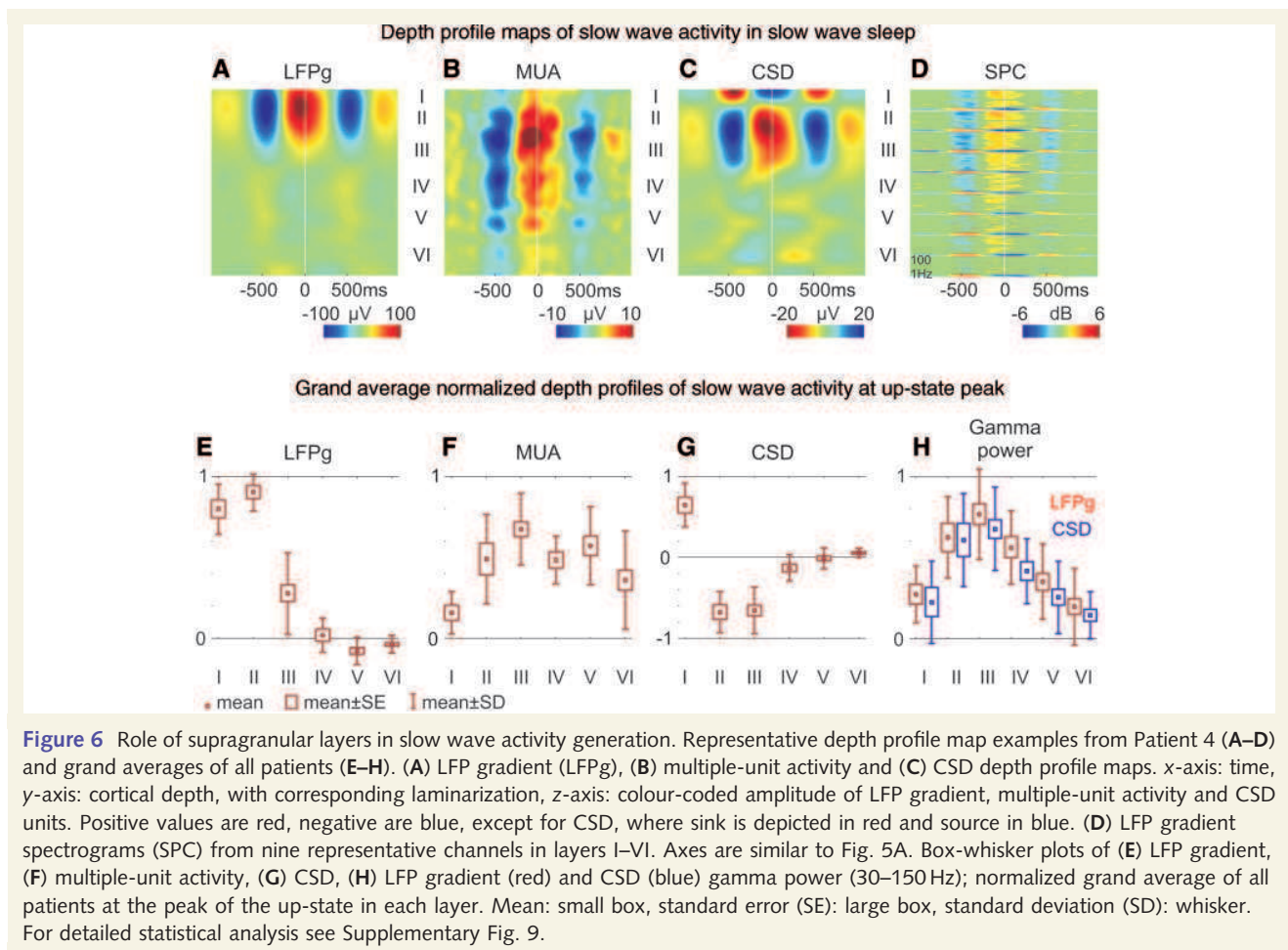
We have shown previously (Ulbert *et al.*, 2001a, b, 2004a, b; Wang *et al.*, 2005; Halgren *et al.*, 2006; Fabo *et al.*, 2008; Cash *et al.*, 2009; Wittner *et al.*, 2009) that our single-unit activity, multiple-unit activity recording and analysis techniques can reliably detect task or epilepsy-related modulation of neuronal firing from each layer of the human cortex and hippocampus.

## Results

Previous studies of slow wave activity in humans (Achermann and Borbely, 1997; Massimini *et al.*, 2004, 2005, 2007; Molle *et al.*, 2004; Marshall *et al.*, 2006) have been limited to macroelectrode recordings that superimpose activity from several squared centimetres of cortex. These recordings are ambiguous as to the circuits involved, are not sensitive to neuronal firing and do not distinguish between excitatory and inhibitory mechanisms. We used laminar multichannel microelectrode array recordings (Ulbert *et al.*, 2001a, b, 2004a, b; Wang *et al.*, 2005; Halgren *et al.*, 2006; Knake *et al.*, 2007; Fabo *et al.*, 2008; Cash *et al.*, 2009; Steinvorth *et al.*, 2009; Wittner *et al.*, 2009) to estimate neuronal firing and synaptic/transmembrane currents in different cortical layers. Since cortical neuronal populations and synaptic inputs are organized into distinct layers, these recordings allowed us to resolve the cortical generators underlying slow wave activity in humans.

## General features of human slow wave activity

Clinical subdural strip and grid electrodes and multichannel microelectrode arrays were implanted into the frontal and parietal cortices of patients ( $n = 5$ ) with intractable epilepsy (Fig. 1) in order to identify the seizure focus and eloquent cortex prior to surgical therapy. The focus was eventually localized to the frontal lobe in four patients and to the temporal lobe in one. Histology of the microelectrode array penetration track was recovered in two patients; it showed intact laminarization (Fig. 2A) and well-preserved interneurons, pyramidal cells and glia (Fig. 2B–D), indicating no discernable epilepsy or implantation-related damage of the examined cortex. None of the patients had pre-operative pathological MRI findings in the 1–2 cm vicinity of the microelectrode array implantation site.



Automatic slow wave activity cycle detection was based on amplitude and phase information using an LFP gradient (Fig. 4A) and ECoG (Fig. 4B) recorded during slow wave sleep (also see Supplementary Figs 1 and 2). On average, 20 slow wave activity cycles (mean = 20 1/min, range = 12–26 1/min, SD = 7 1/min) were detected per minute (Supplementary Figs 3 and 4). Cycle length peaked on average at 0.8 s (mean = 0.8 s, range = 0.6–1.4 s, SD = 0.3 s) (Fig. 3D). Interdetection interval (Fig. 3B) peaked on average at 1.1 s (mean = 1.1 s, range = 0.8–1.2 s, SD = 0.4 s), all comparable to healthy subjects (Massimini *et al.*, 2004). LFP gradient (Fig. 3A and C) and ECoG (not shown) fast Fourier transformation power spectrum and autocorrelation (Fig. 3A and B, Supplementary Fig. 5G and H) also corresponded well to previous human (Achermann and Borbely, 1997) and animal (Isomura *et al.*, 2006) findings, indicating correct slow wave activity cycle identification and relatively normal slow wave activity production.

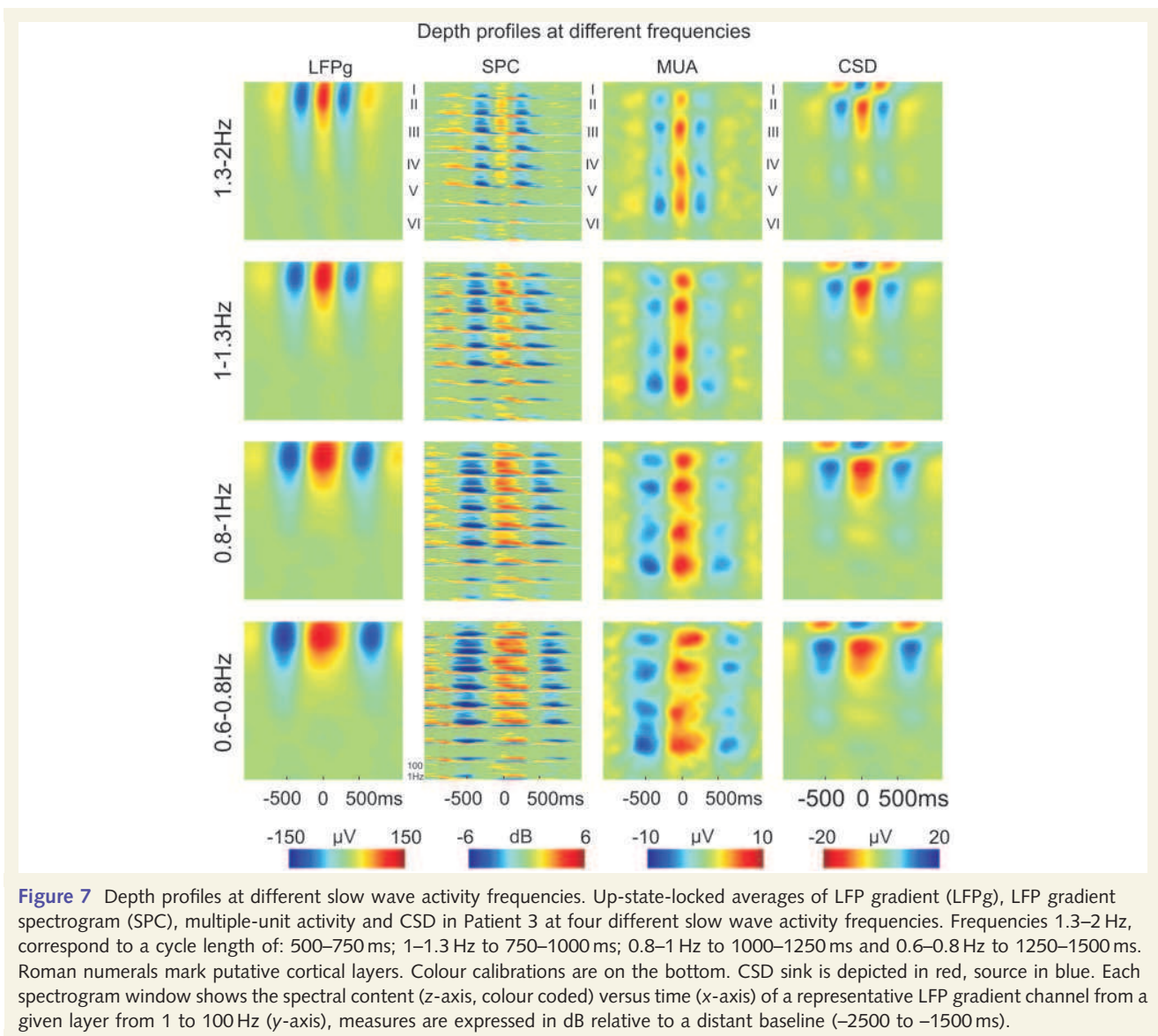
The LFP gradient recorded in layer II (Fig. 4A) closely resembled the locally recorded ECoG (Fig. 4B), with Pearson  $r > 0.9$  ( $P < 0.01$ ) in all patients (Supplementary Fig. 1). Time-locked averages to the peak of the surface positive half-wave (up-state) showed similar LFP gradient and ECoG waveforms regardless if time locking was based on the LFP gradient or ECoG (Fig. 5A, red and green

traces). Both LFP gradient and ECoG (Figs 4C and D and 5A, Supplementary Fig. 5A) showed broadband (10–200 Hz) spectral increases during up-states and decreases during down-states.

## Laminar distribution of slow wave activity

To estimate the laminar contribution of various activities, micro-electrode array channels were assigned into six putative layers (I–VI) based on the histological findings (Fig. 2A) when available and cortical depth when not. This analysis revealed a substantial concentration of the 0.3–3 Hz band LFP gradient fast Fourier transformation power within layers I–III (Fig. 5B, Supplementary Fig. 5B) in each patient, indicating strong supragranular synaptic/transmembrane activity. The slow wave activity shape similarities between electrode contacts were significantly greater in supragranular versus infragranular layers in each patient (0.634 versus 0.423, grand average pairwise coherence, Kruskal–Wallis ANOVA,  $P < 0.01$ ) (Fig. 5C, Supplementary Fig. 5C), while autocorrelation profiles revealed a more precisely paced rhythm supragranularly (Fig. 5D, Supplementary Fig. 5D) in each patient.

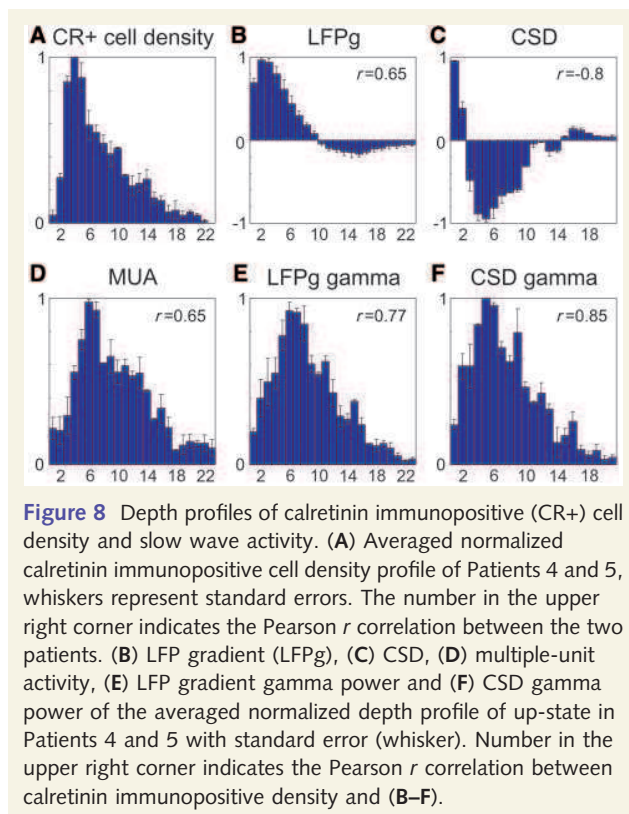
Several measurements, both in individual patients (Fig. 6A–D) and in grand averages (Fig. 6E–H), reflecting different aspects of



population synaptic/transmembrane and firing activity, were maximal in supragranular layers (for detailed statistical analysis, see Supplementary Fig. 9) at the up-state peak. Normalized, grand average depth profiles of LFP gradient (Figs 6E and 8B) were marked by maximally positive deflections in layers I–III, inverting in layers V and VI into a small negativity. Multiple-unit activity was also maximal in layer III (Figs 6F and 8D). The CSD depth profile at the peak of the slow wave activity up-state showed a maximal source (outward current) in layer I and maximal sink (inward current) in layers II and III, and only very small CSD deflections were observed infragranularly (Figs 6G and 8C). In contrast, the CSD depth profile of a population of interictal spikes detected manually and locked to the surface positive LFP gradient (similarly as in the case of the up-state) were markedly different, exhibiting a large sink–source pair in the infragranular layers (Supplementary Fig. 11). Significant increases [bootstrap analysis (Delorme and Makeig, 2004),  $P < 0.01$ ] in LFP gradient spectral

power were detected in all layers at 10–100 Hz frequencies during up-states (Fig. 6D). Gamma power of LFP gradient and CSD was maximal in layer III (Figs 6H, 8E and F). Separate averages of different slow wave activity cycle lengths corresponding to appropriate (0.6–0.8 Hz, 0.8–1 Hz, 1–1.3 Hz and 1.3–2 Hz) oscillation frequencies also yielded qualitatively similar LFP gradient, spectral LFP gradient, multiple-unit activity and CSD distribution (Fig. 7, Supplementary Fig. 6). We have found no statistically significant differences in any layers (ANOVA, Tukey's honestly significant difference *post hoc* test,  $P > 0.3$ ) in the CSD or multiple-unit activity at the peak of the up-state between any of the four frequency bands indicating similar cortical generator mechanisms above (up to 2 Hz) and below 1 Hz (down to 0.6 Hz).

Calretinin immunopositive cell density depth profiles (Fig. 8A) were calculated in two patients and correlated with the depth profile at the up-state peak of the LFP gradient, CSD, multiple-unit activity, LFP gradient and CSD gamma power (Fig. 8B–F).

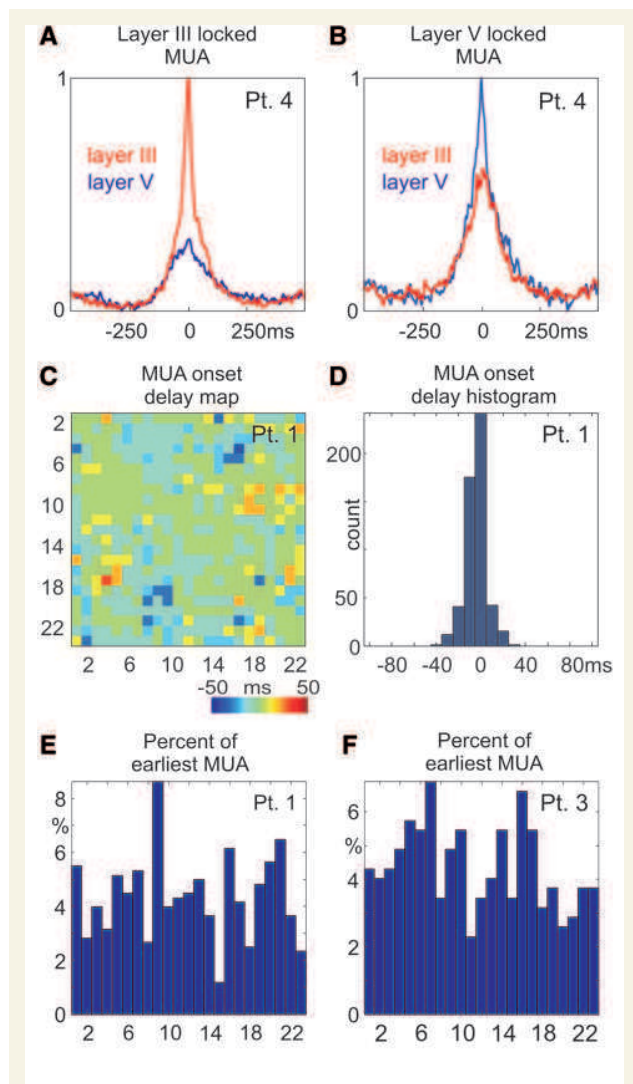


Calretinin immunopositive cell density between Patient 4 and 5 showed high similarity ( $r=0.95$ ,  $P<0.01$ ). The highest positive correlation was found between calretinin immunopositive cell density and CSD gamma power ( $r=0.85$ ,  $P<0.01$ ).

## Multiple-unit activity timing at up-state onset

The time courses of multiple-unit activity were examined to determine if one layer may lead others. It was shown in ferret slices (Sanchez-Vives and McCormick, 2000) that layer V's multiple-unit activity consistently led layers II and III by an average of over 100 ms. In our study, the up-state-associated multiple-unit activity peak-locked averages indicated no evident timing difference in any of the patients, between layers III and V, regardless of whether peak alignment was based on layer III or layer V activity (Fig. 9A and B, Supplementary Fig. 5E and F).

To characterize the multiple-unit activity timing between different layers further, it was cross-correlated (3 SD threshold, 10 ms bin size) between each pair of channels, within 200 ms of every up-state onset. In agreement with animal studies (Sakata and Harris, 2009; Chauvette *et al.*, 2010), delay maps and histograms (Fig. 9C and D) indicated a short inter-laminar multiple-unit activity timing difference at up-state onset; most of the delays were within the  $\pm 10$  ms bin. We also calculated how often (in percentage of all sweeps) any given multiple-unit activity channel shows the earliest firing at up-state onset. In all patients (where multiple-unit activity was available), the initial firing was quite



uniformly distributed across cortical depths. Unlike in a ferret *in vitro* study (Sanchez-Vives and McCormick, 2000), we found no evidence for long ( $\sim 100$  ms) lead or lag times between different layers (Fig. 9E and F).

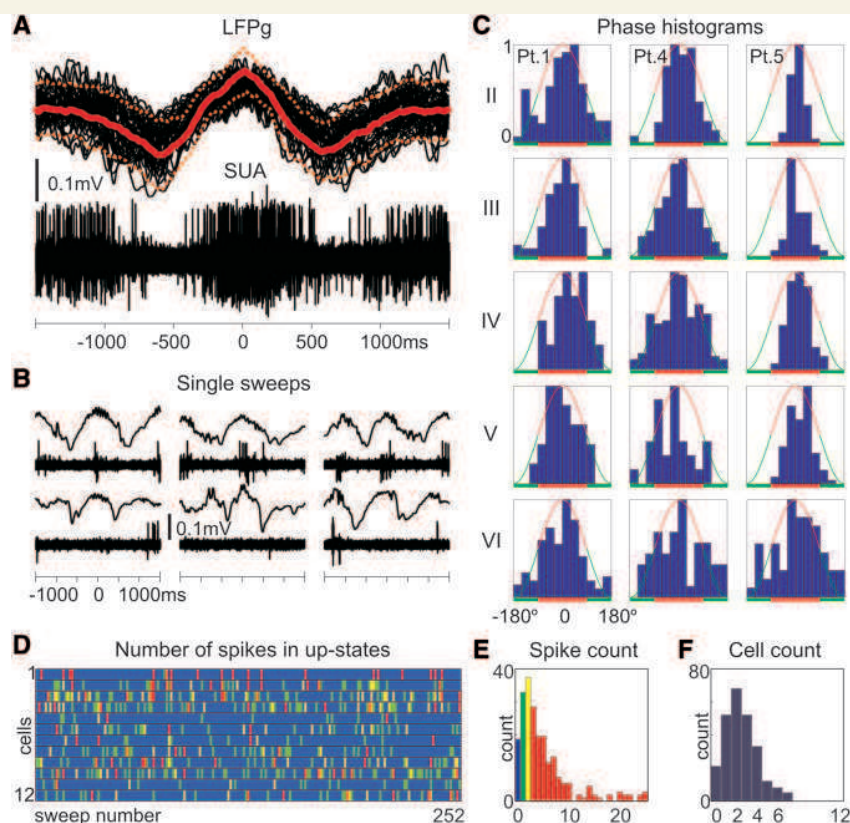


**Figure 10** Single-unit firing in slow wave activity. (A) Superimposed (40 consecutive sweeps) and (B) individual single sweeps of the simultaneously recorded supragranular LFP gradient (LFPg) and multiple-unit activity/single-unit activity (SUA) (Patient 5). Solid and dashed red lines represent LFP gradient mean and standard deviation. (C) Representative normalized (from 0 to 1) firing rate versus phase histograms (from  $-180^\circ$  to  $+180^\circ$ , in  $30^\circ$  bins) of clustered cells from different layers and patients. Red line: positive half-wave (up-state), green line: negative half-wave (down-state). (D) Columns represent individual slow wave activity cycles (1–252), rows represent clustered neurons (cell 1–12 of Patient 4) and colour represents the firing of a given cell. Blue: no firing in the given up-state for the given cell, green: one, yellow: two, red: three or more action potentials. (E) Histogram of the overall number of spikes for all the 12 clustered cells during up-states. (F) Histogram of the number of active cells, firing at least one action potential during up-states. These data illustrate sparse firing in up-states, only a small fraction of the clustered cells fire and these cells together generate only a few action potentials. For additional data, see Supplementary Figs 7 and 8.

## Single-unit correlates of slow oscillation

Recordings from three patients yielded good quality (Supplementary Fig. 7) single-unit activity (Fig. 10). Epochs ( $\sim 1000$ s) showing the largest slow wave activity detection frequencies were selected for analysis from the first sleep cycle. Overall 33 single units were clustered (9, 12 and 12 from Patients 1, 4 and 5) with mean firing rate of 0.66 Hz (range = 0.12–2.0 Hz, SD = 0.48) and mean burst frequency of 3.1 1/min (range = 0–14 1/min, SD = 3.6). Both the average firing rate and the spontaneous burst rate were well below the reported epileptic threshold found in cortical and hippocampal structures (Staba *et al.*, 2002a).

Nearly all cells (31 of 33) showed significantly non-uniform spiking (Fig. 10A and C, Supplementary Fig. 7D and E) over the slow wave activity cycle (Rayleigh test,  $P < 0.01$ ), with a peak up-state firing rate mean of 1.63 Hz (range = 0.45–4.6 Hz, SD = 0.96). We found no significant differences between patients in mean firing rates (Kruskal–Wallis ANOVA,  $P > 0.2$ ), indicating

homogeneous distribution. Although mean firing rates grouped by supra- versus infragranular layers showed no significant differences ( $P > 0.1$ ), supragranular peak up-state firing rates were significantly higher (2.2 Hz versus 1.2 Hz, Kruskal–Wallis ANOVA,  $P < 0.01$ ) than the same measure for infragranular layers. We found the proportion of firing cells and the rate at which they fire in any given up-state (Fig. 10D–F, Supplementary Fig. 8) remarkably low. On average, only 27% of the clustered cells were active (firing at least one spike) during any given up-state (20%, 25% and 36% in each patient). Thus, an average neuron fired in every third to fifth up-state. Moreover, on average, each neuron fired only 0.32 spikes per up-state (0.44, 0.2 and 0.32 in each patient). As an example, out of the 12 clustered neurons in Patient 4, the most probable number of active cells in a given up-state was 2 (Fig. 10F, see also Supplementary Fig. 8C and F), and the most probable number of overall spikes the 12 cells fired within a given up-state was also 2 (Fig. 10E, see also Supplementary Fig. 8B and E).

## Discussion

Our results establish a close similarity between human slow wave activity and the animal slow oscillation at the level of field potential, cellular firing activity and spectral measurements (Steriade, 2006), but they also reveal a number of novel, unexpected findings. Consistent with prior studies in animals, we have shown in humans that the up-state was associated with increased firing and elevated spindle, alpha, beta, gamma and ripple power during the surface-positive LFP half-wave, while the down-state was characterized by the widespread surface negative LFP half-wave with decreased firing and oscillatory activity (Cash *et al.*, 2009). Differences from prior studies were found in the laminar distribution of the up-state, average firing rates during the up-state and the consistency of generators for oscillations above versus below 1 Hz. These contrasts could reflect cortical cytoarchitectonic differences or they could be due to the circumstances of the recordings, including natural sleep versus different types of anaesthesia, or *in vivo* versus *in vitro* preparations. They could also be due to epileptic pathology or to phylogenetic differences.

## Epilepsy and slow wave activity

Epilepsy is a multi-causal disease with diverse aetiology. Focal epilepsies have circumscribed seizure initiating regions without severe pathological alterations in other areas. Surgical candidates are selected exclusively from this patient group during the careful pre-operative evaluation, based on several diagnostic findings (CT, MRI, functional MRI, PET, single-photon emission computed tomography, video-EEG, magnetoencephalography, functional neurophysiological tests, Wada-test and seizure semiology). In the present study we included only patients with evidence for focal disease.

The laminar LFP gradient, CSD, multiple-unit activity and spectral profile of interictal activity *in vivo* and *in vitro* have already been established by our group (Ulbert *et al.*, 2004a, b; Fabo *et al.*, 2008; Wittner *et al.*, 2009). We have shown that the initial phase of the interictal discharges are large amplitude brief events characterized by substantial action potential, LFP gradient, CSD, multiple-unit activity and spectral surges, often emerging from the granular and infragranular (Supplementary Fig. 11) layers of the cortex (Ulbert *et al.*, 2004a). These events are clearly distinct from the background activity and exquisitely visible in single sweeps. Based on our prior knowledge, we carefully excluded any suspicious pathological events from the analysis presented in this article, and we also carefully avoided analysing data derived from electrodes in the proximity of the seizure focus.

Several other considerations suggest that the current findings on the neuronal mechanisms underlying slow wave activity, although recorded in epileptic patients, might also apply to healthy subjects. Our slow wave activity morphology corresponded well to those oscillations collected from standard scalp sleep EEG recordings from healthy subjects. Similarities included not only the slow wave activity frequency and rhythmicity (Achermann and Borbely, 1997), but the asymmetric shape, the briefer and sharper deflection in the down-state (Massimini *et al.*, 2004) and higher beta power content in the up-state (Molle *et al.*, 2002). Our

results of detection frequency, cycle length and interdetection interval histograms are all comparable to previous findings from healthy subjects (Massimini *et al.*, 2004), despite both the recording and analysis methodologies being different. Minor deviations in the exact numbers are therefore natural and may reflect methodological differences rather than disease-related alterations. In addition, neither the firing rate nor the burst rate exceeded the pathological criteria found for single neurons in slow wave sleep (Staba *et al.*, 2002a, b). Finally, the lack of any MRI abnormalities and intact laminarization of the excised tissue strongly suggests that we recorded from structurally intact regions, free of gross functional alterations.

Nevertheless, there are some observations in our study that may be related to the patients' pathology. Out of the 33 clustered units in three patients, two single cells in one patient (Patient 1) showed uniform firing during the slow wave activity cycle (layer III unit #3, average firing rate=1.17 Hz, layer V unit #6, average firing rate=0.54 Hz). While some firing during the down-states could be expected due to biological variability of the slow wave activity or due to inaccuracy of the state detection algorithm, a lack of significant modulation by slow wave activity in these cells may reflect a pathological resistance by a small subgroup of cortical neurons to the network-wide deactivation occurring in the down-state.

## Localization of cortical oscillations in slow wave activity

A consistent CSD pattern of our study was the prominent sink-source pair in the supragranular layers compared with the weak infragranular activation. This localization was true for both the low- (0.5–2 Hz) and the high-frequency (10–200 Hz) oscillations in all patients, in frontal and parietal areas.

In our interpretation, the prominent layer II and III sink during the up-state reflects the large active inward currents flowing across the distal dendritic membrane compartments of layers V and VI pyramidal cells and distal, proximal and basal dendritic membrane compartments and perhaps on the somatic membrane of layers II and III pyramidal cells. The corresponding passive, return, source currents are flowing in layer I, across the most superficial apical dendritic membrane compartments of the pyramidal cells. The spatial CSD pattern in the down-state is inverted, exhibiting a large active current source in layers II and III due to hyperpolarizing currents (likely outward potassium flows from the pyramidal cells) and a passive return sink in layer I (Cash *et al.*, 2009).

Our CSD findings from the frontal and parietal areas in natural sleep are in contrast with a study in the cat suprasylvian area, albeit under ketamine/xylazine anaesthesia (Steriade and Amzica, 1996). At low frequencies (~1 Hz), the maximal up-state-related sink in the cat was located in the middle rather than in the superficial layers, surrounded by not only a superficial but also a large deep source. In addition, a substantial up-state-related sink in the deepest layer was present in the cat, which was practically invisible in our human recordings. The same authors also showed a massive supragranular (layers II and III) up-state-related sink besides one or

two deeper and weaker sinks, during the spontaneous and evoked K-complex (Amzica and Steriade, 1998). Moreover, at higher frequencies ( $\sim 35$  Hz) and during the K-complex, a series of 'alternating microsinks and microsources' was found throughout the depth of the cat suprasylvian area (Steriade and Amzica, 1996; Amzica and Steriade, 1998). Such alternating patterns are best explained by insufficient spatial resolution in the LFP sampling (8 contact,  $250\ \mu\text{m}$  spacing electrode array) and corresponding spatial aliasing error, and not by neuronal sources (Tenke *et al.*, 1993).

A recent study in the cat suprasylvian area in natural sleep with adequate spatial sampling ( $100\ \mu\text{m}$ ) revealed alternation free middle and deep layer sinks and a superficial source during the up-state (Chauvette *et al.*, 2010). Thus, besides cytoarchitectonic differences between different types of cortices (e.g. frontal and parietal areas in humans versus suprasylvian area in the cat), and methodological errors, it is also plausible to assume that neuronal mechanisms of natural sleep and ketamine/xylazine anaesthesia may be different, further accounting for the divergent findings. Another recent study, on the rat primary auditory cortex using high spatial resolution ( $50\ \mu\text{m}$ ) CSD mapping, showed the maximal up-state-related sink to be in the presumed supragranular layers under urethane anaesthesia, while in natural sleep it is rather the presumed granular and probably infragranular layers that exhibited the largest up-state-related sink (see average data, Supplementary Figs 10 and 16 in Sakata and Harris, 2009). Our CSD results in natural sleep are quite close to the results of Sakata and Harris (2009) obtained under urethane anaesthesia, except for the large source deep in the infragranular layers.

Discrepancies between cat, rat and human data thus most probably stem from multiple sources, including but not limited to the recording methodology (spatial density of sampling, electrode types implanted), use of anaesthetics (ketamine/xylazine versus urethane versus natural sleep), cytoarchitectonics of the cortex (suprasylvian cortex in cat versus auditory cortex in rat versus frontal and parietal areas in humans), as well as species differences.

According to our observations, the slow wave activity depth profile, represented by the up-state peaks, was similar between the four investigated frequency ranges including the slow ( $<1$  Hz) and delta band (up to 2 Hz). In our opinion, these frequency bands are thus substantially overlapping, hence a less strict distinction should be applied between activities above versus below 1 Hz. We agree that the slow activity and thalamic delta have obviously different neuronal mechanisms, but it seems that these waves cannot be distinguished using exclusively a frequency band criterion.

We have found similar signs of elementary hierarchical organization of low- and high-frequency oscillations in humans as it was shown in animal models (Lakatos *et al.*, 2005; Steriade, 2006). The organizing substrate was the up-state of the slow wave activity, which gave rise to a wide variety of higher-frequency activity including spindle, alpha, beta, gamma and ripple oscillations. Each of these high-frequency oscillatory bursts was quite different from sweep to sweep, showing for example occasional spindle sequences or marked gamma or ripple band enhancements at various peak frequencies. These observations suggest that each

slow wave activity cycle with unique oscillatory signature reflects individual information content coded differently in the oscillatory process. Given the variability of the high-frequency oscillatory activity during up-states, it is plausible to assume that different underlying neuronal populations might be responsible for the generation of each specific oscillatory pattern. This strategy might be beneficial in the configuration of functional connectivity between neurons to form stable ensembles that may promote the consolidation of memory in sleep.

Paroxysmal activity is known to emerge more often from non-REM sleep compared with REM (Steriade, 2003). Animal studies revealed that cortical hyperexcitability associated with ripple oscillations often results in pathological synchronization leading to epileptic seizures (Grenier *et al.*, 2003). We have shown that up-states are characterized by a large increase in cortical excitability reflected in the increased power of gamma and ripple oscillations. Thus, we hypothesize that the active state of the slow oscillation may play an important role in the generation of seizures and other paroxysmal signs in the cortical epileptic network.

## Laminar calretinin immunopositive interneuron density and slow wave activity

The relatively high correlation in laminar location between LFP gradient, CSD, multiple-unit activity and gamma power during up-states and calretinin immunopositive cell density may provide additional insights into the mechanism for the predominance of oscillatory activity in supragranular layers. Calretinin immunopositive cells are relatively numerous for inhibitory cells, comprising  $\sim 8\%$  of the total number of prefrontal neurons and  $\sim 14.2\text{--}17.6\%$  of layer II and III neurons, in human prefrontal cortex (Gabbott *et al.*, 1997). Calretinin immunopositive cell density in the human, monkey, cat and rat cortex is highest in the supragranular layers (Fonseca and Soriano, 1995; Gabbott *et al.*, 1997; Schwark and Li, 2000). The layer II and III population of calretinin immunopositive cells (78% of all calretinin immunopositive cells) is significantly more numerous (+31%) in humans than in the rat (Gabbott *et al.*, 1997), and the supragranular calretinin immunopositive predominance in humans is not affected by epilepsy (Barinka *et al.*, 2010). The relatively high density and remarkable vertically oriented dendritic alignment (Gabbott *et al.*, 1997) of layers II and III calretinin immunopositive cells (Fig. 2B) suggest that this population on its own may contribute significantly to the CSD. Unlike basket cells that target principal cells (Somogyi *et al.*, 1983) establishing local negative-feedback circuits, layers II and III calretinin immunopositive interneurons preferentially target other inhibitory cells locally in layers II and III and target pyramidal cells in layer V (Meskenaite, 1997), forming local positive-feedback circuits (Dantzker and Callaway, 2000) in the supragranular layers and negative-feedback circuits between supra- and infragranular layers. The negative feedback imposed by the population of calretinin immunopositive cells may relatively attenuate the infragranular activation, while the positive-feedback disinhibition (Tamas *et al.*, 1998) may amplify the supragranular

synaptic/transmembrane oscillations in the gamma band and cellular activity (Whittington *et al.*, 1995).

In addition, GABA<sub>B</sub> receptors are more concentrated in the upper layers of the cortex, at least in rodents (Lopez-Bendito *et al.*, 2002; Tamas *et al.*, 2003), which might also contribute to the potassium current that may play an important role in the down-state generation (Timofeev *et al.*, 2001).

## Action potential activity in slow wave activity

*In vitro* slice studies in animals found that firing in infragranular layers consistently lead supragranular layers by over 100 ms at the onset of the up-state (Sanchez-Vives and McCormick, 2000). In contrast, we found that the onset of activity during up-states differs less than  $\pm 10$  ms between layers. Although the slice preparation is a powerful tool, it severs connections that are present in the intact animal, removing background synaptic input and placing the cell in an artificial medium.

In healthy humans, it is believed that each individual slow wave cycle has a distinct origin and propagates uniquely across a number of brain areas (Murphy *et al.*, 2009). Similar patterns were also found in animal models (Ferezou *et al.*, 2007; Mohajerani *et al.*, 2010). Thus, variable projections may be involved in its propagation, terminating in variable cortical layers making the laminar distribution of the initial unit firing also variable, as it was shown in our study.

The low average firing rate (0.6 Hz) found in here is consistent with a previous human report (Ravagnati *et al.*, 1979). Animal studies using extracellular silicon probes and intracellular sharp electrodes report average firing rates in the 2–20 Hz range from the entire depth of the cortex (Steriade *et al.*, 2001; Isomura *et al.*, 2006; Luczak *et al.*, 2007), and cell-attached and whole-cell patch-clamp studies from layers II and III neurons report average firing rates in the 0.01–0.3 Hz range (Margrie *et al.*, 2002; Waters and Helmchen, 2006; Hromadka *et al.*, 2008). Some of these differences may be related to the laminar location of the neurons and to 'collateral damage' inherent to the different techniques. Extracellular recordings might be biased toward higher average firing rates, because of the use of a minimum spontaneous firing rate (1–2 Hz) constraint (Luczak *et al.*, 2007). We did not use such correction in our unit analysis, thus slower firing cells were also included. Sharp electrode intracellular recordings (Steriade *et al.*, 2001; Isomura *et al.*, 2006) disrupt the cell membrane and introduce leakage current, which may also alter the firing rate. In cell-attached recordings (Margrie *et al.*, 2002; Hromadka *et al.*, 2008), the membrane is partially covered by the recording pipette causing substantial mechanical stress, receptor, ion channel masking and membrane capacitance changes, while the whole-cell configuration (Waters and Helmchen, 2006) disrupts the membrane and causes cell dialysis. Indeed, when establishing the whole-cell configuration, the spontaneous firing rate may double compared with the cell-attached state (Margrie *et al.*, 2002). Given these apparently strong effects of recording methodology on cell firing, it is hard to definitively relate the present findings to animal experiments. However, it seems reasonable to expect that any technique which physically contacts the cell would alter

the firing rate to a greater extent than techniques which do not. To elucidate these differences further, unbiased extracellular action potential techniques need to be implemented in different animal models.

## Concluding remarks

In summary, the differences between our recordings of slow wave activity and those previously described may be due to the observed cortical areas, the experimental preparation, the type of sleep induction and the neurological condition. We suggest that the strong supragranular activity may characterize slow wave activity, in contrast with certain types of epileptic discharges and some specific components of sensory and cognitive-evoked responses, which are mostly localized to the granular and infragranular layers (Ulbert *et al.*, 2001b, 2004a; Wang *et al.*, 2005; Halgren *et al.*, 2006). The strong supragranular oscillatory activity in sleep may be beneficial for the local, higher-order processing of sensory experience and perhaps memory consolidation, since these layers are interconnected by dense cortico-cortical projections forming fine-scale functional networks to perform integrative functions (Yoshimura *et al.*, 2005). The weaker infragranular activity may reflect the relatively suppressed cortical executive, output functions, which may prevent effective connectivity between distant cortical areas from developing in slow wave sleep (Massimini *et al.*, 2005).

Some differences between humans and cats or rats might also be expected given that our last common ancestor was about 75 million years ago, and our prefrontal cortex is more than a hundred times larger, with a striking increase in pyramidal cell dendritic complexity (Elston, 2003; Elston *et al.*, 2006). Our finding that the slow wave activity and corresponding high-frequency rhythms including spindle, alpha, beta, gamma and ripple oscillations may involve supragranular layers is consistent with this massive cortical expansion of neuronal number (Herculano-Houzel *et al.*, 2007), inasmuch as increased dendritic complexity and cortico-cortical association fibres predominantly target these layers (Gonzalez-Burgos *et al.*, 2000).

## Funding

NeuroProbes IST-027017, Epicure LSH-CT-2006-037315, OTKA PD-77864, OTKA K-81357, NKTH-ANR Neurogen, EB9282, NS18741.

## Supplementary material

Supplementary material is available at *Brain* online.

## References

- Achermann P, Borbely AA. Low-frequency (<1 Hz) oscillations in the human sleep electroencephalogram. *Neuroscience* 1997; 81: 213–22.
- Amzica F, Steriade M. Disconnection of intracortical synaptic linkages disrupts synchronization of a slow oscillation. *J Neurosci* 1995; 15: 4658–77.

- Amzica F, Steriade M. Cellular substrates and laminar profile of sleep K-complex. *Neuroscience* 1998; 82: 671–86.
- Axmacher N, Elger CE, Fell J. Ripples in the medial temporal lobe are relevant for human memory consolidation. *Brain* 2008; 131: 1806–17.
- Barinka F, Druga R, Marusic P, Krsek P, Zamecnik J. Calretinin immunoreactivity in focal cortical dysplasias and in non-malformed epileptic cortex. *Epilepsy Res* 2010; 88: 76–86.
- Berger H. Über das Elektroenkephalogramm des Menschen. *Arch Psychiatr Nervenkr* 1929; 87: 527–70.
- Born J, Rasch B, Gais S. Sleep to remember. *Neuroscientist* 2006; 12: 410–24.
- Bragin A, Wilson CL, Staba RJ, Reddick M, Fried I, Engel J Jr. Interictal high-frequency oscillations (80–500 Hz) in the human epileptic brain: entorhinal cortex. *Ann Neurol* 2002; 52: 407–15.
- Buzsaki G, Draguhn A. Neuronal oscillations in cortical networks. *Science* 2004; 304: 1926–9.
- Cash SS, Halgren E, Dehghani N, Rossetti AO, Thesen T, Wang C, et al. The human K-complex represents an isolated cortical down-state. *Science* 2009; 324: 1084–7.
- Chauvette S, Volgushev M, Timofeev I. Origin of active states in local neocortical networks during slow sleep oscillation. *Cereb Cortex* 2010. Advance Access published on March 3, 2010, doi:10.1093/cercor/bhq009.
- Clemens Z, Molle M, Eross L, Barsi P, Halasz P, Born J. Temporal coupling of parahippocampal ripples, sleep spindles and slow oscillations in humans. *Brain* 2007; 130: 2868–78.
- Crepon B, Navarro V, Hasboun D, Clemenceau S, Martinerie J, Baulac M, et al. Mapping interictal oscillations greater than 200 Hz recorded with intracranial macroelectrodes in human epilepsy. *Brain* 2010; 133: 33–45.
- Crunelli V, Hughes SW. The slow (<1 Hz) rhythm of non-REM sleep: a dialogue between three cardinal oscillators. *Nat Neurosci* 2010; 13: 9–17.
- Csicsvari J, Hirase H, Czurko A, Buzsaki G. Reliability and state dependence of pyramidal cell-interneuron synapses in the hippocampus: an ensemble approach in the behaving rat. *Neuron* 1998; 21: 179–89.
- Dantzer JL, Callaway EM. Laminar sources of synaptic input to cortical inhibitory interneurons and pyramidal neurons. *Nat Neurosci* 2000; 3: 701–7.
- Delorme A, Makeig S. EEGLAB: an open source toolbox for analysis of single-trial EEG dynamics including independent component analysis. *J Neurosci Methods* 2004; 134: 9–21.
- Ebersole JS, Pedley TA. Current practice of clinical electroencephalography. Philadelphia, PA: Lippincott Williams & Wilkins, 2003.
- Elston GN. Cortex, cognition and the cell: new insights into the pyramidal neuron and prefrontal function. *Cereb Cortex* 2003; 13: 1124–38.
- Elston GN, Benavides-Piccione R, Elston A, Zietsch B, Defelipe J, Manger P, et al. Specializations of the granular prefrontal cortex of primates: implications for cognitive processing. *Anat Rec A Discov Mol Cell Evol Biol* 2006; 288: 26–35.
- Euston DR, Tatsuno M, McNaughton BL. Fast-forward playback of recent memory sequences in prefrontal cortex during sleep. *Science* 2007; 318: 1147–50.
- Fabo D, Magloczky Z, Wittner L, Pek A, Eross L, Czirjak S, et al. Properties of in vivo interictal spike generation in the human subiculum. *Brain* 2008; 131: 485–99.
- Ferezou I, Haiss F, Gentet LJ, Aronoff R, Weber B, Petersen CC. Spatiotemporal dynamics of cortical sensorimotor integration in behaving mice. *Neuron* 2007; 56: 907–23.
- Fonseca M, Soriano E. Calretinin-immunoreactive neurons in the normal human temporal cortex and in Alzheimer's disease. *Brain Res* 1995; 691: 83–91.
- Freeman JA, Nicholson C. Experimental optimization of current source-density technique for anuran cerebellum. *J Neurophysiol* 1975; 38: 369–82.
- Gabbott PL, Jays PR, Bacon SJ. Calretinin neurons in human medial prefrontal cortex (areas 24a,b,c, 32', and 25). *J Comp Neurol* 1997; 381: 389–410.
- Gonzalez-Burgos G, Barrionuevo G, Lewis DA. Horizontal synaptic connections in monkey prefrontal cortex: an in vitro electrophysiological study. *Cereb Cortex* 2000; 10: 82–92.
- Grenier F, Timofeev I, Steriade M. Neocortical very fast oscillations (ripples, 80–200 Hz) during seizures: intracellular correlates. *J Neurophysiol* 2003; 89: 841–52.
- Haider B, Duque A, Hasenstaub AR, McCormick DA. Neocortical network activity in vivo is generated through a dynamic balance of excitation and inhibition. *J Neurosci* 2006; 26: 4535–45.
- Halgren E, Wang C, Schomer DL, Knake S, Marinkovic K, Wu J, et al. Processing stages underlying word recognition in the anteroventral temporal lobe. *Neuroimage* 2006; 30: 1401–13.
- Harris KD, Henze DA, Csicsvari J, Hirase H, Buzsaki G. Accuracy of tetrode spike separation as determined by simultaneous intracellular and extracellular measurements. *J Neurophysiol* 2000; 84: 401–14.
- Heitler JW. DataView v5: software for the display and analysis of digital signals in neurophysiology. <http://www.st-andrews.ac.uk/~wjh/dataview/> (13 June 2010, date last accessed).
- Herculano-Houzel S, Collins CE, Wong P, Kaas JH. Cellular scaling rules for primate brains. *Proc Natl Acad Sci USA* 2007; 104: 3562–7.
- Hromadka T, Dewese MR, Zador AM. Sparse representation of sounds in the unanesthetized auditory cortex. *PLoS Biol* 2008; 6: e16.
- Huber R, Ghilardi MF, Massimini M, Tononi G. Local sleep and learning. *Nature* 2004; 430: 78–81.
- Iber C, Ancoli-Israel S, Chesson A, Quan SF. The AASM Manual for the Scoring of Sleep and Associated Events: Rules, Terminology and Technical Specifications. Westchester: American Academy of Sleep Medicine; 2007.
- Isomura Y, Sirota A, Ozen S, Montgomery S, Mizuseki K, Henze DA, et al. Integration and segregation of activity in entorhinal-hippocampal subregions by neocortical slow oscillations. *Neuron* 2006; 52: 871–82.
- Jacobs J, Levan P, Chatillon CE, Olivier A, Dubeau F, Gotman J. High frequency oscillations in intracranial EEGs mark epileptogenicity rather than lesion type. *Brain* 2009; 132: 1022–37.
- Jensen O, Kaiser J, Lachaux JP. Human gamma-frequency oscillations associated with attention and memory. *Trends Neurosci* 2007; 30: 317–24.
- Jirsch JD, Urrestarazu E, LeVan P, Olivier A, Dubeau F, Gotman J. High-frequency oscillations during human focal seizures. *Brain* 2006; 129: 1593–608.
- Keller CJ, Cash SS, Narayanan S, Wang C, Kuzniecky R, Carlson C, et al. Intracranial microprobe for evaluating neuro-hemodynamic coupling in unanesthetized human neocortex. *J Neurosci Methods* 2009; 179: 208–18.
- Knake S, Wang CM, Ulbert I, Schomer DL, Halgren E. Specific increase of human entorhinal population synaptic and neuronal activity during retrieval. *Neuroimage* 2007; 37: 618–22.
- Lakatos P, Karmos G, Mehta AD, Ulbert I, Schroeder CE. Entrainment of neuronal oscillations as a mechanism of attentional selection. *Science* 2008; 320: 110–13.
- Lakatos P, Shah AS, Knuth KH, Ulbert I, Karmos G, Schroeder CE. An oscillatory hierarchy controlling neuronal excitability and stimulus processing in the auditory cortex. *J Neurophysiol* 2005; 94: 1904–11.
- Loomis AL, Harvey EN, Hobart GA. Cerebral states during sleep, as studied by human brain potentials. *J Exp Psychol* 1937; 21: 127–44.
- Lopez-Bendito G, Shigemoto R, Kulik A, Paulsen O, Fairen A, Lujan R. Expression and distribution of metabotropic GABA receptor subtypes GABABR1 and GABABR2 during rat neocortical development. *Eur J Neurosci* 2002; 15: 1766–78.
- Luczak A, Bartho P, Marguet SL, Buzsaki G, Harris KD. Sequential structure of neocortical spontaneous activity in vivo. *Proc Natl Acad Sci USA* 2007; 104: 347–52.
- Margrie TW, Brecht M, Sakmann B. In vivo, low-resistance, whole-cell recordings from neurons in the anesthetized and awake mammalian brain. *Pflugers Arch* 2002; 444: 491–8.
- Marshall L, Helgadottir H, Molle M, Born J. Boosting slow oscillations during sleep potentiates memory. *Nature* 2006; 444: 610–13.

- Massimini M, Ferrarelli F, Esser SK, Riedner BA, Huber R, Murphy M, et al. Triggering sleep slow waves by transcranial magnetic stimulation. *Proc Natl Acad Sci USA* 2007; 104: 8496–501.
- Massimini M, Ferrarelli F, Huber R, Esser SK, Singh H, Tononi G. Breakdown of cortical effective connectivity during sleep. *Science* 2005; 309: 2228–32.
- Massimini M, Huber R, Ferrarelli F, Hill S, Tononi G. The sleep slow oscillation as a traveling wave. *J Neurosci* 2004; 24: 6862–70.
- Meskenaite V. Calretinin-immunoreactive local circuit neurons in area 17 of the cynomolgus monkey, *Macaca fascicularis*. *J Comp Neurol* 1997; 379: 113–32.
- Mohajerani MH, McVea DA, Fingas M, Murphy TH. Mirrored bilateral slow-wave cortical activity within local circuits revealed by fast bihemispheric voltage-sensitive dye imaging in anesthetized and awake mice. *J Neurosci* 2010; 30: 3745–51.
- Molle M, Marshall L, Gais S, Born J. Grouping of spindle activity during slow oscillations in human non-rapid eye movement sleep. *J Neurosci* 2002; 22: 10941–7.
- Molle M, Marshall L, Gais S, Born J. Learning increases human electroencephalographic coherence during subsequent slow sleep oscillations. *Proc Natl Acad Sci USA* 2004; 101: 13963–8.
- Murphy M, Riedner BA, Huber R, Massimini M, Ferrarelli F, Tononi G. Source modeling sleep slow waves. *Proc Natl Acad Sci USA* 2009; 106: 1608–13.
- Nicholson C, Freeman JA. Theory of current source-density analysis and determination of conductivity tensor for anuran cerebellum. *J Neurophysiol* 1975; 38: 356–68.
- Ravagnati L, Halgren E, Babb TL, Crandall PH. Activity of human hippocampal formation and amygdala neurons during sleep. *Sleep* 1979; 2: 161–73.
- Sakata S, Harris KD. Laminar structure of spontaneous and sensory-evoked population activity in auditory cortex. *Neuron* 2009; 64: 404–18.
- Sanchez-Vives MV, McCormick DA. Cellular and network mechanisms of rhythmic recurrent activity in neocortex. *Nat Neurosci* 2000; 3: 1027–34.
- Schevon CA, Trevelyan AJ, Schroeder CE, Goodman RR, McKhann G Jr, Emerson RG. Spatial characterization of interictal high frequency oscillations in epileptic neocortex. *Brain* 2009; 132: 3047–59.
- Schroeder CE, Lakatos P. Low-frequency neuronal oscillations as instruments of sensory selection. *Trends Neurosci* 2009; 32: 9–18.
- Schwark HD, Li J. Distribution of neurons immunoreactive for calcium-binding proteins varies across areas of cat primary somatosensory cortex. *Brain Res Bull* 2000; 51: 379–85.
- Shu Y, Hasenstaub A, McCormick DA. Turning on and off recurrent balanced cortical activity. *Nature* 2003; 423: 288–93.
- Somogyi P, Kisvarday ZF, Martin KA, Whitteridge D. Synaptic connections of morphologically identified and physiologically characterized large basket cells in the striate cortex of cat. *Neuroscience* 1983; 10: 261–94.
- Staba RJ, Wilson CL, Bragin A, Fried I, Engel J Jr. Sleep states differentiate single neuron activity recorded from human epileptic hippocampus, entorhinal cortex, and subiculum. *J Neurosci* 2002a; 22: 5694–704.
- Staba RJ, Wilson CL, Fried I, Engel J Jr. Single neuron burst firing in the human hippocampus during sleep. *Hippocampus* 2002b; 12: 724–34.
- Steinorth S, Wang C, Ulbert I, Schomer D, Halgren E. Human entorhinal gamma and theta oscillations selective for remote autobiographical memory. *Hippocampus* 2009; 20 (1): 166–73.
- Steriade M. *Neuronal substrates of sleep and epilepsy*. Cambridge: Cambridge University Press; 2003.
- Steriade M. Grouping of brain rhythms in corticothalamic systems. *Neuroscience* 2006; 137: 1087–106.
- Steriade M, Amzica F. Intracortical and corticothalamic coherency of fast spontaneous oscillations. *Proc Natl Acad Sci USA* 1996; 93: 2533–8.
- Steriade M, Nunez A, Amzica F. Intracellular analysis of relations between the slow (<1 Hz) neocortical oscillation and other sleep rhythms of the electroencephalogram. *J Neurosci* 1993a; 13: 3266–83.
- Steriade M, Nunez A, Amzica F. A novel slow (<1 Hz) oscillation of neocortical neurons in vivo: depolarizing and hyperpolarizing components. *J Neurosci* 1993b; 13: 3252–65.
- Steriade M, Timofeev I. Neuronal plasticity in thalamocortical networks during sleep and waking oscillations. *Neuron* 2003; 37: 563–76.
- Steriade M, Timofeev I, Grenier F. Natural waking and sleep states: a view from inside neocortical neurons. *J Neurophysiol* 2001; 85: 1969–85.
- Tamas G, Lorincz A, Simon A, Szabadics J. Identified sources and targets of slow inhibition in the neocortex. *Science* 2003; 299: 1902–5.
- Tamas G, Somogyi P, Buhl EH. Differentially interconnected networks of GABAergic interneurons in the visual cortex of the cat. *J Neurosci* 1998; 18: 4255–70.
- Tenke CE, Schroeder CE, Arezzo JC, Vaughan HG Jr. Interpretation of high-resolution current source density profiles: a simulation of sublaminar contributions to the visual evoked potential. *Exp Brain Res* 1993; 94: 183–92.
- Timofeev I, Grenier F, Steriade M. Disfacilitation and active inhibition in the neocortex during the natural sleep-wake cycle: an intracellular study. *Proc Natl Acad Sci USA* 2001; 98: 1924–9.
- Turner DA, Li XG, Pyapali GK, Ylinen A, Buzsaki G. Morphometric and electrical properties of reconstructed hippocampal CA3 neurons recorded in vivo. *J Comp Neurol* 1995; 356: 580–94.
- Ulbert I, Halgren E, Heit G, Karmos G. Multiple microelectrode-recording system for human intracortical applications. *J Neurosci Methods* 2001a; 106: 69–79.
- Ulbert I, Heit G, Madsen J, Karmos G, Halgren E. Laminar analysis of human neocortical interictal spike generation and propagation: current source density and multiunit analysis in vivo. *Epilepsia* 2004a; 45 (Suppl 4): 48–56.
- Ulbert I, Karmos G, Heit G, Halgren E. Early discrimination of coherent versus incoherent motion by multiunit and synaptic activity in human putative MT+. *Hum Brain Mapp* 2001b; 13: 226–38.
- Ulbert I, Magloczky Z, Eross L, Czirjak S, Vajda J, Bogner L, et al. In vivo laminar electrophysiology co-registered with histology in the hippocampus of patients with temporal lobe epilepsy. *Exp Neurol* 2004b; 187: 310–8.
- Urrestarazu E, Chander R, Dubeau F, Gotman J. Interictal high-frequency oscillations (100–500 Hz) in the intracerebral EEG of epileptic patients. *Brain* 2007; 130: 2354–66.
- Volgushev M, Chauvette S, Mukovski M, Timofeev I. Precise long-range synchronization of activity and silence in neocortical neurons during slow-wave oscillations [corrected]. *J Neurosci* 2006; 26: 5665–72.
- Vyazovskiy VV, Cirelli C, Pfister-Genskow M, Faraguna U, Tononi G. Molecular and electrophysiological evidence for net synaptic potentiation in wake and depression in sleep. *Nat Neurosci* 2008; 11: 200–8.
- Wang C, Ulbert I, Schomer DL, Marinkovic K, Halgren E. Responses of human anterior cingulate cortex microdomains to error detection, conflict monitoring, stimulus-response mapping, familiarity, and orienting. *J Neurosci* 2005; 25: 604–13.
- Waters J, Helmchen F. Background synaptic activity is sparse in neocortex. *J Neurosci* 2006; 26: 8267–77.
- Whittington MA, Traub RD, Jefferys JG. Synchronized oscillations in interneuron networks driven by metabotropic glutamate receptor activation. *Nature* 1995; 373: 612–15.
- Wittner L, Henze DA, Zaborszky L, Buzsaki G. Hippocampal CA3 pyramidal cells selectively innervate aspiny interneurons. *Eur J Neurosci* 2006; 24: 1286–98.
- Wittner L, Huberfeld G, Clemenceau S, Eross L, Dezamis E, Entz L, et al. The epileptic human hippocampal cornu ammonis 2 region generates spontaneous interictal-like activity in vitro. *Brain* 2009; 132: 3032–46.
- Worrell GA, Gardner AB, Stead SM, Hu S, Goerss S, Cascino GJ, et al. High-frequency oscillations in human temporal lobe: simultaneous microwire and clinical macroelectrode recordings. *Brain* 2008; 131: 928–37.
- Worrell GA, Parish L, Cranstoun SD, Jonas R, Baltuch G, Litt B. High-frequency oscillations and seizure generation in neocortical epilepsy. *Brain* 2004; 127: 1496–506.
- Yoshimura Y, Dantzer JL, Callaway EM. Excitatory cortical neurons form fine-scale functional networks. *Nature* 2005; 433: 868–73.

dc\_303\_11

## 6. Melléklet

# Complex Propagation Patterns Characterize Human Cortical Activity during Slow-Wave Sleep

Balázs Hangya,<sup>1</sup> Benedek T. Tihanyi,<sup>1</sup> László Entz,<sup>2,3</sup> Dániel Fabó,<sup>2,3</sup> Loránd Erőss,<sup>2</sup> Lucia Wittner,<sup>2,3</sup> Rita Jakus,<sup>2</sup> Viktor Varga,<sup>1</sup> Tamás F. Freund,<sup>1</sup> and István Ulbert<sup>2,3,4</sup>

<sup>1</sup>Department of Cellular and Network Neurobiology, Institute of Experimental Medicine, Hungarian Academy of Sciences, Budapest, Hungary, <sup>2</sup>National Institute of Neuroscience, Budapest, Hungary, <sup>3</sup>Institute for Psychology, Hungarian Academy of Sciences, Budapest, Hungary, and <sup>4</sup>Faculty of Information Technology, Péter Pázmány Catholic University, Budapest, Hungary

Cortical electrical activity during nonrapid eye movement (non-REM) sleep is dominated by slow-wave activity (SWA). At larger spatial scales (~2–30 cm), investigated by scalp EEG recordings, SWA has been shown to propagate globally over wide cortical regions as traveling waves, which has been proposed to serve as a temporal framework for neural plasticity. However, whether SWA dynamics at finer spatial scales also reflects the orderly propagation has not previously been investigated in humans. To reveal the local, finer spatial scale (~1–6 cm) patterns of SWA propagation during non-REM sleep, electrocorticographic (ECoG) recordings were conducted from subdurally implanted electrode grids and a nonlinear correlation technique [mutual information (MI)] was implemented. MI analysis revealed spatial maps of correlations between cortical areas demonstrating SWA propagation directions, speed, and association strength. Highest correlations, indicating significant coupling, were detected during the initial positive-going deflection of slow waves. SWA propagated predominantly between adjacent cortical areas, albeit spatial noncontinuities were also frequently observed. MI analysis further uncovered significant convergence and divergence patterns. Areas receiving the most convergent activity were similar to those with high divergence rate, while reciprocal and circular propagation of SWA was also frequent. We hypothesize that SWA is characterized by distinct attributes depending on the spatial scale observed. At larger spatial scales, the orderly SWA propagation dominates; at the finer scale of the ECoG recordings, non-REM sleep is characterized by complex SWA propagation patterns.

## Introduction

Cortical slow-wave activity (SWA; in the ~0.5–2 Hz frequency range) is the EEG correlate of synchronized active (up) and silent (down) states of large populations of neocortical neurons during deep nonrapid eye movement (non-REM) sleep or slow-wave sleep (SWS) (Steriade et al., 1993; Cash et al., 2009; Csercsa et al., 2010; Le Van Quyen et al., 2010). Although synchronous up and down states were observed in isolated neocortex *in vitro* (Cossart et al., 2003), several studies showed that the thalamus might also play an active role in shaping cortical SWA (Sirota and Buzsáki, 2005; Crunelli and Hughes, 2010; Magnin et al., 2010). Large-scale thalamocortical networks were shown to engage in synchronous low-frequency oscillations (Sirota and Buzsáki, 2005; Volgushev et al., 2006). Furthermore, the hippocampus as well as subcortical centers could also participate in this process (Isomura et al., 2006; Wolansky et al., 2006; Mena-Segovia et al., 2008),

indicating that slow oscillations could provide a general clockwork for a large variety of neural operations (Sirota and Buzsáki, 2005; Buzsáki, 2006). This view is further strengthened by a series of observations indicating that SWA is indispensable for precisely coordinating hippocampal and thalamocortical oscillations. Population activity patterns like hippocampal ripples and synchronously appearing cortical spindles are orchestrated by the cortical SWA, being entrained to the first half of the surface positive, active phase or up state of slow-wave cycles (Siapas and Wilson, 1998; Mölle et al., 2006; Clemens et al., 2007; Csercsa et al., 2010). Also, cortical SWA was shown to propagate over large distances as traveling waves (Massimini et al., 2004; Murphy et al., 2009). From another point of view, memory consolidation processes are often reflected in local changes of cortical SWA (Huber et al., 2004; Massimini et al., 2009) and asynchronies in thalamocortical slow rhythms at different recording sites were reported in some studies (Sirota and Buzsáki, 2005, their Fig. 2). Recent reports of regional and temporal heterogeneity of cortical slow waves (Mohajerani et al., 2010), as well as alternative propagation patterns such as spiral waves (Huang et al., 2010), raise the possibility that, in addition to the large-scale orderly traveling of slow waves, complex propagation patterns emerge in a temporal parallel manner at a finer spatial scale.

Signals from subdural electrodes provide substantially better spatial localization compared with scalp recordings as a result of the absence of distorting, integrating, and attenuating effects of interleaved tissues (Buzsáki, 2006; Bangerter et al., 2010). These

Received March 24, 2011; revised April 28, 2011; accepted May 2, 2011.

Author contributions: L. Entz, D.F., L. Erőss, R.J., and I.U. performed research. B.H., V.V., T.F.F., and I.U. designed research; B.H., B.T.T., L. Entz, and L.W. analyzed data; B.H., V.V., and I.U. wrote the paper.

This work was supported by Országos Tudományos Kutatási Alapprogramok (OTKA) PD-77864, OTKA K-81357, Nemzeti Kutatási és Technológiai Hivatal (NKTH)-Agence Nationale de la Recherche Neurogen, NKTH-OTKA CNK77793, and National Institutes of Health Grant MH54671. L.W. was supported by Bolyai János Research Fellowship. We thank Emilia Tóth for helping us with the reconstruction of the Brodmann areas.

Correspondence should be addressed to Balázs Hangya at his present address: Cold Spring Harbor Laboratory, 1 Bungtown Road, Cold Spring Harbor, NY 11724. E-mail: bhangya@cshl.edu.

DOI:10.1523/JNEUROSCI.1498-11.2011

Copyright © 2011 the authors 0270-6474/11/318770-10\$15.00/0

**Table 1. Patient characteristics**

Patient ID	Age at onset (years)	Age at surgery (years)	Epileptic focus (seizure onset zone)	MRI abnormality
Pt. 1	4	26	Left frontobasal–temporopolar	Left temporopolar microgyria
Pt. 2	5	16	Right superior frontal gyrus	Right superior frontal gyrus flair abnormality
Pt. 3	11	34	Right supplementary motor area and cuneus	Negative
Pt. 4	30	42	Left parietal tuber	Left temporoparietal multiplex tubers (sclerosis tuberosa)
Pt. 5	1	40	Left parietal operculum and posterior part of insula	Negative
Pt. 6	1.5	29	Left parietal operculum and posterior part of insula	Left parietal and insular flair abnormality

advantages allowed us to investigate the fine-scale ( $\sim 1$  cm) propagation patterns of sleep slow waves such as convergence, divergence, reciprocal, and circular propagation. We analyzed subdural electrocorticographic (ECoG) recordings by extending classical linear correlation with information theory-based measures characterized by higher sensitivity in detecting nonlinear interactions commonly observed in neural systems (Freiwald et al., 1999). In contrast to the orderly SWA propagation patterns observed in scalp EEG recordings, we found a high prevalence of complex SWA patterns at the finer spatial scale provided by the ECoG traces. This spatial scale-dependent distinction in electrical activity patterns may reflect the different processing strategies at the local and global cortical levels during SWS.

## Materials and Methods

### Patient selection

Patients (Pts.) participating in this study [ $n = 6$ , five men and one woman (Pt. 3)] had medically intractable complex partial seizures and were referred to our epilepsy surgical center for presurgical evaluation (Table 1). All patients underwent intracranial electrode implantation as required for localization of epileptogenic tissue before therapeutic resection. Patients or their legal guardians signed the informed consent form before surgery after detailed explanation of the risks. The consent forms were approved by the local ethical committee of the National Institute of Neuroscience according to the World Medical Association Declaration of Helsinki.

### Electrode implantation and intracranial recording protocols

Since the noninvasive evaluation was inconclusive, all of the patients underwent subdural strip and grid electrode implantation (various subdural electrodes; distance between adjacent electrodes, 10 mm; Ad-Tech Medical Instrument). Implantation site selection was based on results of previous noninvasive clinical studies for seizure focus localization. We used standard craniotomies to insert the electrodes into the subdural space under general anesthesia. The electrode cables were tunneled under the skin to avoid infection and the bone flap was cryopreserved for delayed reimplantation to avoid any complication from significant brain swelling. A postimplantation MRI (3D sequence, 1 mm slice thickness) was routinely performed to visualize the final position of the electrodes. After 3-dimensional reconstruction and skull stripping of the images (Brain Extraction Tool), electrode contacts were individually localized with the aid of intraoperative photographs.

After recovery from surgery, the patients were admitted to the epilepsy monitoring unit and were continuously monitored for seizures. Video-EEG monitoring was performed using a 128 channel Brain Quick System 98 (Micromed). All signals were recorded to a mastoid reference (acquisition rate: 1024 or 512 Hz, filtered between 0.1 and 250 Hz).

### Slow-wave sleep detection

Since the sleep of the patients was fragmented due to medical care and distress from the hospitalization and head wound, we cannot provide the standard hypnograms that are usually obtained from subjects undergoing standard polysomnography studies without recent craniotomy. Craniotomies may also distort the scalp distribution of the EEG due to lack of bone and excessive fluid accumulation below the scalp. Furthermore, scalp electrodes placed close to frontal craniotomy wounds may induce infection; therefore, we avoided placing more than two frontal scalp EEG electrodes. In fact, we attempted to use these scalp EEG elec-

trodes whenever possible to aid our partial sleep staging method, but most of the time their signal was not adequate for this purpose because of the desiccation of the EEG electrode gel and other reasons causing large and variable electrode impedances, electromagnetic interference, and mechanical artifacts. To overcome these hardships, our partial sleep staging method in the clinical environment was based on the recordings from frontal ECoG channels and long-term video, without measures like EMG, EOG, ECG, and respiration monitoring that are usually recorded with EEG in a standard polysomnography environment. Behavioral sleep was confirmed by the all night, long-term video recording, while deep non-REM sleep periods were electrographically identified using frontal ECoG traces by expert neurologists. In particular, deep non-REM sleep periods (or SWS) were identified when a 30-s-long sleep epoch contained  $>20\%$  of slow waves with  $>75$   $\mu\text{V}$  peak-to-peak amplitude falling in the 0.5–2 Hz frequency range. The above criteria are consistent with the staging criteria of N3 or SWS, according to the recent American Academy of Sleep Medicine guidelines (Iber et al., 2007). In our previous work, using similar partial staging techniques based on ECoG traces and video records, we were able to clearly distinguish between light and deep non-REM sleep (Cash et al., 2009, their Fig. 2B,C). In another study using similar staging methods, we were also able to clearly detect the typical SWA pattern in SWS demonstrated in previous animal and human studies (Csicsvari et al., 2010, their Fig. 4B, supplemental Fig. 1). Data containing interictal spikes (within 1 min) and seizures (within overall 60 min; 40 min in Pt. 4) were excluded from the study to avoid epileptic contamination.

### Data analysis

**Data preprocessing.** Subgrids of  $4 \times 4$  (Pts. 1, 3, and 5) or  $4 \times 5$  (Pts. 2, 4, and 6) electrodes were selected for analysis (Fig. 1A). The reduction of the number of grid electrodes was necessary to analyze similar number of channels for comparability reasons and to reduce computational time. Selection of subgrids was based on grid location [an attempt was made to include frontal electrodes where SWA is typically more pronounced (Kurth et al., 2010)] and recording quality (channels not functioning were excluded). For each patient, three to five 1-min-long segments (26 segments in total) of normal SWS were selected. Principles of segment selection were to avoid epileptic contamination (see below) and to include deep-sleep epochs with prominent SWA. In Pt. 6, all segments were recorded in a single night, whereas in the other patients, segments from different nights were also included. Selected segments were preceded and followed by 30 min of seizure-free activity (except Pt. 4, where it was preceded by 30 min and followed by 10 min) and were free from interictal spikes. ECoG traces were resampled at 1000 Hz and bandpass filtered (0.1–40 Hz) with a finite impulse response filter using zero phase shift filtering (fir1.m and filtfilt.m built-in Matlab functions) to remove high-frequency ECoG components and electrical noise.

**Calculation of propagation maps.** We assessed associations between ECoG traces from different channels using mutual information (MI). MI provides the amount of information shared by two variables and is considered a nonlinear measure of covariation (Na et al., 2002; Kajikawa and Hackett, 2005; Hangya et al., 2009). The choice of MI instead of linear correlations was motivated by its ability to detect any kind of dependency without assumptions about the structure of correlations or the underlying distributions (Na et al., 2002; Kajikawa and Hackett, 2005; Paz et al., 2010), which is important because nonlinear correlations are generally common among neural signals (Freiwald et al., 1999; Hangya et al., 2009). We further justified this choice by comparing MI with linear cross-correlation analysis (see Results, below) (Fig. 2).

For each 1000 ms segment, ECoG values were binned into fixed bins between the overall minimal and maximal value. MI was calculated between different ECoG channels using the classic formulation in combination with Panzeri–Treves bias correction (Shannon, 1948; Panzeri et al., 2007), as described previously (Hangya et al., 2009). The basic idea of time-shifted correlations or cross-correlations was applied (Ostojic et al., 2009), using MI instead of linear correlation, as follows. On each channel, 1-s-long ECoG segments ( $X_t$  to  $X_{t+1000}$ ) were correlated to later segments from all other electrodes separately ( $Y_{t+\tau}$  to  $Y_{t+\tau+1000}$ ,  $0 < \tau < 1000$  ms) by calculating MI (temporal resolution, 1 ms) (Fig. 1*B*). Maximal MI in the function of the time lags ( $\tau$ ) was calculated for all time points ( $t$ ) and channel pairs. The choice of 1-s-long time windows was motivated by the observation that SWA frequency is around or below 1 Hz (Crunelli and Hughes, 2010; Csercsa et al., 2010; Diekelmann and Born, 2010), thus these time windows were able to approximately include a slow-wave cycle. However, it has been shown that MI calculations are robust in the selection of the time windows (Paz et al., 2010). The above calculations were repeated for overlapping 1-s-long ECoG segments (900 ms overlap). Next, correlations were destructured by cutting the ECoG data to 1–1.2-s-long segments, which were then shuffled using the `randperm.m` built-in Matlab function, which randomly permutes integers based on a uniform distribution. Permutation was repeated if a data segment remained in its original position. Significance of maximal MI was tested by comparing it to a distribution of MI values calculated from such shuffled versions of the original data (number of shuffles ranged from 151,296 to 236,400). A significance level of  $p = 0.0001$  was used to reduce the number of false-positive detections according to high numbers of statistical tests (this choice corresponds to approximately one false detection in 2.5 s). In case a significant maximal MI was found, waveform correlation was established between the two channels at time point  $t$ . It should be noted that according to the binning between the minimal and maximal data values, MI reflected predictability between slow-wave cycles rather than higher frequency (lower amplitude) oscillations such as spindles (see Results, below). Thus, significant maximal MI showed the propagation of SWA between two cortical areas, the temporal maximum location provided propagation time, and the maximal MI value indicated correlation strength. Propagation speed was calculated by dividing electrode distances by propagation time values. Time-resolved propagation maps were created using the above parameters, visualized as movies and further analyzed (see below). Unitary propagation events (Fig. 1*C*, bottom left, arrows) were assessed by significant propagation between two ECoG channels. Start and end points of such events were defined by the zero ( $t$ ) and maximal location ( $t + \tau$ ) points in the time lag–MI plot (Fig. 1*B*, right). According to the overlap-

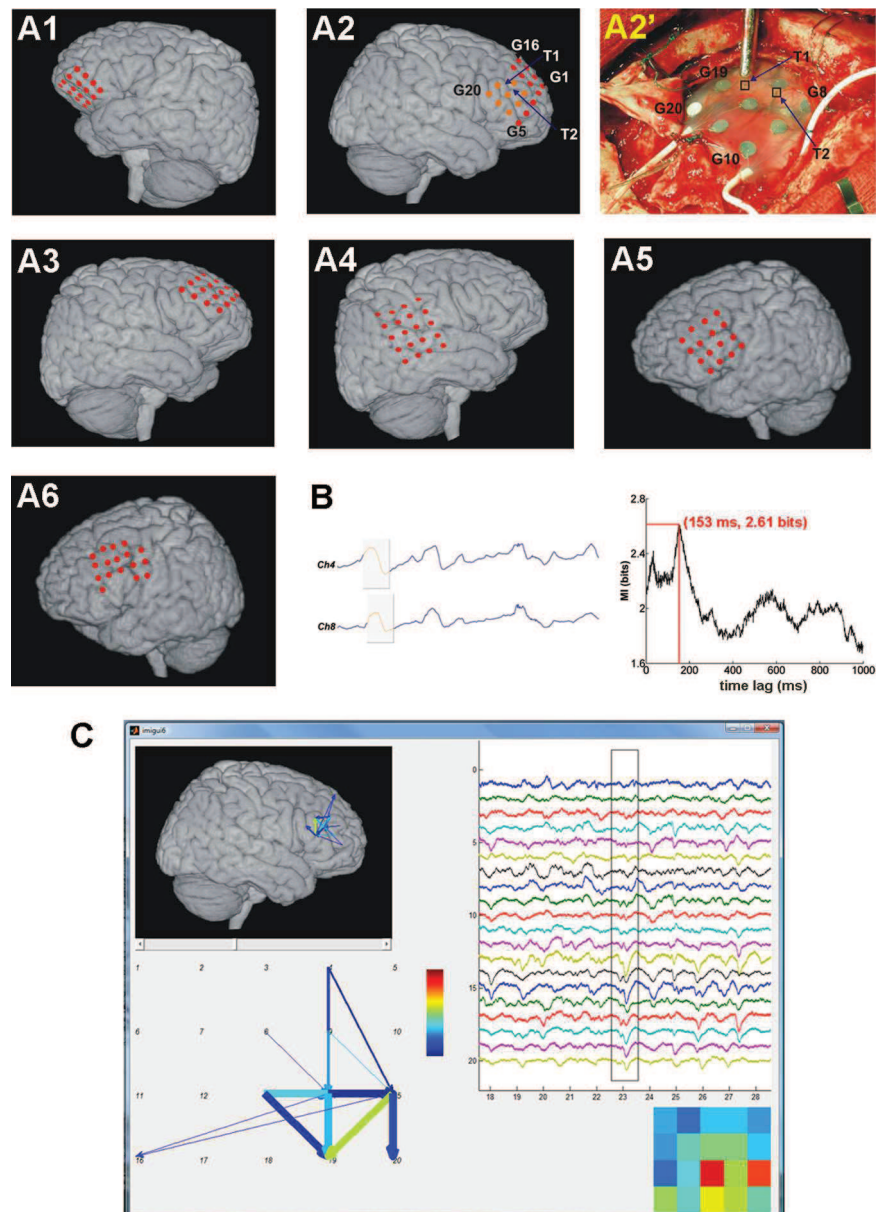


**Figure 1.** Recording and analysis of SWA propagation. **A**, Estimations of the positions of recording sites on standard human brain images based on intraoperative photographs and postoperative structural MR images (**A1–A6** correspond to Pts. 1–6, respectively). **A2'**, Photograph taken during the operation. Marked points and electrodes are also exhibited in the corresponding reconstruction image (**A2**). Recording sites visible in **A2'** are displayed in orange in **A2**. Channel 18 in Pt. 2 as well as channels 5, 17, and 18 in Pt. 6 were dysfunctional (i.e., either no data were recorded by the electrode, or a disproportionate amount of nonbiological noise showed the malfunction of the contact site) and thus left out from the analysis. **B**, Filtered (0.1–40 Hz) ECoG data were subjected to MI analysis for all pairs of recording channels (see Materials and Methods). One-second-long data segments were compared with time-lagged data from the other channel and the extent of nonlinear correlation (predictability) was measured by MI. Left, Short data segments from two ECoG channels (Ch). Gray shading designates examples of 1-s-long temporal windows for MI calculations. Right, MI was displayed as the function of time lags (1 ms resolution). A significant maximal MI (in this case, 2.61 bits at 153 ms temporal delay) was considered to be a sign of significant correlation between the two channels, which corresponded to propagating sleep slow waves (see Materials and Methods and Results). Left, Time lag between the data windows (gray) was set to the optimal delay (153 ms) at the given time point. Note the similarity of slow-wave cycles (orange) in the windows. This analysis was repeated for all fixed time instances and for all pairs of recording channels. **C**, Based on the MI analysis, SWA propagation time, distance, and association strength could be assessed for all significant unitary propagation events, from which a time-resolved propagation map was drawn and visualized in a custom-built graphical user interface. A screenshot from this interface is shown with all ECoG channels (top right), amplitude map [bottom right; coldest/warmest color correspond to smallest/largest ECoG amplitude (color bar)];  $5 \times 4$  squares correspond to the  $5 \times 4$  grid electrodes; amplitude was calculated as the difference of maximal and minimal ECoG value in the data window; propagation map displayed in a schematic form (bottom left) and also projected to the brain surface (top left). For every time point, arrows on the propagation map designate unitary propagation events between two recording sites (marked by numbers on the schematic view). The color of each arrow shows association strength (warmer colors are stronger) and the width corresponds to propagation time (thicker lines show shorter time).

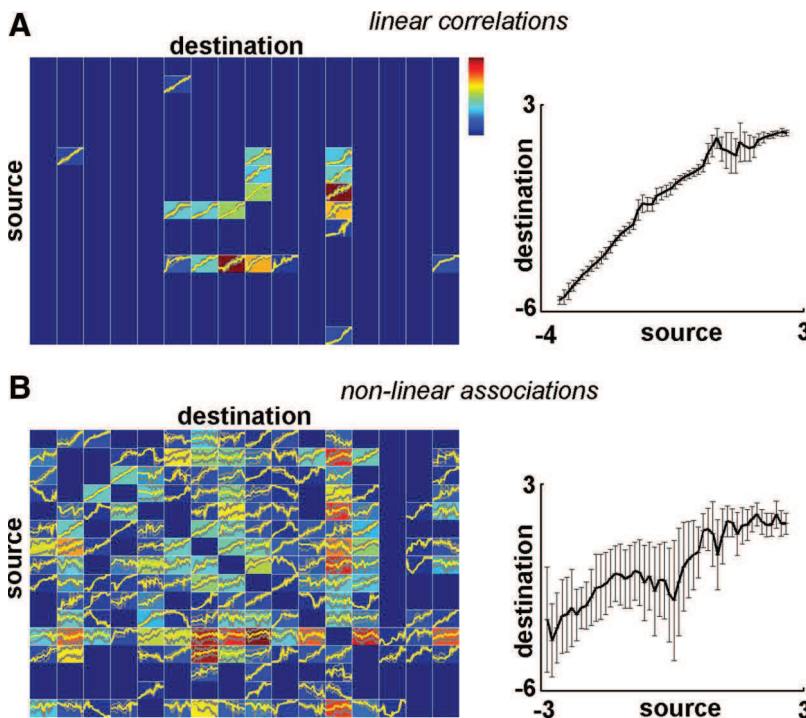


**Figure 2.** Nonlinear associations during SWA propagation. **A**, Left, Correlation profile and input–output curves of linear cross-correlation analysis from a representative subject. Each colored field corresponds to a pair of recording channels (*y*-axis, source channel; *x*-axis, destination channel). Colors indicate the total strength of (significant) directional correlation between the source and destination channels (i.e., significant cross-correlation with a positive time lag when calculated with reference to the source channel; warm colors are high correlation values) (for significance testing of linear and nonlinear correlations, see Materials and Methods). A significant cross-correlation between two channels at  $\tau$  milliseconds means that the ECoG segment of the source channel is correlated with that of the destination channel shifted by  $\tau$  milliseconds. We collected these correlated pairs of data segments for each pair of channels and plotted the ECoG values of the destination channel against corresponding values of the source channel (binned and averaged). These input–output functions are plotted in the colored fields for all channel pairs (yellow, mean; gray, SD). Right, A typical input–output function (source, channel 8; destination, channel 9) is enlarged. Error bars indicate SD. ECoG segments were standardized (i.e., transformed to zero mean and unitary SD); thus, tick labels on both axes show standardized voltage values. Note the line-like shape of these input–output curves. **B**, Left, Nonlinear correlation profiles and input–output curves for the same sleep segment calculated by the MI method. Arrangement follows that of **A**. Right, An example input–output function (source, channel 2; destination, channel 11) is enlarged. Note the higher abundance of significant nonlinear associations, the moderate similarities of linear and nonlinear correlation profiles (e.g., low rate/absence of correlations for channels 14 and 15, strong correlation between channels 8 and 12), and the more complex and variable shape of nonlinear input–output curves. Higher SD values and noisier appearance of the nonlinear input–output functions show that the nonlinear correlation functions between pairs of channels exhibit temporal changes.

ping windows (see above), the time resolution of propagation map frames was 100 ms, whereas the temporal resolution of time delays was 1 ms (see above). Consistency of time delays for direct and indirect associations was checked to test the robustness of the method.

**Correlation triggered average.** To visualize ECoG patterns giving rise to significant correlations, we calculated ECoG averages triggered by significant MI values (Fig. 3A). That is, if a significant MI was detected at a certain time, a 1-s-long ECoG segment centered to that time point was stored. At the end, these segments were averaged for each recording channel. The average signal reflected typical ECoG patterns underlying significant correlations.

**Analysis of propagation patterns.** Convergence/divergence of SWA was defined as unitary propagation events ending/starting at the same recording site within a 100 ms time window. Divergence maps were smoothed over two consecutive frames because of the discrete nature of the starting points of unitary propagation events. Two-dimensional distributions showing relative contribution to the convergence/divergence at a single location were termed “contribution maps.” Cortical centers with high convergence/divergence rate did not show correlation with epileptic foci. Reciprocal connections were defined as reciprocal propagation between two sites within 100 ms. Three-point circles (i.e., directed three-point trajectories of which the end points are the same as the starting points) were defined in an

analogous way. Controls for the above measures were generated by within-frame random shuffling (uniform distribution using `randperm.m` built-in Matlab function) of unitary propagation events among the electrode pairs. Control distributions for reciprocal connections and three-point circles were generated by 250 or 1000 shuffles. If the value derived from the real data was out of the entire range of control distributions, we used the  $p \approx 0$  notation, which can be translated to at least  $p < 0.004$ . Normalization with individual control distributions (Figs. 4, 5) was performed by subtracting the mean and dividing by the SD of the corresponding control distribution. The application of this procedure results in standardized control distributions and allows the comparison across subjects. Significance of correlations among slow-wave propagation characteristics, convergence, divergence, and contribution maps was assessed using *F* test. Statistical tests were judged at a significance level of  $p = 0.05$  unless stated otherwise. We performed a signal-to-noise ratio analysis that confirmed that potential differences in recording quality did not have a significant effect on the propagation map evaluation (data not shown).

**Linear cross-correlations.** Linear cross-correlation analysis was conducted by replacing time-shifted mutual information values with linear cross-correlations. To facilitate the comparison of the results of linear and nonlinear analyses, all other parameters of the calculations were left unchanged (including significance testing using shuffled data; see above). Thus, a directional correlation was established when a significant cross-correlation with a positive time lag was observed (positive and negative correlation were not differentiated to allow the comparison with the MI measure). We also calculated the input–output functions related to significant linear (cross-correlation) and nonlinear (MI) correlations. For each pair of recording channels, we collected pairs of ECoG segments where a significant association was found, and plotted average ECoG amplitude values of a recording channel as a function of binned ECoG values of the other channel.

All data analysis procedures were implemented in Matlab development environment (MathWorks) using custom-built and built-in functions.

## Results

### Nonlinear associations during human SWS

The nonlinear nature of neural communication was shown in several systems (Freiwald et al., 1999; Darvas et al., 2009; Chen et al., 2010); however, it is unclear whether such nonlinearities also appear in the course of slow oscillation propagation. We investigated 1-min-long segments of SWS in six epileptic patients. ECoGs from 16–20 subdural recording sites were analyzed in each patient. We first searched for associations between ECoG waveforms recorded from different brain areas and compared the results of a linear (cross-correlation) and a nonlinear (MI) correlation analysis (see Materials and Methods, above).

Both linear and nonlinear types of dependencies were present in ECoG channels in all analyzed sleep segments. Significant linear correlation and MI values were summed over time for each

pair of recording channels for each recording segment, resulting in linear and nonlinear correlation profiles. Although some similarities between the two types of profiles were discoverable (Fig. 2), significant nonlinear correlations were more abundant [5687 of 7266 channel pairs in all recordings (78.3%) compared with 1292 of 7266 (17.8%)], showing additional associations compared with the linear analysis. It should be noted however, that linear correlations were detected in a very few cases where nonlinear correlations were not (36 of 7266 channel pair comparisons, 0.5%), showing that in cases of pure linear associations, cross-correlation analysis can be more sensitive than MI.

To visualize the associations between channel pairs, we calculated the input–output functions related to significant linear and nonlinear correlations. If all such input–output curves are line-shaped even for the MI calculations, then nonlinear analysis is unnecessary and the cross-correlation technique is sufficient to detect all associations. As expected, cross-correlations mainly captured linear relationships (Fig. 2A). However, we found that input–output curves were highly complex and often nonlinear in a number of cases for MI analysis (Fig. 2B). Thus, as nonlinear associations were present during human SWS, the MI analysis was more appropriate in characterizing slow oscillation propagation.

### Characteristics of SWA propagation

The significant correlation of time-shifted waveforms recorded from pairs of electrodes was established by the MI technique. The resulting associations at each time point (Fig. 1B,C) served as unitary events for the subsequent calculations.

First, we investigated what characteristic patterns in the ECoG traces gave rise to significant waveform correlations. Raw ECoG segments showing significant nonlinear correlation with data segments recorded from other electrodes were averaged for each recording site (see Correlation triggered average, above). Significant waveform correlations usually corresponded to the rising phase of cortical SWA (Fig. 3A), which further supports the view that waveform correlations detected by the MI method reflect slow-wave propagation between different cortical areas. Moreover, it implies that the most conservative segment of the slow-wave cycle is its ascending phase, showing more pronounced correlation across areas compared with other phases of the oscillation.

Next, we calculated general characteristics of SWA propagation. The distribution of propagation distance (Fig. 1C, length distribution of the arrows) showed that SWA correlations were most common among neighboring cortical areas, although associations between distant sites were also observed (Fig. 3B). These unexpected spatial noncontinuities, or jumps, of SWA do not fit the general idea of traveling waves, i.e., propagation of slow waves as single lines over large cortical areas (Massimini et al., 2004). Propagation speed of cortical slow waves (calculated by dividing electrode distances with propagation time values; see Materi-

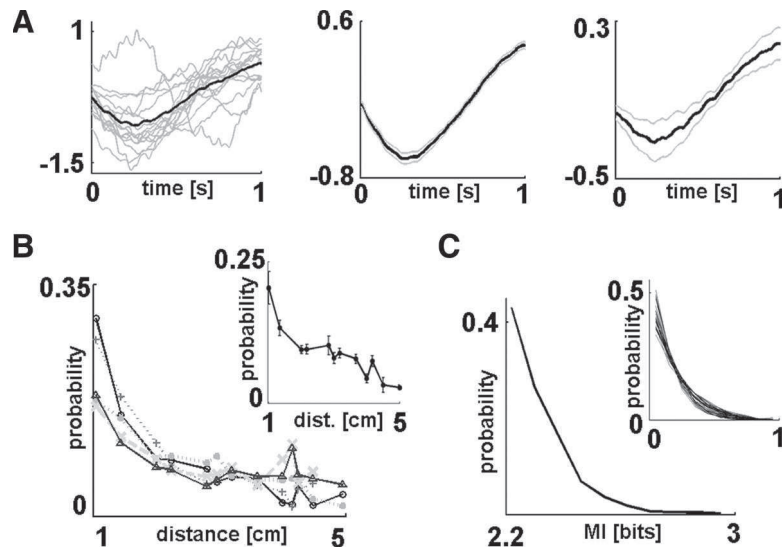


**Figure 3.** SWA propagation characteristics. **A**, Average waveforms of data segments with significant nonlinear correlations across ECoG channels. Left, Mean waveform from all ECoG channels separately (gray) and averaged (black) from a representative sleep segment of a single subject. Only data segments that showed significant correlations with other recording channels were included in these calculations. Middle, Mean waveform of significantly correlated data segments from the same subject including all analyzed sleep segments (black). Gray lines show SEM. Right, Grand average from all patients (black, mean; gray, SEM across patients). It should be noted that ECoG segments were standardized before the calculation of waveform averages; thus, tick labels of the *y*-axis show standardized voltage values. Average waveforms of data segments with significant waveform correlations across channels showed characteristic down-to-up state transitions, including the rising phase of SWA. **B**, Propagation distance distributions of unitary propagation events (Fig. 1C, length distribution of single arrows). Propagation distance distributions from the five analyzed sleep segments of a representative subject. Inset, Average distribution from all subjects. Error bars indicate SEM. SWA propagation to adjacent locations were significantly more frequent than spread to more distant loci ( $p = 7.12 \times 10^{-21}$ , Mann–Whitney *U* test); however, spatial noncontinuities of SWA propagation between areas located 5 cm away (largest distance covered) could also be detected. **C**, Distribution of association strength (Fig. 1C, maximal MI values of unitary propagation events indicated by the colors of the arrows). MI distribution from a representative sleep segment is shown. Inset, Connection strength distributions overlaid for all analyzed recording segments of all subjects. Because the range of connection strength values could vary, MI values were normalized between 0 and 1 for this plot. The shape of the distribution was similar across sleep segments and subjects.

als and Methods, above) showed large variability with an overall mean  $\pm$  SEM of  $3.33 \pm 0.96$  m/s, which is approximately in agreement with previous studies (Massimini et al., 2004; Hill and Tononi, 2005; Murphy et al., 2009). The distribution shape of correlation strength (MI) showed marked similarity across recording segments and subjects (Fig. 3C).

These propagation statistics were not statistically independent. Specifically, weak but significant negative correlations were found between correlation strength and propagation time [significant correlation ( $p < 0.01$ ) in 24 of 26 sleep segments with a mean  $\pm$  SEM correlation coefficient of  $-0.17 \pm 0.01$ ] as well as propagation distance [significant correlation ( $p < 0.01$ ) in 22 of 26 sleep segments with a mean correlation coefficient of  $-0.16 \pm 0.01$ ], whereas it was positively correlated with propagation speed [significant correlation ( $p < 0.01$ ) in 19 of 26 sleep segments with a mean correlation coefficient of  $0.10 \pm 0.01$ ]. Thus, fast propagation to short distances was accompanied by higher correlation strength. Expectedly, propagation time was usually positively correlated with propagation distance [positive correlation ( $p < 0.01$ ) in 23 of 26 sleep segments with a mean correlation coefficient of  $0.28 \pm 0.02$ ; negative correlation in one and no significant correlation in two cases].

### Complex patterns of SWA propagation

Sleep slow waves detected using scalp EEG recordings were shown to propagate along anteroposterior lines, sweeping across large areas of the cortical mantle (Massimini et al., 2004). The high signal quality of ECoG recordings (Buzsáki, 2006) allowed us to investigate SWA propagation at a finer scale. We tested

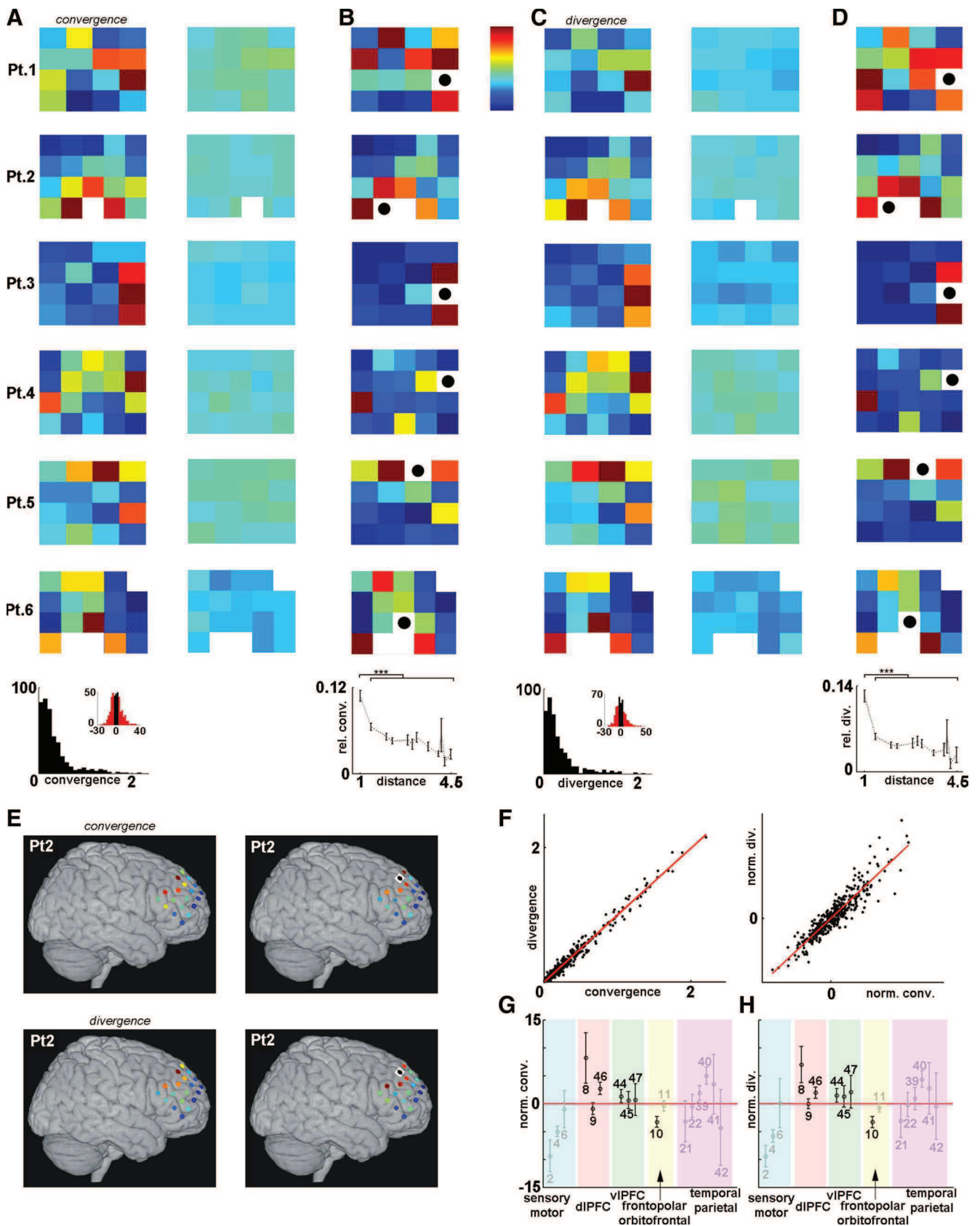


**Figure 4.** Convergence and divergence of SWA. **A**, Rate of SWA convergence on different electrodes. Warm colors indicate high number of convergent inputs (color bar). The  $4 \times 4$  or  $4 \times 5$  arrangements correspond to the configuration of the electrode grids (Fig. 1A). Left, Representative sleep segments from all subjects; right, corresponding control maps of randomized data (unitary propagation events were randomly shuffled among electrode pairs within each time frame, see Materials and Methods). Bottom, Distribution of the mean number of convergent inputs for all channels of all subjects. Inset, Distribution of the same values but normalized with individual control distributions (see Materials and Methods). Red bars fall out of the range of control distributions. **B**, Contribution maps for recording sites with the highest convergence rate (black dot in white field). Warm colors indicate high proportion of contribution to the SWA (Figure legend continues.)

whether more localized propagation patterns merely reflect line-like spreading found at larger scales, or whether a more complex propagation pattern characterizes smaller cortical regions.

First we analyzed convergence and divergence patterns. Convergence was assessed when an area received cortical activity from at least two distinct sites within a 100 ms time window, a temporal frame that allows different types of synaptic plasticity (Caporale and Dan, 2008). Locations with a high occurrence of convergent activity were observed in all subjects (see convergence maps in Fig. 4*A, E*). Sites of high convergence were preserved over different periods of SWS during the same night ( $n = 6$  subjects) and also, albeit to a lesser extent, different nights (significant correlation of convergence maps were found in all subjects in 13 of 16 within-night and 13 of 30 between-night comparisons; correlation coefficient for significant within- and between-night comparisons of  $0.70 \pm 0.05$  and  $0.65 \pm 0.04$ , respectively) (Fig. 5*A*). Recorded cortical areas contributed differentially to all convergent inputs to these sites (see contribution maps in Fig. 4*B*). These contribution maps were also statistically similar within subjects for sleep segments recorded during the same or different nights (significant correlations of contribution maps for the cortical site with the highest rate of convergence were found in all subjects in 12 of 16 within-night and 16 of 30 between-night comparisons; correlation coefficient for significant within- and between-night comparisons of  $0.67 \pm 0.05$  and  $0.70 \pm 0.04$ , respectively) (Fig. 5*A*). Areas with high rate of convergence received activity mostly, but not exclusively, from neighboring cortical locations (Fig. 4*B*).

Divergence of SWA was defined as propagation to different cortical areas from a single recording site within a 100 ms time window. Divergence maps showed hot spots with high divergence rates in all subjects (Fig. 4*C, E*) and were similar across different sleep segments of the same night as well as across different nights within subjects (significant correlation of divergence maps were found in all subjects in 11 of 16 within-night and 12 of 30 between-night comparisons; correlation coefficient for significant within- and between-night comparisons of  $0.75 \pm 0.05$  and  $0.66 \pm 0.04$ , respectively) (Fig. 5*B*). Moreover, these maps were markedly similar to the corresponding convergence maps of the same segment (significant correlation in all cases,  $n = 26$ ; correlation coefficient of  $0.93 \pm 0.01$ ) (compare Fig. 4, *A* and *C*; see

also Fig. 4*F*). Thus, convergence and divergence maps changed in a correlated fashion across different nights (Fig. 5). Maps showing relative distribution of divergent outputs from these hot spots of SWA propagation (Fig. 4*D*) were preserved among recording segments (significant correlations were found in all subjects in 12 of 16 within-night and 18 of 30 between-night comparisons; correlation coefficient for significant within- and between-night comparisons of  $0.71 \pm 0.05$  and  $0.69 \pm 0.03$ , respectively) (Fig. 5*B*) and were similar to corresponding convergence contribution maps (significant correlation in 25 of 26 cases; correlation coefficient of  $0.87 \pm 0.02$ ) (compare Fig. 4, *B* and *D*).

The placement of the grids was determined by clinical demands resulting in only a partial overlap among patients (Fig. 1*A*). Although this arrangement prevented detailed anatomical localization of convergence and divergence centers and the construction of topographic maps for convergence and divergence rates, we nevertheless analyzed the spatial organization of these activities according to Brodmann areas (BA). BA8, BA9, and BA46 (dorsolateral prefrontal cortex); BA10 (frontopolar cortex); and BA44 and BA45 (ventrolateral prefrontal cortex; Broca area in Pts. 5 and 6, where the grid was above the left hemisphere) were partially covered by the grid in at least two patients. We found that both convergence (Fig. 4*G*) and divergence (Fig. 4*H*) rates were high in parts of the dorsolateral prefrontal cortex (BA46 and particularly in BA8) and in the ventrolateral prefrontal cortex (BA44 and BA45), whereas it was low in the frontopolar cortex and adjacent areas (BA9 and BA10). The grids in Pts. 4 and 6 covered primary sensory and motor areas, respectively (BA2 in Pt. 4 and BA4 in Pt. 6), where the occurrence of convergent and divergent activity was the lowest. In Pt. 4, variable rates of convergence and divergence were found in the middle-superior temporal area and adjacent parietal regions (BA21, BA22, BA39, BA40, BA41, BA42).

The high correlation between input and output patterns of convergence–divergence centers found in this report suggests the presence of reciprocal and short-range circular propagation of SWA. We tested these possibilities as follows. For each unitary propagation event of SWA between two cortical recording sites, we investigated whether reciprocal propagation between those areas appears within 100 ms. The number of reciprocal associations was highly above chance in all analyzed sleep episodes of all subjects ( $p \approx 0$  in comparison with control distributions) (Fig. 6*A*). Finally, three-point circles (i.e., directed three-point trajectories of which the end points are the same as the starting points) of SWA propagation were detected. Three-point circles were abundant in all analyzed epochs (Fig. 6*B*), showing that propagating SWA often reenters previously visited cortical areas within a short time interval.

## Discussion

Here we analyzed the ECoG patterns of sleep slow waves in humans using a nonlinear correlation technique based on mutual information calculations supplemented by linear correlation measures. While high-density scalp EEG provides nearly complete spatial coverage over both hemispheres with a spatial resolution of  $\sim 2$  cm at the level of the scalp, its localizing capacity is hampered by the spatial smoothing effects of the scalp, skull, pia, and CSF. In contrast, while ECoG recordings provide lower spatial coverage, with a higher spatial resolution of  $\sim 1$  cm at the level of the cortical surface, it is not burdened by the spatial smoothing effects of the interleaving tissue (Buzsaki, 2006).

Correlations among SWA cycles recorded from different ECoG channels were highest during the first part of the up states where

(Figure legend continued.) convergence. Maps in the same row correspond to the same sleep segment. Bottom, Group results showing relative contribution to the convergence on the most prominent convergence center in the function of propagation distance (mean  $\pm$  SEM; only distance values with at least four sample elements are shown to allow reliable statistical estimates). Adjacent cortical areas showed significantly larger relative contribution ( $p = 1.07 \times 10^{-15}$ , Mann–Whitney  $U$  test), although distant sites could also contribute substantially (see Pts. 1 and 4). *C*, Rate of SWA divergence for all electrodes. Warm colors indicate high number of divergent outputs. Arrangement follows that of *A*. Right, Control maps. Note the similarity with corresponding convergence maps (*A*). *D*, Relative distribution of divergent outputs from sites with highest divergence rates. Arrangement follows that of *B*. Diverging SWA propagated dominantly to adjacent loci ( $p = 2.07 \times 10^{-20}$ , Mann–Whitney  $U$  test), but distant areas also received substantial diverging SWA (see Pts. 1, 4, and 6). *E*, The four maps of Pt. 2 shown in *A–D* are projected onto the brain surface (left, convergence and divergence map; right, corresponding contribution maps). *F*, Left, Convergence and divergence rates are plotted against each other for all recording sites and sleep segments in all patients. Right, The same rates were normalized to individual controls. Convergence and divergence rates were strongly correlated ( $r = 0.988$  and  $r = 0.921$  in the raw and normalized cases, respectively;  $p \approx 0$  in both cases). *G, H*, Distribution of convergence (conv., *G*) and divergence (div., *H*) rates [normalized (norm.) to controls] over different Brodmann areas. Mean  $\pm$  SEM values are displayed for each Brodmann area (numbers). Black, Regions covered in at least two patients; gray, areas covered in only one patient. dlPFC, Dorsolateral prefrontal cortex; vlPFC, ventrolateral prefrontal cortex.

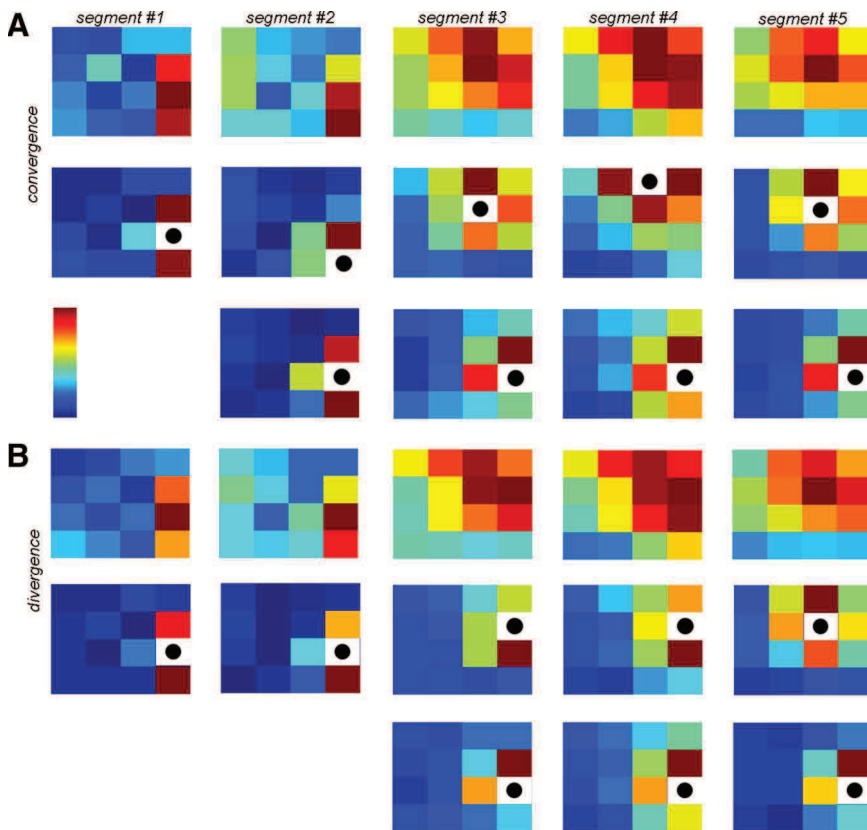


**Figure 5.** Convergence and divergence maps were similar within patients across sleep segments. **A**, Top, Convergence maps of Pt. 3 (see color bar). First and second segments were recorded during the second postoperative night; third and fourth segments are from the fourth postoperative night; fifth segment was recorded during the fifth postoperative night. Middle, Relative contribution to convergent inputs to the area with highest convergence rate. Bottom, Relative contribution to convergent inputs of the site receiving the most convergent activity during the first segment. **B**, Divergence maps and relative distribution of diverging activities arranged similarly as convergence maps in **A**. Note that maps for SWS segments recorded during a single night (first and second; third and fourth) were markedly similar in all cases. Maps in the fifth column are clearly similar to those of the third and fourth segments, despite being recorded during two different (but consecutive) nights.

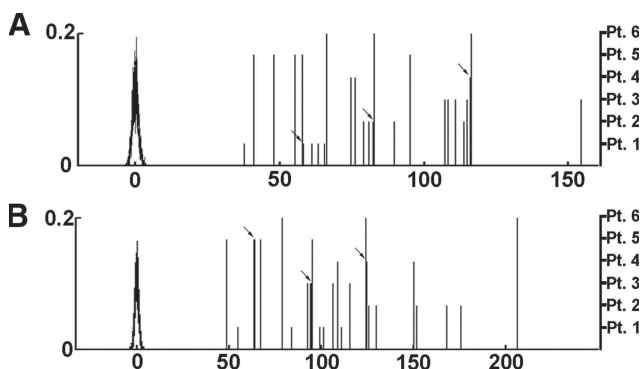


**Figure 6.** Reciprocal connections and short circles in the course of SWA propagation. **A**, Normalized number of reciprocal connections calculated for all analyzed sleep segments in all subjects. Normalization was performed using control distributions (see Materials and Methods). Normalized control distributions are superimposed in black (left y-axis shows probabilities). Normalized numbers of reciprocal propagations are indicated as vertical bars (different lengths correspond to different patients; right y-axis). The number of reciprocal connections was found to be highly above control values in all cases ( $p \approx 0$ ). Arrows point to overlapping values. **B**, Normalized number of three-point circles displayed in a similar way as reciprocal connections. The number of circles was significantly above control values ( $p \approx 0$ ).

most of the neuronal spiking interactions take place, confirming that this phase of the oscillation provides an optimal window for neuronal interactions (Luczak et al., 2009). It is also in line with previous findings showing that sleep spindles and hippocampal ripples are phase locked to this segment of the slow-wave cycle, indicating that the flow of information both among cortical regions and between the thalamocortical and hippocampal circuits would be connected to the down-to-up state transition period (Mölle et al., 2006; Clemens et al., 2007).

SWA, recorded by ECoG, showed complex propagation patterns such as convergence, divergence, reciprocal propagation, and short circles. Correlations were strongest between neighboring recording sites, although unexpected spatial noncontinuities of slow-wave propagation were also observed. Cortical areas were shown to receive convergent activity from other regions as well as to disseminate SWA. Centers (or hot spots) of SWA propagation with high convergence and divergence rates were identified in all subjects. Hot spots were stable during and, although to a lesser extent, across nights. These complex patterns of SWA propagation might reflect the differential aspects of local and global mechanisms of neural interactions revealed by cortical electrical activity during SWS.

Our choice of the nonlinear correlation measure was based on our observation and other reports that, in addition to linear associations, nonlinear dependencies are frequently detected among different brain regions during various brain states (Freiwald et al., 1999; Darvas et al., 2009; Chen et al., 2010). Although linear methods (e.g., cross-correlation, partial directed coherence, directed transfer function) may in certain situations perform better than nonlinear ones (e.g., MI, transfer entropy, nonlinear Granger causality), they have common drawbacks, such as bias toward the detection of linear associations and a lack of scaling independence (for review, see Pereda et al., 2005). The well established information theory-based MI analysis (Na et al., 2002; Kajikawa and Hackett, 2005; Pereda et al., 2005; Paz et al., 2010) was capable of detecting a larger number of significant associations when compared with linear cross-correlations. These nonlinear associations were often characterized by complex and variable input–output functions. Our choices of cross-correlation and MI were in concert with the recommendations of Pereda et al. (2005) for EEG-type data. Functional connections are inferred from linear or nonlinear correlation or coherence measures, such as significant short-latency peaks in cross-correlation functions when established between single neurons (Csicsvari et al., 1998; Barthó et al., 2004; Hangya et al., 2010) or significant waveform and phase correlations in cases of neural networks or brain areas (Buzsáki, 2006; Womelsdorf et al., 2007; Bullmore and Sporns, 2009; Singer and Uhlhaas et al., 2009). Thus, we speculate that nonlinear correlation of SWA activity might reflect functional connections among brain areas.

Associations reported in this study may be mediated by both corticocortical and corticothalamocortical routes of information transmission (Crunelli and Hughes, 2010). Although it is theoretically possible that the two types of communication operate with different temporal delays, consistent bimodality of propagation time distributions could not be revealed. Also, influences of common information sources cannot completely be ruled out (Hangya et al., 2009), although a recent study suggested that such sources do not necessarily cause detectable correlations (Renart et al., 2010).

Based on the concept of traveling waves, a propagating slow wave rarely if ever reenters previously visited cortical sites. However, anatomical studies of cortical structural connectivity show an especially rich repertoire of reciprocal connections and loops within and across brain areas (Bullmore and Sporns, 2009). In concert with the complex patterns of cortical connectivity, we also found a rich source of reciprocal and short circle propagation patterns, which may suggest that electrical activity underlying neuronal processing was often bidirectional, or reentered previously visited areas.

We propose that cortical centers with high convergence and divergence rates might serve as hot spots for neuronal interaction in sleep. This view is supported by the relative stability of these hot spots and their tendency to have a larger correlation with neighboring cortical areas. Spatial distances between correlated channels were found to be short on average, which further emphasizes the importance of the finely structured, local neuronal circuitry in electrical activity pattern generation. Longer range correlations arose occasionally, presumably as a consequence of the communication between high connectivity centers. These associations could appear as noncontinuous propagation between relatively distant areas. It should be noted, however, that rapid step-by-step spread along a continuous array of recording sites could be masked sometimes by higher noise levels on some of the electrodes or reduced signal quality over sulci. Between-night correlations appeared less frequently compared with within-night correlations, which may be a result of slow temporal changes in cortical activity. This hypothesis is in agreement with previous results showing that local changes in cortical SWA are largely related to daytime experiences (Huber et al., 2004). We did not observe a systematic change of correlation stability with increasing time after the surgery. However, an effect of gradual recovery after the surgical intervention on the stability of convergence and divergence centers cannot be completely ruled out.

Although different placements of the electrode grid on the six patients limited the possibilities of mapping hot spots onto anatomical structures, averaging normalized convergence and divergence rates in different Brodmann areas showed an elevated activity in the ventrolateral and dorsolateral prefrontal cortex. These observations are in accordance with previous studies showing the strong involvement of human prefrontal areas in memory consolidation and related delta band oscillatory activity during deep stages of sleep (Diekelmann and Born, 2010). Our findings are also in agreement with the prominent participation of the middle and inferior frontal gyri in SWS propagation (Murphy et al., 2009).

The long-standing observation that sleep is beneficial to remembering (Jenkins and Dallenbach, 1924) has recently been linked to cortical sleep slow waves (Fowler et al., 1973; Marshall et al., 2006). Although large brain areas can engage in synchronous low-frequency oscillations (Sirota and Buzsáki, 2005; Volgushev et al., 2006), a number of studies showed localized increase of SWA after learning correlated with memory performance after

sleep (Huber et al., 2004; Schmidt et al., 2006; Huber et al., 2007; Massimini et al., 2009 and references therein). Thus, a growing body of evidence suggests that memory consolidation during sleep involves localized cortical processes, which are accompanied by regional changes in SWA. In addition to reports of SWA propagation over wide cortical areas (Massimini et al., 2004; Hill and Tononi, 2005; Murphy et al., 2009), propagation dynamics should be examined at a finer spatial scale to detect phenomena possibly underlying local cortical processing (Luczak et al., 2007; Mohajerani et al., 2010). The use of subdural electrode grids, which lack the major drawbacks of scalp recordings, such as spatial smoothing and attenuation exerted by the intermediate tissues (Buzsáki, 2006; Bangera et al., 2010), allowed us to unravel an unexpected complexity of localized SWA propagation patterns, e.g., short circles and convergence–divergence centers. Thus, our results provide the first step in filling the gap between global SWA traveling (Massimini et al., 2004) and local operations of cortical networks (Huber et al., 2004; Mohajerani et al., 2010).

## Notes

Supplemental material for this article is available at [http://www.koki.hu/supp\\_materials/Hangya\\_et\\_al\\_Supplemental\\_Material\\_JN2011.html](http://www.koki.hu/supp_materials/Hangya_et_al_Supplemental_Material_JN2011.html). The supplemental material includes three movies showing slow oscillation propagation (two for real and one for simulated data); additional analysis showing robustness of our results, including an analysis of signal-to-noise ratios with three figures; and three tables showing individual propagation speed and convergence/divergence map correlation results, as well as coverage of Brodmann areas by the electrode grids for each patient. This material has not been peer reviewed.

## References

- Bangera NB, Schomer DL, Dehghani N, Ulbert I, Cash S, Papavasiliou S, Eisenberg SR, Dale AM, Halgren E (2010) Experimental validation of the influence of white matter anisotropy on the intracranial EEG forward solution. *J Comput Neurosci* 29:371–387.
- Barthó P, Hirase H, Monconduit L, Zugaro M, Harris KD, Buzsáki G (2004) Characterization of neocortical principal cells and interneurons by network interactions and extracellular features. *J Neurophysiol* 92:600–608.
- Bullmore E, Sporns O (2009) Complex brain networks: graph theoretical analysis of structural and functional systems. *Nat Rev Neurosci* 10:186–198.
- Buzsáki G (2006) *Rhythms of the brain*. New York: Oxford University.
- Caporale N, Dan Y (2008) Spike timing-dependent plasticity: a Hebbian learning rule. *Annu Rev Neurosci* 31:25–46.
- Cash SS, Halgren E, Dehghani N, Rossetti AO, Thesen T, Wang C, Devinsky O, Kuzniecky R, Doyle W, Madsen JR, Bromfield E, Eross L, Halász P, Karmos G, Csercsa R, Wittner L, Ulbert I (2009) The human K-complex represents an isolated cortical down-state. *Science* 324:1084–1087.
- Chen CC, Kilner JM, Friston KJ, Kiebel SJ, Jolly RK, Ward NS (2010) Non-linear coupling in the human motor system. *J Neurosci* 30:8393–8399.
- Clemens Z, Mölle M, Eross L, Barsi P, Halász P, Born J (2007) Temporal coupling of parahippocampal ripples, sleep spindles and slow oscillations in humans. *Brain* 130:2868–2878.
- Cossart R, Aronov D, Yuste R (2003) Attractor dynamics of network UP states in the neocortex. *Nature* 423:283–288.
- Crunelli V, Hughes SW (2010) The slow (<1 Hz) rhythm of non-REM sleep: a dialogue between three cardinal oscillators. *Nat Neurosci* 13:9–17.
- Csercsa R, Dombóvári B, Fabó D, Wittner L, Eross L, Entz L, Sólyom A, Rásonyi G, Szucs A, Kelemen A, Jakus R, Juhas V, Grand L, Magony A, Halász P, Freund TF, Maglóczy Z, Cash SS, Papp L, Karmos G, et al. (2010) Laminar analysis of slow wave activity in humans. *Brain* 133:2814–2829.
- Csicsvari J, Hirase H, Czurko A, Buzsáki G (1998) Reliability and state dependence of pyramidal cell-interneuron synapses in the hippocampus: an ensemble approach in the behaving rat. *Neuron* 21:179–189.
- Darvas F, Ojemann JG, Sorensen LB (2009) Bi-phase locking—a tool for

- probing non-linear interaction in the human brain. *Neuroimage* 46:123–132.
- Diekelmann S, Born J (2010) The memory function of sleep. *Nat Rev Neurosci* 11:114–126.
- Fowler MJ, Sullivan MJ, Ekstrand BR (1973) Sleep and memory. *Science* 179:302–304.
- Freiwald WA, Valdes P, Bosch J, Biscay R, Jimenez JC, Rodriguez LM, Rodriguez V, Kreiter AK, Singer W (1999) Testing non-linearity and directedness of interactions between neural groups in the macaque inferotemporal cortex. *J Neurosci Methods* 94:105–119.
- Hangya B, Borhegyi Z, Szilágyi N, Freund TF, Varga V (2009) GABAergic neurons of the medial septum lead the hippocampal network during theta activity. *J Neurosci* 29:8094–8102.
- Hangya B, Li Y, Muller RU, Czurkó A (2010) Complementary spatial firing in place cell-interneuron pairs. *J Physiol* 588:4165–4175.
- Hill S, Tononi G (2005) Modeling sleep and wakefulness in the thalamocortical system. *J Neurophysiol* 93:1671–1698.
- Huang X, Xu W, Liang J, Takagaki K, Gao X, Wu JY (2010) Spiral wave dynamics in neocortex. *Neuron* 68:978–990.
- Huber R, Ghilardi MF, Massimini M, Tononi G (2004) Local sleep and learning. *Nature* 430:78–81.
- Huber R, Esser SK, Ferrarelli F, Massimini M, Peterson MJ, Tononi G (2007) TMS-induced cortical potentiation during wakefulness locally increases slow wave activity during sleep. *PLoS One* 2:e276.
- Iber C, Ancoli-Israel S, Chesson A, Quan SF (2007) The AASM manual for the scoring of sleep and associated events: rules, terminology and technical specifications. Westchester: American Academy of Sleep Medicine.
- Isomura Y, Sirota A, Ozen S, Montgomery S, Mizuseki K, Henze DA, Buzsáki G (2006) Integration and segregation of activity in entorhinal-hippocampal subregions by neocortical slow oscillations. *Neuron* 52:871–882.
- Jenkins JC, Dallenbach KM (1924) Obliviscence during sleep and waking. *Am J Psychol* 35:605–612.
- Kajikawa Y, Hackett TA (2005) Entropy analysis of neuronal spike train synchrony. *J Neurosci Methods* 149:90–93.
- Kurth S, Ringli M, Geiger A, LeBourgeois M, Jenni OG, Huber R (2010) Mapping of cortical activity in the first two decades of life: a high-density sleep electroencephalogram study. *J Neurosci* 30:13211–13219.
- Le Van Quyen M, Staba R, Bragin A, Dickson C, Valderrama M, Fried I, Engel J (2010) Large-scale microelectrode recordings of high-frequency gamma oscillations in human cortex during sleep. *J Neurosci* 30:7770–7782.
- Luczak A, Barthó P, Marguet SL, Buzsáki G, Harris KD (2007) Sequential structure of neocortical spontaneous activity *in vivo*. *Proc Natl Acad Sci U S A* 104:347–352.
- Luczak A, Barthó P, Harris KD (2009) Spontaneous events outline the realm of possible sensory responses in neocortical populations. *Neuron* 62:413–425.
- Magnin M, Rey M, Bastuji H, Guillemant P, Mauguière F, Garcia-Larrea L (2010) Thalamic deactivation at sleep onset precedes that of the cerebral cortex in humans. *Proc Natl Acad Sci U S A* 107:3829–3833.
- Marshall L, Helgadóttir H, Mölle M, Born J (2006) Boosting slow oscillations during sleep potentiates memory. *Nature* 444:610–613.
- Massimini M, Huber R, Ferrarelli F, Hill S, Tononi G (2004) The sleep slow oscillation as a traveling wave. *J Neurosci* 24:6862–6870.
- Massimini M, Tononi G, Huber R (2009) Slow waves, synaptic plasticity and information processing: insights from transcranial magnetic stimulation and high-density EEG experiments. *Eur J Neurosci* 29:1761–1770.
- Mena-Segovia J, Sims HM, Magill PJ, Bolam JP (2008) Cholinergic brainstem neurons modulate cortical gamma activity during slow oscillations. *J Physiol* 586:2947–2960.
- Mohajerani MH, McVea DA, Fingas M, Murphy TH (2010) Mirrored bilateral slow-wave cortical activity within local circuits revealed by fast bi-hemispheric voltage-sensitive dye imaging in anesthetized and awake mice. *J Neurosci* 30:3745–3751.
- Mölle M, Yeshenko O, Marshall L, Sara SJ, Born J (2006) Hippocampal sharp wave-ripples linked to slow oscillations in rat slow-wave sleep. *J Neurophysiol* 96:62–70.
- Murphy M, Riedner BA, Huber R, Massimini M, Ferrarelli F, Tononi G (2009) Source modeling sleep slow waves. *Proc Natl Acad Sci U S A* 106:1608–1613.
- Na SH, Jin SH, Kim SY, Ham BJ (2002) EEG in schizophrenic patients: mutual information analysis. *Clin Neurophysiol* 113:1954–1960.
- Ostojic S, Brunel N, Hakim V (2009) How connectivity, background activity, and synaptic properties shape the cross-correlation between spike trains. *J Neurosci* 29:10234–10253.
- Panzeri S, Senatore R, Montemurro MA, Petersen RS (2007) Correcting for the sampling bias problem in spike train information measures. *J Neurophysiol* 98:1064–1072.
- Paz R, Gelbard-Sagiv H, Mukamel R, Harel M, Malach R, Fried I (2010) A neural substrate in the human hippocampus for linking successive events. *Proc Natl Acad Sci U S A* 107:6046–6051.
- Pereda E, Quiroga RQ, Bhattacharya J (2005) Nonlinear multivariate analysis of neurophysiological signals. *Prog Neurobiol* 77:1–37.
- Renart A, de la Rocha J, Bartho P, Hollender L, Parga N, Reyes A, Harris KD (2010) The asynchronous state in cortical circuits. *Science* 327:587–590.
- Schmidt C, Peigneux P, Muto V, Schenkel M, Knoblauch V, Münch M, de Quervain DJ, Wirz-Justice A, Cajochen C (2006) Encoding difficulty promotes postlearning changes in sleep spindle activity during napping. *J Neurosci* 26:8976–8982.
- Shannon C (1948) A mathematical theory of communication. *Bell Syst Tech J* 27:379–423, 623–656.
- Siapas AG, Wilson MA (1998) Coordinated interactions between hippocampal ripples and cortical spindles during slow-wave sleep. *Neuron* 21:1123–1128.
- Sirota A, Buzsáki G (2005) Interaction between neocortical and hippocampal networks via slow oscillations. *Thalamus Relat Syst* 3:245–259.
- Steriade M, Nuñez A, Amzica F (1993) A novel slow (< 1 Hz) oscillation of neocortical neurons in vivo: depolarizing and hyperpolarizing components. *J Neurosci* 13:3252–3265.
- Uhlhaas PJ, Pipa G, Lima B, Melloni L, Neuenschwander S, Nikolić D, Singer W (2009) Neural synchrony in cortical networks: history, concept and current status. *Front Integr Neurosci* 3:17.
- Volgushev M, Chauvette S, Mukovski M, Timofeev I (2006) Precise long-range synchronization of activity and silence in neocortical neurons during slow-wave oscillations. *J Neurosci* [Erratum (2006) 26:table of contents] 26:5665–5672.
- Wolansky T, Clement EA, Peters SR, Palczak MA, Dickson CT (2006) Hippocampal slow oscillation: a novel EEG state and its coordination with ongoing neocortical activity. *J Neurosci* 26:6213–6229.
- Womelsdorf T, Schoffelen JM, Oostenveld R, Singer W, Desimone R, Engel AK, Fries P (2007) Modulation of neuronal interactions through neuronal synchronization. *Science* 316:1609–1612.

dc\_303\_11

## **7. Melléklet**



## In vivo laminar electrophysiology co-registered with histology in the hippocampus of patients with temporal lobe epilepsy

István Ulbert,<sup>a,b,\*</sup> Zsófia Maglóczky,<sup>c</sup> Loránd Eröss,<sup>d</sup> Sándor Czirják,<sup>e</sup> János Vajda,<sup>e</sup>  
László Bognár,<sup>e</sup> Szabolcs Tóth,<sup>d</sup> Zerind Szabó,<sup>d</sup> Péter Halász,<sup>f</sup> Dániel Fabó,<sup>f</sup>  
Eric Halgren,<sup>b,g</sup> Tamás F. Freund,<sup>c</sup> and George Karmos<sup>a</sup>

<sup>a</sup>Institute for Psychology of the Hungarian Academy of Sciences, Budapest 1068, Hungary

<sup>b</sup>Athinoula A. Martinos Center for Biomedical Imaging, Massachusetts General Hospital, Massachusetts Institute of Technology, Harvard Medical School, Charlestown, MA 02129, USA

<sup>c</sup>Institute of Experimental Medicine of the Hungarian Academy of Sciences, Budapest 1450, Hungary

<sup>d</sup>Department of Neurosurgery, MÁV Hospital, Budapest 1062, Hungary

<sup>e</sup>National Institute for Neurosurgery, Budapest 1577, Hungary

<sup>f</sup>National Institute of Psychiatry and Neurology, Epilepsy Center, Budapest 1021, Hungary

<sup>g</sup>INSERM, Marseilles, France

Received 27 August 2003; revised 4 December 2003; accepted 8 December 2003

Available online 10 February 2004

### Abstract

Laminar multiple microelectrodes have been developed to sample cortical and hippocampal activity in animals. If these measurements are adequately co-registered with the anatomy of the region, they can yield important information about its function and structure. In vivo laminar electrophysiological recordings from the human epileptic hippocampus are rare. However, histological and immunohistochemical analyses are widely used to determine the structural changes associated with temporal lobe epilepsy (TLE). Here we present data obtained by a combined approach: intraoperative recording of laminar field potentials, single and multiple unit activity under anesthesia, accompanied by histology and immunohistochemistry from the same hippocampal region of epileptic patients undergoing temporal lobectomy for drug-resistant TLE. The stability of the electrophysiology and the accuracy of its co-registration with histology were tested successfully. We have found large field potential spikes associated with bursting single units in CA1. Intracortical and subdural strip recordings from the lateral temporal cortex showed similar field potential activation patterns. A prominent oscillatory activity was present in the dentate gyrus with highly localized field potential gradient and multiple unit activity. This pattern could be used as a landmark defining the position of the electrode in the hippocampus. Our findings indicate that some aspects of the local and network epileptiform activity in the hippocampal formation are likely preserved under anesthesia. Electrophysiological identification of the functional state of the hippocampus together with its local structural correlates could further enhance our understanding of this disease.

© 2004 Elsevier Inc. All rights reserved.

**Keywords:** Temporal lobe epilepsy; Hippocampus; Human; Laminar electrophysiology; Histology; CA1; DG; Interictal spike; Bursting unit

### Introduction

Temporal lobe epilepsy (TLE) is a devastating disease, causing cognitive impairment and decreased quality of life.

The hippocampus plays a central role in the generation and maintenance of the paroxysmal activity in TLE. Numerous morphological and in vivo electrophysiological studies have assessed the structural and functional disturbances in the human hippocampus caused by TLE; however, these studies lack accurate co-registration of histology and electrophysiology. We believe that co-registration of the in vivo functional and morphological findings is a very important issue to elucidate the anatomical sources and network bases of

\* Corresponding author. Department of Psychophysiology, Institute for Psychology of the Hungarian Academy of Sciences, Szondi u. 83-85, Budapest 1068, Hungary. Fax: +36-1-354-2416.

E-mail address: ulbert@cogpsyphy.hu (I. Ulbert).

paroxysmal events, and define the functional connections between the closely spaced structures of the human hippocampus.

In the last two decades, powerful electrophysiological techniques have been developed to reveal the network interactions of the rodent hippocampus in vivo (Csicsvari et al., 2003). Silicone probes were implanted chronically mostly into rats, and a significant amount of information has been collected during several tasks, various stages of vigilance, and induced seizures (Bragin et al., 1997, 2002a). Laminar field potentials recorded from the hippocampus yield information about its synaptic and cellular properties (Buzsaki et al., 1986). Multiple, single unit activity (MUA, SUA) and current source density (CSD) analysis (Freeman and Nicholson, 1975; Nicholson and Freeman, 1975) have been developed and utilized to investigate hippocampal circuitry. Together with histological co-registration, CSD and MUA can identify the micro-anatomical sources of postsynaptic currents and spiking activity (Bragin et al., 1997, 2000). However, the morphology and the connections of the human hippocampus are more complex than in rodents (Lim et al., 1997a,b), consequently their electrophysiological properties may also seem different. As an example, it is still debated whether the classically defined theta oscillation—a fundamental electrographic element of the rodent hippocampal activity—exists at all in the human hippocampus (Bodizs et al., 2001; Caplan et al., 2003; Halgren, 1991; Kahana et al., 2001; O'Keefe and Burgess, 1999).

In epileptic humans, together with the clinical depth electrodes, microwires (Babb et al., 1973; Halgren et al., 1978; Staba et al., 2002a,b; Wyler et al., 1982) were implanted to record neuronal activity from the hippocampus. These devices were not designed to resolve the laminar potential profile to produce CSD traces and spatially dense laminar information about action potential spiking activity (MUA, SUA). To record laminar field potentials and MUA, SUA, multicontact linear array electrodes with 500  $\mu\text{m}$  spacing were implemented (Bragin et al., 2002b), but these devices are still not optimal for the CSD analysis. Another shortcoming of the above methods is the uncertainty of electrode tip localization. MR scans were used to define the electrode coordinates, but MR has a limited resolution and often considerable spatial distortion. Moreover, the hippocampus could not be recovered after resection to verify the location of the electrode track and to investigate the degree of structural reorganization in the vicinity of the electrophysiological recordings.

Here we present a combined approach that allows recording of laminar field potentials and spiking activity together with identification of the microanatomy at the recording sites in the hippocampus of epileptic patients undergoing temporal lobectomy. In addition, the methodology yields very important information about the reorganization of the hippocampus surrounding the electrode track via immunohistochemical techniques. Examples of laminar field potential and

MUA, SUA traces from various depths of the hippocampus will be presented, together with the histological/immunohistochemical analysis. With the aid of this technique, we can have a better insight into the functional and structural properties of the hippocampal involvement in TLE.

## Methods

A crucial aspect of this investigation is the coordination among neurosurgery, electrophysiology, and histology. Patients who participated in this research all underwent temporal lobectomy (hippocampectomy) as treatment for long-standing medically intractable TLE. Each subject was fully informed and consented under the auspices of the Hungarian Medical Research Council, in accordance with the Declaration of Helsinki. Intraoperative recordings were only done in the hippocampus and in the middle temporal gyrus (T2) to be resected, thus no additional risks that may stem from the invasive nature of our investigation were anticipated.

### *Electrophysiology and surgery*

Laminar multicontact microelectrodes (multielectrodes, ME) were designed for animals with a long shaft to reach deep structures in the brain (Barna et al., 1981; Mehta et al., 2000a,b). In a previous paper (Ulbert et al., 2001a), thumb-tack MEs (tME) were introduced to sample cortical structures (Ulbert et al., 2001b) from humans. These MEs were not adequate for quick intraoperative hippocampal insertion, so they were redesigned to minimize the additional time needed to mount the device and record during the surgery.

The depth ME (dME) is manufactured the same way as the tME (Ulbert et al., 2001a). The recent design is a 10-cm-long, 350- $\mu\text{m}$ -diameter, stainless steel shaft, sharp tip device, with 24 contacts, formed by the cut end of 25- $\mu\text{m}$ -diameter Pt/Ir wires, center-to-center distance is 100  $\mu\text{m}$  (Fig. 1A). To mount the dME, it was glued on a precision small sledge with epoxy, which was then attached to a micromanipulator with a screw lock system, so it could be roughly positioned before the insertion. The micromanipulator was equipped with a precision dial advancing mechanism and a measure, so the depth of the penetration could be controlled with 100  $\mu\text{m}$  accuracy after securing the rough positioning screw. All the equipment, preamplifiers and cables going into the surgical field were sterilized in ethylene oxide. The micromanipulator was mounted on a medical instrument holder during surgery, which could be fixed in position and allowed the surgeon to aim toward the hippocampus. Under visual control using an operating microscope, the electrode tip was advanced into the hippocampus after temporal pole resection. The pole resection was done under general anesthesia (Fentanyl, Diprivan and  $\text{N}_2\text{O}$  or Isofluran or Sevofluran and  $\text{N}_2\text{O}$ ) from a small craniotomy (3–5 cm) to reveal the head and the initial part of

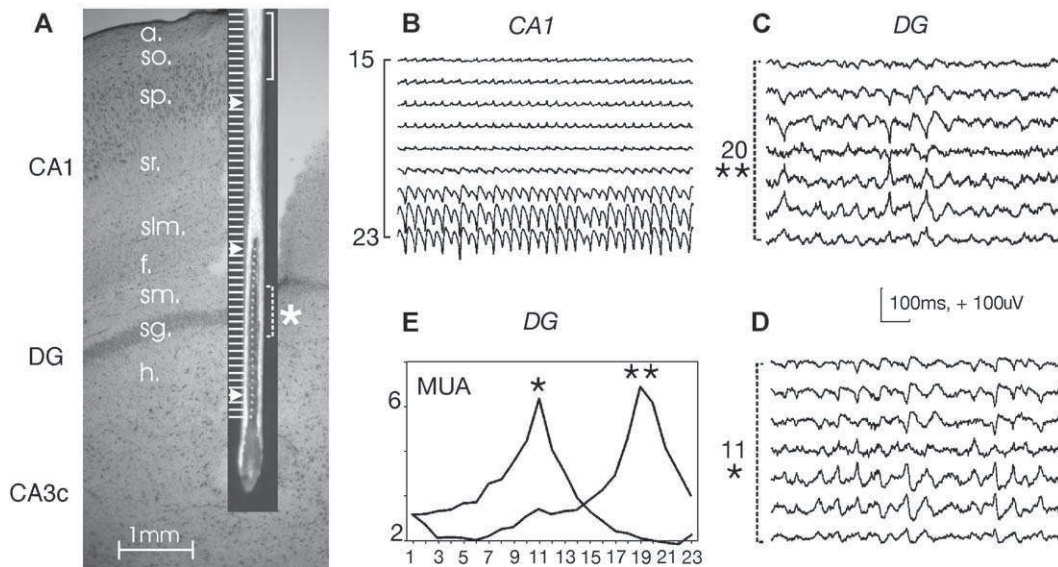


Fig. 1. (A) Reconstruction of pt.1 electrode track with the dME superimposed. Calibration bar: 1 mm, 60- $\mu$ m-thick Nissl-stained section. The photomicrograph of the dME was inserted in the slide to illustrate its position in the hippocampus. DG: dentate gyrus, a.: alveus, so.: stratum oriens, sp.: stratum pyramidale, sr.: stratum radiatum, slm.: stratum lacunosum-moleculare, f.: fissura hippocampi, sm.: stratum moleculare of the DG, sg.: stratum granulosum, h.: hilus. White grating (100  $\mu$ m apart) on the side of the dME indicates the depth of the recording sites, distance between arrows: 2 mm. Solid white bracket refers to the location of the field potential gradient shown in B (solid black bracket), dashed white bracket refers to the location of the field potential gradient shown in C and D (dashed black brackets). Double black asterisks denote the sg. in the first electrode position, while single black asterisk denotes sg. in the second (lowered 1 mm) electrode position. A shows the approximate location of the dME in the tissue, in the second (lowered 1 mm) electrode position. (B) Injury potentials from the CA1 subfield. Representative single sweep PG traces show oscillatory activity after the dME entered the hippocampus for the first time. The oscillation lasted only for about 60 s, and then diminished. No single unit spikes were detected. Note that PG is positive in so. and inverts rapidly in sp., the same profile is apparent in Fig. 2B (CA1) with nearly identical inversion depth. Calibration: 100 ms, +100  $\mu$ V, positive potentials are depicted upwards in all of the figures. (C and D) Oscillatory activity in DG while the manipulator was moved down with  $\sim$ 1 mm, representative traces. C was recorded before the movement, the PG inversion is at channel 20 (marked with \*\*), after the movement PG inversion slides to channel 11 (marked with \*), accounting for  $\sim$ 1 mm displacement of the dME in the tissue. (E) The depth profile of the ongoing MUA averaged during a 1-min period before and after repositioning the dME. X-axis: channel numbers, Y-axis intensity, arbitrary units. Note that the MUA peak moved from channel 19–20 to channel 11, as the zero zone on C and D.

the body of the hippocampus, which is a routine approach for hippocampectomy. After positioning onto the hippocampal surface, the electrode was advanced into the hippocampus with 2-mm increments. At each 2-mm step, we recorded for 2–5 min continuously. One or two penetrations were made, usually crossing the CA1, dentate gyrus (DG), hilus, and CA3c. Spatial field potential gradient (PG, first spatial derivative of the laminar field potentials) was collected in the low-frequency band (EEG; 0.1–500 Hz, sampled at 2 kHz/channel, 16 bit) and high-frequency band (MUA; 150–5000 Hz, sampled at 20 kHz/channel, 12 bit) simultaneously. In two patients, intraoperative electrocorticography (ECoG), and in one patient intracortical tME observations were performed. Details about the amplifier and acquisition system were published previously (Ulbert et al., 2001a).

After the recordings were done, the dME was pulled out, and the hippocampus was resected en bloc. The neurosurgeon and the histologist confirmed and recorded the region and angle of the electrode insertion based on the surface vascularization of the hippocampus, because the entrance point of the dME was sometimes not apparent. Digital photograph was taken of the removed hippocampal part, and then the block was cut into 4- to 5-mm-thick slabs in the

operating room, parallel with the electrode trajectory. Another photograph was taken of the cut slab containing the electrode track, it was measured to allow subsequent estimation of shrinkage, and finally all of the slabs were put into fixative separately.

#### *Histology, immunohistochemistry*

The fixative contained 4% paraformaldehyde, 0.05% glutaraldehyde, and 0.2% picric acid in 0.1 M phosphate buffer (PB, pH = 7.4), it was hourly changed to a fresh solution during constant agitation for 6 h, and then the blocks were postfixated in the same solution overnight. Vibratome sections (60  $\mu$ m thick) were cut from the blocks, and following washing in PB, they were immersed in 30% sucrose for 1–2 days, and then frozen three times over liquid nitrogen.

Sections were processed for immunostaining as follows: They were transferred to TRIS-buffered saline (TBS, pH = 7.4), and then endogenous peroxidase activity was blocked by 1% H<sub>2</sub>O<sub>2</sub> in TBS for 10 min. TBS was used for all the washes (3  $\times$  10 min between each antiserum) and for dilution of the antisera. Nonspecific immunostaining was blocked by

5% milk powder and 2% bovine serum albumin. A polyclonal rabbit antiserum against glutamate receptor 2 and 3 subunit (GluR2/3, 1:100, Chemicon, Temecula) was used to label the principal cells for 2 days at 4°C. For the visualization of immunopositive elements, biotinylated anti-rabbit IgG (1:250, Vector) was applied as secondary serum followed by avidin–biotinylated horseradish peroxidase complex (ABC, 1:250, Vector). The immunoperoxidase reaction was developed by 3,3'-diaminobenzidine tetrahydrochloride (DAB, Sigma) as a chromogene dissolved in TRIS buffer (TB, pH = 7.6). Sections were then treated with 1% OsO<sub>4</sub> in PB for 40 min, dehydrated in ethanol (1% uranyl acetate was added at the 70% ethanol stage for 40 min) and mounted in Durcupan (ACM, Fluka). The specificity of the antiserum has been thoroughly tested by the laboratory of origin.

Controls of the method included the incubation of sections in the same way, but primary antisera were replaced by the respective normal sera. No specific immunostaining could be detected under these conditions. Alternate sections (every sixth) were mounted from gelatin, and processed for cresyl violet (Nissl) staining, air-dried, dehydrated in xylene, and covered with Depex neutral medium for identification of the electrode track. Control hippocampal tissue was obtained from two patients, who died by accident, with no neurological disorder (Magloczky et al., 2000).

## Results

Eleven patients were implanted with the dME. We recovered the full electrode track in six patients, while parts of the track were found in five patients. From all of the patients, we were able to obtain electrophysiology data. Complete co-registration of the electrophysiology with the histology was done in four patients. In three out of the four co-registered patients, the electrode track was found in the CA1/DG/CA3 axis, in the remaining co-registered patient, the electrode track was from CA1/CA1i (internal digitations). Two out of the four patients with fully reconstructed electrode track had a well-preserved CA1 region with numerous pyramidal cells, while the other subjects showed hippocampal sclerosis with moderate to massive CA1 pyramidal cell loss and gliosis. Here we present histological and electrophysiological data from the CA1 and DG of the two nonsclerotic hippocampi (left side). Both patients were anesthetized with N<sub>2</sub>O, Diprivan (propofol), and Fentanyl.

Patient 1 (pt.1, male, age 14, right handed) had complex partial seizures (CPS) since age of 4, seizure frequency of 6–20 per week, localized left temporal EEG seizure onset, severe bilateral temporal mental status, left temporal medio-basal dysgenesis on the MR. After the surgery, this patient remained seizure-free with highly recovered cognitive status (improved memory and social skills) at 9 months follow up. The electrode was placed in the posterior part of the hippocampal head with CA1, DG, hilus, CA3c trajectory

(Fig. 1A), where it crossed the principal cell layers close to perpendicular in the coronal plane.

Patient 2 (pt.2, male, age 46, right handed) had 8 years history of CPS, seizure frequency was 1 per week, EEG showed left fronto-temporal seizure onset, no significant MR findings. After the surgery, one seizure was detected at 6 months follow up. The electrode was placed in the hippocampal digitations, with CA1, CA1i (internal digitations) trajectory (Fig. 2A), in addition, intracortical recordings in T2 were also made before removing the temporal pole (Figs. 2C, E).

GluR2/3 is known to be present predominantly in principal cells of the human hippocampus (de Lanerolle et al., 1998). GluR2/3 immunocytochemistry and cresyl violet staining were used to identify the exact hippocampal regions containing the electrode track and the pattern of principal cell loss. Hippocampal regions were identified in coronal sections according to Duvernoy (1998) and Amaral and Insausti (1990).

### *Co-registration and verification*

Co-registration of the electrophysiological data with the anatomical structures was done on the 60- $\mu$ m-thick Nissl-stained sections showing the longest electrode track to minimize distortion stemming from the deviation of the trajectory and the cutting angle (Fig. 1A). Here we show the detailed procedure in pt.1 with CA1, DG, hilus trajectory. The measured tissue shrinkage was about 30%. The best section was digitized at high resolution with distance calibration and transferred into CorelDraw (Corel Inc., Dallas, TX), an accurate vector graphics software, to reconstruct the electrode tract and potential profile corresponding to the individual recording sites and epochs. Using the 30% shrinkage value, the readings from the micromanipulator and additional information from the height of the first penetration (tracked by the operating microscope), all the spatial positions of the recording epochs were marked on the digitized slide (Fig. 1A). We acquired separate files for each movement of the dME. Figs. 1B and 2B show the PG profile after the first 2-mm penetration into the hippocampus. The profiles are quite similar, which—together with the similar positions of the two CA1s derived from histology—suggests uniform initial insertion. The acquisition started before the movement, so we could compare the electrical activity before and after advancing the electrode. The result of the graphical co-registration procedure was then combined with the electrophysiology. Samples of single sweep electrical activity were displayed on the side of the graphical co-registration depicting all the channels in the corresponding depth of each recording site (as illustrated in Fig. 1).

On the basis of the graphical co-registration, in all of the patients, where the dME penetrated the DG ( $n = 6$ ), a typical sharply contoured oscillatory activity was observed on the electrode sites falling in the region of the DG. Depending on the penetrating angle and thickness of the granule cell layer

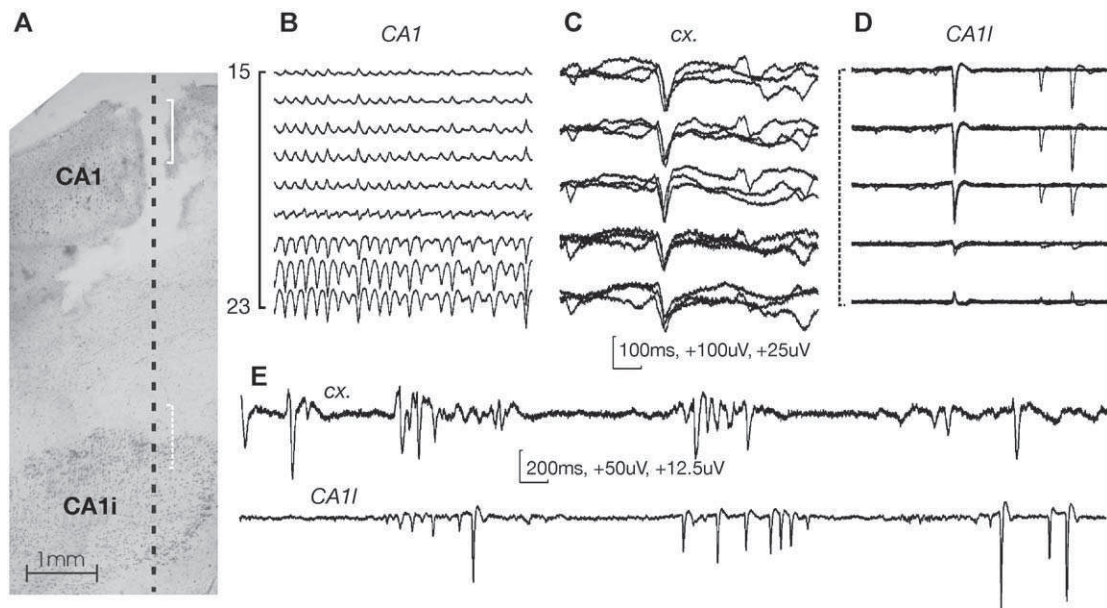


Fig. 2. (A) Reconstructive montage of pt.2. CA1 and CA1i in the hippocampal digitations. Nissl-stained, 60- $\mu$ m-thick section, calibration bar: 1 mm. Slightly oblique section, the track is only visible in CA1. Dashed line indicates the continuation of the penetration that crosses CA1i nearly parallel with the axis of the pyramidal cells. Solid bracket refers to the CA1, dashed bracket refers to the CA1i recording. (B) Injury potentials from CA1. Identical to Fig. 1B. Note that the inversion is nearly at the same channel as in Fig. 1B, the shape and frequency of the activity is quite similar too. Calibration: 100 ms, +100  $\mu$ V. (C) Interictal spikes collected before temporal pole resection from the middle temporal gyrus (T2). Recordings from layers II to III, three representative single sweeps are superimposed. The tMEs were implanted for 10 min to record temporal cortex spikes, to test if hippocampal activity after pole resection has common patterns with T2. Calibration: 100 ms, +25  $\mu$ V. (D) Interictal spikes from CA1i. Representative traces recorded close to the sp. Three sweeps superimposed. The spike latency is shorter than in T2, and the morphology of the separate spikes has much less variation, than in T2. Every second channel is shown. Calibration: 100 ms, +100  $\mu$ V. (E) Long time scale plots of T2 (upper trace) and CA1i (lower trace) activity. Similar timing of single spikes and polyspike trains in T2 and CA1i suggesting common generator mechanisms; however, the intracortical activity is slower and shows larger variation, suggesting cortical network modulation of epileptic discharges. Calibration: 100 ms, +50  $\mu$ V for the CA1i; 100 ms, +12.5  $\mu$ V for the cortex.

(stratum granulosum: sg.), an abrupt potential inversion (Figs. 1C, D) and a highly localized spatial MUA profile (Fig. 1E) was apparent. This way, sg. served as a natural landmark allowing us to verify the graphical co-registration. Granule cells are known to generate oscillatory synaptic and spiking activity in the rat under epileptogenic conditions (Cohen et al., 2003; Kobayashi and Buckmaster, 2003; Towers et al., 2002). Earlier data indicated that the human DG can also produce this type of population discharge pattern (Williamson et al., 1995a,b). Because MUA is generated by the discharge of neurons surrounding the electrode contacts, it is most pronounced around the cell body layer, and decays rapidly with distance. Thus, comparing the depth of the maximal spiking activity with the location of the sg. would give us a good measure to verify the graphical co-registration procedure, because (i) the sg. of the human DG is easily identified in the Nissl-stained sections (Fig. 1A), (ii) it is quite thin (about 200  $\mu$ m) in contrast to the CA1 pyramidal layer (stratum pyramidale: sp.), and (iii) no other dense cell layer is located around it.

To test the relative movement of the dME in the tissue, we constructed the spatial amplitude profile of the spiking activity via averaging the ongoing MUA (Ulbert et al., 2001a,b) in a 1-min interval in two consecutive epochs, recorded 1 mm apart from each other (Fig. 1E) as indexed by the reading on the microdrive. As the dME moved 1 mm

downward, the MUA maximum shifted about 1 mm too. The PG inversion (compare Figs. 1C and D) showed a similar shift, providing additional evidence that the relative movement is accurate. The same measures were used to define absolute error of the co-registration process. While moving the dME by 6 mm, the maximal MUA fell within the sg. of the DG (Figs. 1A, E), indicating that our graphical co-registration procedure had less than 200  $\mu$ m error during total electrode movement, which is consistent with a  $\sim$ 4% gross localization error. The position of the potential inversion (zero zone) was concordant with the above findings (Figs. 1C, D), strengthening the accuracy of our localization procedure.

#### Stability of the recordings

Displacement of the ME against the tissue could stem from two sources. The first is the instability of the microdrive: it can slowly drift down because of the weight of the ME, preamplifier, and cabling. The second is the movement of the tissue: rebound from the initial deformation of the insertion. Because this kind of movement could be very small, it would be extremely hard to detect in an intraoperative setting, based only on physical distance measurements. Good physiological localization information can be drawn from the spatial pattern of the SUA. In vivo hippocampal recordings in rats with 25  $\mu$ m

intercontact spacing laminar electrodes (Henze et al., 2000) showed a rapidly changing spatial action potential profile of CA1 pyramidal cells. A 50- $\mu\text{m}$  displacement parallel with the axis of the pyramidal cell could reduce the action potential peak measured at a given site by as much as 40%. Here we measured the changes of the peak action potential amplitude of a CA1 (Figs. 2A and 3) presumably pyramidal cell during a 4-min recording session in pt.2. As seen in Fig. 3B, the peak decrement was less than 20%, which translates to an electrode shift smaller than 50  $\mu\text{m}$ .

#### *Injury-related potentials and effects of anesthesia*

In patients where CA1 pyramids were preserved in the vicinity of the electrode track ( $n = 2$ ), a characteristic fast and sharp oscillation occurred after the first penetration (compare Figs. 1A, B and 2A, B), which faded usually in 1 min. The frequency started at about 30–40 Hz and gradually decreased together with the peak amplitude, until it vanished. The DG ( $n = 6$ ) showed similar sharp oscillation (40–50 Hz), which was faster and larger during the first 1 min of recording immediately after penetrating the granule cell layer. The spatial PG and MUA distribution of this oscillation was the same before and after the frequency stabilized to 8–18 Hz (Figs. 1C, D), and this ongoing spatial distribution did not change for the rest of the recordings (more than 5 min), suggesting intrinsic rather than injury-related activity.

In two patients, subdural strip recordings were performed before the depth observations and in pt.2 we implanted a tME in the medial temporal gyrus (Fig. 2E upper trace, long time scale) before temporal pole resection, and before the

hippocampal recordings (Fig. 2E lower trace, long time scale). In all of these cases, frequent interictal spiking was apparent both in the cortex and the hippocampus, suggesting the preservation of active epileptic processes in these patients under anesthesia.

In pt.2, where both tME and dME were implanted (albeit not simultaneously), we measured the mean recurrence frequency of single interictal spikes for the hippocampus (hc.):  $1.3 \pm 0.4$  Hz and cortex (cx.):  $1 \pm 0.3$  Hz,  $n = 25$ , the mean latency between individual spikes in polyspike trains in hc.:  $89.2 \pm 25.5$  ms and cx.:  $116.8 \pm 48.1$  ms,  $n = 50$ , and mean onset to peak spike latency of hc.:  $9.73 \pm 1.7$  ms and cx.:  $19.6 \pm 3.9$  ms,  $n = 25$ , to characterize cortical (T2) and hippocampal activity. Interictal spikes were selected by the neurologist with a custom Matlab (The MathWorks Inc., Natick, MA) code, based on peak detection. Polyspike trains were defined based on interspike interval criteria. If an initial spike was followed by at least one spike in less than 300 ms, it was regarded as a polyspike train. Onset to peak latency was defined as the time needed for the spike to reach from 10% to maximum peak amplitude, baseline was calculated from the 75- to 50-ms interval before the spike peak. Individual short time scale traces from cortex (supragranular layers) and hippocampus (CA1i) are presented in Figs. 2C and D. The similarity of their shape and temporal recurrence pattern (see also Fig. 2E) suggests, that these large field potential spikes reflect epileptic network activity, rather than injury-related potentials. It is also notable, that the single unit bursting activity showed close relationship with the field potential spikes in CA1i (Fig. 3D), 85% of the bursts happened on the descending part of the spikes, suggesting synaptic and cellular coupling in certain parts of the hippocampus.

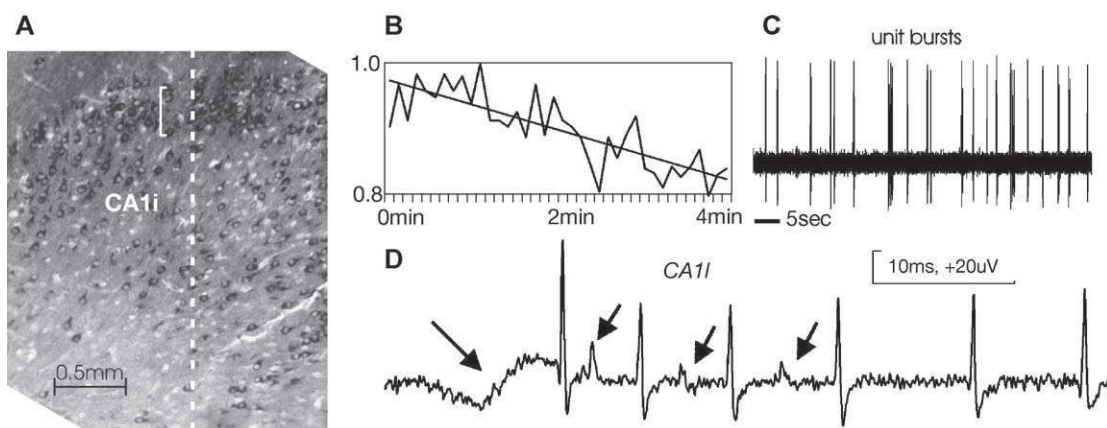


Fig. 3. (A) GluR2/3 stain of pt.2 CA1i region. Calibration bar: 500  $\mu\text{m}$ , white bracket shows the approximate location of the bursting putative pyramidal cell. Dashed white line indicates the electrode track, which was located approximately 250–300  $\mu\text{m}$  from this section. Note the dense cell body layer which is nearly perpendicular to the electrode trajectory. (B) Peak amplitude change of a bursting unit. Normalized peak amplitude of the first firing of a burst is plotted against recording time. The figure indicates less than 20% change during the 4-min interval. (C) Unit recordings from CA1i. This figure shows the stability of the unit recordings with very good signal-to-noise ratio. (D) Burst discharges. One putative pyramidal neuron (corresponds to the location marked with the white bracket in A) exhibits prolonged bursting (5–10 spikes at  $\sim 150$ –100 Hz) at the descending part of the large field potential spike. Raw waveform, note that positivity is up, since we used differential recording (PG). Long arrow points on the preceding interictal spike peak. Small arrows point to the interdigitating firing of another neuron. This pattern was observed very frequently during the recording. Calibration: 10 ms, +20  $\mu\text{V}$ .

## Discussion

A depth laminar multielectrode system and surgical positioning device have been developed, optimized for intraoperative electrophysiological observations, and combined with histology/reconstruction techniques for co-registration with the hippocampal micro-anatomy. The spatial stability, accuracy of the recording apparatus, and co-registration of functional and morphological data were tested and verified successfully.

Despite of the ongoing debate on acute monitoring during epilepsy surgery (Tran et al., 1995), intraoperative ECoG and/or direct hippocampal recordings are used, to localize epileptic network activity, and to tailor focus resection (Alarcon et al., 1997; McKhann et al., 2000; Polkey et al., 1989). These studies were conducted under general anesthesia, in an acute setting, similar to our observations, and their results confirmed that intraoperative ECoG and/or hippocampal recordings can be useful diagnostic tools in certain cases. In our opinion, outcome and long-term follow up could serve, at least as a partial substitute for the direct electrophysiological control, though we do not have direct evidences that some effect of injury can be ruled out. Nitrous oxide does not modify interictal spiking during intraoperative ECoG (Hosain et al., 1997), fentanyl (and its derivatives) is rather a specific agent to assist focus localization during surgery (Manninen et al., 1999; McGuire et al., 2003), while propofol showed no sign of intrinsic epileptogenicity in a sleep study (Leijten et al., 2001), its effect on intraoperative spiking was significant, but did not interfere with the ECoG interpretation (Herrick et al., 1997). Though it was not explicitly tested in here, it is feasible, that the anesthesia used, had no major nonspecific epileptogenic effect. Also the outcomes of the surgeries were favorable, suggesting that the structures examined (and then resected) might have been involved in the network, generating paroxysmal events.

During the experiments we experienced no bleeding or other complications, and no post-surgery neurological deficits of any kind occurred due to the electrode implantations. We have found several different patterns of hippocampal activation, such as pyramidal cell bursting, large field potential spikes originating in CA1, and rhythmic activity both in the DG and CA1.

Cellular bursting in the epileptic hippocampus was observed in vivo during waking, slow wave, and paradoxical sleep (Colder et al., 1996; Ravagnati et al., 1979; Staba et al., 2002b). Here we demonstrated that CA1i pyramidal bursting activity can be detected under anesthesia (Fig. 3).

We could identify hippocampal locations with about  $\pm 100 \mu\text{m}$  error, which exceeds the MRI localization accuracy. This allowed us to determine the anatomical structure, where the bursting cell was located (CA1i in this case). Because immunohistochemistry reveals the fine structure of the surrounding tissue, including the degree of cell loss and

reorganization, this technique puts the electrophysiological information into a structural context.

Large field potential spikes occur in the subiculum (Cohen et al., 2002), and other regions of the limbic system (Babb et al., 1987; Wyler et al., 1982). Here we demonstrated, for the first time, similar activity in the histologically identified human CA1i under anesthesia. The CA1i spike waveforms (Figs. 2D, E) from our experiments are quite similar to the in vitro subicular ones suggesting similar mechanisms underlying the epileptic discharges. Intracortical recordings from T2 before temporal pole resection revealed similar temporal spiking patterns and spike morphology as recorded from the CA1i after temporal pole resection in pt.2 (Fig. 2E). This result is in accordance with the findings of Cohen et al. (2002), implicating functional connections between the CA1-subicular region and lateral temporal structures.

In addition, the nonsclerotic CA1 produced transient injury-related potentials, which were remarkably similar among patients, suggesting homologous generator mechanisms and elevated CA1 excitability. Though this rhythmic pattern faded rapidly, its underlying mechanisms could participate in the epileptic network activity.

In TLE, the main mass of the DG is preserved (Margerison and Corsellis, 1966). DG cells contribute to epileptic reorganization via mossy fiber sprouting (Sutula et al., 1989). Various findings indicate that the DG is heavily involved in the generation and maintenance of paroxysmal activity in TLE, because of the reorganization/imbalance of its inhibitory and/or excitatory circuits (Isokawa-Akesson et al., 1989; Magloczky et al., 2000; Prince and Jacobs, 1998; Williamson et al., 1995b, 1999; Wittner et al., 2001). Until now, no in vivo electrophysiological recordings were obtained from anatomically identified laminae of the human DG. We have found sharp, rhythmic field potential oscillations and elevated cellular spiking activity originating in the DG under anesthesia. The spatial extent of the PG activity was confined to a 500- to 600- $\mu\text{m}$ -wide region coinciding with the DG, while the MUA fell even more rapidly in space, allowing us to define the granule cell layer as an electrophysiological landmark in most of the patients implanted (Fig. 1). Whether this oscillatory DG activity in humans reflects its normal gating mechanism, or it is a consequence of build-up of recurrent excitation caused by mossy fiber sprouting (Buckmaster et al., 2002), cannot be answered solely from these observations, mostly because the dimensions of the electrode did not allow us to record from other structures simultaneously to test their interactions. Given the large size of the human hippocampus, if we want to record—for example—from CA1 and DG simultaneously, either we have to increase the intercontact spacing or use two or more dMEs. To further examine the effect of anesthesia and injury, the authors are planning to design new electrodes, which are suitable to record chronically from the implanted, awake patients.

These observations indicate that there is a high degree of preserved hippocampal and temporal cortex activity in anesthetized humans with TLE. Large-scale network connections might also be in operation under these conditions, allowing the experimenter to investigate the medial and lateral temporal lobe interactions. Similarity of local electrophysiological patterns across patients in CA1 and also in DG further strengthens our conclusion that intraoperative observations of electrical activity patterns, together with appropriate post hoc identification of the precise anatomical sites of their origin, could further enhance our knowledge about the differential and specific involvement of hippocampal subfields in TLE.

### Acknowledgments

This work was supported in part by: EUM (ETT442-04), OTKA (T032251), NIH (NS18741, NS44623), NIH (MH54671), and the Howard Hughes Medical Institute. We thank Dr. György Kollár and Dr. András Fogarasi for their neurological support and László Papp for his technical support.

### References

- Alarcon, G., Garcia Seoane, J.J., Binnie, C.D., Martin Miguel, M.C., Juler, J., Polkey, C.E., Elwes, R.D., Ortiz Blasco, J.M., 1997. Origin and propagation of interictal discharges in the acute electrocorticogram. Implications for pathophysiology and surgical treatment of temporal lobe epilepsy. *Brain* 120 (Pt 12), 2259–2282.
- Amaral, D.G., Insausti, R., 1990. *Hippocampal Formation*. Academic Press, New York.
- Babb, T.L., Carr, E., Crandall, P.H., 1973. Analysis of extracellular firing patterns of deep temporal lobe structures in man. *Electroencephalogr. Clin. Neurophysiol.* 34, 247–257.
- Babb, T.L., Wilson, C.L., Isokawa-Akesson, M., 1987. Firing patterns of human limbic neurons during stereoencephalography (SEEG) and clinical temporal lobe seizures. *Electroencephalogr. Clin. Neurophysiol.* 66, 467–482.
- Barna, J.S., Arezzo, J.C., Vaughan Jr., H.G., 1981. A new multielectrode array for the simultaneous recording of field potentials and unit activity. *Electroencephalogr. Clin. Neurophysiol.* 52, 494–496.
- Bodizs, R., Kantor, S., Szabo, G., Szucs, A., Eross, L., Halasz, P., 2001. Rhythmic hippocampal slow oscillation characterizes REM sleep in humans. *Hippocampus* 11, 747–753.
- Bragin, A., Csicsvari, J., Penttonen, M., Buzsaki, G., 1997. Epileptic after-discharge in the hippocampal–entorhinal system: current source density and unit studies. *Neuroscience* 76, 1187–1203.
- Bragin, A., Hetke, J., Wilson, C.L., Anderson, D.J., Engel Jr., J., Buzsaki, G., 2000. Multiple site silicon-based probes for chronic recordings in freely moving rats: implantation, recording and histological verification. *J. Neurosci. Methods* 98, 77–82.
- Bragin, A., Wilson, C.L., Engel Jr., J., 2002a. Rate of interictal events and spontaneous seizures in epileptic rats after electrical stimulation of hippocampus and its afferents. *Epilepsia* 43 (Suppl. 5), 81–85.
- Bragin, A., Wilson, C.L., Staba, R.J., Reddick, M., Fried, I., Engel Jr., J., 2002b. Interictal high-frequency oscillations (80–500 Hz) in the human epileptic brain: entorhinal cortex. *Ann. Neurol.* 52, 407–415.
- Buckmaster, P.S., Zhang, G.F., Yamawaki, R., 2002. Axon sprouting in a model of temporal lobe epilepsy creates a predominantly excitatory feedback circuit. *J. Neurosci.* 22, 6650–6658.
- Buzsaki, G., Czopf, J., Kondakor, I., Kellenyi, L., 1986. Laminar distribution of hippocampal rhythmic slow activity (RSA) in the behaving rat: current-source density analysis, effects of urethane and atropine. *Brain Res.* 365, 125–137.
- Caplan, J.B., Madsen, J.R., Schulze-Bonhage, A., Aschenbrenner-Scheibe, R., Newman, E.L., Kahana, M.J., 2003. Human theta oscillations related to sensorimotor integration and spatial learning. *J. Neurosci.* 23, 4726–4736.
- Cohen, I., Navarro, V., Clemenceau, S., Baulac, M., Miles, R., 2002. On the origin of interictal activity in human temporal lobe epilepsy in vitro. *Science* 298, 1418–1421.
- Cohen, A.S., Lin, D.D., Quirk, G.L., Coulter, D.A., 2003. Dentate granule cell GABA(A) receptors in epileptic hippocampus: enhanced synaptic efficacy and altered pharmacology. *Eur. J. Neurosci.* 17, 1607–1616.
- Colder, B.W., Wilson, C.L., Frysinger, R.C., Chao, L.C., Harper, R.M., Engel Jr., J., 1996. Neuronal synchrony in relation to burst discharge in epileptic human temporal lobes. *J. Neurophysiol.* 75, 2496–2508.
- Csicsvari, J., Jamieson, B., Wise, K.D., Buzsaki, G., 2003. Mechanisms of gamma oscillations in the hippocampus of the behaving rat. *Neuron* 37, 311–322.
- de Lanerolle, N.C., Eid, T., von Campe, G., Kovacs, I., Spencer, D.D., Brines, M., 1998. Glutamate receptor subunits GluR1 and GluR2/3 distribution shows reorganization in the human epileptogenic hippocampus. *Eur. J. Neurosci.* 10, 1687–1703.
- Duvernoy, H.M., 1998. *The Human Hippocampus*. Springer-Verlag, Berlin.
- Freeman, J.A., Nicholson, C., 1975. Experimental optimization of current source-density technique for anuran cerebellum. *J. Neurophysiol.* 38, 369–382.
- Halgren, E., 1991. Firing of human hippocampal units in relation to voluntary movements. *Hippocampus* 1, 153–161.
- Halgren, E., Babb, T.L., Crandall, P.H., 1978. Activity of human hippocampal formation and amygdala neurons during memory testing. *Electroencephalogr. Clin. Neurophysiol.* 45, 585–601.
- Henze, D.A., Borhegyi, Z., Csicsvari, J., Mamiya, A., Harris, K.D., Buzsaki, G., 2000. Intracellular features predicted by extracellular recordings in the hippocampus in vivo. *J. Neurophysiol.* 84, 390–400.
- Herrick, I.A., Craen, R.A., Gelb, A.W., McLachlan, R.S., Girvin, J.P., Parrent, A.G., Eliasziw, M., Kirkby, J., 1997. Propofol sedation during awake craniotomy for seizures: electrocorticographic and epileptogenic effects. *Anesth. Analg.* 84, 1280–1284.
- Hosain, S., Nagarajan, L., Fraser, R., Van Poznak, A., Labar, D., 1997. Effects of nitrous oxide on electrocorticography during epilepsy surgery. *Electroencephalogr. Clin. Neurophysiol.* 102, 340–342.
- Isokawa-Akesson, M., Wilson, C.L., Babb, T.L., 1989. Inhibition in synchronously firing human hippocampal neurons. *Epilepsy Res.* 3, 236–247.
- Kahana, M.J., Seelig, D., Madsen, J.R., 2001. Theta returns. *Curr. Opin. Neurobiol.* 11, 739–744.
- Kobayashi, M., Buckmaster, P.S., 2003. Reduced inhibition of dentate granule cells in a model of temporal lobe epilepsy. *J. Neurosci.* 23, 2440–2452.
- Leijten, F.S., Teunissen, N.W., Wieneke, G.H., Knape, J.T., Schobben, A.F., van Huffelen, A.C., 2001. Activation of interictal spiking in mesiotemporal lobe epilepsy by propofol-induced sleep. *J. Clin. Neurophysiol.* 18, 291–298.
- Lim, C., Blume, H.W., Madsen, J.R., Saper, C.B., 1997a. Connections of the hippocampal formation in humans: I. The mossy fiber pathway. *J. Comp. Neurol.* 385, 325–351.
- Lim, C., Mufson, E.J., Kordower, J.H., Blume, H.W., Madsen, J.R., Saper, C.B., 1997b. Connections of the hippocampal formation in humans: II. The endfolial fiber pathway. *J. Comp. Neurol.* 385, 352–371.
- Magloczky, Z., Wittner, L., Borhegyi, Z., Halasz, P., Vajda, J., Czizjak, S., Freund, T.F., 2000. Changes in the distribution and connectivity of interneurons in the epileptic human dentate gyrus. *Neuroscience* 96, 7–25.

- Manninen, P.H., Burke, S.J., Wennberg, R., Lozano, A.M., El Beheiry, H., 1999. Intraoperative localization of an epileptogenic focus with alfentanil and fentanyl. *Anesth. Analg.* 88, 1101–1106.
- Margerison, J.H., Corsellis, J.A., 1966. Epilepsy and the temporal lobes. A clinical, electroencephalographic and neuropathological study of the brain in epilepsy, with particular reference to the temporal lobes. *Brain* 89, 499–530.
- McGuire, G., El-Beheiry, H., Manninen, P., Lozano, A., Wennberg, R., 2003. Activation of electrocorticographic activity with remifentanyl and alfentanil during neurosurgical excision of epileptogenic focus. *Br. J. Anaesth.* 91, 651–655.
- McKhann II, G.M., Schoenfeld-McNeill, J., Born, D.E., Haglund, M.M., Ojemann, G.A., 2000. Intraoperative hippocampal electrocorticography to predict the extent of hippocampal resection in temporal lobe epilepsy surgery. *J. Neurosurg.* 93, 44–52.
- Mehta, A.D., Ulbert, I., Schroeder, C.E., 2000a. Intermodal selective attention in monkeys. I: Distribution and timing of effects across visual areas. *Cereb. Cortex* 10, 343–358.
- Mehta, A.D., Ulbert, I., Schroeder, C.E., 2000b. Intermodal selective attention in monkeys. II: Physiological mechanisms of modulation. *Cereb. Cortex* 10, 359–370.
- Nicholson, C., Freeman, J.A., 1975. Theory of current source-density analysis and determination of conductivity tensor for anuran cerebellum. *J. Neurophysiol.* 38, 356–368.
- O'Keefe, J., Burgess, N., 1999. Theta activity, virtual navigation and the human hippocampus. *Trends Cogn. Sci.* 3, 403–406.
- Polkey, C.E., Binnie, C.D., Janota, I., 1989. Acute hippocampal recording and pathology at temporal lobe resection and amygdalo-hippocampectomy for epilepsy. *J. Neurol. Neurosurg. Psychiatry* 52, 1050–1057.
- Prince, D.A., Jacobs, K., 1998. Inhibitory function in two models of chronic epileptogenesis. *Epilepsy Res.* 32, 83–92.
- Ravagnati, L., Halgren, E., Babb, T.L., Crandall, P.H., 1979. Activity of human hippocampal formation and amygdala neurons during sleep. *Sleep* 2, 161–173.
- Staba, R.J., Wilson, C.L., Bragin, A., Fried, I., Engel Jr., J., 2002a. Quantitative analysis of high-frequency oscillations (80–500 Hz) recorded in human epileptic hippocampus and entorhinal cortex. *J. Neurophysiol.* 88, 1743–1752.
- Staba, R.J., Wilson, C.L., Fried, I., Engel Jr., J., 2002b. Single neuron burst firing in the human hippocampus during sleep. *Hippocampus* 12, 724–734.
- Sutula, T., Cascino, G., Cavazos, J., Parada, I., Ramirez, L., 1989. Mossy fiber synaptic reorganization in the epileptic human temporal lobe. *Ann. Neurol.* 26, 321–330.
- Towers, S.K., LeBeau, F.E., Gloveli, T., Traub, R.D., Whittington, M.A., Buhl, E.H., 2002. Fast network oscillations in the rat dentate gyrus in vitro. *J. Neurophysiol.* 87, 1165–1168.
- Tran, T.A., Spencer, S.S., Marks, D., Javidan, M., Pacia, S., Spencer, D.D., 1995. Significance of spikes recorded on electrocorticography in non-lesional medial temporal lobe epilepsy. *Ann. Neurol.* 38, 763–770.
- Ulbert, I., Halgren, E., Heit, G., Karmos, G., 2001a. Multiple microelectrode-recording system for human intracortical applications. *J. Neurosci. Methods* 106, 69–79.
- Ulbert, I., Karmos, G., Heit, G., Halgren, E., 2001b. Early discrimination of coherent versus incoherent motion by multiunit and synaptic activity in human putative MT+. *Hum. Brain Mapp.* 13, 226–238.
- Williamson, A., Spencer, S.S., Spencer, D.D., 1995a. Depth electrode studies and intracellular dentate granule cell recordings in temporal lobe epilepsy. *Ann. Neurol.* 38, 778–787.
- Williamson, A., Telfeian, A.E., Spencer, D.D., 1995b. Prolonged GABA responses in dentate granule cells in slices isolated from patients with temporal lobe sclerosis. *J. Neurophysiol.* 74, 378–387.
- Williamson, A., Patrylo, P.R., Spencer, D.D., 1999. Decrease in inhibition in dentate granule cells from patients with medial temporal lobe epilepsy. *Ann. Neurol.* 45, 92–99.
- Wittner, L., Magloczky, Z., Borhegyi, Z., Halasz, P., Toth, S., Eross, L., Szabo, Z., Freund, T.F., 2001. Preservation of perisomatic inhibitory input of granule cells in the epileptic human dentate gyrus. *Neuroscience* 108, 587–600.
- Wyler, A.R., Ojemann, G.A., Ward Jr., A.A., 1982. Neurons in human epileptic cortex: correlation between unit and EEG activity. *Ann. Neurol.* 11, 301–308.

dc\_303\_11

## **8. Melléklet**

# Properties of *in vivo* interictal spike generation in the human subiculum

Dániel Fabó,<sup>1,2</sup> Zsófia Maglóczky,<sup>3</sup> Lucia Wittner,<sup>1</sup> Ágnes Pék,<sup>1</sup> Loránd Eröss,<sup>4</sup> Sándor Czirják,<sup>4</sup> János Vajda,<sup>4</sup> András Sólyom,<sup>4</sup> György Rásonyi,<sup>2</sup> Anna Szűcs,<sup>2</sup> Anna Kelemen,<sup>2</sup> Vera Juhos,<sup>5</sup> László Grand,<sup>1,7</sup> Balázs Dombóvári,<sup>1,7</sup> Péter Halász,<sup>2</sup> Tamás F. Freund,<sup>3</sup> Eric Halgren,<sup>6</sup> György Karmos<sup>1,7</sup> and István Ulbert<sup>1,7</sup>

<sup>1</sup>Institute for Psychology, Hungarian Academy of Sciences, <sup>2</sup>National Institute of Psychiatry and Neurology, Epilepsy Centre, <sup>3</sup>Institute of Experimental Medicine, Hungarian Academy of Sciences, <sup>4</sup>National Institute of Neurosurgery, <sup>5</sup>Szent István Hospital, Department of Neurology, Budapest, Hungary, <sup>6</sup>University of California, San Diego, Departments of Radiology, Neuroscience and Psychiatry, La Jolla, California, USA and <sup>7</sup>Pázmány Péter Catholic University, Department of Information Technology, Budapest, Hungary

Correspondence to: István Ulbert, Institute for Psychology, Hungarian Academy of Sciences, 1068 Budapest, Szondi u. 83-85, Hungary

E-mail: ulbert@cogpsyphy.hu

**A large proportion of hippocampal afferents and efferents are relayed through the subiculum. It is also thought to be a key structure in the generation and maintenance of epileptic activity; rhythmic interictal-like discharges were recorded in previous studies of subicular slices excised from temporal lobe epilepsy patients. In order to investigate if and how the subiculum is involved in the generation of epileptic discharges *in vivo*, subicular and lateral temporal lobe electrical activity were recorded under anesthesia in 11 drug-resistant epilepsy patients undergoing temporal lobectomy. Based on laminar field potential gradient, current source density, multiple unit activity (MUA) and spectral analyses, two types of interictal spikes were distinguished in the subiculum. The more frequently occurring spike started with an initial excitatory current (current source density sink) in the pyramidal cell layer associated with increased MUA in the same location, followed by later inhibitory currents (current source density source) and decreased MUA. In the other spike type, the initial excitation was confined to the apical dendritic region and it was associated with a less-prominent increase in MUA. Interictal spikes were highly synchronized at spatially distinct locations of the subiculum. Laminar data showed that the peak of the initial excitation occurred within 0–4 ms at subicular sites separated by 6 mm at the anterior–posterior axis. In addition, initial spike peak amplitudes were highly correlated in most recordings. A subset of subicular and temporal lobe spikes were also highly synchronous, in one case the subicular spikes reliably preceded the temporal lobe discharges. Our results indicate that multiple spike generator mechanisms exist in the human epileptic subiculum suggesting a complex network interplay between medial and lateral temporal structures during interictal epileptic activity. The observed widespread intra-subicular synchrony may reflect both of its intrinsic and extrinsically triggered activity supporting the hypothesis that subiculum may also play an active role in the distribution of epileptiform activity to other brain regions. Limited data suggest that subiculum might even play a pacemaker role in the generation of paroxysmal discharges.**

**Keywords:** epilepsy; hippocampus; current source density; multiple unit activity; laminar recording

**Abbreviations:** CSD = current source density; EC = entorhinal cortex; FPG = field potential gradient; MUA = multiple unit activity

Received September 21, 2007. Revised October 28, 2007. Accepted November 16, 2007. Advance Access publication December 14, 2007

## Introduction

Recently accumulating knowledge about the function and structure of the subiculum suggest its essential role in a

number of normal and pathological processes. Besides its task in the formation and retrieval of short-term memory (Gabrieli *et al.*, 1997; Hampson and Deadwyler, 2003) and

in the creation of cognitive maps (Sharp and Green, 1994), the subiculum is involved in Alzheimer's disease (Davies *et al.*, 1988), schizophrenia (Roberts and Greene, 2003) and temporal lobe epilepsy (Cohen *et al.*, 2002; Arellano *et al.*, 2004; Wozny *et al.*, 2005; Huberfeld *et al.*, 2007).

Animal studies show that the subiculum controls the input and output of the hippocampal formation by virtue of its position between the CA1 region and entorhinal cortex (EC) (Van Hoesen *et al.*, 1979; Witter and Groenewegen, 1990; Witter *et al.*, 1990; Naber and Witter, 1998; Naber *et al.*, 2001; Menendez de la Prida, 2006). The local connections of subicular pyramidal cells form a characteristic pattern, hypothesized to facilitate the appearance of internal recurrent network activity (Harris and Stewart, 2001; Harris *et al.*, 2001; Witter, 2006) that is under the control of local GABA-ergic inhibition (Seress *et al.*, 1993; Arellano *et al.*, 2004; Menendez de la Prida, 2006). The organization of both its extrinsic and intrinsic connections promotes multiple reentrant pathway formation, which might lead to synchronized reverberating circuits and under pathological conditions to epileptogenic plasticity (Kloosterman *et al.*, 2004; Knopp *et al.*, 2005).

Anatomical examination of human tissue derived from temporal lobe epilepsy patients has revealed varying levels of hippocampal size reduction and signs of tissue damage termed as hippocampal (or Ammon's horn) sclerosis (Corsellis, 1957). This damage features pathological alteration and reorganization of both excitatory and inhibitory circuits of the Ammon's horn (Cornu Ammonis) and the dentate gyrus manifesting in cell loss, axonal sprouting and gliosis (Sutula *et al.*, 1989; Babb, 1999; Wittner *et al.*, 2002, 2005; Magloczky and Freund, 2005). In contrast with the damaged Cornu Ammonis and dentate gyrus, the subiculum is relatively well preserved (Fisher *et al.*, 1998; Cavazos *et al.*, 2004). *In vitro* slice studies on excised human hippocampal tissue showed that spontaneous rhythmic synchronized network activity similar to interictal discharges is present in the subiculum, sometimes even in the absence of hippocampal sclerosis (Cohen *et al.*, 2002; Wozny *et al.*, 2003, 2005; Huberfeld *et al.*, 2007). Recurrence rate and certain morphological analogies between *in vitro* subicular events and *in vivo* interictal spikes suggested that they may represent similar epileptic processes (Cohen *et al.*, 2002; Wozny *et al.*, 2003).

Subicular discharges can result from intrinsic (local subicular origin), extrinsic (extra-subicular input) or mixed network mechanisms. In non-epileptic animals, intrinsic generation of spontaneous, rhythmic, spatially synchronized subicular (Wu *et al.*, 2005a, b, 2006) and hippocampal (Papatheodoropoulos and Kostopoulos, 2002; Kubota *et al.*, 2003; Maier *et al.*, 2003; Colgin *et al.*, 2004) *in vitro* activity resembling interictal spikes share a number of similarities with that of the epileptic human (Cohen *et al.*, 2002; Wozny *et al.*, 2003, 2005; Huberfeld *et al.*, 2007) *in vitro* studies, all using physiological incubation medium.

Subicular responses to hippocampal or cortical electrical stimulation also reproduce some basic features of subicular interictal spikes (Naber *et al.*, 1999; Gigg *et al.*, 2000; Naber *et al.*, 2001; Cappaert *et al.*, 2007). These spikes show differential laminar and cellular patterns (Behr *et al.*, 1998; Naber *et al.*, 1999; Gigg *et al.*, 2000; Naber *et al.*, 2001; Cappaert *et al.*, 2007) corresponding to known anatomical connections (Finch and Babb, 1981; Amaral *et al.*, 1991; Witter *et al.*, 2000; O'Mara, 2006; Witter, 2006).

While *in vitro* preparations have yielded valuable data on the epileptiform activity of the subiculum, there is a lack of microphysiological information concerning its *in vivo* behaviour in epileptic humans. In the present paper we investigate the electrophysiological events associated with interictal activity of the anatomically identified human subiculum and temporal lobe *in vivo* under general anaesthesia using laminar multielectrodes in patients with drug-resistant temporal lobe epilepsy. High spatial resolution laminar field potential gradient (FPG), multiple unit activity (MUA), current source density (CSD) from the subiculum and concurrently recorded temporal lobe electrocorticogram (ECoG) were analysed to elucidate the neuronal network mechanisms underlying interictal activity. The results suggest that multiple forms of interictal spike activity are generated in the subiculum, some of which may be projected to lateral temporal areas.

## Methods

### Surgery and recording

Eleven temporal lobe epilepsy patients undergoing standard anterior temporal lobectomy were included in this study. Intraoperative recordings were made under general anaesthesia (Propofol and N<sub>2</sub>O or Isofluran and N<sub>2</sub>O). All of the patients underwent MR imaging and video-EEG monitoring before the operation for localizing their seizure onset zone and diagnosed as having unilateral mesial temporal lobe seizure onset. Informed consent was obtained from the patients under the auspices of the local ethical committee according to the Declaration of Helsinki. For intrahippocampal recordings, one or two laminar multielectrodes were used. Each 10 cm long, 350 µm shaft diameter multielectrode had twenty-four 25 µm diameter Pt/Ir recording contacts separated by 100 µm (two cases) or 200 µm (nine cases). The multielectrode was mounted on a hydraulic micromanipulator together with the attached high impedance preamplifiers. In the case of dual laminar recordings, the electrodes were mounted in parallel, about 6 mm apart. All the equipment going into the surgical field was sterilized in ethylene-oxide. The manipulator with the mounted multielectrodes and preamplifiers was attached to a medical instrument holder, which allowed the surgeon to aim towards the hippocampus under visual control using an operating microscope. In order to conserve medial-lateral temporal pathways, the lateral ventricle was opened from a small incision involving the deep aspect of the superior temporal sulcus to reveal the head and body of the hippocampus. Under visual control, the multielectrode tip was positioned onto the ependymal surface of the hippocampus through the incision. After the initial positioning, the electrodes were advanced into the tissue

with 2–4 mm increments using the hydraulic manipulator. At each step, the signal was recorded for 3–8 min continuously. One or two penetrations were made reaching the proximal and distal (with respect to CA1) or anterior and posterior part of the subiculum. Spatial FPG, the first spatial derivative of the local field potentials was digitized and stored (24 or 48 channels of data, depending on single or dual multielectrode recording) both in the low-frequency band (pass band: 0.1–300 Hz, each channel sampled at 2 kHz with 16-bit resolution) and in high-frequency band (150–5000 Hz, each channel sampled at 20 kHz with 12-bit resolution) simultaneously for off-line analysis. Details about the multielectrode, amplifier and recording system were published previously (Ulbert *et al.*, 2001, 2004a, b). In addition to laminar multielectrode implantation, in two cases an 8-contact clinical strip electrode (Ad-Tech Medical Instrument Corporation, Racine, USA) was positioned over the temporo-basal cortical areas going around the pole of the temporal lobe. Based on the angle and visual inspection of the strip, it reached the temporo-polar (Brodmann, Br. 38), perirhinal (Br. 35–36) and inferotemporal (Br. 20) areas, but not the entorhinal (Br. 28) area. ECoG was filtered (0.1–1000 Hz), digitized at 5 kHz with 16-bit resolution and stored for off-line analysis (Brainvision Recorder, Brain Products GmbH, Gilching, Germany). Laminar and strip recordings were co-registered using a common trigger channel.

### Histology

At the end of the session, the multielectrodes were pulled out, and the hippocampus was resected *en bloc*. The neurosurgeon and the histologist confirmed and registered the region and angle of the electrode insertion based on the surface vascularization of the hippocampus. Digital photographs were taken of the removed tissue, and then it was cut into smaller, 4–5 mm thick blocks in the operating room, parallel with the suspected electrode trajectory. Additional photographs were taken of the blocks, they were measured to allow subsequent estimation of shrinkage, and then immersed separately into fixative containing 4% paraformaldehyde, 0.05% glutaraldehyde and 0.2% picric acid in 0.1 M phosphate buffer (PB, pH 7.4), as described earlier (Magloczky *et al.*, 1997). The fixative was changed every hour to a fresh solution during constant agitation for 6 h, and then the blocks were post-fixed in the same fixative overnight. Vibratome sections (60 µm thick) were cut from the blocks, and photographs were taken from the electrode tracks (Fig. 1B). Following washing in PB, sections were immersed in 30% saccharose for 1–2 days then frozen three times over liquid nitrogen. Sections containing the electrode track were either stained with cresyl violet, or processed for immunostaining against glutamate receptor subunit 2 and 3 (GluR2/3), as follows. Sections were transferred to Tris-buffered saline (TBS, pH 7.4), then endogenous peroxidase was blocked by 1% H<sub>2</sub>O<sub>2</sub> in TBS for 10 min. TBS was used for all the washes (3 × 3–10 min between each step) and dilution of the antisera. Non-specific immunostaining was blocked by 5% milk powder and 2% bovine serum albumin. A polyclonal rabbit antibody against GluR2/3 (1:100, Chemicon, Temecula) was used for 2 days at 4°C. The specificity of the antibody has been thoroughly tested by the manufacturer. For visualization of immunopositive elements, biotinylated anti-rabbit immunoglobulin G (1:300, Vector) was applied as secondary antiserum followed by avidin-biotinylated horseradish peroxidase complex (ABC; 1:300, Vector). The immunoperoxidase reaction was developed

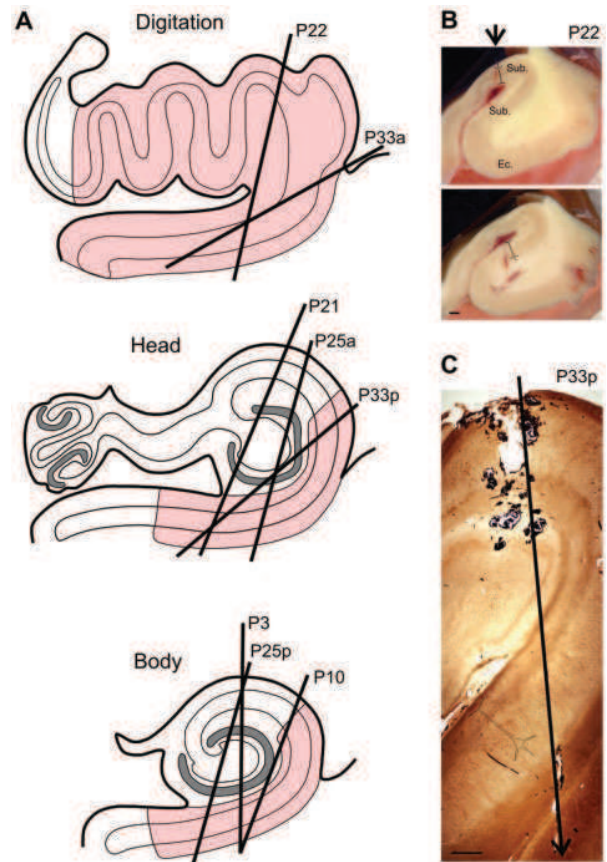


**Fig. 1** (A) Schematic drawings showing the location of the electrodes for the six patients included in the detailed analysis (P3, P10, P21, P22, P25 and P33). In two of these cases we inserted two electrodes, 6 mm apart from each other. The anterior traces are marked with *a*, while the posterior traces are marked with *p*. The subiculum is indicated with pink colour, modified from Duvernoy (Duvernoy, 1998) (B) Photographs showing the electrode track in patient 22 (arrow), taken during sectioning of the resected block. The exact location of the electrode was determined after light microscopic examination. Ec.: entorhinal cortex. Schematic neuron illustrates principal cell orientation and approximate location of the pyramidal and apical dendritic layer. (C) Light micrograph of a GluR2/3-immunostained section containing the posterior electrode track (arrow) in patient 33. A bleeding (black patches in the proximal subiculum) occurred after the removal of the electrode. Scale bars: 1 mm.

by 3,3'-diaminobenzidine tetrahydrochloride (DAB; Sigma) dissolved in Tris buffer (TB, pH 7.6) as a chromogen. Sections were then osmicated (1% OsO<sub>4</sub> in PB, 40 min) and dehydrated in ethanol (1% uranyl acetate was added at the 70% ethanol stage for 40 min) and mounted in Durcupan (ACM, Fluka).

The location of the electrode tracks were defined based on light microscopic examination. Only cases were included in this study, where the electrode passed through the subicular complex (including the subiculum, pre- and prosubiculum). In the cases without hippocampal sclerosis, the border between the CA1 region and the subiculum was determined by the increased extension of the pyramidal cell layer, with two sublaminae (Amaral and Insausti, 1990). In the sclerotic cases, the CA1-subiculum border

was determined by the absence or presence of pyramidal cells, respectively. The entorhinal cortex was distinguished based on the presence of six cortical layers (including lamina dissecans) and islands of modified pyramidal cells in layer II (Amaral and Insausti, 1990). More details about the anatomy-electrophysiology co-registration were published earlier (Ulbert *et al.*, 2004b).

### Data analysis

The second spatial derivative of the field potentials approximates the depth distribution of the extracellular sources and sinks of currents in laminated structures expressed in current source density units. Since we recorded the spatial gradient of the field potential, the CSD calculation involved only one spatial derivation of the FPG. Inhomogeneous conductivity and electrode distance were not taken into account. Hamming-window spatial smoothing, additional 0.1–100 Hz band pass filtering (zero phase shift, 12 dB/oct) and baseline correction (–500 to –100 ms) were applied if needed on the low-frequency band data. As shown on Fig. 1B and C, the directions of the penetrations were usually equal to or less than 30° compared to the perpendicular axis. Assuming a penetration angle of 30°, a pyramidal layer thickness of 2 mm, and an intra-subicular conduction velocity of 1.5 m/s (the lowest estimated value, see results), then linear estimation yields an expected timing error compared to the perpendicular insertion of about 0.75 ms between two contacts separated by 2 mm, and 0.075 ms between adjacent contacts. This would result in the steepest part of the CSD (initial sink) changing by an about 5–10% compared to its entire swing during the estimated timing error. Based on the above assumptions we expect an approximately 0.75 ms timing error and about 5–10% amplitude inaccuracy in our oblique recordings between sites separated by 2 mm and negligible errors at adjacent contacts.

A continuous estimate of the multiple unit activity was derived by additional band pass filtering (zero phase shift, 500–5000 Hz, 48 dB/oct), full wave rectifying and finally low pass filtering (zero phase shift, 100 Hz, 12 dB/oct) of the high-frequency band data. NeuroScan (Compumedics, El Paso, TX, USA) and home written MatLab (MathWorks, Natick, MA, USA) tools were used for data analysis. Details about CSD and MUA calculations were published earlier (Ulbert *et al.*, 2001, 2004a).

Subicular spikes were detected using amplitude criteria based on the polarity of FPG and CSD traces and their relationship to the local anatomy. An event was detected if the amplitude of the FPG exceeded the 2 standard deviation (SD) threshold calculated from a spike-free period. The earliest sharp CSD peak in the pyramidal layer was designated as time zero for further event triggered averaging. FPG is presented on line plots with positive deflections upwards, CSD data is presented on line plots and depth versus time maps, with colour-coded sink (red, negative values) and source (blue, positive values) amplitudes. MUA averages are presented on colour-coded depth versus time maps. Warm colours (red) depict MUA increase, cold colours (blue) depict MUA decrease compared to the pre-spike baseline period (–500 to –100 ms). *T*-test was used for CSD and MUA to reveal significant ( $P < 0.01$ ) alterations compared to baseline activity and between event comparison ( $P < 0.01$ ). For ECoG spike detection the 2 SD threshold criterion was used, time zero was defined by the earliest peak after threshold crossing. Expert neurologists classified ECoG events as interictal spikes when they had a short (<50 ms) initial peak width with a following slow wave (Gotman, 1980).

We also assessed the temporal synchrony and amplitude relationship of spikes recorded from two spatially distinct parts of the subiculum ( $n = 3$ ) either on the same or on different electrodes. Temporal synchrony was expressed in percent; the number of coinciding FPG spikes within a  $\pm 10$  ms window was divided by the total number of spikes. The correlation of peak FPG amplitudes between two spatially distinct subicular spikes and its significance was calculated using linear regression model.

Spectro-temporal analysis was performed using wavelet-based methods modified from EEGLAB (Delorme and Makeig, 2004). Spectral content of the spikes was calculated from single sweeps (FPG) followed by averaging of the individual time–frequency measures. Dividing the resultant values with the baseline (–500 to –100 ms) activation in each frequency band gives the relative change of spectral activity in time termed as the individual trial event-related spectral perturbation (iERSP) expressed in dB. Statistical significance (bootstrap,  $P < 0.01$ ) of the iERSP against baseline was assessed using bootstrap analysis (Delorme and Makeig, 2004). Significant spectral activity increase and decrease is marked with warm (red) and cold (blue) colours, respectively, while non-significant values are shaded green. A non-parametric statistical test (Kruskal–Wallis ANOVA) was used to compare iERSP of different spike types with a  $P < 0.05$  significance level.

### Results

We recorded subicular laminar electrical activity from 11 patients in 13 multielectrode penetrations under general anaesthesia. Hippocampus was removed *en bloc* after the implantation, containing the electrode track. In seven cases we found direct histological evidence that the electrodes reached the target and recorded subicular activity. In four cases the subiculum was damaged and lost during the removal. In the remaining four cases, reconstructions by expert morphologist based on the remnant tissue and the general anatomy revealed that it is highly likely that the electrodes also reached the target and recorded subicular activity. All available tissue was analysed with respect to cell loss and reorganization in the CA1 and subiculum with immunohistochemical methods (Wittner *et al.*, 2005). In seven patients we observed severe cell loss in the CA1 region (severe hippocampal sclerosis, sHS); in four patients relatively mild cell loss was detected (mild hippocampal sclerosis, mHS, see Table 1). Subicular structure was well preserved and it appeared to be control-like in all but two cases. P4 showed patchy cell loss close to the electrode track, while in P25, one discrete patch of cell loss was detected at the border of the subiculum and CA1, remote from the electrode location (Table 1).

Nine out of the eleven patients ( $n = 6$  with sHS,  $n = 3$  with mHS) showed at least one spike exceeding the  $\pm 2$  SD threshold for spike detection in the subiculum during the entire recording session (10–25 min). Overall spike frequency in six (P3, P10, P21, P22, P25 and P33) patients ( $n = 4$  with sHS,  $n = 2$  with mHS) exceeded the 1 spike/min value and yielded enough events to permit detailed analysis of their FPG, CSD, MUA and spectra. In five of the six patients the complete histology of the electrode track was

**Table 1** Summary of patient characteristics

Patient	Included in detailed analysis	Age (years)	Impl. side	Gender	Duration of epilepsy (years)	MRI finding	Hippocampal damage	Subiculum damage	Elec. 1 loc.	Elec. 2 loc.	Anesthesia
P3	Yes	47	Left	F	36	Bilateral HS	sHS	c-l.	Body	NA	Propofol
P4	No	35	Left	F	30	Left HS	sHS	Patchy	Head	NA	Isoflurane
PI0	Yes	24	Left	F	20	Left HS	sHS	c-l.	Body	Body	Propofol
PI7	No	31	Right	M	22	Right HS	sHS	c-l.	Body	Head	Isoflurane
P20	No	56	Left	F	7	Tumour (left temporo-polar)	mHS	c-l.	Body	Digit.	Propofol
P21	Yes	26	Right	F	7	Right HS	mHS	c-l.	Body	Body	Propofol
P22	Yes	46	Left	F	10	Bilateral HS	sHS	c-l.	Head	Digit.	Propofol
P25	Yes	36	Left	F	6	Left HS	sHS	One patch	Body*	Head*	Propofol
P26	No	40	Right	F	26	Bilateral HS	sHS	c-l.	Body	Body	Isoflurane
P30	No	40	Right	F	15	Tumour (right temporo-lateral)	mHS	c-l.	Head	Head	Propofol
P33	Yes	51	Left	F	32	Tumour (left amygdala)	mHS	c-l.	Head*	Head*	Propofol

Impl. Side = implantation and resection side; F = female; M = male; HS = hippocampal sclerosis; sHS = severe cell loss and reorganization of hippocampus (severe hippocampal sclerosis); mHS = mild cell loss and reorganization of hippocampus (mild hippocampal sclerosis); c-l. = control-like; Elec. loc. = electrode location; digit. = hippocampal digitations; according to (Duvernoy, 1998). NA = not applicable. Dual electrode experiments, where both electrodes were implanted to and recorded successfully from the subiculum are marked by an asterisk.

available. In two of the six patients, ECoG was obtained concurrently from strip electrodes placed on the pial surface of the temporal lobe in addition to the subicular recordings. All of the six patients were anaesthetized by the combination of Propofol and N<sub>2</sub>O. Table 1 summarizes the patient data and Fig. 1 shows the reconstructed trajectories, block photos and typical histology of the electrode penetrations.

### Spike classification

In general, the detected subicular events closely resembled the well-known interictal discharges frequently recorded from the temporal lobe of epileptic patients: the early sharp spike component was followed by a late slow wave component (Gotman, 1980; Altafullah *et al.*, 1986; de Curtis and Avanzini, 2001). Detection, assignment of discharges into different subtypes and time zero definition for event triggered averages was established in all cases selected for detailed signal analysis. Subicular discharge morphology was differentiated based on single-sweep FPG and CSD waveforms and their spatial relationship to the anatomy of the region, as described later.

Overall, 347 spikes were analysed from the six patients, and two clusters were distinguished. Type 1 spike (marked by triangle on Figs 2 and 3) was characterized by a positive, while Type 2 (marked by diamond) was characterized by a negative initial sharp FPG peak located in the pyramidal layer. In a fraction of the cases, visual inspection revealed biphasic activation; these were manually assigned to the second type. Type 1 ( $n=255$ , 73.5%) spike was detected in all six, while Type 2 ( $n=92$ , 26.5%) was detected in four subjects. Patients with sHS showed a significantly

(Fisher exact test,  $P<0.05$ ) greater number of Type 2 spikes than patients with mHS. Average spike frequency in sHS was 9.59 spike/min (Type 1: 7.71 spike/min, Type 2: 1.88 spike/min), in mHS it was 9.14 spike/min (Type 1: 8.93 spike/min, Type 2: 0.43 spike/min). Occasional epochs of rhythmic Type 1 spiking activity (0.3–1 Hz) were observed in four patients. As an illustration, Fig. 7C depicts the instantaneous recurrence frequency fluctuation of P33 Type 1 events, indicating non-stationary spiking activity. Autocorrelograms (Fig. 7D, left column, P33 and P25 Type 1 spike) peaking around 1600 ms further confirm the occasional occurrence of rhythmic spikes. To define time zero in each spike cluster for accurate analysis, single-sweep CSD traces were further investigated. As a result, time zero was arbitrarily assigned to the peak of the initial CSD activation after threshold crossing.

Recordings from a single electrode that penetrated both the proximal (to CA1) and distal segments of the subiculum in one track (P22, P33) are illustrated on Fig. 2. In the majority of the spikes, the proximal part of the subiculum showed an initial sharp negative FPG peak around the somatic layer while the distal segment of the subiculum produced a positive FPG peak (Fig. 2A). A minority of the spikes were characterized by inverted polarity FPG peaks with more complex morphology (Fig. 2B). Note that FPG is a directional measurement, and thus will be inverted depending upon whether the electrode tip is pointed toward the soma versus apical dendrites. This orientation in each recording was deduced from careful co-registration of electrophysiology and anatomy, permitting consistent interpretation of FPG recordings.

Dual electrode recording experiments were made in two patients (P25, P33). Activity was simultaneously recorded

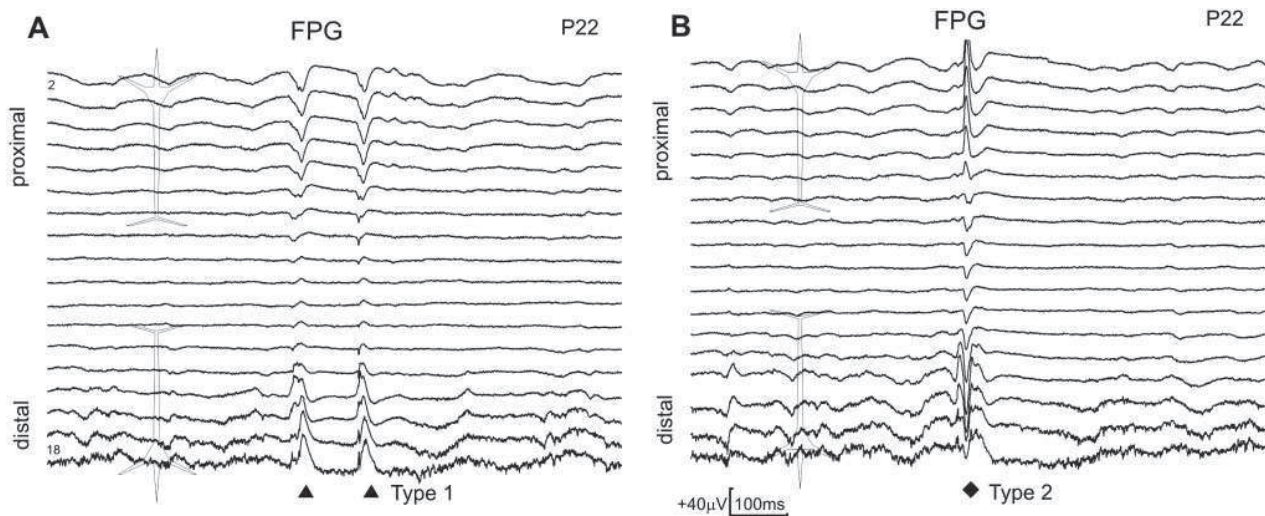


**Fig. 2** Simultaneous FPG recordings of different types of interictal spikes from the proximal and distal subiculum of patient 22. Continuous, non-averaged data. The multielectrode crossed both the proximal and the distal part of the subiculum in one penetration. Upper traces (channel 2) are close to the base of the multielectrode; lower traces (channel 18) are close to the tip. Spatial separation between traces is 200  $\mu\text{m}$ . Schematic neuron illustrates principal cell orientation and approximate location of the pyramidal and apical dendritic layers. Calibration: +40  $\mu\text{V}$ , 100 ms, positivity upwards. The spikes appeared in a close temporal relationship to each other at both subicular locations. **(A)** Type 1 spikes (marked by triangles) with the major FPG deflection being positive in the distal and negative in the proximal subiculum. **(B)** Type 2 spike (marked by a diamond) with the major negative deflection in the distal subiculum. In the proximal subiculum, the corresponding component is positive. Of note, a smaller positive peak (preceding the major negative deflection) was observed in the distal recordings, which was much less pronounced in the proximal traces, indicating the variability of Type 2 spikes.

from the anterior and posterior parts of the subiculum separated by 6 mm. Typical single-sweep FPG and the corresponding CSD traces are shown from a dual electrode experiment in Fig. 3. For simplicity, only 12 channels are shown.

### Complex CSD, MUA and spectral characterization

Event triggered CSD, MUA and spectral averages for separate discharge classes were constructed for all the selected patients. Type 1 discharges revealed a brief initial CSD sink ( $25 \pm 7$  ms half amplitude duration) in the pyramidal layer (Fig. 4), while the late wave component was associated with a longer lasting (range: 50–300 ms) source current in the same location (Fig. 5). Both the early somatic sinks and late sources were complemented by early sources and late sinks, respectively in the apical dendritic region (Fig. 5). MUA showed a significant ( $t$ -test,  $P < 0.01$ ) increase during the peak of the initial spike component, while it decreased below baseline during the late wave component in the somatic region ( $P < 0.01$ ). iERSP analysis revealed significantly increased ( $P < 0.01$ ) broad-band spectral activity (10–200 Hz) during the spike, and a later decrease ( $P < 0.01$ ) mostly in the 15–100 Hz range during the wave in the somatic region (Fig. 5).

Type 2 discharges showed greater inter- and intra-subject variability (Fig. 4). In essence, the initial spike component ( $40 \pm 22$  ms half-amplitude width) was accompanied by

sources in the somatic region and sinks in the apical dendritic region followed by another fast, but lower amplitude sink–source pair concluding with a slow source–sink pair contributing to the wave component (range: 50–500 ms) of the discharge. MUA related to the Type 2 initial spike component in the somatic layer was significantly smaller than in Type 1 discharge (Fig. 4,  $t$ -test,  $P < 0.01$ ), but still significantly greater than the baseline activity (Fig. 5,  $P < 0.01$ ). The MUA decrease during the late wave component was detectable, but highly variable. In different subjects, this decrease could either be unchanged compared to Type 1 MUA or significantly smaller or larger. Type 1 event iERSP compared to Type 2 showed a significantly larger (Fig. 5, Kruskal–Wallis ANOVA,  $P < 0.05$ ) initial spectral activation increase mostly in the higher frequency range (100–200 Hz). A decrease in spectral activity during the wave component of Type 2 events was also present, mostly in the higher frequencies (80–200 Hz) (Fig. 5).

### Intra-subicular and temporal lobe interactions

In order to further characterize intra-subicular ( $n = 3$ ) and subiculum-temporal lobe ( $n = 2$ ) discharge relationships, FPG, CSD and ECoG were analysed. Spike time delay, synchrony index and spike amplitude correlations were computed using data obtained from spatially distinct subicular locations. In addition, spike onset and peak time delays and perievent time histograms (PETH) were

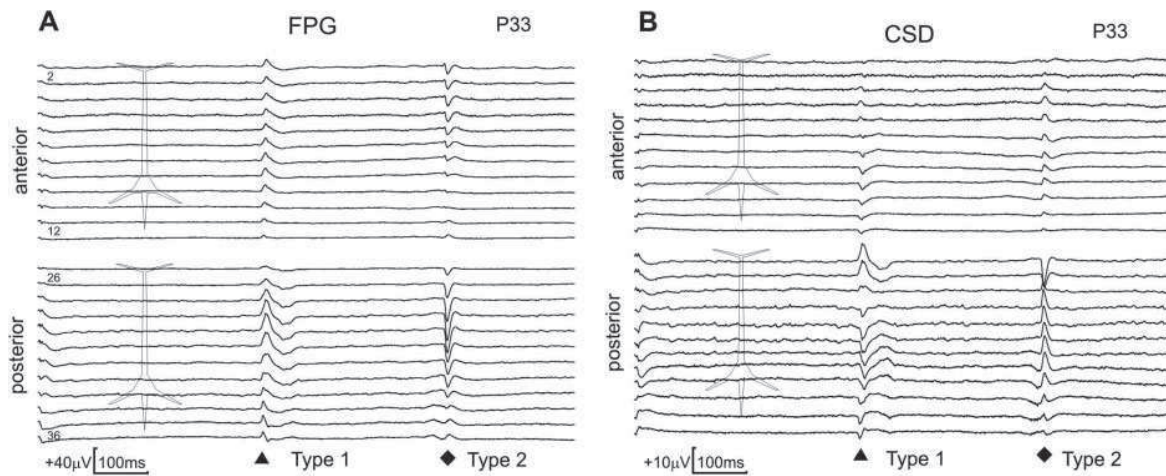


**Fig. 3** Dual multi-electrode, simultaneous FPG and CSD recordings from the anterior and posterior part of the subiculum indicating successively appearing Type 1 (triangle) and Type 2 (diamond) spikes in a somatically oriented penetration. Continuous, non-averaged data. As in the previous figure, the spikes appeared in a close temporal relationship to each other at both subicular locations. **(A)** FPG traces, 12 channels are shown from the anterior (channels 1–12) and from the posterior (channels 25–36) multi-electrodes, recorded simultaneously. Spatial separation between traces on a given multi-electrode is 200  $\mu\text{m}$ . Schematic neuron illustrates principal cell orientation and approximate location of the pyramidal and apical dendritic layers. Calibration: +40  $\mu\text{V}$ , 100 ms, positivity upwards. **(B)** Continuous non-averaged CSD traces from the anterior and posterior multi-electrodes computed from the corresponding FPG. Calibration: +10  $\mu\text{V}$ , 100 ms. Positive deflections indicate sources (outward currents), negative deflections indicate sink (inward currents). Since the tissue conductivity and electrode spacing were not taken into account, the CSD measurement unit is expressed in  $\mu\text{V}$ . Type 1 spike initial component is associated with brief somatic sink, inward, presumably depolarizing current complemented by sources from the dendritic region. Type 2 spike initial component shows an inverted sink–source pattern indicating a possible initial apical dendritic depolarizing mechanism.

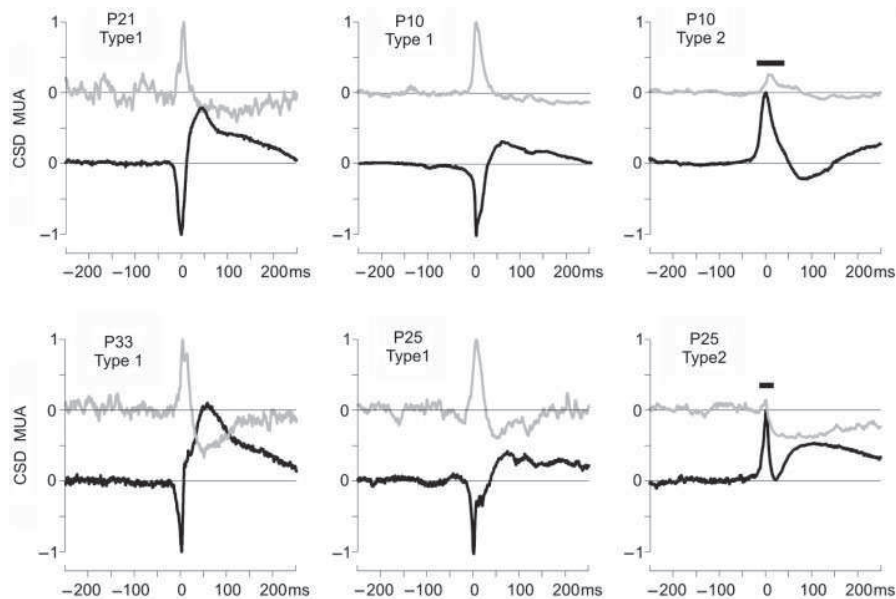


**Fig. 4** Averaged CSD and MUA traces recorded from the pyramidal layer. Representative data from four patients indicating Type 1 (P10, P21, P25, P33: left two columns) and Type 2 (P10, P25: right column) spikes. In order to compare the time course of Type 1 spikes between patients, CSD and MUA averages (P10, P21, P25, P33: left two columns) were scaled to 1 using the peak values of the initial activation. In the right column, indicating Type 2 spike, only the CSD peak was scaled to 1, while MUA was scaled with the value derived from the Type 1 peak. This permits comparison of the MUA amplitude ratio between Type 1 and Type 2 spikes recorded from two patients (P10 and P25). For Type 1 spikes, the CSD and MUA time courses show remarkable similarities between patients. The shape and timing of the initial sink and MUA increase nearly overlap, while the late source and MUA decrease are also similar in appearance. The CSD and MUA time courses of Type 2 spikes show less correspondence between patients, but the main characteristics are similar: the initial source is followed by a developing sink and concludes with a slow source. MUA recordings revealed an initial small firing rate increase followed by a variable firing rate decrease during the late part of Type 2 spike. Comparison of Type 1 (middle column) and Type 2 (right column) spikes in the same patient (P10, P25) revealed inverted initial CSD activation pattern, while the late wave component appeared to be quite similar. MUA during the initial part of Type 1 spikes was significantly larger (indicated by the thick line above the plot) than in Type 2 spikes ( $t$ -test,  $P < 0.01$ ) in both cases.

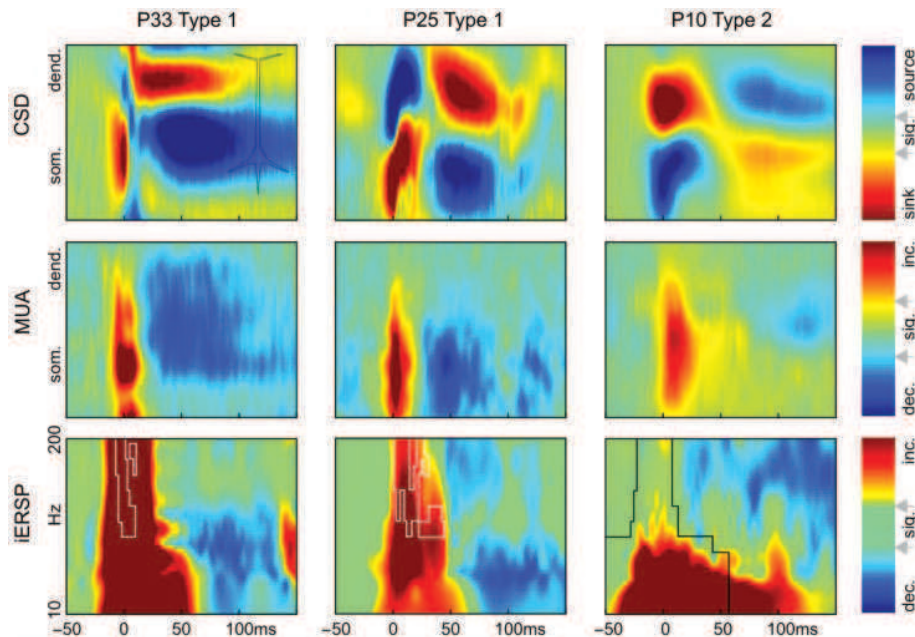


**Fig. 5** CSD, MUA and iERSP maps of Type 1 and Type 2 spikes in different patients (P10, P25 and P33). X-axis indicates time: from  $-50$  to  $150$  ms, Y-axis indicates depth: covering  $2$  mm of the subiculum. Approximate locations of somatic and apical dendritic layers are abbreviated on the figure. Small schematic pyramidal cell shows the orientation of the recording. Cold (blue) colours indicate activity decrease (dec.) compared to baseline, while warm (red) colours indicate activity increase (inc.) compared to baseline for MUA and iERSP. CSD sink is depicted in red, source in blue. Colour range was adjusted so that both increases and decreases were visible. iERSP is shown from one channel located in the pyramidal layer. Statistical comparison to baseline was performed using a  $t$ -test for CSD and MUA, and bootstrap analysis for iERSP. Significance level (bootstrap:  $P < 0.01$ ,  $t$ -test:  $P < 0.01$ ) is indicated on the side colour bar by arrows. Statistically non-significant activity in iERSP is shaded green. Type 1 spike is initiated by an inward current and firing rate increase in the pyramidal layer, accompanied by a presumably passive source in the dendritic region. iERSP during this period revealed a significant wide band oscillatory power increase up to  $200$  Hz. The wave component was accompanied by a source and firing rate decrease in the pyramidal layer, accompanied by a presumably passive current sink in the apical dendritic region. iERSP during the wave component showed a significant oscillatory power decrease. Type 2 spikes showed an inverted initial CSD pattern with an MUA increase in the pyramidal layer and accompanying spectral activity increase up to  $100$  Hz. The wave component was associated with later CSD inversion, as well as firing rate and spectral activity decreases. Significant differences (Kruskal–Wallis ANOVA,  $P < 0.05$ ) between Type 1 and Type 2 spikes are indicated by the inclusion area of white (Type 1 activity is significantly higher than Type 2 activity) and black (Type 2 activity is significantly smaller than Type 1 activity) lines in the iERSP color map for the initial spike component.

calculated using data obtained from simultaneous subicular and temporal lobe ECoG recordings.

In both single (Fig. 2) and dual (Figs 3 and 6) multi-electrode experiments reaching distinct subicular locations, a high degree of spike synchrony was observed. Detailed analysis revealed that synchronous subicular discharges (within a  $\pm 10$  ms window) were almost exclusively of the same type. Figure 7D (right column) PETH illustrates that P25 and P33 Type 1 discharges were not preceded or followed by a Type 2 spike within a  $\pm 100$  ms time window.

Intra-subicular spike time delays in dual multi-electrode experiments were estimated from the event triggered CSD to eliminate volume conduction effects. The peaks of the largest amplitude sink (in the case of Type 1 event) and source (in the case of Type 2 event) at a given multi-electrode were chosen as triggering base for the averages. We found that a certain discharge type emerged at anterior and posterior subicular locations separated by  $6$  mm with a short, but variable sink or source peak time delay (Fig. 7A, values:  $-4$ ,  $0$  and  $2$  ms) corresponding to a lowest estimate

conduction velocity of  $1.5$ – $2$  m/s. In cases when a single multi-electrode covered both the proximal and distal parts of the subiculum in one track (Fig. 2), the initial sink and/or source were not concurrently available due to positioning problems, thus discharge timing was estimated from FPG threshold crossing. Absolute time delays between the proximal and distal subicular locations were in the range of  $0$ – $10$  ms. Assuming an axonal path length of  $15$  mm between proximal and distal locations, the corresponding lowest estimate of conduction velocity would be around  $1.5$  m/s. Given the short distances ( $6$ – $15$  mm) between subiculum sites and the  $0.5$  ms sampling (corresponding to  $2000$  Hz digitization rate) accuracy in the low-frequency band, an upper conduction velocity estimate of  $12$ – $30$  m/s can be reasonably measured between the subiculum sites investigated in here. Next we examined how often the spikes emerged in such a close temporal relationship at distinct subicular locations. We found that a large proportion ( $89$ – $100\%$ ) of similar type spikes occurred concurrently (within a  $\pm 10$  ms window) between

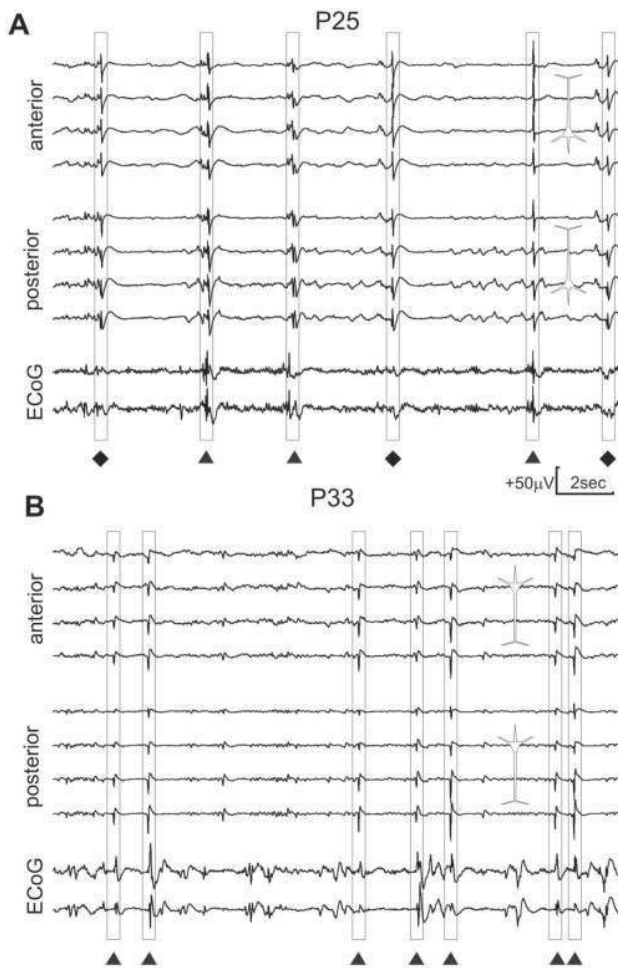


**Fig. 6** Relationship of subicular and temporal lobe spiking. **(A)** Simultaneous dual laminar and ECoG strip electrode recordings from the anterior and posterior subiculum, and temporal lobe in patient 25 in a somatically oriented penetration. Continuous, non-averaged data. Temporal lobe strip electrode contacts were localized at the base of the temporal lobe, lateral to the inferotemporal sulcus. Four representative subicular traces separated by  $400\ \mu\text{m}$  are shown from both anterior and posterior regions, while two representative ECoG traces are shown from the strip recordings. Type 1 (triangles) and Type 2 (diamonds) spikes arise synchronously at both subicular locations. Temporal lobe interictal spikes with a sharp initial component show a close timing relationship with Type 1 subicular discharges, while much less activity was seen in the temporal lobe during Type 2 (diamonds) spikes. **(B)** Similar recordings from patient 33. In this case the penetration was oriented dendritically as depicted by the inverted pyramidal cell. Each detected Type 1 (triangle) subicular spike was accompanied by a temporal lobe interictal spike. Local generation of temporal lobe spikes is highly possible, since in most cases the initial component of the ECoG spike inverted between strip contacts 5 and 6. Of note, smaller (not detected) subicular spikes were not clearly associated with temporal lobe spikes, in addition, several temporal lobe spikes lack corresponding subicular spikes.

anterior–posterior and proximal–distal sites, expressed by the synchrony index (Fig. 7B), suggesting strong functional coupling within the subiculum. Correlation between spike peak FPG amplitudes measured at different locations was

moderate to high, and it was significant in all except one case (Fig. 7B), indicating a strong linear relationship between activities at distinct subicular locations.

In addition to intra-subicular discharge synchronization, we found that temporal lobe spiking was clearly associated in time with the subicular events (Figs 6 and 8). Long time scale PETH revealed temporal spike coupling between the subiculum and temporal lobe in P25 and P33 (Figs 6 and 8A and B). This association was strong for Type 1 events in P33, weaker and broader in P25 for the same type, and virtually absent in P25 for Type 2 discharges (Fig. 8C). We found significantly more spikes (two-tailed Fisher exact test, significance level of  $P < 0.01$ ) in the range of  $\pm 200$  ms around the zero point of the PETHs than expected from a random (uncorrelated) spike distribution both in P33 Type 1 ( $P < 0.00001$ ) and P25 Type 1 ( $P < 0.00001$ ) events, while P25 Type 2 ( $P = 0.7432$ ) subiculum and cortical spikes appeared to be uncorrelated. We also quantified the statistical properties of lead or lag between subiculum and temporal cortex spikes occurring within  $\pm 200$  ms of each other. Two-tailed Fisher exact test (significance level of  $P < 0.01$ ) revealed that P33 Type 1 subicular events were significantly ( $P < 0.00001$ ) more likely to occur before the cortical spikes than after them, indicating a highly reliable subicular lead over the cortex. Such preference was not seen in either P25 Type 1 events ( $P = 0.3771$ ) or in P33 Type 2 events ( $P = 0.6843$ ).

To investigate temporal directionality between subiculum and temporal lobe in P33, spike onset and peak timing were further analysed for Type 1 events. The timing of the initial sink peak and the earliest initial ECoG positive peak were correlated. Short time scale PETH showed that the earliest ECoG positivity follows the subicular sink peak with a  $5.5 \pm 1$  ms delay (Fig. 8D). The delay was further confirmed by event triggered averaging based on the sink peak. Assuming a distance of about 30–60 mm between subiculum and temporal lobe recording sites, the estimated conduction velocity is in the range of 4.5–10 m/s. In Fig. 8B,  $t$ -scores (compared to baseline period) of CSD (multiplied by  $-1$  for better visualization) from the anterior and posterior subiculum and the  $t$ -score of temporal lobe ECoG are shown. It is evident that both the onset and peak of activity are earlier in the subiculum than in the temporal lobe, suggesting a possible subicular driving role.

## Discussion

Detailed FPG, CSD, MUA and spectral analysis of anatomically identified subicular electrical activity was performed on six mesial temporal lobe epilepsy patients during anterior temporal lobectomy under general anaesthesia. In two of the six cases, ECoG spikes were simultaneously obtained from the temporal lobe and were correlated with the subicular events. We found multiple and complex spike generation mechanisms. The general

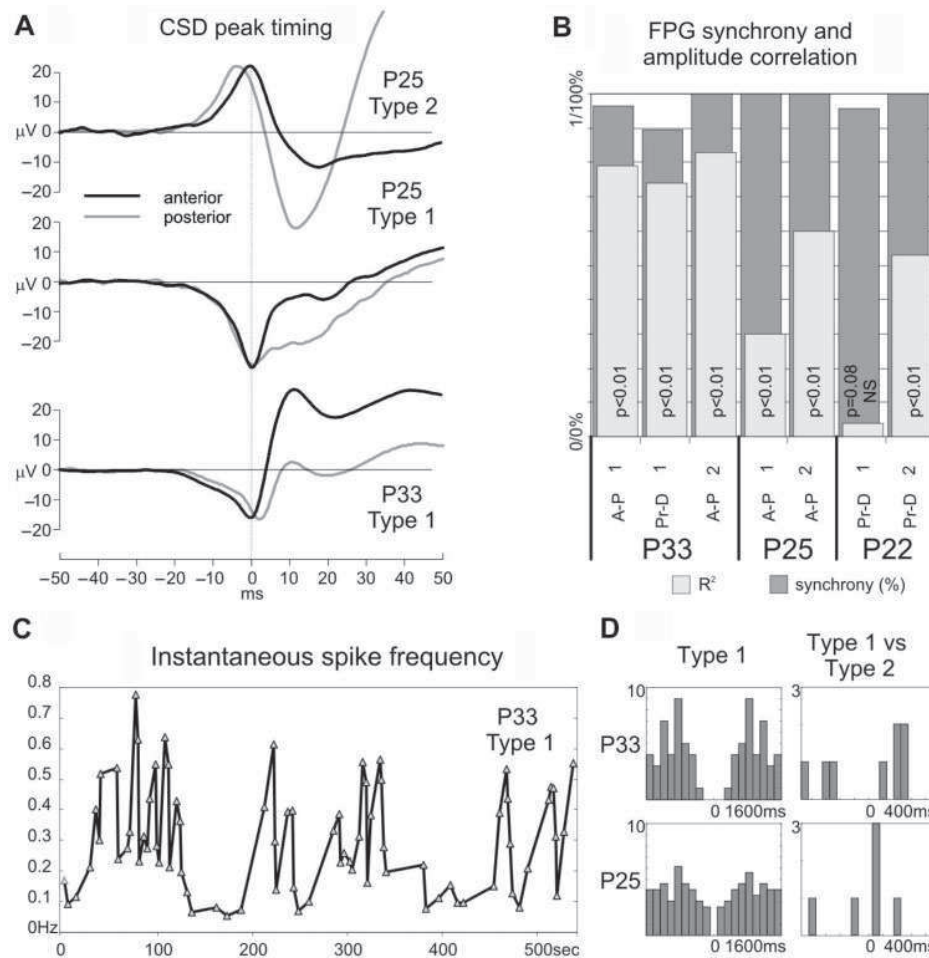


**Fig. 7** (A) Examples of event-triggered CSD averages at different subicular locations. Upper superimposed traces show Type 2 spike CSD derived from the pyramidal layer. Event triggering was based on the anterior subiculum electrode (dark trace). The resulting CSD peak at the posterior subiculum (light grey trace) preceded the anterior subiculum CSD peak by 4 ms. Middle superimposed traces show Type 1 spike CSD derived from the pyramidal layer of the same patient (P25). In this case event triggered CSD peaks were concurrent, with no delay. Lower superimposed traces depict spike Type 1 event (anterior subiculum peak) triggered CSD from patient 33. In this case, the posterior subiculum (light grey trace) follows the anterior (black trace) subiculum CSD peak by 2 ms delay. (B) FPG synchrony index and amplitude correlation. Correlation coefficient (Pearson's  $r^2$ ) and its significance is shown with light grey bars between the peak FPG amplitude at distinct subicular locations in three patients (P22, P25, P33) with proximal–distal and/or anterior–posterior penetrations for separate spike types (1 and 2). Synchrony index is shown with dark grey bars. (C) Instantaneous spike frequency of P33 Type 1 events calculated from the average time differences of three consecutively occurring spikes, expressed in Hz. (D) Left column shows the auto-correlograms (in 400 ms bins) of P33 (upper) and P25 (lower) Type 1 events indicating rhythmicity in spike occurrence. Right column shows PETHs of Type 1 and Type 2 events based on Type 1 events (in 200 ms bins) indicating sparse interaction between them.

appearance of the subicular spikes closely resembled that previously described for spike-wave discharges (Gotman, 1980; Altafullah *et al.*, 1986; de Curtis and Avanzini, 2001). Based on waveform morphology, two distinct discharge types were classified.

In Type 1 events (comprising 73.5% of all discharges), the initial component started with a brief inward current (sink) accompanied by increased cell firing and broad-band spectral activity in the pyramidal layer, and a simultaneous outward current (source) in the apical dendrites. These characteristics strongly suggest active depolarizing perisomatic excitatory mechanisms with passive, electrotonic return currents drawn from the apical dendrites. Based on

previous studies, the time course and localization of the early depolarizing current is at least partially compatible with the presence of fast glutamatergic excitation (Menendez de la Prida and Gal, 2004) in the pyramidal cell layer delivered through the local recurrent excitatory network (Harris *et al.*, 2001; Witter, 2006). The wave component was characterized by longer lasting outward currents together with decreases in firing rate and spectral activity in the somatic layer, and simultaneous inward currents in the dendritic region. These characteristics strongly suggest active hyperpolarizing, inhibitory mechanisms at the soma of principal cells with passive, electrotonic return currents drawn from the dendrites. Membrane

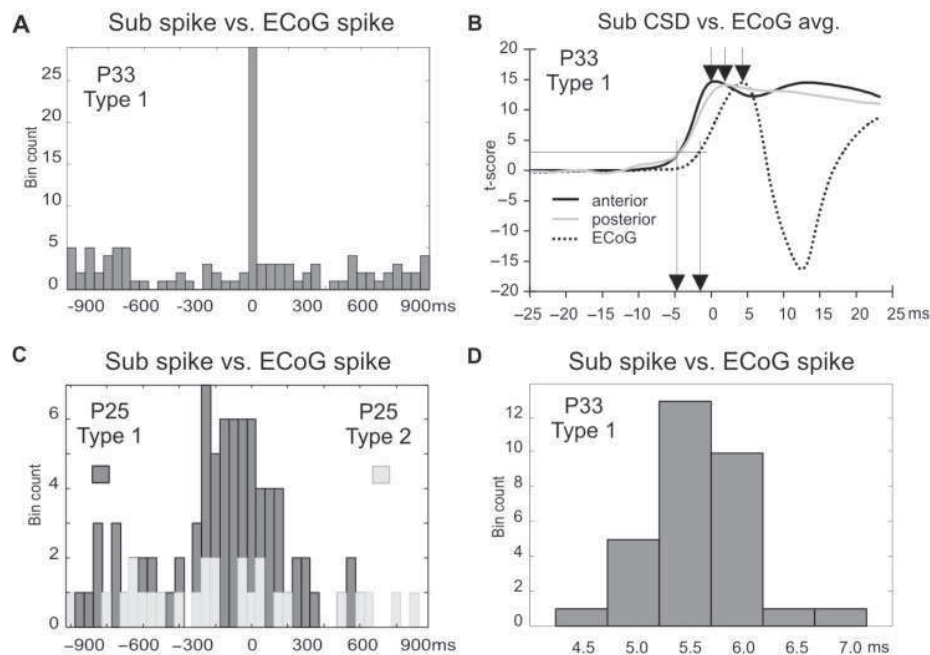


**Fig. 8** (A) Timing relationship between Type 1 subicular spikes and temporal lobe ECoG spikes (P33); peri-event time histogram,  $-1000$  to  $1000$  ms,  $50$  ms bins. (B) Onsets and peaks of averaged, event triggered (based on the anterior spike peak) subicular CSD and temporal lobe ECoG spike, t-score plots (P33). The CSD of Type 1 spikes derived from the pyramidal layer was inverted in order to illustrate onset and peak differences compared to the ECoG. Anterior subiculum CSD: dark line; posterior subiculum CSD: light grey line; temporal lobe ECoG: dashed line. Long arrows indicate the onset (t-test:  $P < 0.05$ ) of activity. The onset of subicular activation is followed by the onset of the temporal cortex spike by  $4$  ms. Short arrows indicate the peak of the activity. Both subiculum CSD peaks are earlier than the ECoG spike peak by  $3$ – $5$  ms. (C) Timing relationship between Type 1 (dark grey) and Type 2 (light grey) subicular spikes, and temporal lobe ECoG spikes (P25); peri-event time histogram,  $-1000$  to  $1000$  ms,  $50$  ms bins. (D) Short time peri-event histogram (bin size:  $0.5$  ms) of subiculum CSD peak (time zero) and temporal lobe ECoG spike initial peak. All of the detected subiculum spikes preceded temporal lobe spikes with a median latency of  $5.5$  ms.

conductances underlying the late hyperpolarizing current cannot be clearly identified from extracellular measurements. The rapid decay of the initial excitation is compatible with local circuit GABAergic inhibition (Cohen *et al.*, 2002), while the later hyperpolarizing component is most likely to be a mixture of other synaptic (Cohen *et al.*, 2006) and intrinsic (Alger and Nicoll, 1980) membrane currents, such as different kinds of potassium currents (Fernandez de Sevilla *et al.*, 2006) or even disfacilitation (Gigg *et al.*, 2000). Similar to the Type 1 spike in humans described here, electrical stimulation of CA1 in animals resulted in broad subicular excitation including the pyramidal layer (Cappaert *et al.*, 2007) with initially increased pyramidal cell firing, followed by decreased firing (Gigg *et al.*, 2000) and hyperpolarizing currents (Behr *et al.*, 1998). A similar activation sequence was observed in human *in vitro* subicular slice preparations spontaneously or in response to electrical stimulation (Cohen *et al.*, 2002; Huberfeld *et al.*, 2007), suggesting that intrinsic activity can also be triggered.

Type 2 events (comprising 26.5% of all discharges) showed considerably more spatio-temporal variability than Type 1 events, suggesting more complex and/or less-stable generator mechanisms. The initial component of Type 2

events started as a brief outward current in the somatic layer and an inward current in the apical dendritic layer, with a relatively small increase in firing rate and spectral power. One plausible interpretation of this pattern is that the flow of active excitatory, depolarizing currents located in the apical dendritic region cause a passive return source linked by electrotonic conduction with the active dendritic sink (Uva and de Curtis, 2003; Wu and Leung, 2003). The following wave component emerged variably from the fading somatic source as a longer lasting outward current, accompanied by variable decreases in firing rate and spectral power. The most probable generator mechanism of this wave component is, as in the case of Type 1 events, a mixture of synaptic and intrinsic hyperpolarizing currents confined to the somatic layer. Similar to the Type 2 *in vivo* human spike activation sequence described here, cortical electrical stimulation in animals revealed an initial superficial molecular layer excitation in the subiculum (Cappaert *et al.*, 2007) with increased pyramidal firing, and then a later action potential decrease (Gigg *et al.*, 2000) accompanied by hyperpolarizing currents (Behr *et al.*, 1998).

Opposing polarity spikes were observed in different phases of kindling in rats, dogs (Lopes da Silva *et al.*, 1982; Wadman *et al.*, 1983) and rabbits (Kogure, 1997).

In humans, opposing polarity spikes were shown in the entorhinal cortex (Bragin *et al.*, 2002). Also in humans, interictal discharges in the neocortex were found to have different laminar characteristics depending upon whether they were *de novo* generated or propagated (Ulbert *et al.*, 2004a). The seizure protective or promoting nature of interictal spikes is under debate (de Curtis and Avanzini, 2001), however it seems to be clear that some spikes are strongly linked to seizures. Recent data demonstrate that provoked spikes are good indicators of the epileptogenic area in the frontal and temporal lobes, including the hippocampus (Valentin *et al.*, 2002, 2005a, b). Furthermore, high-frequency oscillations during spikes were associated with epileptogenesis in animal models of epilepsy (Bragin *et al.*, 2004) and in humans (Staba *et al.*, 2004, 2007). We have shown that a greater amount of high-frequency (100–200 Hz) activity and cellular firing was associated with Type 1 than with Type 2 spikes (Fig. 5), further suggesting that different spike types take different roles in epileptogenesis.

Measured over a relatively long time period, spike frequency was in the range of 9 and 1 spike/min for Type 1 and Type 2 events, respectively. Type 1 discharges showed occasional episodes of rhythmicity in four patients at 0.3–1 Hz. Interictal spike rate computed from long epochs in the human mesial temporal lobe under *in vivo* conditions show a large variability (Clemens *et al.*, 2003). In general, however, spike frequencies *in vivo*, in human epilepsy are closer to our findings than has been observed *in vitro* (Cohen *et al.*, 2002; Wozny *et al.*, 2003, 2005), nonetheless bouts of rhythmic discharges at higher frequencies are not uncommon *in vivo*.

The effect of propofol anaesthesia on paroxysmal activity has been investigated by several authors. While there is an ongoing debate of its pro- or antiepileptic influence, a blood level controlled study demonstrated that interictal spiking was not significantly influenced by the infusion of the drug in a dose-dependent manner (Samra *et al.*, 1995).

The anaesthetized state is characterized by large fluctuations in synaptic and action potential activity (Steriade, 2006). The slow oscillation ( $\sim 1$  Hz) detected in various species including humans (Massimini *et al.*, 2004) during anaesthesia and natural slow wave sleep is composed of alternating phases of active (up-state) and inactive states (down-state). Human studies have revealed significant cortical excitability changes between up- and down-states (Massimini *et al.*, 2003). In addition, the slow oscillation is modulated by the infraslow oscillation ( $\sim 0.02$  Hz), which was also shown to group interictal spikes in humans (Vanhatalo *et al.*, 2004). Recent work of Clemens and co-workers (Clemens *et al.*, 2007) pointed out the relationship of cortical slow oscillation, parahippocampal spiking and sharp wave-ripples in humans. The occasional rhythmicity (0.3–1 Hz) of subicular spiking observed by us, may be consistent with the coordinative role of the cortical slow oscillation ( $\sim 1$  Hz) in the cortico-hippocampal dialogue,

not only in relatively mild (Clemens *et al.*, 2007) but even in cases of more severe mesial temporal damage. The long-term subicular spiking frequency fluctuation may reflect the modulating role of the infraslow oscillation impinging on the cortical slow oscillation.

In addition to fluctuations in interictal spike frequency, variations in spike amplitude may also be related to the varying level of excitability stemming from the slow and infraslow oscillations. Furthermore, cortical excitability cycles may also differentially modulate spike thresholds in different temporal structures, and thus the transfer of interictal discharges between the subiculum and temporal neocortex. Further investigations are needed to test these speculations.

Locally generated interictal events were found to be synchronous within  $\pm 10$  ms with high reliability at different locations of the subiculum. This was true for both Type 1 and Type 2 events. Presumably, in addition to *de novo* local generation or projected activity from the lateral temporal lobe, other limbic structures such as entorhinal cortex may also initiate widespread subicular and lateral temporal lobe synchrony. Subicular spike frequency did not correlate with the level of HS, but significantly more Type 2 discharges were detected in sHS than in mHS patients. Although the number of subjects is too small to formulate far-reaching conclusions, the reorganized input patterns of the subiculum due to the significant cell loss in the CA1 region might be related to this phenomenon. Besides the remarkable degree of intra-subicular synchrony, subicular spikes were also closely associated with temporal lobe spiking. We have shown that Type 1 discharges reliably preceded temporal lobe spikes with a short but accurate ( $5.5 \pm 1$  ms) delay.

One limitation of our acute intraoperative study stems from the unexplored effects of anaesthesia on the microphysiology of temporal lobe interictal spikes and seizures. Chronically implanted laminar multielectrodes would provide comparative data between different states of vigilance and anaesthesia, in addition to revealing more completely the relationship between spikes and seizures. Detailed evaluation of the spread of subicular activity requires implantation of more than one or two multielectrodes. Recent advances in silicone probe design may allow brain activity to be sampled in three-dimensions. The implantation of recording devices may itself have an unpredictable influence on brain activity. However, the size of our devices is a fraction of the conventionally used depth electrodes, probably inducing less damage, and thus improving the detection of pathological events.

Concerning for example the perisomatic inhibitory input of hippocampal principal cells, controversial results have been found in different rat models of epilepsy (Morin *et al.*, 1999; Cossart *et al.*, 2001) and in human studies (Wittner *et al.*, 2005). These conflicting results require an extensive comparison and correlation of human and animal data to be able to extrapolate model predictions from animals to

human. In addition to animal model validation, laminar microphysiology yields accurate templates for source localization procedures, which may further advance non-invasive diagnostic efforts. Elucidating the role of the subiculum in the generation and spread of epileptic activity within the temporal lobe may also result in a less invasive and more selective treatment of temporal lobe epilepsy.

Analysis of the ECoG, CSD, MUA and spectral fingerprints of subicular and temporal lobe events in our study revealed multiple spike generator mechanisms suggesting a complex network interplay between medial and lateral temporal lobe during epileptic activity. We have shown that spikes are generated locally and synchronously in the subiculum, and that a subset of subicular discharges had close timing association with temporal lobe spikes. These results support the hypothesis that a subicular focus might also take an active role in the distribution of epileptiform activity to other brain regions (de la Prida *et al.*, 2006).

### Acknowledgements

We thank László Papp, Katalin Lengyel, Emőke Simon and Katalin Iványi for their excellent technical assistance. This work was supported by ETT 135/2006, OTKA T049122, NeuroProbes IP 027017, LSH-CT-2006-037315 (EPICURE), NS44623 and János Szentágothai Knowledge Center RET 05/2004.

### References

- Alger BE, Nicoll RA. Epileptiform burst afterhyperpolarization: calcium-dependent potassium potential in hippocampal CA1 pyramidal cells. *Science* 1980; 210: 1122–4.
- Altfulah I, Halgren E, Stapleton JM, Crandall PH. Interictal spike-wave complexes in the human medial temporal lobe: typical topography and comparisons with cognitive potentials. *Electroencephalogr Clin Neurophysiol* 1986; 63: 503–16.
- Amaral DG, Dolorfo C, Alvarez-Royo P. Organization of CA1 projections to the subiculum: a PHA-L analysis in the rat. *Hippocampus* 1991; 1: 415–35.
- Amaral DG, Insausti R. Hippocampal formation. In: Paxinos G, editor. *The human nervous system*. San Diego: Academic Press, Inc.; 1990. p. 711–55.
- Arellano JI, Munoz A, Ballesteros-Yanez I, Sola RG, DeFelipe J. Histopathology and reorganization of chandelier cells in the human epileptic sclerotic hippocampus. *Brain* 2004; 127: 45–64.
- Babb TL. Synaptic reorganizations in human and rat hippocampal epilepsy. *Adv Neurol* 1999; 79: 763–79.
- Behr J, Gloveli T, Heinemann U. The perforant path projection from the medial entorhinal cortex layer III to the subiculum in the rat combined hippocampal-entorhinal cortex slice. *Eur J Neurosci* 1998; 10: 1011–8.
- Bragin A, Wilson CL, Almajano J, Mody I, Engel J Jr. High-frequency oscillations after status epilepticus: epileptogenesis and seizure genesis. *Epilepsia* 2004; 45: 1017–23.
- Bragin A, Wilson CL, Staba RJ, Reddick M, Fried I, Engel J Jr. Interictal high-frequency oscillations (80–500 Hz) in the human epileptic brain: entorhinal cortex. *Ann Neurol* 2002; 52: 407–15.
- Cappaert NL, Wadman WJ, Witter MP. Spatiotemporal analyses of interactions between entorhinal and CA1 projections to the subiculum in rat brain slices. *Hippocampus* 2007; 17: 909–21.
- Cavazos JE, Jones SM, Cross DJ. Sprouting and synaptic reorganization in the subiculum and CA1 region of the hippocampus in acute and chronic models of partial-onset epilepsy. *Neuroscience* 2004; 126: 677–88.
- Clemens Z, Janszky J, Szucs A, Bekecs M, Clemens B, Halasz P. Interictal epileptic spiking during sleep and wakefulness in mesial temporal lobe epilepsy: a comparative study of scalp and foramen ovale electrodes. *Epilepsia* 2003; 44: 186–92.
- Clemens Z, Molle M, Eross L, Barsi P, Halasz P, Born J. Temporal coupling of parahippocampal ripples, sleep spindles and slow oscillations in humans. *Brain* 2007; Jul 5 [Epub ahead of print].
- Cohen I, Huberfeld G, Miles R. Emergence of disinhibition-induced synchrony in the CA3 region of the guinea pig hippocampus in vitro. *J Physiol* 2006; 570: 583–94.
- Cohen I, Navarro V, Clemenceau S, Baulac M, Miles R. On the origin of interictal activity in human temporal lobe epilepsy in vitro. *Science* 2002; 298: 1418–21.
- Colgin LL, Kubota D, Brucher FA, Jia Y, Branyan E, Gall CM, et al. Spontaneous waves in the dentate gyrus of slices from the ventral hippocampus. *J Neurophysiol* 2004; 92: 3385–98.
- Corseellis JAN. The incidence of Ammon's horn sclerosis. *Brain* 1957; 80: 193–208.
- Cossart R, Dinocourt C, Hirsch JC, Merchan-Perez A, De Felipe J, Ben-Ari Y, et al. Dendritic but not somatic GABAergic inhibition is decreased in experimental epilepsy. *Nat Neurosci* 2001; 4: 52–62.
- Davies DC, Wilmott AC, Mann DM. Senile plaques are concentrated in the subicular region of the hippocampal formation in Alzheimer's disease. *Neurosci Lett* 1988; 94: 228–33.
- de Curtis M, Avanzini G. Interictal spikes in focal epileptogenesis. *Prog Neurobiol* 2001; 63: 541–67.
- de la Prida LM, Totterdell S, Gigg J, Miles R. The subiculum comes of age. *Hippocampus* 2006; 16: 916–23.
- Delorme A, Makeig S. EEGLAB: an open source toolbox for analysis of single-trial EEG dynamics including independent component analysis. *J Neurosci Methods* 2004; 134: 9–21.
- Duvernoy HM. *The human hippocampus*. Berlin: Springer-Verlag; 1998.
- Fernandez de Sevilla D, Garduno J, Galvan E, Buno W. Calcium-activated afterhyperpolarizations regulate synchronization and timing of epileptiform bursts in hippocampal CA3 pyramidal neurons. *J Neurophysiol* 2006; 96: 3028–41.
- Finch DM, Babb TL. Demonstration of caudally directed hippocampal efferents in the rat by intracellular injection of horseradish peroxidase. *Brain Res* 1981; 214: 405–10.
- Fisher PD, Sperber EF, Moshe SL. Hippocampal sclerosis revisited. *Brain Dev* 1998; 20: 563–73.
- Gabrieli JD, Brewer JB, Desmond JE, Glover GH. Separate neural bases of two fundamental memory processes in the human medial temporal lobe. *Science* 1997; 276: 264–6.
- Gigg J, Finch DM, O'Mara SM. Responses of rat subicular neurons to convergent stimulation of lateral entorhinal cortex and CA1 in vivo. *Brain Res* 2000; 884: 35–50.
- Gotman J. Quantitative measurements of epileptic spike morphology in the human EEG. *Electroencephalogr Clin Neurophysiol* 1980; 48: 551–7.
- Hampson RE, Deadwyler SA. Temporal firing characteristics and the strategic role of subicular neurons in short-term memory. *Hippocampus* 2003; 13: 529–41.
- Harris E, Stewart M. Intrinsic connectivity of the rat subiculum: II. Properties of synchronous spontaneous activity and a demonstration of multiple generator regions. *J Comp Neurol* 2001; 435: 506–18.
- Harris E, Witter MP, Weinstein G, Stewart M. Intrinsic connectivity of the rat subiculum: I. Dendritic morphology and patterns of axonal arborization by pyramidal neurons. *J Comp Neurol* 2001; 435: 490–505.
- Huberfeld G, Wittner L, Clemenceau S, Baulac M, Kaila K, Miles R, et al. Perturbed chloride homeostasis and GABAergic signaling in human temporal lobe epilepsy. *J Neurosci* 2007; 27: 9866–73.

- Kloosterman F, van Haeften T, Lopes da Silva FH. Two reentrant pathways in the hippocampal-entorhinal system. *Hippocampus* 2004; 14: 1026–39.
- Knopp A, Kivi A, Wozny C, Heinemann U, Behr J. Cellular and network properties of the subiculum in the pilocarpine model of temporal lobe epilepsy. *J Comp Neurol* 2005; 483: 476–88.
- Kogure S. Properties of interictal discharges induced by hippocampal kindling. *Epilepsy Res* 1997; 27: 139–48.
- Kubota D, Colgin LL, Casale M, Brucher FA, Lynch G. Endogenous waves in hippocampal slices. *J Neurophysiol* 2003; 89: 81–9.
- Lopes da Silva FH, Wadman WJ, Leung LS, Van Hulten K. Common aspects of the development of a kindling epileptogenic focus in the prepyriform cortex of the dog and in the hippocampus of the rat: spontaneous interictal transients with changing polarities. *Electroencephalogr Clin Neurophysiol Suppl* 1982; 36: 274–87.
- Magloczky Z, Freund TF. Impaired and repaired inhibitory circuits in the epileptic human hippocampus. *Trends Neurosci* 2005; 28: 334–40.
- Magloczky Z, Halasz P, Vajda J, Czirjak S, Freund TF. Loss of Calbindin-D28K immunoreactivity from dentate granule cells in human temporal lobe epilepsy. *Neuroscience* 1997; 76: 377–85.
- Maier N, Nimrich V, Draguhn A. Cellular and network mechanisms underlying spontaneous sharp wave-ripple complexes in mouse hippocampal slices. *J Physiol* 2003; 550: 873–87.
- Massimini M, Huber R, Ferrarelli F, Hill S, Tononi G. The sleep slow oscillation as a traveling wave. *J Neurosci* 2004; 24: 6862–70.
- Massimini M, Rosanova M, Mariotti M. EEG slow (approximately 1 Hz) waves are associated with nonstationarity of thalamo-cortical sensory processing in the sleeping human. *J Neurophysiol* 2003; 89: 1205–13.
- Menendez de la Prida L. Functional features of the rat subicular microcircuits studied in vitro. *Behav Brain Res* 2006; 174: 198–205.
- Menendez de la Prida L, Gal B. Synaptic contributions to focal and widespread spatiotemporal dynamics in the isolated rat subiculum in vitro. *J Neurosci* 2004; 24: 5525–36.
- Morin F, Beaulieu C, Lacaille JC. Alterations of perisomatic GABA synapses on hippocampal CA1 inhibitory interneurons and pyramidal cells in the kainate model of epilepsy. *Neuroscience* 1999; 93: 457–67.
- Naber PA, Witter MP. Subicular efferents are organized mostly as parallel projections: a double-labeling, retrograde-tracing study in the rat. *J Comp Neurol* 1998; 393: 284–97.
- Naber PA, Witter MP, Lopes da Silva FH. Perirhinal cortex input to the hippocampus in the rat: evidence for parallel pathways, both direct and indirect. A combined physiological and anatomical study. *Eur J Neurosci* 1999; 11: 4119–33.
- Naber PA, Witter MP, Lopes da Silva FH. Evidence for a direct projection from the postrhinal cortex to the subiculum in the rat. *Hippocampus* 2001; 11: 105–17.
- O'Mara S. Controlling hippocampal output: the central role of subiculum in hippocampal information processing. *Behav Brain Res* 2006; 174: 304–12.
- Papathodoropoulos C, Kostopoulos G. Spontaneous, low frequency (approximately 2–3 Hz) field activity generated in rat ventral hippocampal slices perfused with normal medium. *Brain Res Bull* 2002; 57: 187–93.
- Roberts L, Greene JR. Post-weaning social isolation of rats leads to a diminution of LTP in the CA1 to subiculum pathway. *Brain Res* 2003; 991: 271–3.
- Samra SK, Sneyd JR, Ross DA, Henry TR. Effects of propofol sedation on seizures and intracranially recorded epileptiform activity in patients with partial epilepsy. *Anesthesiology* 1995; 82: 843–51.
- Seress L, Gulyas AI, Ferrer I, Tunon T, Soriano E, Freund TF. Distribution, morphological features, and synaptic connections of parvalbumin- and calbindin D28k-immunoreactive neurons in the human hippocampal formation. *J Comp Neurol* 1993; 337: 208–30.
- Sharp PE, Green C. Spatial correlates of firing patterns of single cells in the subiculum of the freely moving rat. *J Neurosci* 1994; 14: 2339–56.
- Staba RJ, Frigetto L, Behnke EJ, Mathern GW, Fields T, Bragin A, et al. Increased fast ripple to ripple ratios correlate with reduced hippocampal volumes and neuron loss in temporal lobe epilepsy patients. *Epilepsia* 2007; 48: 2130–8.
- Staba RJ, Wilson CL, Bragin A, Jhung D, Fried I, Engel J Jr. High-frequency oscillations recorded in human medial temporal lobe during sleep. *Ann Neurol* 2004; 56: 108–15.
- Steriade M. Grouping of brain rhythms in corticothalamic systems. *Neuroscience* 2006; 137: 1087–106.
- Sutula T, Cascino G, Cavazos J, Parada I, Ramirez L. Mossy fiber synaptic reorganization in the epileptic human temporal lobe. *Ann Neurol* 1989; 26: 321–30.
- Ulbert I, Halgren E, Heit G, Karmos G. Multiple microelectrode-recording system for human intracortical applications. *J Neurosci Methods* 2001; 106: 69–79.
- Ulbert I, Heit G, Madsen J, Karmos G, Halgren E. Laminar analysis of human neocortical interictal spike generation and propagation: current source density and multiunit analysis in vivo. *Epilepsia* 2004a; 45 (Suppl 4): 48–56.
- Ulbert I, Magloczky Z, Eross L, Czirjak S, Vajda J, Bogner L, et al. In vivo laminar electrophysiology co-registered with histology in the hippocampus of patients with temporal lobe epilepsy. *Exp Neurol* 2004b; 187: 310–8.
- Uva L, de Curtis M. Propagation pattern of entorhinal cortex subfields to the dentate gyrus in the guinea-pig: an electrophysiological study. *Neuroscience* 2003; 122: 843–51.
- Valentin A, Alarcon G, Garcia-Seoane JJ, Lacruz ME, Nayak SD, Honavar M, et al. Single-pulse electrical stimulation identifies epileptogenic frontal cortex in the human brain. *Neurology* 2005a; 65: 426–35.
- Valentin A, Alarcon G, Honavar M, Garcia Seoane JJ, Selway RP, Polkey CE, et al. Single pulse electrical stimulation for identification of structural abnormalities and prediction of seizure outcome after epilepsy surgery: a prospective study. *Lancet Neurol* 2005b; 4: 718–26.
- Valentin A, Anderson M, Alarcon G, Seoane JJ, Selway R, Binnie CD, et al. Responses to single pulse electrical stimulation identify epileptogenesis in the human brain in vivo. *Brain* 2002; 125: 1709–18.
- Vanhatalo S, Palva JM, Holmes MD, Miller JW, Voipio J, Kaila K. Infraslow oscillations modulate excitability and interictal epileptic activity in the human cortex during sleep. *Proc Natl Acad Sci USA* 2004; 101: 5053–7.
- Van Hoesen GW, Rosene DL, Mesulam MM. Subicular input from temporal cortex in the rhesus monkey. *Science* 1979; 205: 608–10.
- Wadman WJ, Da Silva FH, Leung LW. Two types of interictal transients of reversed polarity in rat hippocampus during kindling. *Electroencephalogr Clin Neurophysiol* 1983; 55: 314–9.
- Witter MP. Connections of the subiculum of the rat: topography in relation to columnar and laminar organization. *Behav Brain Res* 2006; 174: 251–64.
- Witter MP, Groenewegen HJ. The subiculum: cytoarchitectonically a simple structure, but hodologically complex. *Prog Brain Res* 1990; 83: 47–58.
- Witter MP, Ostendorf RH, Groenewegen HJ. Heterogeneity in the dorsal subiculum of the rat. Distinct neuronal zones project to different cortical and subcortical targets. *Eur J Neurosci* 1990; 2: 718–25.
- Witter MP, Wouterlood FG, Naber PA, Van Haeften T. Anatomical organization of the parahippocampal-hippocampal network. *Ann N Y Acad Sci* 2000; 911: 1–24.
- Wittner L, Eross L, Czirjak S, Halasz P, Freund TF, Magloczky Z. Surviving CA1 pyramidal cells receive intact perisomatic inhibitory input in the human epileptic hippocampus. *Brain* 2005; 128: 138–52.
- Wittner L, Eross L, Szabo Z, Toth S, Czirjak S, Halasz P, et al. Synaptic reorganization of calbindin-positive neurons in the human hippocampal CA1 region in temporal lobe epilepsy. *Neuroscience* 2002; 115: 961–78.

- Wozny C, Kivi A, Lehmann TN, Dehnicke C, Heinemann U, Behr J. Comment on “On the origin of interictal activity in human temporal lobe epilepsy in vitro”. *Science* 2003; 301: 463; author reply 463.
- Wozny C, Knopp A, Lehmann TN, Heinemann U, Behr J. The subiculum: a potential site of ictogenesis in human temporal lobe epilepsy. *Epilepsia* 2005; 46 (Suppl 5): 17–21.
- Wu C, Asl MN, Gillis J, Skinner FK, Zhang L. An in vitro model of hippocampal sharp waves: regional initiation and intracellular correlates. *J Neurophysiol* 2005a; 94: 741–53.
- Wu CP, Huang HL, Asl MN, He JW, Gillis J, Skinner FK, et al. Spontaneous rhythmic field potentials of isolated mouse hippocampal-subicular-entorhinal cortices in vitro. *J Physiol* 2006; 576: 457–76.
- Wu K, Leung LS. Increased dendritic excitability in hippocampal cal in vivo in the kainic acid model of temporal lobe epilepsy: a study using current source density analysis. *Neuroscience* 2003; 116: 599–616.
- Wu C, Luk WP, Gillis J, Skinner F, Zhang L. Size does matter: generation of intrinsic network rhythms in thick mouse hippocampal slices. *J Neurophysiol* 2005b; 93: 2302–17.

dc\_303\_11

## **9. Melléklet**

## Laminar Analysis of Human Neocortical Interictal Spike Generation and Propagation: Current Source Density and Multiunit Analysis In Vivo

\*†‡Istvan Ulbert, \*Gary Heit, §Joseph Madsen, †George Karmos, and ‡||Eric Halgren

\**Department of Neurosurgery, Stanford University Medical Center, Stanford, California, U.S.A.*; †*Institute for Psychology, Hungarian Academy of Sciences, Budapest, Hungary*; ‡*Martinos Center, Massachusetts General Hospital, Harvard Medical School, and Massachusetts Institute of Technology, Charlestown, and §Department of Neurosurgery, Children's Hospital, Harvard Medical School, Boston, Massachusetts, U.S.A.*; and ||*INSERM, Marseilles, France*

**Summary:** Multicontact microelectrodes were chronically implanted in epilepsy patients undergoing subdural grid implantation for seizure localization. Current source density and multiple unit activity of interictal spikes (IISs) were sampled every  $\sim 150 \mu\text{m}$  in a line traversing all layers of a cortical column. Our data suggest that interictal epileptiform events in humans are initiated by large postsynaptic depolarizations, consistent with the hypothesis that human IISs correspond to animal

paroxysmal depolarization shifts. Furthermore, the cortical layer where the initial depolarization occurs may differ according to whether the IIS is locally generated or propagated from a distant location, and among the propagated IISs, whether the IIS is in the direct path of propagation or on the periphery of that path. **Key Words:** Current source density—Epilepsy—Human neocortex—Interictal spikes—Multiple unit activity.

Although the defining feature of epileptic brain is its ability to generate seizures, the ability to generate interictal spikes (IISs) may be equally characteristic (1,2). Human IISs are thought to be homologous to the paroxysmal depolarization shifts (PDSs) that have been studied in animal models of epilepsy (3,4) and have been shown to be giant excitatory postsynaptic potentials (EPSPs) (5–8). In addition to PSPs, other synchronizing mechanisms may contribute to IISs, including voltage-sensitive ion channels, gap junctions, electrical field effects, glial currents, and changes in the extracellular ionic milieu (9–13). In many models of epilepsy, the spike is followed by a slow wave (SW), which represents  $\gamma$ -aminobutyric acid (GABA)-mediated recurrent inhibition, as well as intraneuronal processes such as afterhyperpolarization and other K currents (14).

Numerous fundamental studies have allowed animal IISs/SWs to be understood as a paroxysmal recruitment of excitatory synapses, accompanied by feedforward and then feedback inhibition, with the whole interacting with intrinsic membrane properties and extraneuronal elements. This understanding is fundamental to current concepts of the IIS as a final common neurophysiologic event

in human epileptogenesis. Although it is reasonable to assume that human IISs share neural mechanisms with animal PDSs, direct evidence for this assumption is not strong. Bursting may occur in human epileptogenic tissue removed in therapeutic surgery, but spontaneous PDSs are seldom seen (15,16). In any case, these studies have been performed in vitro. Because epilepsy is fundamentally a property of neuronal networks, removal of tissue from its physiologic milieu permits elementary processes to be probed but may not provide a complete view of how these processes contribute to epileptogenesis (17). In vivo studies of human epileptic tissue have also failed to reveal properties that were expected, given animal models of PDSs. In particular, the number of bursting cells and the quantity of bursts were found actually to decrease in epileptogenic areas in human limbic cortex recorded in vivo (18).

Interictal spikes also are clinically important because they are a widely used indicator for the location of the epileptogenic zone. Although ultimately, the origin of the seizure is at issue, IISs are much easier to analyze because usually thousands of IISs are found to each seizure, and they can be obtained without accompanying movement artifacts. However, the reliability of IISs in indicating the seizure focus is limited because they may propagate from their initial site of origin. Thus most epileptologists

Address correspondence and reprint requests to Dr. E. Halgren at MGH-NMR, Room 2301, Building 149, 13th Street, Charlestown, MA 02129, U.S.A. E-mail: halgren@nmr.mgh.harvard.edu

currently believe that surgical treatment requires localization of the seizure discharge itself, but consider IIS to provide crucial complementary information (19).

This study attempted to describe the laminar microphysiology of IISs in vivo in humans, first to understand better their neural basis, and second, to determine whether microphysiologic characteristics may potentially be used to identify those IISs that are generated locally.

## METHODS

Patients with medically intractable epilepsy underwent subdural grid implantation for localization and removal of their seizure focus. Grids usually consisted of 32–64 contacts, each ~8 mm in diameter and spaced at 10-mm centers. One or two multielectrodes (MEs) were placed underneath the grid. The choice of patients for intracranial studies, the location of the clinical electrodes, and the duration of implantation were all determined entirely by clinical considerations unrelated to the experimental protocol. The patients consented to the experimental procedure after a complete explanation of the risks, under procedures monitored and approved by the Institutional Review Boards at Stanford University and Children's Hospital, Boston, according to the Declaration of Helsinki. Details of electrode construction, recordings, and analysis techniques can be found in (20,21).

### Patients

Patient A (age 49 years) had complex partial seizures (CPSs) for 30 years. A right frontal osteoma with underlying encephalomalacia/scarring was resected at age 31 years. Surface grids covered the right superior frontal gyrus (SFG) and the temporal regions. ME1 was placed in the SFG 3 cm from the right frontal pole, and ME2, close to the scarring, 1.5 cm posterolaterally. Grid recordings revealed that some spontaneous seizures arose from the vicinity of ME2, but most began more posteriorly.

Patient B (age 29 years) had frontal lobe epilepsy with seizures mostly arising from sleep. Multielectrodes were implanted into the left SFG 1.5 cm from midline, 1.5 (ME1) and 2.5 cm (ME2) anterior to the premotor area (grid contact: G14). Grid recordings showed consistent seizure spread from the medial surface of the SFG (grid IH15) toward the location of the MEs (G14).

Patient C (age 11 years) with CPSs was implanted with two MEs ~1 cm apart in the left superior parietal area, close to the sensory strip and ~3 cm superior to a cyst in the vicinity of G31. Grid recordings showed frequent IISs and seizure spread toward the MEs originating from the region of G71.

Patient D (age 33 years) was implanted with one ME near the left temporoparietooccipital junction (TPO). Grid recordings showed a posterior parietooccipital seizure focus with frequent IIS propagation toward the TPO.

### Laminar recordings

Multielectrodes were implanted underneath the clinical grid electrodes (Fig. 1). Each ME (350- $\mu$ m shaft diameter) spanned a cortical column, with its base in layer I and its tip in layer VI, with 24 individual recording sites spaced evenly at 150 or 175  $\mu$ m. Low-frequency band spatial potential gradient (PG; 0.1–500 Hz, sampled at 2 kHz/channel, 16 bit) and high-frequency band multiple (MUA) and occasionally single-unit activity (200–5,000 Hz, sampled at 20 kHz/channel, 12 bit) associated with IISs were recorded from the MEs simultaneously, while the patients were watching TV or sleeping in the epilepsy intensive care unit after electrode implantation. Grid recordings (1–70 Hz, sampled at 200 Hz/channel on the clinical video-EEG system) were coregistered with ME recordings by using a common marker in patients. A, B, and C during 1- to 3-h periods of the 5- to 10-day postoperative observation, before the second, resective surgery.

The MEs were placed within the planned cortical topectomy by using the following protocol. At the time of subdural electrode placement, intraoperative corticography was used to find the region of maximal EEG abnormalities. An intraoperative navigation system was used to place the ME on the boundary of any structural abnormality that was concordant with the maximal EEG pathology. Lacking radiographic lesions, it was placed in the zone of maximal electrographic pathology. Care was taken to insert the ME perpendicular to the cortical surface in the middle of the selected gyrus. At the time of resection, the ME site was removed en bloc, in patients A, B, and D, fixed, and embedded in paraffin. Serial 15- $\mu$ m sections were stained with H&E and Luxol Fast Blue to localize the electrode position to the respective cortical lamina. An illustration of the implantation site, schematic picture of the ME, and the penetration track is presented in Fig. 1. Patients B, C, and D remained seizure free at 6- to 24-month follow-up, whereas patient A had 70% seizure reduction at 2-year follow-up.

### CSD, unit, and MUA analysis

One-dimensional CSD data are presented on depth-versus-time maps, with color-coded sink (red) and source (blue) amplitudes. The second spatial derivative of the field potentials approximates the depth distribution of the current sources in laminated structures, such as the cerebral neocortex. Inhomogeneous conductivity was not taken into account. Hamming-window spatial smoothing and additional 0.1- to 100-Hz bandpass filtering (zero phase shift, 12 dB/oct) was applied on the continuous CSD data derived from the low-frequency band recordings. The stop band power did not exceed 0.01% of the pass band. The CSD maps are representative (single sweep, not averaged) samples of the ongoing activity, because the variance of the IISs was quite small. Comparing the single sweeps with the average showed no significant differences

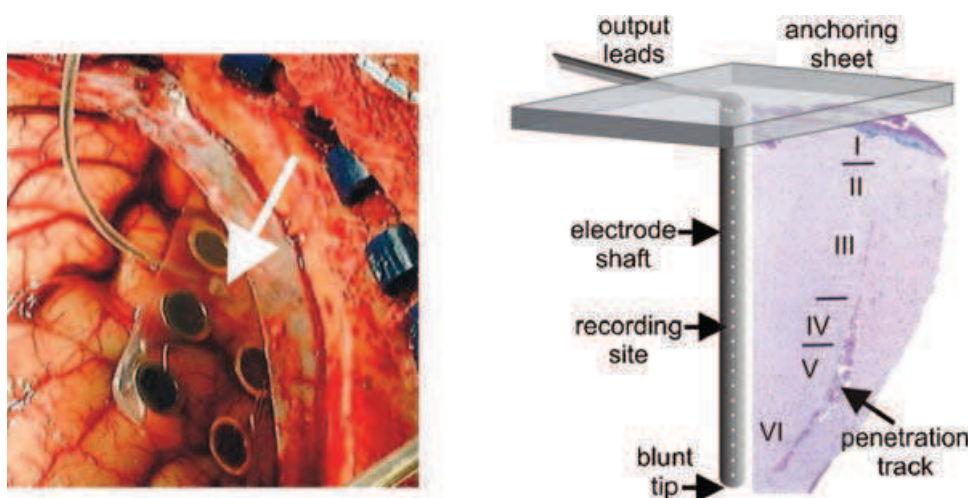


**FIG. 1.** Implantation site and multielectrode schematic drawing with histology. **Left:** intraoperative photo of patient D implantation site. The multielectrode was inserted into the TPO underneath the clinical grid. White arrow, the top of the multielectrode. **Right:** schematic drawing of the multielectrode and the histology from the same patient. Grey bars (representing  $300\ \mu\text{m}$ ) on the histology indicate approximately the boundaries between layers I/II, III/IV, and IV/V. Luxol fast blue.

(z-score,  $\leq 0.75$ ;  $p \geq 0.45$ ). A continuous estimate of the population cellular activity (MUA) was derived by additional bandpass filtering (zero phase shift, 500–5,000 Hz, 48 dB/oct), full-wave rectifying, and finally low-pass filtering (zero phase, 100 Hz, 12 dB/oct) the high-frequency band data. To enhance the signal-to-noise ratio of the MUA, spike-triggered averaging was used based on the CSD of the IISs.

Single units were sorted via traditional threshold detection and clustering of the bandpass filtered (zero phase shift, 500–5,000 Hz, 48 dB/oct), high-frequency band data. Perispike histograms (PSPHs) constructed with 2-ms bin size from the sorted units based on the timestamp of the PG spike. When no apparent single unit was present on a given channel, the filtered high-frequency band data were threshold detected without clustering, and the PSPH was calculated the same way.

## RESULTS

### Classification of IISs

The large areas covered by the clinical grids allowed the sequence of activation of different cortical areas by the IISs to be examined. This sequence generally corresponded to that observed for spontaneous clinical seizures and IISs. The macro- and microrecordings were coregistered to reveal the connection between surface potentials and intracortical activity. The surface potentials and intracortical patterns observed at six recording sites in four patients were quite stable during the 1- to 3-h time course of the daily recording, suggesting a corresponding stability in the corticocortical pathways and intracortical mechanisms that give rise to epileptiform events. Based on the timing and spatial distribution of the surface recordings, we distinguished two types of IISs at a particular site.

If the spike at a particular site was consistently preceded by an initial activation at another location, we called it a “propagated” IIS at this particular site (Fig. 2C, D: G14, G31). When a spike was recorded at a particular site without any sign of consistently preceding activity at another location, we called it a “de novo” IIS at this particular site (Fig. 2B, C: G12, IH15). In Patient A, the G12 site was able to generate both propagated and de novo IISs (Fig. 2A, B), but in the rest of the cases, all of the ME sites generated only one type of IIS.

Two distinct intracortical CSD/MUA patterns were found to be related to the propagated IISs. The most common pattern—granular—was encountered in five implantation sites. This pattern was characterized by an earliest layer IV CSD sink and MUA onset, with delayed CSD sink and MUA in layer III, and also delayed sources and MUA in layers V–VI. The second pattern—supragranular—which was observed in three recording sites, revealed a major layer I–III CSD sink with enhanced MUA, and later sinks and sources in the deep layers. In the case of the de novo IIS, one site showed initial layer V CSD sink and MUA enhancement, followed by layer IV and supragranular activation.

### Propagated spikes: Granular pattern

Both MEs in Pts. B (Fig. 3, left and middle panels) and C (Fig. 3, right panel), and in some cases the focal ME of Patient A showed initial activation during IISs in layer IV. The sequence of CSD and MUA patterns in this granular type of IISs was as follows.

Preceding the spike component, a strong sink in layers I–II and a strong source in layers III–IV were present at the four ME locations of patients B and C. MUA generally decreased during the layers III–IV source, suggesting hyperpolarizing processes centered on these layers (see

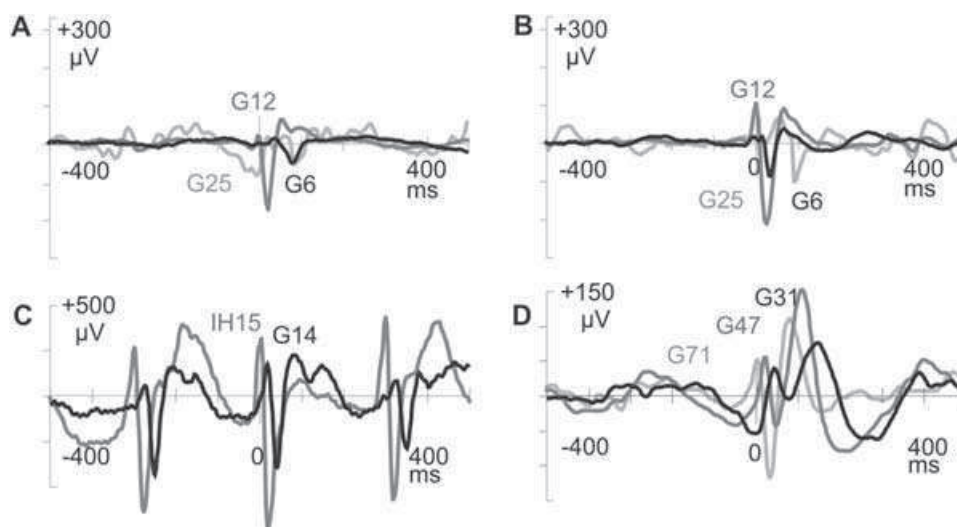


**FIG. 2.** Propagation of interictal spikes (IISs), surface grid recordings. **A:** Averaged EEG during IISs in patient A indicate a posterior to anterior propagation in the SFG from G25 (small negative deflection in *light grey trace*) to G12 (*dark grey trace*) and then G6 (*black trace*). During these IISs, ME2 (close to G12) showed an initial sink in supragranular layers. **B:** Other IISs (averaged traces) from the same patient showed initial activity in G12, followed by G6 and G25. During these IISs, ME2 (close to G12) showed an initial sink in infragranular layers, whereas ME1 (close to G6) showed an initial sink in supragranular layers. **C:** Single EEG sweeps in patient B indicate that the IISs originate near IH15 (*light grey*), followed after 20–30 ms by an IIS in G14 (*black trace*). During wakefulness, rhythmic 3-Hz IIS recurrence was observed. The multielectrodes close to G14 showed an initial granular layer sink. **D:** IISs in patient C were averaged by triggering on the positive peak recorded at G71 in the posterior parietal region. A continuous spread from G71→G47→G31 is clearly seen. Because the amplitude of the earliest G71 peak was quite small compared with the other potentials, it was enlarged 3 times in amplitude and plotted in *light grey*. The patient was awake during the recordings, and 3-Hz rhythmic IIS recurrence was present, similar to that observed in patient B. IISs recorded by ME near G47 began with a granular sink.

PSPH during the preceding source in Fig. 3). Surface-grid potentials during this period showed a small negative deflection consistent with a current sink in superficial layers (Fig. 3, IH15 and G14).

Onset of the sharp component of the spike started in layer IV with an excitatory component arising from preceding layers III–IV hyperpolarization. From layer IV, the excitation spread to layer III. While the layer III excitation propagated toward the surface, sequential inhibitory processes or current returns took place in layers III–IV. By this time, layers V–VI exhibited action-potential firing, which was later than the initial firing of layer IV (see arrow with feather in Fig. 3). The spatiotemporal pattern of the sink rising from layers IV to II–III gave the visual impression of a continuous propagation in all of the sites with propagated spikes. Calculating peak sink delay between layers IV and upper III from individual IISs, propagation velocity was in the range of 0.033–0.15 m/s. In Patient A, the mean velocity (mv) of IISs was 0.054 m/s; SD, 0.008 m/s;  $n = 50$ ; Patient B, mv, 0.058 m/s; SD, 0.01 m/s;  $n = 50$ ; Patient C, mv, 0.075 m/s; SD, 0.023 m/s;  $n = 50$ . Surface grid potentials resembled the superficial sink-source pattern rather than the layer IV activation, resulting in a biphasic spike morphology at the surface.

The SW component of the IIS/SW complex appeared to start with a long-lasting rebound excitation of layers III–IV; finally, this excitation then inverted into a strong hyperpolarization, completing the IIS/SW cycle, and usually giving rise to another IIS.

#### Propagated spikes: supragranular pattern

This pattern was observed in patient A (CSD maps are not presented) and patient D (for details, see Fig. 4). In contrast with the granular pattern, the most prominent early activation arose from layers I–II and upper layer III (Fig. 4). Preceding the spike component, CSD revealed a layer I–II and upper layer III source, and lower-layer small sinks (Fig. 4). In Patient D, a strong layer V MUA decrement was observed (Fig. 4; red MUA trace). At the onset of the spike, sinks started in layers I–II, followed by layer III (mv, 0.02 m/s; SD, 0.004 m/s;  $n = 50$ ), together with MUA increment. A characteristic source extending from layer III to layers V–VI accompanied these changes. Layers V–VI neurons fired by that time. The most prominent MUA peaks were detected in layers III and V–VI. Prolonged sinks in layer III coincided with a prolonged increase of MUA. About 100 ms after spike onset, layers I–II and III sinks inverted into sources, while MUA decreased to baseline or below. This decrement was strong in layer V and weaker in layer III.

#### De novo generation

The ME2 close to the scar (secondary seizure focus) showed both propagated and de novo spike generation in Patient A. Comparing Fig. 5 left and right panels, propagated versus de novo generation; it is clear that only the initial part of the IIS/SW complex is different. The de novo spike started deeper, in layer V, and from there it propagated to layer IV. It consisted of an initial large sink

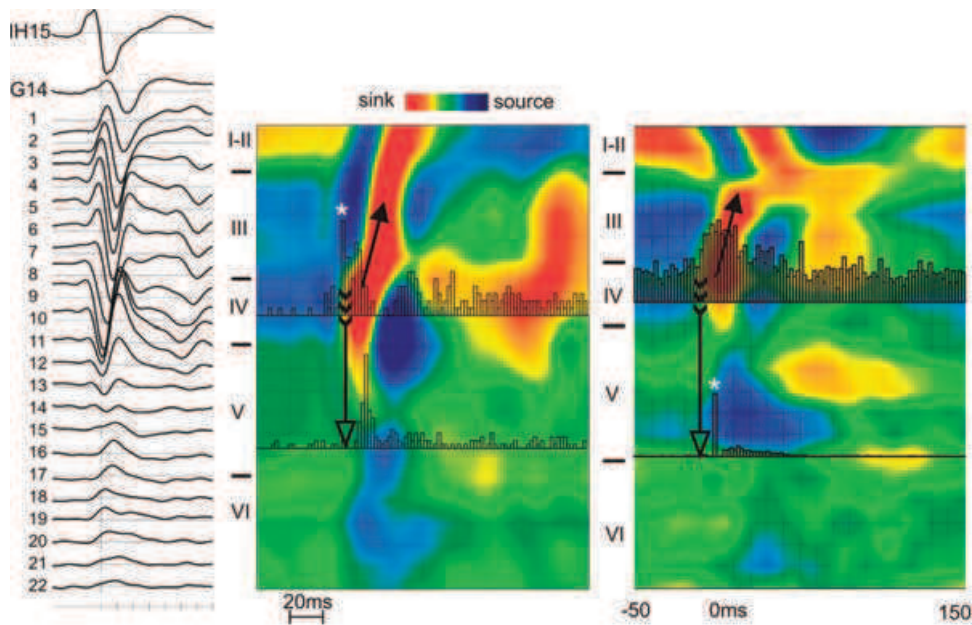


**FIG. 3.** Relation of the surface grid recordings to the current source density (CSD) during granular IIS. **Left:** CSD line plots of a granular IIS (single sweep) in patient B coregistered with the surface recordings from a nearby subdural electrode (G14) and with the intrahemispheric (medial surface of the SFG) focal surface electrode (IH15). Sinks downward, time tick 20 ms, arbitrary units. **Middle:** The map was constructed from a representative single sweep corresponding to the left panel, plotting depth (Y-axis) versus time (X-axis). CSD amplitude (arbitrary units) is color coded, sinks are yellow/red, and sources are blue/purple. Single unit activity (white asterisk) and multiunit analysis (MUA) histograms are superimposed on the color maps in black. Horizontal lines represent the recording sites, Roman numerals on the side shows the laminarization of the cortex, time mark is 20 ms. Well-isolated action potentials were recorded from multielectrode channel 10. The PSPH onset was later in layer V than in layer IV, by ~10 ms (see downward-pointing arrow with feathers). Black arrows pointing diagonally upward show intracortical spread of the layer IV origin sink toward the cortical surface. **Right:** Patient C granular IIS. Note the similarity between the two patterns. Time tick: 10 ms.

and MUA increase in layer V. From this point, the CSD and MUA patterns were highly similar to the granular pattern; however de novo generation evoked larger-amplitude sinks and sources in the superficial layers. The corresponding initial surface positivity also was larger than in the propagating spikes, but the rest of the sequence was quite similar (compare Fig. 2A and B; G12 traces).

#### Relation of IIS patterns to seizure onset and propagation zones

The epileptogenic network consists of a seizure-generating focus, and an area where the seizure spreads. Only one ME was located in a seizure focus (patient A, ME2), and that was a satellite to the primary focus based on the neurologic diagnosis. However, the fact that ME2 in patient A was also the only one to show layer V spike initiation, and was the only one to generate IIS de novo, suggested correlations that should be tested in further patients. Layer IV origin propagating spikes were observed in five ME locations of three patients. All of these sites were in the mainstream of seizure and spike propagation (the focal site in patient A also acted as a spike and a satellite seizure focus). All of the layer IV-origin spikes were temporally preceded by activation of the surrounding area. The layers I–III origin spike was observed in three recording sites of three patients. In two patients, the implantation site was located at the marginal area of the seizure prop-

agation (patient A focal site was able to initiate both IISs and seizures). The same spatiotemporal causality was observed as with the layer IV origin propagating IISs. As patient A had apparently multifocal epilepsy and the rest of the patients did not (as indicated by the follow-up), this might have accounted for these exceptions.

#### DISCUSSION

We found that human IISs can originate with initial synaptic activity centered in either supragranular, infragranular, or granular lamina. Similarly, CSD/MUA recordings in a variety of animal models have found that IISs originate in supragranular (22–29), infragranular (30–34), or granular layers (35). The laminar origin of the IIS was related to the role of the recorded area in IIS generation and propagation. Some studies in animal models also found distinct pathways for IIS generation and propagation (36–38), whereas others revealed that both supra- and infragranular layers can take part, even independently, in the epileptic process (8,39–42). The only previous CSD study of human IISs was in vitro; it suggested more frequent supragranular origin (43).

Regardless of the laminar distribution of the initial synaptic activity, the human IIS in the current study was characterized by a large initial current sink together

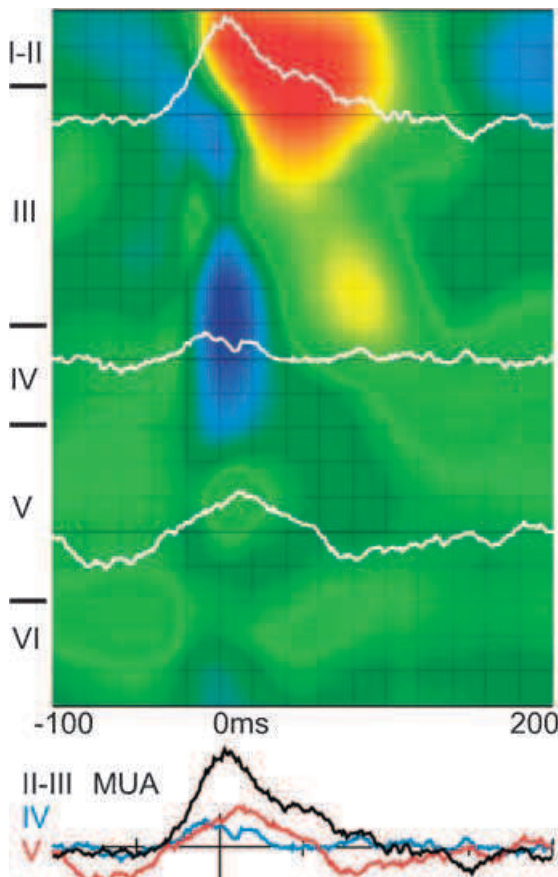


**FIG. 4.** Current source density (CSD) and multiunit analysis (MUA) of supragranular spike in patient D. Single-sweep CSD map color coded as in Fig. 3. Spike-triggered, averaged MUA from the corresponding layers superimposed on the maps in white. Time mark: 20 ms. Below the maps, the line plots of MUA from the different layers. Upper layer III, black lines; layer IV, blue lines; layer V, red lines, arbitrary units.

with an extended increase in firing. The extended increase in firing is generally consistent with that observed during sustained polysynaptic EPSPs, which may occur with activation of local associative fibers (44). The fibers have been shown in animal models to be important in the generation of PDSs (29,33,45). Nonsynaptic mechanisms also could contribute to the PDS and local neuronal synchronization (9–13). Whether these effects are in operation during human spike generation and propagation, and if so, to what extent, remains to be determined.

The human IIS was always followed by a large source and decreased firing. Cellular processes contributing to the post-IIS source probably include GABA-mediated feedforward and recurrent inhibition (46,47), as well as intrinsic K currents (24). Overall, these data provide good evidence for the validity of the PDS model for human IISs.

### Granular pattern

The described CSD/MUA timing and intracortical distribution (Fig. 3) highly resembles the feedforward patterns recorded in animals in primary and secondary sensory cortices elicited by natural stimuli or thalamic electrical stimulation (26,48,49). A similar activation sequence was observed by Kandel and Buzsáki (35) in rats during spontaneous high-voltage spikes and sleep spindles. Thalamic disinhibition evoked layer IV-centered earliest activity in rats, including the prespike source as described here (40).

The propagation of the current sink from layer IV through layer III to layer II has also been observed in previous studies in the rat, evoked by thalamic stimulation (49) and thalamic disinhibition (40). The mechanism of this propagation is still unclear, but it appears unlikely that it reflects somatodendritic backpropagation of the action potential, which is about 5 times faster than the rate of 0.033–0.15 m/s observed in the current study (50,51).

Our surface-recorded data strongly suggest corticocortical IIS propagation with  $\geq 1$  m/s velocity. Similar values of intrahemispheric corticocortical spread were found in different animal models (52–55). Intracortical spread is consistently several times slower than propagating action potentials, implicating a polysynaptic accumulation of excitation (regulated by inhibition) (33,56). The morphology of the surface-recorded potentials—brief initial positivity, then larger fast negativity followed by the slower positive–negative sequence of the wave component—also is in agreement with previous findings.

### Supragranular pattern

The initial supragranular sink in these IISs suggests activation of intrinsic collaterals, as their main inputs (44,57). Supragranular layers also receive afferents from nonspecific thalamic nuclei as well as from higher cortical areas (58–60). Stimulation of the later feedback afferents evokes a prolonged polysynaptic EPSP, with little subsequent inhibitory postsynaptic potential (61,62), consistent with the current observations.

Direct cortical electrical stimulation (24,47) elicited similar surface and CSD/MUA activation patterns as seen in Fig. 4. Besides cortical stimulation, cortical disinhibition can produce similar superficial CSD sinks in animals. Epicortical penicillin application in rabbit evoked prominent negative surface potentials (63) with sinks in layers I–II and upper layer III, and deeper sources. Cortical GABA<sub>A</sub> blockade in the rat also elicited layer III sinks and enhanced MUA (8).

### De novo generation

In agreement with our results (Fig. 5, right), layer V was found to be the initiation area of paroxysmal events in a number of slice studies involving disinhibition and neocortical isolation (64–66), where burst generating cells and axonal sprouting (67) were implicated. In vivo CSD

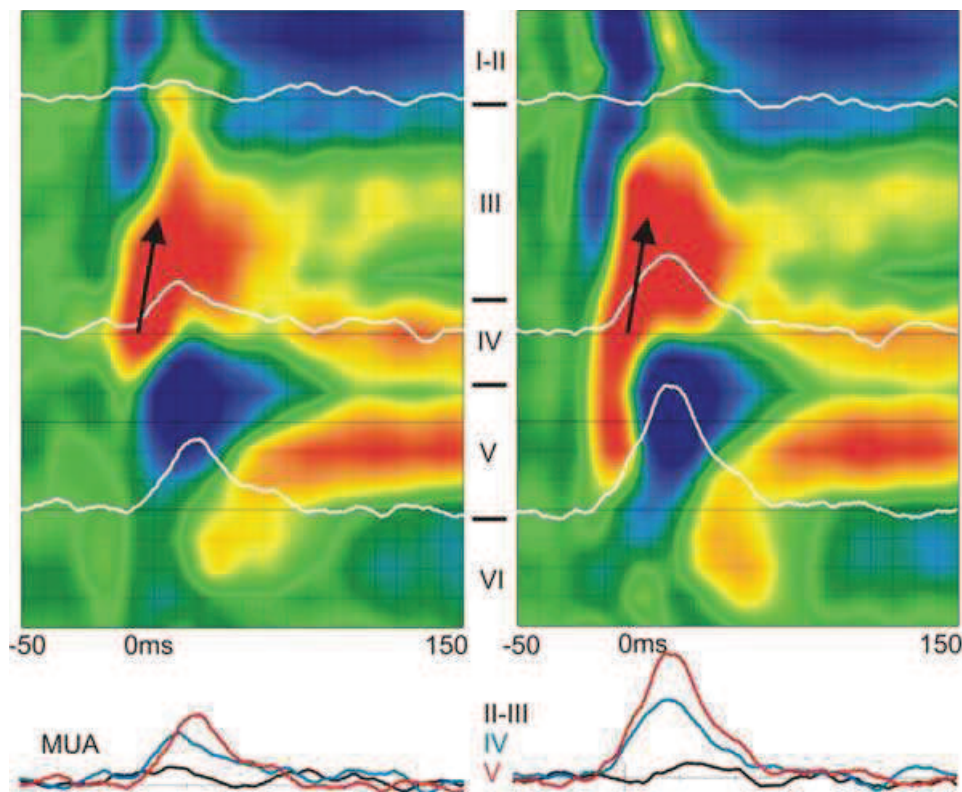


**FIG. 5.** Current source density (CSD) and multiunit analysis (MUA) of granular versus de novo spike. **Left:** Single-sweep CSD and spike-triggered, averaged MUA pattern of granular IIS from ME2 in patient A (close to G12). Color CSD codes are as in Fig. 3. Time mark: 10 ms. Below the maps: line plots of MUA, as in Fig. 4. **Right:** De novo spike from the same patient and location. Surface recordings during these IISs are shown in Fig. 2A for the left panel and Fig. 2B for the right panel. For details, see text.

experiments with cortical disinhibition in rats and rabbits (8,63) also showed that layer V plays an important role in spike generation. In a human slice CSD study, Kohling (43) demonstrated that layer V can be the initiation area of spiking; however, they found that superficial layers generate spikes more frequently.

### CONCLUDING REMARKS

PDSs are characteristic of animal epilepsy; IISs are characteristic of human epilepsy; our findings confirm that they are the same phenomenon. Beyond the defining feature of a large prolonged population EPSP, the current results confirm in humans the intracortical laminar pattern of synaptic activity during PDSs that has been described in animals.

In cortical regions on the main route of ictal spread, IISs begin with powerful depolarizations in layer IV, which spread to both supra- and infragranular laminae, resembling the normal cortical response to strong feedforward corticocortical or thalamic input. In the periphery of the main route of spread, the depolarization begins and remains supragranular. Limited data suggest that within the spike-initiation zone itself, the IIS originates in layer V. Within cortical columns, as well as between cortical ar-

reas, the spread of the IISs appears to involve the buildup of polysynaptic excitation (31,44,62).

**Acknowledgment:** This work was funded by NIH grants NS18741 and NS44623. We thank Drs. Robert Fisher, Michael Risinger, Blaise Bourgeois, Michael Kahana, and Bruce Rosen. Special thanks for Laszlo Papp for excellent technical support.

### REFERENCES

1. Penfield W, Jasper H. *Epilepsy and the functional anatomy of the human brain*. Boston: Little, Brown, 1954.
2. Pedley T. *Epilepsy and the human electroencephalogram*. London: Academic Press, 1984:1–30.
3. Wheal HV, Ashwood TJ, Lancaster B. A comparative in vitro study of the kainic acid lesioned and bicuculline treated hippocampus: chronic and acute models of focal epilepsy. In: Schwartzkroin PA, Wheal HV, eds. *Electrophysiology of epilepsy*. New York: Academic Press, 1984:176–200.
4. Wong R, Traub R, Miles R. Epileptogenic mechanisms as reviewed by studies of the hippocampal slice. In: Schwartzkroin PA, Wheal HV, eds. *Electrophysiology of epilepsy*. London: Academic Press, 253–76.
5. Ayala GF, Dichter M, Gummit RJ, et al. Genesis of epileptic interictal spikes: new knowledge of cortical feedback systems suggests a neurophysiological explanation of brief paroxysms. *Brain Res* 1973;52:1–17.
6. Steriade M, Amzica F, Neckelmann D, et al. Spike-wave complexes and fast components of cortically generated seizures, II: extra- and intracellular patterns. *J Neurophysiol* 1998;80:1456–79.

7. Steriade M, Contreras D. Spike-wave complexes and fast components of cortically generated seizures, I: role of neocortex and thalamus. *J Neurophysiol* 1998;80:1439–55.
8. Castro-Alamancos MA. Origin of synchronized oscillations induced by neocortical disinhibition in vivo. *J Neurosci* 2000;20:9195–206.
9. Taylor C, Dudek F. Excitation of hippocampal pyramidal cells by an electrical field effect. *J Neurophysiol* 1984;52:126–42.
10. Korn S, Giacchino J, Chamberlin N, et al. Epileptiform burst activity induced by potassium in the hippocampus and its regulation by GABA-mediated inhibition. *J Neurophysiol* 1987;57:325–40.
11. Amzica F, Steriade M. Neuronal and glial membrane potentials during sleep and paroxysmal oscillations in the neocortex. *J Neurosci* 2000;20:6648–65.
12. Kohling R, Gladwell SJ, Bracci E, et al. Prolonged epileptiform bursting induced by 0-Mg(2+) in rat hippocampal slices depends on gap junctional coupling. *Neuroscience* 2001;105:579–87.
13. Traub RD, Whittington MA, Buhl EH, et al. A possible role for gap junctions in generation of very fast EEG oscillations preceding the onset of, and perhaps initiating, seizures. *Epilepsia* 2001;42:153–70.
14. McCormick DA, Contreras D. On the cellular and network bases of epileptic seizures. *Annu Rev Physiol* 2001;63:815–46.
15. Schwartzkroin PA. Cellular electrophysiology of human epilepsy. *Epilepsy Res* 1994;17:185–92.
16. Williamson A, Spencer DD. Electrophysiological characterization of CA2 pyramidal cells from epileptic humans. *Hippocampus* 1994;4:226–37.
17. Steriade M. Impact of network activities on neuronal properties in corticothalamic systems. *J Neurophysiol* 2001;86:1–39.
18. Colder B, Frysinger R, Wilson C, et al. Decreased neuronal burst discharge near site of seizure onset in epileptic human temporal lobes. *Epilepsia* 1996;37:113–21.
19. Blume WT. Current trends in electroencephalography. *Curr Opin Neurol* 2001;14:193–7.
20. Ulbert I, Halgren E, Heit G, et al. Multiple microelectrode-recording system for human intracortical applications. *J Neurosci Methods* 2001;106:69–79.
21. Ulbert I, Karmos G, Heit G, et al. Early discrimination of coherent vs incoherent motion by multiunit and synaptic activity in human putative MT+. *Hum Brain Mapp* 2001;13:226–38.
22. Holmes O, Lockton JW. Penicillin epileptogenesis in the rat: diffusion and the differential laminar sensitivity of the cortex cerebri. *Brain Res* 1982;231:131–41.
23. Silva-Barrat C, Brailowsky S, Levesque G, et al. Epileptic discharges induced by intermittent light stimulation in photosensitive baboons: a current source density study. *Epilepsy Res* 1988;2:1–8.
24. Barth DS, Sutherling W. Current source-density and neuromagnetic analysis of the direct cortical response in rat cortex. *Brain Res* 1988;450:280–94.
25. Barth DS, Sutherling W. Neuromagnetic studies of evoked and spontaneous activity in animals. *Adv Neurol* 1990;54:119–31.
26. Schroeder CE, Tenke CE, Givre SJ, et al. Laminar analysis of bicuculline-induced epileptiform activity in area 17 of the awake macaque. *Brain Res* 1990;515:326–30.
27. Louvel J, Pumain R, Roux FX, et al. Recent advances in understanding epileptogenesis in animal models and in humans. *Adv Neurol* 1992;57:517–23.
28. Albowitz B, Kuhnt U. Epileptiform activity in the guinea-pig neocortical slice spreads preferentially along supragranular layers: recordings with voltage-sensitive dyes. *Eur J Neurosci* 1995;7:1273–84.
29. Albowitz B, Kuhnt U, Kohling R, et al. Spatio-temporal distribution of epileptiform activity in slices from human neocortex: recordings with voltage-sensitive dyes. *Epilepsy Res* 1998;32:224–32.
30. Connors BW. Initiation of synchronized neuronal bursting in neocortex. *Nature* 1984;310:685–7.
31. Prince DA, Connors BW. Mechanisms of epileptogenesis in cortical structures. *Ann Neurol* 1984;16:S59–64.
32. Hoffman NW, Wuarin JP, Dudek FE. Whole-cell recordings of spontaneous synaptic currents in medial preoptic neurons from rat hypothalamic slices: mediation by amino acid neurotransmitters. *Brain Res* 1994;660:349–52.
33. Demir R, Haberly LB, Jackson MB. Voltage imaging of epileptiform activity in slices from rat piriform cortex: onset and propagation. *J Neurophysiol* 1988;80:2727–42.
34. Telfeian AE, Spencer DD, Williamson A. Lack of correlation between neuronal hyperexcitability and electrocorticographic responsiveness in epileptogenic human neocortex. *J Neurosurg* 1999;90:939–45.
35. Kandel A, Buzsaki G. Cellular-synaptic generation of sleep spindles, spike-and-wave discharges, and evoked thalamocortical responses in the neocortex of the rat. *J Neurosci* 1997;17:6783–97.
36. Biella G, Forti M, de Curtis M. Propagation of epileptiform potentials in the guinea-pig piriform cortex is sustained by associative fibres. *Epilepsy Res* 1996;24:137–46.
37. Eiselt M, Zweiner U, Wagner H, et al. Intracortical functional heterogeneity in area striate during penicillin-induced spikes in rabbits. *Epilepsy Res* 1988;30:177–86.
38. Telfeian AE, Connors BW. Layer-specific pathways for the horizontal propagation of epileptiform discharges in neocortex. *Epilepsia* 1998;39:700–8.
39. Pockberger H, Rappelsberger P, Petsche H. Penicillin-induced epileptic phenomena in the rabbit's neocortex, II: laminar specific generation of interictal spikes after the application of penicillin to different cortical depths. *Brain Res* 1984;309:261–9.
40. Castro-Alamancos MA. Neocortical synchronized oscillations induced by thalamic disinhibition in vivo. *J Neurosci* 1999;19:RC27:1–7.
41. Kubota T, Aso K, Negoro T, et al. Epileptic spasms preceded by partial seizures with a close temporal association. *Epilepsia* 1999;40:1572–9.
42. Tsau Y, Guan L, Wu JY. Epileptiform activity can be initiated in various neocortical layers: an optical imaging study. *J Neurophysiol* 1999;82:1965–73.
43. Kohling R, Qu M, Zilles K, et al. Current-source-density profiles associated with sharp waves in human epileptic neocortical tissue. *Neuroscience* 1999;94:1039–50.
44. Douglas RJ, Koch C, Mahowald M, et al. Recurrent excitation in neocortical circuits. *Science* 1995;269:981–5.
45. Demir R, Haberly LB, Jackson MB. Epileptiform discharges with in-vivo-like features in slices of rat piriform cortex with longitudinal association fibers. *J Neurophysiol* 2001;86:2445–60.
46. Connors BW, Malenka RC, Silva LR. Two inhibitory postsynaptic potentials, and GABA<sub>A</sub> and GABA<sub>B</sub> receptor-mediated responses in neocortex of rat and cat. *J Physiol* 1988;406:443–68.
47. Biella G, Uva L, de Curtis M. Network activity evoked by neocortical stimulation in area 36 of the guinea pig perirhinal cortex. *J Neurophysiol* 2001;86:164–72.
48. Mitzdorf U. Current source-density method and application in cat cerebral cortex: investigation of evoked potentials and EEG phenomena. *Physiol Rev* 1985;65:37–100.
49. Castro-Alamancos MA, Connors BW. Thalamocortical synapses. *Prog Neurobiol* 1997;51:581–606.
50. Buzsaki G, Kandel A. Somadendritic backpropagation of action potentials in cortical pyramidal cells of the awake rat. *J Neurophysiol* 1998;79:1587–91.
51. Antic S, Major G, Zecevic D. Fast optical recordings of membrane potential changes from dendrites of pyramidal neurons. *J Neurophysiol* 1999;82:1615–21.
52. Steriade M, Amzica F. Dynamic coupling among neocortical neurons during evoked and spontaneous spike-wave seizure activity. *J Neurophysiol* 1994;72:2051–69.
53. Castro-Alamancos MA, Connors BW. Spatiotemporal properties of short-term plasticity sensorimotor thalamocortical pathways of the rat. *J Neurosci* 1996;16:2767–79.
54. Neckelmann D, Amzica F, Steriade M. Spike-wave complexes and fast components of cortically generated seizures, III: synchronizing mechanisms. *J Neurophysiol* 1998;80:1480–94.
55. Meeren HK, Pijn JP, Van Luijckelaar EL, et al. Cortical focus drives widespread corticothalamic networks during spontaneous absence seizures in rats. *J Neurosci* 2002;22:1480–95.
56. Traub RD, Knowles WD, Miles R, et al. Models of the cellular mechanism underlying propagation of epileptiform activity in the CA2-CA3 region of the hippocampal slice. *Neuroscience* 1987;21:457–70.
57. Thomson AM, Bannister AP. Interlaminar connections in the neocortex. *Cereb Cortex* 2003;13:5–14.

58. Szentagothai J. The Ferrier Lecture, 1977. The neuron network of the cerebral cortex: a functional interpretation. *Proc R Soc Lond B Biol Sci* 1978;201:219–48.
59. Rockland KS, Pandya DN. Laminar origins and terminations of cortical connections of the occipital lobe in the rhesus monkey. *Brain Res* 1979;179:3–20.
60. Szentagothai J. The modular architectonic principle of neural centers. *Rev Physiol Biochem Pharmacol* 1983;98:11–61.
61. Johnson RR, Burkhalter A. Microcircuitry of forward and feedback connections within rat visual cortex. *J Comp Neurol* 1996;368:383–98.
62. Shao Z, Burkhalter A. Role of GABA<sub>B</sub> receptor-mediated inhibition in reciprocal interareal pathways of rat visual cortex. *J Neurophysiol* 1999;81:1014–24.
63. Pockberger H, Rappelsberger P, Petsche H. Penicillin-induced epileptic phenomena in the rabbit's neocortex, I: the development of interictal spikes after epicortical application of penicillin. *Brain Res* 1984;309:247–60.
64. Connors BW, Benardo LS, Prince DA. Carbon dioxide sensitivity of dye coupling among glia and neurons of the neocortex. *J Neurosci* 1984;4:1324–30.
65. Chagnac-Amitai Y, Connors BW. Synchronized excitation and inhibition driven by intrinsically bursting neurons in neocortex. *J Neurophysiol* 1989;62:1149–62.
66. Hoffman SN, Salin PA, Prince DA. Chronic neocortical epileptogenesis in vitro. *J Neurophysiol* 1994;71:1762–73.
67. Salin P, Tseng GF, Hoffman S, et al. Axonal sprouting in layer V pyramidal neurons of chronically injured cerebral cortex. *J Neurosci* 1995;15:8234–45.

dc\_303\_11

## **10. Melléklet**

# Heterogeneous neuronal firing patterns during interictal epileptiform discharges in the human cortex

Corey J. Keller,<sup>1,2</sup> Wilson Truccolo,<sup>1,3</sup> John T. Gale,<sup>4,5</sup> Emad Eskandar,<sup>4,5</sup> Thomas Thesen,<sup>6</sup> Chad Carlson,<sup>6</sup> Orrin Devinsky,<sup>6</sup> Ruben Kuzniecky,<sup>6</sup> Werner K. Doyle,<sup>6</sup> Joseph R. Madsen,<sup>7,8</sup> Donald L. Schomer,<sup>9</sup> Ashesh D. Mehta,<sup>10,11</sup> Emery N. Brown,<sup>12,13,14</sup> Leigh R. Hochberg,<sup>1,14,15,16</sup> István Ulbert,<sup>17,18,19</sup> Eric Halgren<sup>20</sup> and Sydney S. Cash<sup>1</sup>

1 Department of Neurology, Massachusetts General Hospital and Harvard Medical School, Boston, MA, 02114, USA

2 Albert Einstein College of Medicine, Bronx, NY, 10461, USA

3 Department of Neuroscience, Brown University, Providence, RI, 02912, USA

4 Department of Neurosurgery, Massachusetts General Hospital and Harvard Medical School, Boston, MA, 02114, USA

5 Nayef Al-Rodhan Laboratories for Cellular Neurosurgery and Neurosurgical Technology, Massachusetts General Hospital, Harvard Medical School, Boston, MA, 02114, USA

6 Comprehensive Epilepsy Center, New York University School of Medicine, New York, NY, 10016, USA

7 Department of Neurosurgery, Children's Hospital, Boston, MA, 02115, USA

8 Department of Neurosurgery, Brigham and Women's Hospital, Boston, MA, 02115, USA

9 Beth Israel Deaconess Medical Center, Boston, Department of Neurology, MA, 02215, USA

10 Departments of Neurology and Neurosurgery, North Shore LIJ Health System, New Hyde Park, NY, 11030, USA

11 Feinstein Institute for Medical Research, North Shore LIJ Health System, Manhasset, NY, 11030, USA

12 Department of Anesthesia, Critical Care and Pain Medicine, Massachusetts General Hospital and Harvard Medical School, Boston, MA, 02114, USA

13 Department of Brain and Cognitive Sciences, Massachusetts Institute of Technology, Cambridge, MA, 02139, USA

14 Rehabilitation Research and Development Service, Department of Veterans Affairs, Providence, RI, 02912, USA

15 Department of Neurology, Brigham and Women's Hospital and Harvard Medical School, Boston, MA, 02115, USA

16 Division of Engineering, Brown University, Providence, RI, 02912, USA

17 National Institute of Neuroscience, Budapest, Hungary

18 Institute for Psychology, Hungarian Academy of Sciences, Budapest, Hungary

19 Péter Pázmány Catholic University, Department of Information Technology, Budapest, Hungary

20 Departments of Radiology, Neurosciences and Psychiatry, University of California, San Diego, San Diego, CA, 92093, USA

Correspondence to: Sydney S. Cash,  
Department of Neurology,  
30 Massachusetts General Hospital,  
55 Fruit Street,  
Boston, MA 02114 USA  
E-mail: scash@partners.org

**Epileptic cortex is characterized by paroxysmal electrical discharges. Analysis of these interictal discharges typically manifests as spike-wave complexes on electroencephalography, and plays a critical role in diagnosing and treating epilepsy. Despite their fundamental importance, little is known about the neurophysiological mechanisms generating these events in human focal epilepsy. Using three different systems of microelectrodes, we recorded local field potentials and single-unit action potentials during interictal discharges in patients with medically intractable focal epilepsy undergoing diagnostic workup for localization of seizure foci. We studied 336 single units in 20 patients. Ten different cortical areas and the hippocampus, including regions both inside and outside the seizure focus, were sampled. In three of these patients, high density microelectrode arrays**

simultaneously recorded between 43 and 166 single units from a small (4 mm × 4 mm) patch of cortex. We examined how the firing rates of individual neurons changed during interictal discharges by determining whether the firing rate during the event was the same, above or below a median baseline firing rate estimated from interictal discharge-free periods (Kruskal–Wallis one-way analysis,  $P < 0.05$ ). Only 48% of the recorded units showed such a modulation in firing rate within 500 ms of the discharge. Units modulated during the discharge exhibited significantly higher baseline firing and bursting rates than unmodulated units. As expected, many units (27% of the modulated population) showed an increase in firing rate during the fast segment of the discharge ( $\pm 35$  ms from the peak of the discharge), while 50% showed a decrease during the slow wave. Notably, in direct contrast to predictions based on models of a pure paroxysmal depolarizing shift, 7.7% of modulated units recorded in or near the seizure focus showed a decrease in activity well ahead (0–300 ms) of the discharge onset, while 12.2% of units increased in activity in this period. No such pre-discharge changes were seen in regions well outside the seizure focus. In many recordings there was also a decrease in broadband field potential activity during this same pre-discharge period. The different patterns of interictal discharge-modulated firing were classified into more than 15 different categories. This heterogeneity in single unit activity was present within small cortical regions as well as inside and outside the seizure onset zone, suggesting that interictal epileptiform activity in patients with epilepsy is not a simple paroxysm of hypersynchronous excitatory activity, but rather represents an interplay of multiple distinct neuronal types within complex neuronal networks.

**Keywords:** microelectrodes; focal epilepsy; spike–wave; single unit; microphysiology

**Abbreviations:** EEG = electroencephalogram

## Introduction

### Importance of the interictal discharge

Epileptogenic cortex is characterized by paroxysmal bursts of activity (Gibbs *et al.*, 1935) that occur independently from the synchronous neural activity that comprises a seizure. These interictal discharges, referred to as a spike, spike and wave or sharp wave on the electroencephalogram (EEG), are thought to represent pathologic alterations in normal cellular excitability and synchronization (Kooi, 1966; Chatrian *et al.*, 1974; Gotman, 1980; Walczac and Jayakar, 1997). Many authors, particularly those trained as electroencephalographers, refer to interictal spikes. Instead, we have chosen the term interictal discharge in order to encompass all components of the event, including the slow wave, and to avoid confusion with single-unit action potentials that are also referred to as spikes, primarily by cellular physiologists (Niedermeyer *et al.*, 1982). While the relationship between interictal abnormalities in the EEG and ictal events remains somewhat unclear, interictal discharges are important indicators of epileptogenicity, are routinely used in the diagnosis of epilepsy and play a critical role in the localization of seizure foci (Penfield and Jasper, 1954; Pedley, 1984; Baumgartner *et al.*, 1995; Holmes *et al.*, 2000; Blume *et al.*, 2001a and b; de Curtis and Avanzini, 2001). A deeper and more comprehensive understanding of the neurophysiological mechanisms underlying the interictal discharge is crucial to developing more complete models of epileptic activity and more principled and effective methods for controlling seizures.

Prior studies in animal models suggest that interictal discharges reflect synchronous and excessive discharges from a large population of neurons. In these models, the interictal discharge results from a burst of action potentials at 200–500 Hz superimposed on a slow depolarizing potential, the paroxysmal depolarizing shift (Goldensohn and Purpura, 1963; Matsumoto and Ajmone

Marsan, 1964). This has been observed in many models of focal epilepsy (see de Curtis and Avanzini, 2001 for a review). Whether this same mechanism underlies interictal events in human patients with idiopathic focal epilepsy is uncertain. In particular, does the interictal discharge arise from endogenous membrane instability leading to a paroxysmal depolarizing shift or is it the consequence of exogenous, perhaps network wide, activities? Examination of the relationship between single unit activity and the interictal discharge appears more complex than model systems would suggest. For example, only a subset of neurons seem to increase firing during the fast component of the interictal discharge (Wyler *et al.*, 1982; Altafullah *et al.*, 1986; Isokawa *et al.*, 1989; Ulbert *et al.*, 2004) and most human studies have not found a predictable correlation between neuronal firing or bursting of single units and interictal spikes (Ward and Thomas, 1955; Rayport and Waller, 1967; Babb, 1973; Wyler *et al.*, 1982; Schwartzkroin *et al.*, 1983; Williamson and Spencer, 1994). There is more consistency, however, with regard to the slow component of the discharge. During the slow wave there is a diminished rate of neuronal activity corresponding to a period of relative inhibition. In patients with focal epilepsy, for example, a decrease in multi-unit firing during the slow-wave (Altafullah *et al.*, 1986) is accompanied by large current sources in middle cortical layers (Ulbert *et al.*, 2004). Taken together, these studies point to greater complexity in the generation of the interictal discharge than the paroxysmal depolarizing shift model accounts for and raise the possibility that neuronal interactions and network relationships drive the paroxysm.

To understand the physiological basis of the interictal discharge in human epilepsy more completely, particularly the relationship between single unit activity and interictal discharges, we simultaneously recorded single unit activity and local field potentials in patients with intractable focal epilepsy. Consistent with prior studies, we found that many single units show an increase in

neuronal firing at the discharge as well as a decrease during the following slow-wave. In contrast with those studies, however, for many units in or near the seizure focus there is either a decrease or an increase in their firing preceding the interictal discharge. There was also a wide variety of different unit firing patterns seen during the fast component of the discharge and the following slow wave that have not been described previously. This diversity in types of modulation was observed even within small cortical regions and was true in regions inside and outside the seizure focus. Together these patterns suggest that the interictal discharge does not result from a physiologic event limited to a single population of neurons but, instead, reflects a dynamic and complex network phenomenon, emerging from a heterogeneous population.

## Materials and methods

### Subjects

Twenty patients (ages 10–58 years, nine females) with medically intractable focal epilepsy who were already scheduled for clinically-indicated intracranial cortical recordings for epilepsy monitoring (Delgado-Escueta and Walsh, 1983; Engel *et al.*, 1983) were enrolled in the study after informed consent was obtained. These procedures were monitored by local Institutional Review Boards in accordance with the ethical standards of the Declaration of Helsinki. Electrode targets and the duration of implantation were determined solely on clinical grounds.

### Clinical electrodes and recordings

Patients were implanted with intracranial subdural grids, strips and/or depth electrodes (Adtech Medical Instrument Corporation, Racine, WI) for 5–10 days. They were monitored in a specialized hospital setting until sufficient data were collected to identify the seizure focus, at which time the electrodes were removed and, if appropriate, the seizure focus was resected. Continuous intracranial EEG was recorded with standard recording systems (XLTEK, Ontario Canada; BMSI, Viasys NeuroCare, Conshohocken, PA; CEEGRAPH, Bio-logic Systems, Mundelein, IL; and BIDMC/Apropos Medical, Boston, MA) with sampling rates between 200 and 500 Hz. All steps of the analysis of intracranial EEG data were performed using Neuroscan Edit 4.3 software (Compumedics, El Paso, TX) and custom designed MATLAB (MathWorks, Natick, MA) software.

### Microelectrodes

Three types of microelectrodes were implanted in addition to the clinical macroelectrodes. The first type of electrode was the NeuroPort array ( $n=3$  patients, Cyberkinetics Inc/Blackrock Microsystems, Salt Lake City, UT), which has been used in several previous studies (Hochberg *et al.*, 2006; Schevon *et al.*, 2008; Truccolo *et al.*, 2008; Waziri *et al.*, 2009). The 4 mm  $\times$  4 mm microelectrode array is composed of 100 platinum-tipped silicon probes that are inserted 1.0 mm into the cortex. Recordings were made from 96 active electrodes and data were sampled at 30 kHz per electrode (0.3–7 kHz bandwidth).

The second type was a system of microelectrodes implanted perpendicularly to the cortical surface to sample the width of the cortex ( $n=13$  patients). This laminar microelectrode array has been described

previously (Ulbert *et al.*, 2001a) and also used in a number of studies (Ulbert *et al.*, 2001b, 2004; Wang *et al.*, 2005; Fabó *et al.*, 2008; Cash *et al.*, 2009; Keller *et al.*, 2009). Each array was comprised of 24 electrodes in a single row with diameters of 40  $\mu$ m spaced at 150  $\mu$ m centre-to-centre. The entire array had a length of 3.6 mm. Differential recordings were made from each pair of successive contacts to establish a potential gradient across the cortical lamina. After wideband filtering (DC–10 kHz) and preamplification (gain 10 $\times$ , CMRR 90 db, input impedance 10<sup>12</sup> ohms), the signal was split into a low frequency field potential band (filtered at 0.2–500 Hz, gain 1000 $\times$ , digitized at 2 kHz, 16 bit) and a high frequency multi- and single unit activity band (zero-phase digital high pass filtering above 300 Hz, 48 dB/oct, gain 1000 $\times$ , digitized at 20 kHz, 12 bit) and stored continuously with stimulus markers.

The third type of microelectrode used in this study ( $n=4$  patients) was a microwire bundle (Adtech Medical Instrument Corporation, Racine, WI) that has, in similar form, also been used in several previous studies (Cameron *et al.*, 2001; Staba *et al.*, 2002; Ekstrom *et al.*, 2003; Worrell *et al.*, 2008). Patients were implanted with hybrid depth electrodes consisting of the microwire bundle located inside the clinical depth electrodes. The microwires protruded  $\sim$ 3 mm beyond the macroelectrode tip and were used to record from mesial temporal structures (primarily hippocampus). Recordings were made from seven active electrodes and data were acquired at 30 kHz (0.3–7 kHz bandwidth) using the NeuroPort recording amplifiers.

### Selection of interictal discharges

Interictal discharges were selected based on morphological characteristics typical for sharp waves, spikes and spike-wave discharges, as detected on subdural grids or strips in clinical practice. Events showing a biphasic or triphasic morphology with an initial fast phase of 200 ms or less which may or may not have been followed by a prolonged, slower phase were chosen through visual inspection. Time zero was defined as the peak of the fast component of the discharge. Events were selected from the microelectrode field potentials and verified by the adjacent macroelectrode EEG record to minimize potential variability due to the distance between the two types of electrodes. Discharges were selected from epochs in which the patient was awake as determined by inspection of the macroelectrode EEG recordings and video monitoring. Although interictal spikes may be present during sleep, we did not include such recordings since the background rhythmicity of slow wave sleep would confound our analysis regarding grouping and inter-relationships between single units (Staba *et al.*, 2002). Only discharges separated by more than one hour from any ictal event were included in this analysis. The median firing rate of interictal discharges across all subjects was 3.46 discharges/min (minimum was 0.23, maximum 13.06). This high variability in rate resulted in a high variability of total number of discharges being examined for each patient (31–608 discharges).

### Localization of electrodes

To co-register the electrodes to anatomical structures, we used Freesurfer software to compute the reconstruction of the cortical surface (Dale *et al.*, 1999). A combination of in-house MATLAB software and Freesurfer was then used to co-register the preoperative MRI and post-operative CT or MRI scan and later align the electrodes on the cortical surface and to deeper structures. Such localization was checked against intraoperative notes and photographs of the placement of the microelectrode arrays. Determination of the seizure onset zone was performed by clinical neurophysiologists. For the purposes of

this study, the seizure onset region was demarcated by electrodes that were involved in the initiation of the seizure as recorded with the intracranial electrodes. This determination was made without any knowledge of the research.

## Data and statistical analysis

Time-frequency analysis of single trial interictal discharges was used to determine peri-event spectral changes and compare these changes to modulated unit firing rates. A sinusoidal wavelet method (short-time DFT) that returns the mean event-related spectral perturbation was employed using the EEGLAB toolbox for MATLAB (Delorme and Makeig, 2004). We used 100 linear-spaced frequencies up to 50 Hz for this analysis. To compute statistical power, we used a bootstrap method of 200 surrogate data trials.

Although single units were isolated slightly differently for each recording system, they were sorted similarly. For the laminar microelectrode, continuous microphysiology data were high-pass filtered (200 Hz–20 kHz, zero-phase shift, 48 dB/oct) and amplitude thresholded offline with Offline Sorter (Plexon, Dallas, TX). For the microwire bundle and NeuroPort array, the full analogue signal was automatically amplitude thresholded and reduced to waveform snapshots using Cerebus Online Classification software (Blackrock, Inc. Salt Lake City, UT) and then sorted with Plexon's Offline Sorter.

Great care was taken to ensure that single, stable neurons were used for this analysis. Units sorted with the method described above were treated as single units based on criteria including waveform morphology and autocorrelation functions (Lewicki, 1994; Gale *et al.*, 2009). Only neurons with an absence of spikes in a refractory period (2 ms) were considered single units; putative units with spikes during the refractory period were considered to represent multi-unit activity and were omitted.

To visualize the discharge-related activity of single neurons, peri-stimulus raster plots and timing histograms were constructed for a period 1 s before and after each event. After visual inspection of the local field potential of the event for all patients, we defined five distinct time periods around an interictal discharge. These were a pre-interictal discharge baseline period (–500 to –200 ms), a pre-interictal discharge period (–200 to –35 ms), the interictal discharge (–35 to 35 ms), the slow-wave (35–200 ms) and a post-interictal discharge period (200–500 ms).

Interictal discharges can be rhythmic and can occur at high frequencies, therefore activity directly before the interictal discharge cannot be taken as a distinct baseline. For this reason, baseline periods were created by randomly selecting epochs during interictal discharge-free interictal recording segments. A Kruskal–Wallis one-way analysis of variance tested the equality ( $P < 0.05$ ) of medians for the firing rate of baseline periods and each period of interest around the interictal discharge (Gibbons, 1985; Hollander and Wolfe, 1999). This test accounts for the non-parametric distribution of spike trains. We used a Bonferroni correction to account for the multiple number of time periods being compared.

To study the effect of neuronal attributes on different populations, we dually characterized each unit. The 'average firing rate' was calculated by dividing the total number of spikes by the recording length of the segment. The 'average bursting rate' of a neuron was calculated by the algorithm described in Staba *et al.* (2002), in which a burst is defined by groups of three action potentials occurring within 20 ms such that none are observed 20 ms on either side of the first and last action potential in the cluster.

To study the effects of firing and bursting rate, a Kolmogorov–Smirnov test was used to compare the data set with a normal

distribution (Massey, 1951; Marsaglia *et al.*, 2003). In each case, the data were determined to be non-parametric ( $P < 0.05$ ) and the Kruskal–Wallis test was utilized. Additionally, the peak:trough ratio (the maximum peak amplitude divided by the minimum trough amplitude) and spike half width (a spike's duration at half-spike amplitude) were calculated in order to characterize action potential morphology and attempt to discriminate between cortical pyramidal cells and interneurons as described previously (Swadlow, 2003; Merchant *et al.*, 2008; Cardin *et al.*, 2009). We observed low variability in these calculations for a given recording system; however, we observed a high variability between modalities. This was presumably due to filtering differences in the different recording systems as well as distinct electrode properties.

## Results

### Clinical characteristics of patients

We recorded interictal discharges from 20 patients (11 males, 9 females) with intractable epilepsy, from five collaborating institutions (Beth Israel Deaconess Medical Centre, Boston; Brigham and Women's Hospital, Boston; The Children's Hospital, Boston; Massachusetts General Hospital, Boston; and New York University Medical Centre, New York City). The mean age was  $30.0 \pm 13.7$  years (SD). Different aetiologies accounted for patient's epilepsy including cortical dysplasias and heterotopias, perinatal ischaemia, mesial temporal sclerosis, tumours (oligoastrocytoma and ganglioglioma), arteriovenous malformation and post-traumatic injury. In six patients the aetiology was not definitively established. In three cases this was because a resection was not performed, because the seizure onset zone involved eloquent cortex ( $n = 1$ ) or was not fully defined ( $n = 2$ ). In the remaining three cases, the pathology obtained was unremarkable. Similarly, different brain regions were affected, although the temporal lobe was most commonly involved. Microelectrodes were implanted into both the lateral neocortex (13 patients, 10 with laminar microelectrodes, three with NeuroPort) and mesial cortical structures (seven patients, three with laminar microelectrodes, four with microwires). Microelectrode arrays were placed within as well as outside the seizure focus (as determined by a team of clinical neurophysiologists). These data are summarized in Table 1.

### Some, but not all, neurons change their firing rate during or near the interictal discharge

For each patient, the microelectrode array and macroelectrode contacts were localized with respect to cortical and subcortical structures. A common trigger system was used to ensure alignment of the corticography data and the microelectrode signals. An example of electrode localization, macro and microelectrode recordings and single unit analysis is shown in Fig. 1. Additionally, an example of the laminar recordings and unit bursting can be found in the online supplementary material (Supplementary Fig. 1).

We examined 336 isolated single units across the 20 patients. We defined a unit to be 'modulated' if the firing rate, in at least

**Table 1** Patient characteristics

ID	Age	Gender	Electrode type	Anatomical structure	Proximity to seizure focus	Number of units	Seizure focus	Aetiology
S1	27	F	Laminar	Cingulate gyrus	Far	8	Temporal	Cryptogenic (1)
S2	31	M	Microwire	Hippocampus	Near	3	Temporal	Cryptogenic (2)
S3	58	F	Microwire	Hippocampus	Far	2	Temporal	Cryptogenic (1)
S4	45	F	Microwire	Hippocampus	Near	10	Parietal-occipital	Cryptogenic (3)
S5	28	M	Microwire	Hippocampus	Within	4	Temporal	Post-traumatic
S6	17	M	Laminar	Hippocampus	Within	8	Temporal	Cortical dysplasia
S7	47	M	Laminar	Hippocampus	Far	7	Temporal	Hippocampal sclerosis
S8	19	M	Laminar	Superior temporal gyrus	Within	3	Temporal	Cortical gliosis/hippocampal sclerosis
S9	21	M	NeuroPort	Middle frontal gyrus	Near	43	Temporal	Cortical dysplasia
S10	52	F	NeuroPort	Middle temporal gyrus	Near	166	Temporal	Cortical dysplasia
S11	43	M	Laminar	Pre-central gyrus	Within	2	Temporal	Oligoastrocytoma
S12	29	F	Laminar	Lateral occipital cortex	Near	3	Parietal	Heterotopia
S13	24	M	Laminar(s)	Pre-central and middle temporal gyri	Far	2	Frontal	Cortical dysplasia
S14	12	M	Laminar	Pre-central gyrus	Near	9	Parietal-occipital	Perinatal ischaemic injury
S15	10	F	Laminar	Inferior temporal gyrus	Within	8	Temporal	Ganglioglioma with adjacent dysplasia
S16	14	M	Laminar(s)	Inferior and middle temporal gyri	Near	3	Temporal	Hippocampal sclerosis
S17	34	F	Laminar	Occipital lateral gyrus	Within	2	Occipital	AVM
S18	27	F	Laminar	Inferior frontal gyrus	Far	1	Frontal	Cryptogenic (2)
S19	40	M	Laminar	Middle temporal gyrus	Far	2	Frontal	Cryptogenic (2)
S20	22	F	NeuroPort	Middle temporal gyrus	Within	50	Temporal	Cortical dysplasia

Anatomical structure from which the microelectrode recording was made was determined by comparison of intra-operative notes and photographs and co-registration of pre- and post-operative imaging (MRI and/or CT). Proximity to seizure focus was established by comparison to clinically determined seizure onset regions. If the electrode was within the determined area it was considered within, near if within 3 cm and far if outside of 3 cm. Aetiology was determined based on pathology studies in the context of the other clinical data. Aetiology notes: multifocal or site of onset not defined so no resection was performed (1), pathology was unremarkable (2), eloquent cortex involved therefore no resection was performed (3). AVM = arteriovenous malformation.

one of five defined time periods around the interictal discharge, was significantly different from a baseline firing rate (Kruskal–Wallis one-way analysis of variance with Bonferroni correction for multiple comparison). Based on this categorization, we found that 48% (158/336) of the units were modulated ( $P < 0.05$ ) during the interictal discharge.

To determine if all the modulated units were participating in a given event or if only a subset contribute, we calculated the firing probabilities on a per unit basis. On average, a given modulated unit only had a 39.6% ( $\pm 2.0\%$  standard error) probability of firing during the five time periods previously defined during any single interictal discharge. Additionally, during any given interictal discharge period only 28.2% ( $\pm 5.95\%$  standard error) of the modulated units fired. Thus, for any given event only a small, and changing, population of neurons participated.

To determine if the modulated and non-modulated neurons had distinct characteristics we compared the firing and bursting rate of these populations. Median baseline frequencies in the modulated and non-modulated groups were 2.55 and 0.66 spikes/s and 1.20 and 0.20 bursts/min, respectively (Kruskal–Wallis,  $n_1 = 158$ ,  $n_2 = 178$ ,  $P < 0.01$  for both measures, two-tailed). We recalculated

these parameters excluding the interictal discharge to ensure that the difference was not solely due to the interictal discharge itself. The modulated population still had significantly higher firing and bursting rates than the non-modulated population (Fig. 2;  $Med_{modulated} = 2.56$  spikes/s and 0.65 bursts/min;  $Med_{non-modulated} = 1.02$  spikes/s and 0.20 bursts/min; for both measures  $P < 0.01$ ).

We additionally calculated each unit's spike half-width (a spike's duration at half-spike amplitude) and peak:trough ratio (peak amplitude divided by the trough amplitude) as a possible measure of different neuronal types (Cardin *et al.*, 2009). There were no noticeable effects of modulation on neuronal properties within a given recording modality (Supplementary Fig. 2). There were, however, significant changes in these values between modalities. Spike half-width values were significantly lower for units recorded by the laminar system when compared to the others ( $P < 0.01$ ). Additionally, those units recorded by the NeuroPort system had significantly lower peak:trough ratios when compared to microwire-recorded units (Supplementary Fig. 2,  $P < 0.05$ ).

We also examined if there were differences in these characteristics based on mesial temporal or cortical location. Overall,

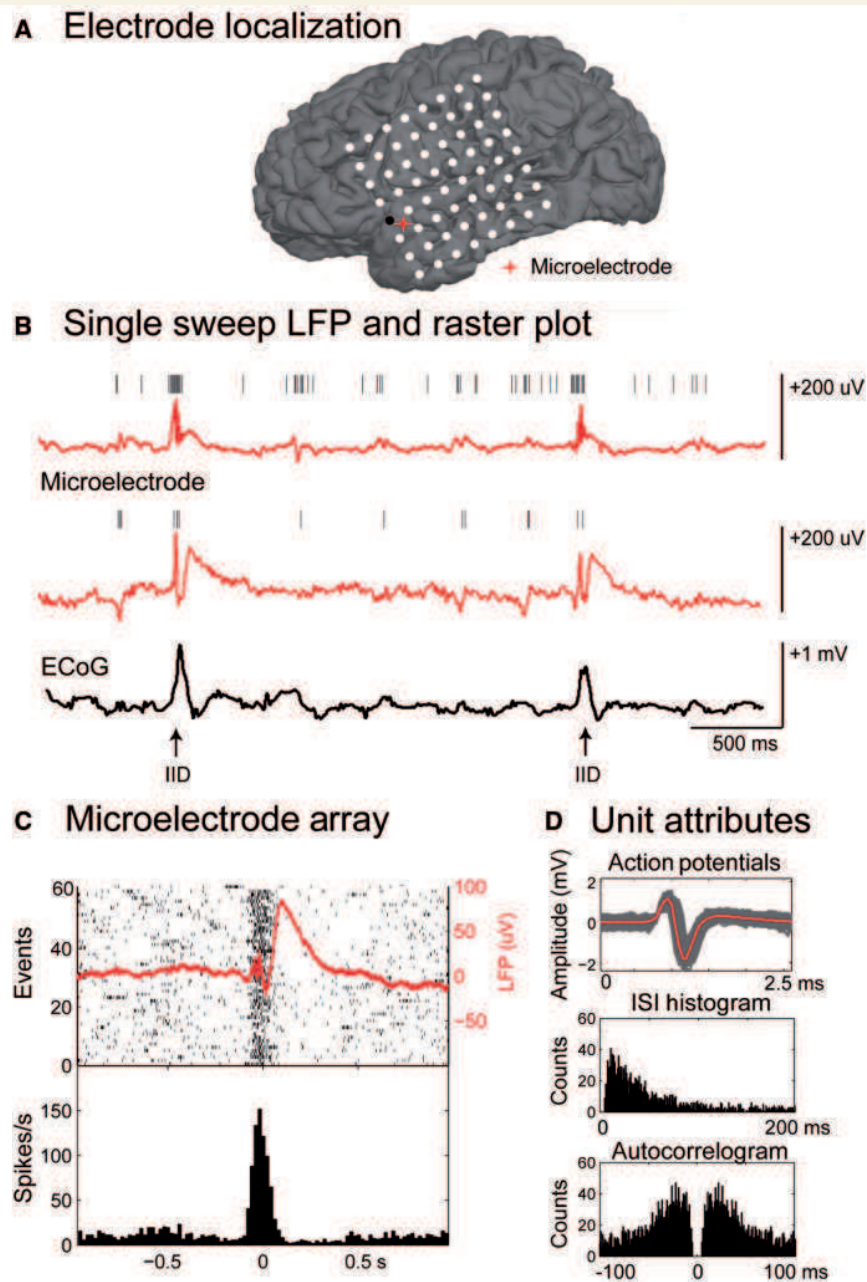


**Figure 1** Relationship between macroelectrodes, microelectrodes and single unit activity during an interictal discharge. (A) Co-registration of pre-operative MRI and post-operative CT or MRI allows identification of the electrodes and anatomical structures. (B) Single sweep of microelectrode local field potential (LFP; red) and corticography (ECoG; black) from an adjacent electrode. Hash marks indicate discriminated action potentials. Selected interictal discharges (IID) are indicated with arrows. Note the increase in action potentials from both units during the fast component of the interictal discharge. (C) Raster plot and peri-spike timing histogram from one of the microelectrode channels shown above during the interictal discharge ( $n = 60$ ). The averaged local field potential is overlaid on the raster plot in red. Histogram bin width is 5 ms. (D) Unit attributes: action potentials (each in grey, average in red), neuronal inter-spike time interval (ISI) histogram (1 ms bin width) and autocorrelogram ( $-100$  to  $100$  ms; 1 ms bin width) from the unit isolated in (C).

there was no statistically significant difference between the bursting or firing rates in mesial temporal versus cortical neurons. The spike half-width of mesial temporal neurons was slightly faster than cortical neurons. There were no significant differences in the peak:trough ratio (Supplementary Fig. 3).

## Characterization of the modulated neuronal population

To categorize these different patterns of modulation further, we grouped the neurons based on changes in each of five time

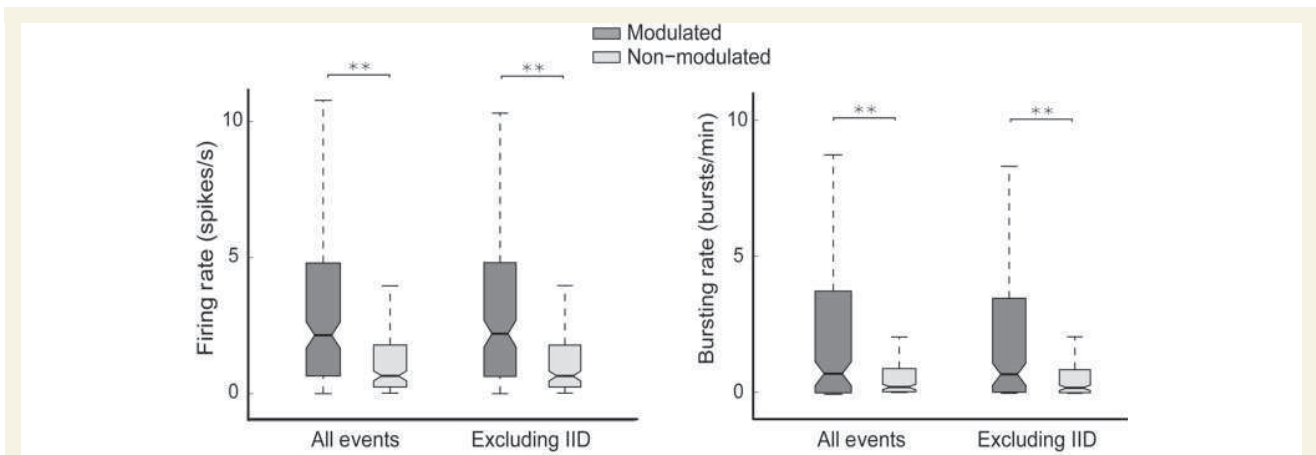


**Figure 2** Firing and bursting rate for neurons modulated or not during the interictal discharge. Boxplots show the median (Med,  $\times 5$ ), lower (Q1,  $\times 25$ ) and upper quartile (Q3,  $\times 75$ ) in the shaded regions and the largest non-outlier observations (whiskers shown with dotted lines). The modulated population had significantly higher firing and bursting rates compared to the non-modulated population both including and excluding the interictal event (Med modulated = 2.56 spikes/s and 0.65 bursts/min; Med non-modulated = 1.02 spikes/s and 0.20 bursts/min;  $**P < 0.01$ , Kruskal-Wallis test,  $n_1 = 158$ ,  $n_2 = 178$ ). IID = interictal discharge.

**Table 2** Classification of neuronal responses during interictal discharge

Class	Number of units	Modulated neurons (%)	Patients represented (%)	Pre-IID (-500 to -200 ms)	Pre-IID (-200 to -35 ms)	IID (-35 to 35 ms)	Slow wave (35 to 200 ms)	Post-slow wave (200 to 500 ms)
1	57	36.1	60	-	-	-	↓	-
2	24	15.2	50	-	-	↑	-	-
3	14	8.9	35	-	-	↑	↓	-
4	13	8.2	5	-	-	-	↑	-
5	8	5.1	20	-	-	↓	↓	-
6	5	3.2	20	-	↓	↑	↓	-
7	4	2.5	15	-	↑	-	↓	-
8	4	2.5	10	-	↓	-	↓	-
9	3	1.9	10	↑	-	-	-	-
10	3	1.9	5	↑	-	-	↓	-
11	3	1.9	5	-	-	-	↓	↓
12	2	1.3	10	-	↑	-	↑	-
13	2	1.3	5	-	-	-	-	↑
14	2	1.3	10	-	-	↑	↓	↓
15	2	1.3	10	-	↓	↑	↓	↓
16	2	1.3	10	-	-	↑	↑	-

Arrows indicate a significant change in firing during the selected time period as defined in the 'Materials and methods' section. IID = interictal discharge.

periods. Of the possible permutations (five time periods, each with either a significant increase, decrease or no change results in 243 possible outcomes), 16 different firing patterns occurred in more than one unit (Table 2). Five main groups constituted about 75% of the modulated neurons and were observed both inside and outside the seizure focus. In addition, modulated units were observed in both cortical (154 of 304 units) and mesial temporal locations (4 of 32). Figure 3 demonstrates a representative neuron and population averages for the five most common firing patterns. The average local field potential of the same microelectrode channel is overlaid on the raster plot with the peri-spike timing histogram of the representative neuron.

Firing of Type 1 units significantly decreased during the slow-wave but was unchanged during the interictal discharge. They represented 36.1% of the modulated population and occurred in 60% of the patients. Type 2 units had an increase in firing rate only during the fast component of the interictal discharge ( $\pm 35$  ms from the peak, 15.2% of the modulated units) and were found in 50% of the patients. In contrast, for Type 3, units firing increased during the interictal discharge but decreased during the slow-wave. Type 4 neurons were not modulated during the spike itself but increased in activity during the slow-wave and were only found in one patient. Action potentials of Type 5 units decreased during both the spike and slow-wave.

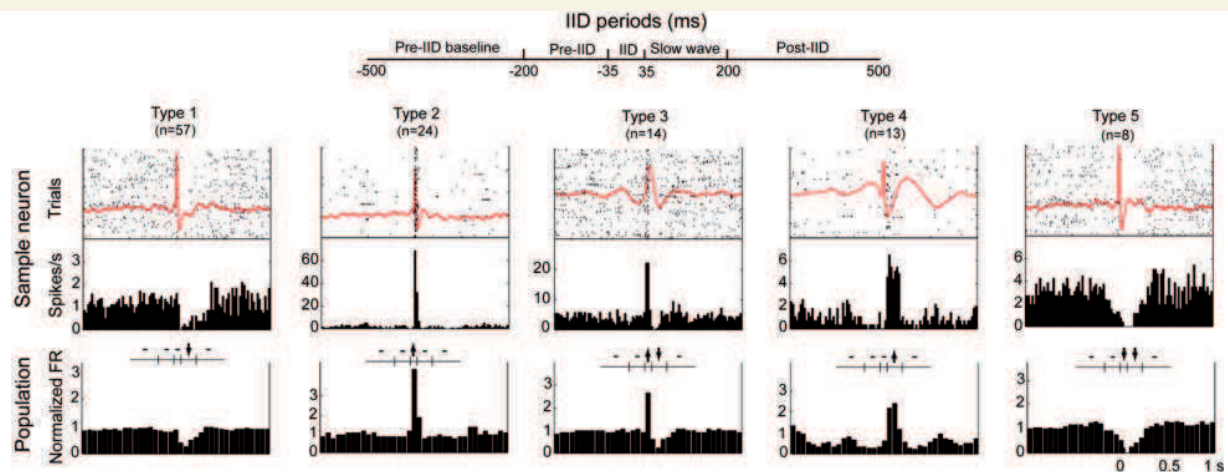


**Figure 3** Classification of neuronal responses during the interictal discharge (IID). Five defined interictal discharge periods are shown in the schematic at top. The averaged local field potential, raster plot and peri-event time histogram of a sample neuron and the population average peri-event time histogram of the top five modulated firing patterns around the interictal event are shown in each column. FR = firing rate. Dashes indicate no significant change and arrows up or down denote an increase or decrease in significance in the middle diagrams ( $P < 0.05$ , Kruskal–Wallis test, Bonferroni corrected).

In an attempt to understand which classes of neurons may constitute any given type of firing pattern, we examined the baseline firing and action potential characteristics of each of the 10 most frequent types of patterns. Most patterns showed the same characteristics in terms of firing rate and bursting rate with the exception of Type 5 units. These showed a significantly higher firing and bursting rate than other types. This type is the only one of the most common types to have a decrease in firing during the fast component of the discharge. Types 3 and 4 appeared to have a lower firing and bursting rate than other types. Spike half-width and peak:trough values were not significantly different between different firing patterns (Supplementary Fig. 3).

### Changes in neuronal firing preceding interictal discharges are found within or near the seizure focus

In addition to the five main types of single unit activity described above, many units showed a significant change in firing preceding the interictal discharge. Twelve single units (7.6% of the modulated population) significantly decreased their firing rate and 19 units (12.0%) significantly increased in one of the two time periods preceding the interictal discharge. Two of the 12 units (1.3% of the modulated population) decreased far before the interictal discharge (–500 to –200 ms) while 11 of the 19 units (7.0%) increased far before. We also found three units that increased long after the interictal discharge (200–500 ms; Fig. 4). These types of patterns were found only within or near the seizure focus. In fact, 70% of identified units within the seizure focus showed a pre-discharge change in activity. No such changes were seen in units well outside the seizure onset zone.

Comparison of firing rates, bursting rates and action potential characteristics amongst these different groups revealed few

differences. There were no statistically significant differences between units which increased, decreased or had no change in their firing rate in terms of baseline firing rate, bursting rate or peak:trough ratio. Units with a decrease in firing before the event had a significantly shorter time at half peak (Supplementary Fig. 3).

### Broadband (local field potential) and neuronal firing decrement preceding interictal discharge observed across subjects

Given the plurality of neurons demonstrating a decrement in single unit firing preceding the interictal discharge, we were interested in increasing our understanding of the relationship between this decrement and local field potentials during the pre-spike period. We identified units across subjects that exhibited similar attributes—a decrement before the interictal discharge (–200 to –35 ms), an increase during the interictal discharge (–35 to 35 ms) and a decrement after the fast component (–35 to 200 ms or 200–500 ms; Fig. 5). In four subjects we observed this neuronal firing pattern. In addition, we quantified the local field potential frequency components by averaging the single trial event-related spectral power around the interictal discharge. All of the subjects demonstrated a significant ( $P < 0.01$ ) broadband decrement in spectral power preceding the event, a significant increase in spectral power during the fast component and a significant decrement again during the slow wave. These changes in spectral power correlate closely with the changes in neuronal firing and together suggest a cortical inhibitory period preceding the fast component, followed by an excitatory period during the fast component of the interictal discharge and an inhibitory period during the slow wave.

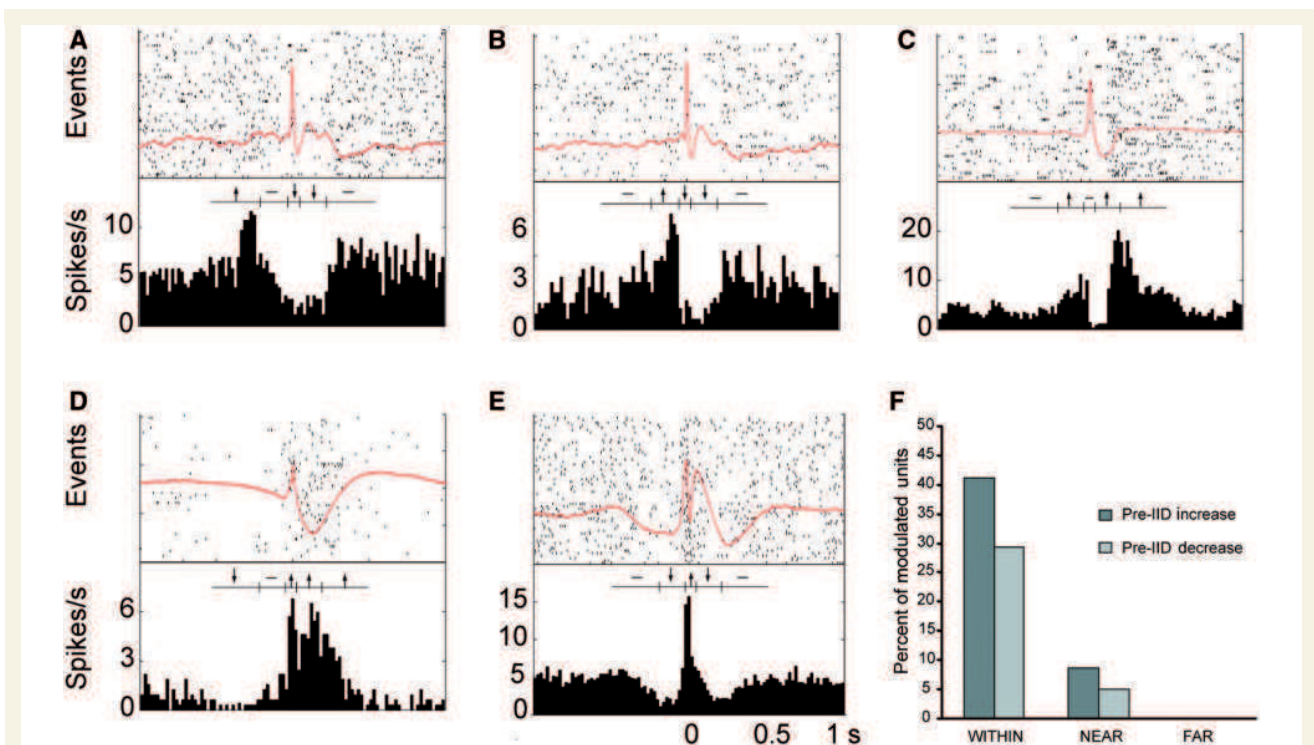


**Figure 4** Neuronal units whose firing changes preceded the interictal discharge (IID). Examples of units that (A) increase long before, (B) increase just before, (C) increase after, (D) decrease long before and (E) decrease just before the interictal discharge. (F) Histogram of percent of modulated units which show an increase or decrease before the interictal discharge in regions which were within, near or far from the seizure onset zone.

## Firing patterns are heterogeneous even within a small cortical region and such variation is present inside and outside the seizure focus

In each subject we found that the several different firing patterns of individual neuronal units could be observed even within a small area of cortex. Units with entirely different firing characteristics could be recorded from a single microelectrode or from microelectrodes within a few 100  $\mu\text{m}$  of each other. These results are demonstrated in Fig. 6, in which the variability in firing patterns of a population of neurons in a restricted cortical region from a single patient is displayed. In this example, the recordings were made within a radius of  $\sim 2.5\text{mm}$  in layers III–IV of the neocortex, as determined from post-resection histology. Note that the local field potentials of all recordings are extremely similar in morphology despite the large variation in firing patterns of the single units. Unit attributes for this example (action potentials, interictal spike histograms, and autocorrelograms) can be found in the online supplementary material (Supplementary Fig. 4). In addition, not only were many different firing patterns found within a small region but many of the different patterns were observed in recordings made both inside and outside of the seizure focus.

## Discussion

### A heterogeneous sub-population of neurons are involved in interictal discharge generation

We studied hundreds of neurons in ten different cortical and sub-cortical structures, both inside and outside the seizure focus, in 20 patients with intractable focal epilepsy. This is perhaps the most extensive survey of single unit activity during human interictal activity reported. In contrast to previous studies, our datasets included large numbers of simultaneously recorded single units—up to 166 units from a small patch of cortex—and covered a larger number of different regions and aetiologies. In this systematic characterization of cortical neuronal activities surrounding interictal discharge events we found a remarkable variety of distinct firing patterns, which we classified into more than 15 categories. Only about half of the recorded units showed some change in firing in or around the interictal discharge. This percentage of modulated neurons agrees with that described by Wyler *et al.* (1982), who found that 44% of recorded neurons showed primarily an increase in firing rate near the interictal discharge peak. Surprisingly, a considerable subset of units showed either an increase or decrease in firing rates well ahead of the interictal

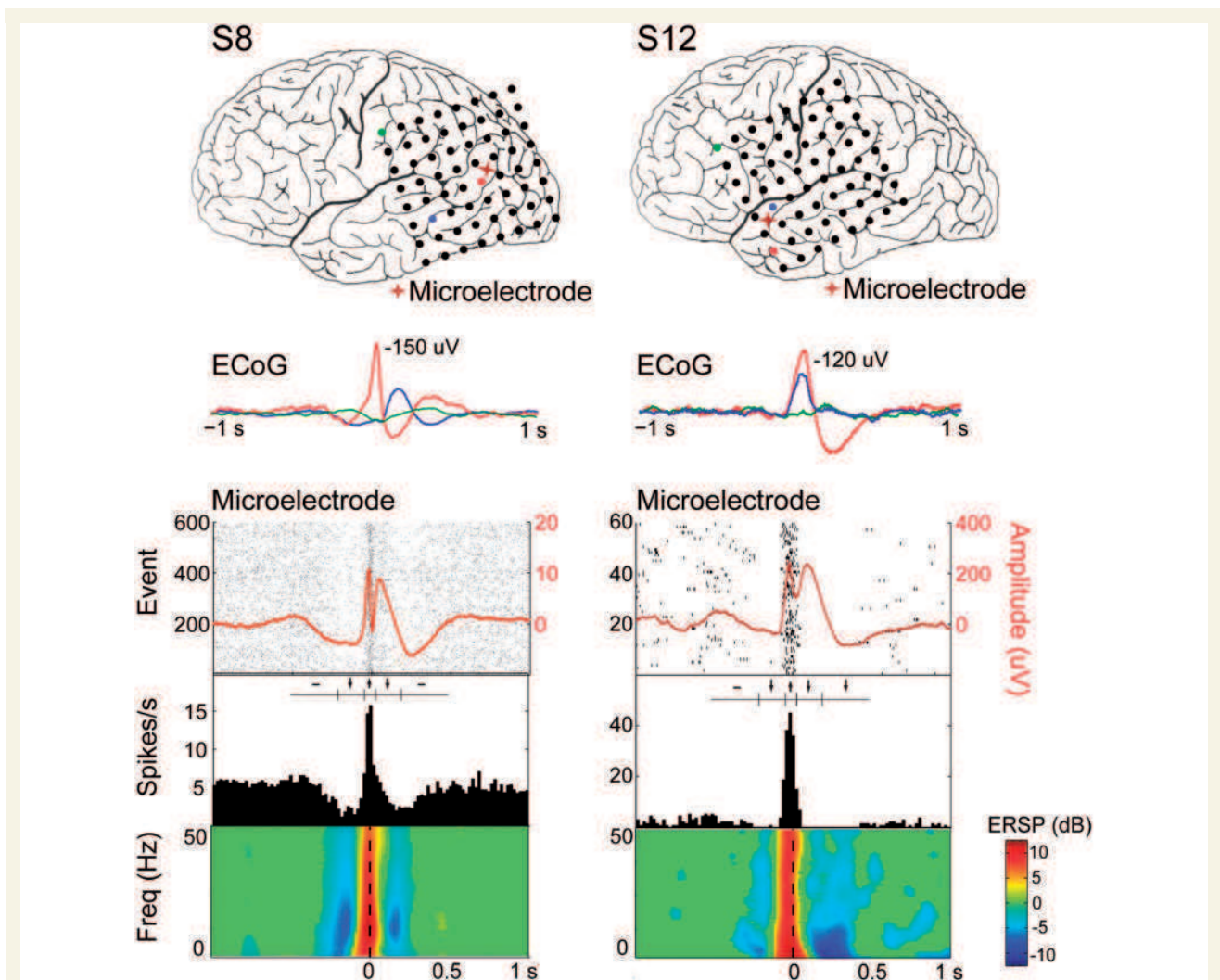


**Figure 5** Transient decrease in both local field potential spectral power and neuronal firing rates precede interictal discharges. Upper panels show the average LFP (red) overlaid on raster plots of neuronal firing. Below is the peri-event time histogram and then time-frequency plots of the LFP (non-significant values are plotted in green. Red indicates a significant increase and blue indicates a decrease ( $P < 0.01$ ). The two columns are from two different patients.

discharge event, in direct contrast to simple models of a paroxysmal depolarizing shift. These results have several implications for the mechanisms underlying epileptiform activity.

First, our results suggest that epileptiform activity, rather than requiring a large mass of neurons, can occur with relatively sparse single neuron participation. That is, for any given event, only a fraction of available neurons participate or are necessary for the generation of the epileptic discharge. In addition, it appears that a different subset of modulated neurons participated in any given event since any given interictal discharge only involved  $\sim 30\%$  of the total pool of recorded modulated units. This finding suggests that at the microphysiological level epileptiform activity can involve multiple neuronal groups or pathways. Certainly, our recording techniques are biased toward sampling the activities of neurons with large cell bodies. Smaller cells and neurons with low amplitude events may not be recorded and therefore their

behaviour during the interictal discharge may not be revealed. As a result, it is possible that the total percentage of neurons involved in any given discharge is larger. Nonetheless, it is clear that (i) a substantial number of neurons are not necessary for, or perhaps are not able to, participate in the epileptic activity; and (ii) the same set of neurons are not always involved. Advances in recording techniques and comparisons with intracellular studies done in model systems should help to complete this picture in more detail.

Second, neurons that were modulated during the interictal discharge had significantly higher bursting and firing rates than those that did not. It is possible that the increase in bursting and firing rates found during the interictal state may be due solely to the interictal discharge itself. To exclude this possibility we analysed recording periods without interictal discharge and found that the modulated population still demonstrated higher firing and bursting

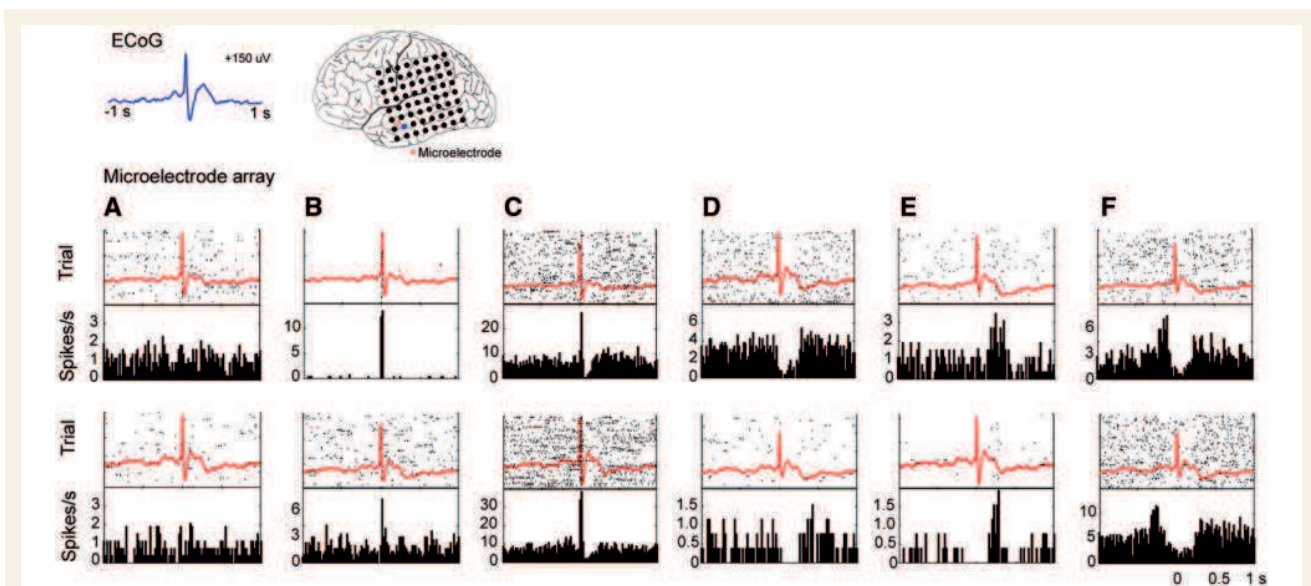


**Figure 6** Neuronal responses are variable in a small cortical region. All 12 units in this analysis were found within 2.5 mm at the same depth in cortex and therefore, the same cortical layer. In each plot, the top panel shows the raster plot (60 events) overlaid with the average local field potential. The lower panel shows the peri-event time histogram. Each column shows examples of similar firing patterns in two different units. Neuronal responses to the interictal discharge were seen that (A) did not change, (B) increased during the fast component, (C) increased during the fast component and decreased during the slow wave, (D) did not change during the fast component but decreased during the wave, (E) increased after the IID peak and wave, and (F) increased before the fast component of the interictal discharge.

propensities. These data lead to two possible conclusions. On the one hand, these findings support the notion, widely expressed in the literature, that neurons crucial for epileptic activity have distinct, if not abnormal, intrinsic activities. On the other hand, it is possible that these increased burst and firing rates reflect purely network phenomena; they are an essential reflection of the network properties in which the neuron is embedded. In either case, the distinct characteristics of these neurons do not explain how an interictal discharge is generated. Examination of the diversity of firing patterns seen before and during the interictal discharge suggests that a particular cascade of neuronal interactions is crucial for formation of the paroxysmal event.

## Modulated firing patterns include changes preceding the interictal discharge

Of the subset of units whose activity was modulated during the interictal discharge, we observed multiple firing patterns both within and across patients. Some of these patterns are expected—an increase in firing during the fast component, a decrease during the slow wave, or both an increase during and a decrease after have all been reported previously (Wyler *et al.*, 1982; Altafullah *et al.*, 1986; Ulbert *et al.*, 2004) and together constitute 60% of the units in our study. These patterns are consistent with the paroxysmal depolarizing shift mechanism—a burst of action potentials followed by a period of relative inhibition. The other activity patterns observed, however, depart from

predictions of the simple paroxysmal depolarizing shift model. Most significantly, almost 20% of the units significantly increased or decreased their firing well before the interictal discharge. Such changes were only seen in or near the seizure onset zone. This is consistent with the common notion that autonomously generated epileptiform activity would have a different origin than similar activity which is propagated and may point toward methods for further delineation of the seizure onset-zone.

These pre-discharge changes were not an artefact of the recording process. While the morphology of the interictal discharge was highly variable across patients, we selected events such that time zero would be aligned to the peak of the fast component of the interictal discharge. Additionally, these local field potentials were derived from the local microelectrode channel; therefore, this temporal shift in different neuronal firing patterns could not result from a shift between the macroelectrode intracranial EEG recording and the microelectrode local field potential recording.

Concomitant with the decrease in firing rate for certain neurons, at least in some patients and locations, is a decrease in broadband local field potential activity. In addition, a different population of neurons displays an increase in firing rates during this same period. These results support the hypothesis that neuronal inhibition may be responsible, in part, for synchronizing cortical activity and generating the interictal discharge. Unfortunately, our analysis of the action potential characteristics associated with units which changed before the discharge showed only modest differentiation between classes. Thus, it is difficult to point conclusively to one type as excitatory and the other as inhibitory. This is, in part, due to our

use of different recording systems but may also reflect the heterogeneity of aetiologies, brain regions and many other factors. Nevertheless, such pre-event changes have also been seen in advance of seizures in an animal model of temporal lobe epilepsy (Bower and Buckmaster, 2008) and around seizure onset in human temporal lobe epilepsy (Verzeano *et al.*, 1971; Babb and Crandall, 1976; Babb *et al.*, 1987). In addition, this period prior to the fast component of the interictal discharge appears similar to the cortical downstate in animal models of sleep (Amzica and Steriade, 1998; Steriade and Amzica, 1998) and in humans during slow wave sleep and evoked during K-complexes of sleep (Cash *et al.*, 2009).

Previously evidence for this type of mechanism was confined mainly to animal studies of generalized epilepsy. Decreased neuronal firing in reticular thalamic cells during a depth positive EEG wave preceding the interictal discharge was recorded from cat cortex during generalized epilepsy (Steriade *et al.*, 1995). Additionally, a correlation in firing was found between interneurons and high frequency oscillations preceded the interictal discharge in rat hippocampus (Ylinen *et al.*, 1995). Based on these studies, it has been proposed that synchronously firing cortical interneurons that decrease firing directly before the interictal discharge permit the bursting of excitatory neurons that make up the fast component of the interictal discharge (de Curtis and Avanzini, 2001). This mechanism may certainly account for our data in which we observed some neurons with decreased firing immediately preceding the interictal discharge. The timescale of this event, however, may be fairly prolonged as there were clear changes for certain neurons hundreds of milliseconds before the event.

In this data set, there was remarkably little that distinguished units of one pattern from another. The action potential or firing characteristics of the neurons at baseline were not very different between different classes of units (with the exception of the Type 5 unit). It is possible that other measures of classification might distinguish these different neuronal types. It is also possible that both the numbers of units recorded here and the recording technologies themselves, being variants on extracellular systems, are not powerful or consistent enough to allow us to reliably distinguish between the neuron types. Further work with larger numbers of examples may eventually allow us to separate more precisely the physiological features corresponding to each neuronal firing pattern and within different brain regions.

## An overall model of the interictal discharge

While the results presented here do not establish causal links between observed neuronal firing patterns and the recorded paroxysm, the existence of these different patterns suggests that activity in multiple different neuronal types, linked in a local but remarkable heterogeneous network, gives rise to the interictal event. One possible sequence of events is that chronic excitation in and around the seizure focus leads to a compensatory, chronic up-regulation of both excitatory and inhibitory activity. As a result, the bursting and firing rates of the neurons are generally

increased. A subset of inhibitory neurons firing together may initially decrease the activity of other neurons in the network. Subsequently, these inhibitory interneurons cease to fire resulting in a hyper-synchronous, excitatory rebound. The post-synaptic effects of this rebound are manifest in the EEG recording of the interictal discharge. During the slow wave there is primarily a decrease in firing—though a small number of neurons increase during this period—suggesting, like the pre-ictal period, that this is an active event representative of network interactions and not just intrinsic currents. Of course, this sequence of events begs the question of what initiates the inhibitory wave of activity to start with. In some situations, sleep for example, ongoing slow oscillations may provide the underlying drive. In other states it may be a purely stochastic process. Further study will be necessary to provide further details of this sequence but the overall scheme highlights the possible importance of inhibition in sculpting epileptic events which have largely been considered purely excitatory in nature.

## Conclusion

In this study we have used microelectrode recordings to quantify and characterize cortical neuronal firing patterns during interictal discharges in patients with focal seizures, finding a tremendous diversity of response including changes in firing that precede the defining interictal discharge itself. Such a variety of neuronal activities supports the hypothesis that interictal discharges are an emergent manifestation of a complex set of network interactions and highlights the potential importance of inhibitory activity in seemingly excitatory paroxysmal events.

## Acknowledgements

The authors thank Alex Chan, Andrew Dykstra, Nima Dehghani, Justine Cormier, Chris Sherman, Jacob Donoghue, Caroline Raclin and Rodrigo Zepeda for their invaluable comments during the preparation of the manuscript. The authors are enormously indebted to the patients that participated in this study, as well as the nursing and physician staff at each facility.

## Funding

This work was supported by CIMIT under U.S. Army Medical Research Acquisition Activity Cooperative Agreement W81XWH-09-2-0001, an EFA-Grass-Morison Fellowship, Rappaport Fellowship and the National Institutes of Health: NIH-NS062092 to SSC.; NIH-NS018741 to EH.; EE was supported by NEI R01EY017658, NIDA R01NS063249, NSF IOB 0645886, the HHMI, and the Klingenstein Foundation; ENB was supported by DP1-0D003646. The information contained herein does not necessarily reflect the position or policy of the Government, and no official endorsement should be inferred.

## Supplementary material

Supplementary material is available at *Brain* online.

## References

- Altafullah I, Halgren E, Stapleton JM, Crandall PH. Interictal spike-wave complexes in the human medial temporal lobe: typical topography and comparisons with cognitive potentials. *Electroencephalogr Clin Neurophysiol* 1986; 63: 503–16.
- Amirnovin R, Williams ZM, Cosgrove GR, Eskandar EN. Visually guided movements suppress subthalamic oscillations in Parkinson's disease patients. *J Neurosci* 2004; 24: 11302–6.
- Amzica F, Steriade M. Electrophysiological correlates of sleep delta waves. *Electroencephalogr Clin Neurophysiol* 1998; 107: 69–83.
- Babb TL, Carr E, Crandall PH. Analysis of extracellular firing patterns of deep temporal lobe structures in man. *Electroencephalogr Clin Neurophysiol* 1973; 34: 247–57.
- Babb TL, Crandall PH. Epileptogenesis of human limbic neurons in psychomotor epileptics. *Electroencephalogr Clin Neurophysiol* 1976; 40: 225–43.
- Babb TL, Pretorius JK, Kupfer WR, Crandall PH. Glutamate decarboxylase-immunoreactive neurons are preserved in human epileptic hippocampus. *J Neurosci* 1989; 9: 2562–74.
- Babb TL, Wilson CL, Isokawa-Akesson M. Firing of human limbic neurons during stereoencephalography (SEEG) and clinical temporal lobe seizures. *Electroencephalogr Clin Neurophysiol* 1987; 66: 467–82.
- Baumgartner C, Lindinger G, Ebner A, Aull S, Sesles W, Olbrich A, Lurger S, Czeck T, Burgess R, Lüders H. Propagation of interictal epileptic activity in temporal lobe epilepsy. *Neurology* 1995; 45: 118–22.
- Blume WT. Current trends in electroencephalography. *Curr Opin Neurol* 2001; 14: 193–7.
- Blume WT, Holloway GM, Wiebe S. Temporal epileptogenesis: localizing value of scalp and subdural interictal and ictal EEG data. *Epilepsia* 2001; 42: 508–14.
- Blume WT, Kaibara M. Localization of epileptic foci in children. *Can J Neurol Sci* 1991; 18: 570–2.
- Bower MR, Buckmaster PS. Changes in granule cell firing rates precede locally recorded spontaneous seizures by minutes in an animal model of temporal lobe epilepsy. *Neurophysiol* 2008; 99: 2431–42.
- Cameron KA, Yashar S, Wilson CL, Fried I. Human hippocampal neurons predict how well word pairs will be remembered. *Neuron* 2001; 30: 289–98.
- Cardin JA, Carlen M, Meletis K, Knoblich U, Zhang F, Deisseroth K, et al. Driving fast-spiking cells induces gamma rhythm and controls sensory responses. *Nature* 2009; 459: 663–7.
- Cash SS, Halgren E, Dehghani N, Rossetti AO, Thesen T, Wang C, et al. The human K-complex represents an isolated cortical down-state. *Science* 2009; 324: 1084–7.
- Chatrian GE, Bergamini L, Dondey M, Klass DW, Lennox-Buchthal M, Petersen I. A glossary of terms most commonly used by clinical electroencephalographers. *Electroencephalogr Clin Neurophysiol* 1974; 37: 538–48.
- Colder BW, Frysinger RC, Wilson CL, Harper RM, Engel J Jr. Decreased neuronal burst discharge near site of seizure onset in epileptic human temporal lobes. *Epilepsia* 1996; 37: 113–21.
- de Curtis M, Avanzini G. Interictal spikes in focal epileptogenesis. *Prog Neurobiol* 2001; 63: 541–67.
- Dale AM, Fischl B, Sereno MI. Cortical surface-based analysis. I. Segmentation and surface reconstruction. *Neuroimage* 1999; 9: 179–94.
- Delgado-Escueta AV, Walsh GO. The selection process for surgery of intractable complex partial seizures: Surface EEG and depth electrography. In: Ward AA Jr, Penry JK, Purpura DP, editors. *Epilepsy*. New York: Raven press; 1983. p. 295–326.
- Delorme A, Makeig S. EEGLAB: an open source toolbox for analysis of single-trial EEG dynamics including independent component analysis. *J Neurosci Methods* 2004; 134: 9–21.
- Ekstrom AD, Kahana MJ, Caplan JB, Fields TA, Isham EA, Newman EL, et al. Cellular networks underlying human spatial navigation. *Nature* 2003; 425: 184–8.
- Engel J, Crandall PH, Rausch P. Surgical treatment of partial epilepsies. In: Rosenberg RN, Grossman RG, Schoclet S, editors. *The clinical Neurosciences*. New York: Churchill Livingstone; 1983. p. 1349–80.
- Engel J, Rausch R, Lieb JP, Kulh DE, Crandall PH. Correlation of criteria used for localizing epileptic foci in patients considered for surgical therapy of epilepsy. *Ann Neurol* 1981; 9: 215–24.
- Fabó D, Maglóczy Z, Wittner L, Pék A, Erő L, Czirják S, et al. Properties of in vivo interictal spike generation in the human subiculum. *Brain* 2008; 131: 485–99.
- Gale JT, Shields DC, Jain FA, Amirnovin R, Eskandar EN. Subthalamic nucleus discharge patterns during movement in the normal monkey and Parkinsonian patient. *Brain Res* 2009; 1260: 15–23.
- Gibbons J. *Nonparametric Statistical Inference*. New York: Marcel Dekker; 1985.
- Gibbs FA, Davis H, Lennox WG. The electroencephalogram in epilepsy and conditions with impaired consciousness. *Archives of Neurology and Psychiatry* 1935; 34: 1133–48.
- Goldensohn ES, Purpura DP. Intracellular potentials of cortical neurons during focal epileptogenic discharges. *Science* 1963; 139: 840–2.
- Gotman J. Quantitative measurements of epileptic spike morphology in the human EEG. *Electroencephalogr Clin Neurophysiol* 1980; 48: 551–7.
- Hochberg LR, Serruya MD, Friehs GM, Mukand JA, Saleh M, Caplan AH, et al. Neuronal ensemble control of prosthetic devices by a human with tetraplegia. *Nature* 2006; 442: 164–71.
- Hogg RV LJ. *Engineering statistics*. New York: MacMillan Publishing; 1987.
- Hollander M, Wolfe DA. *Nonparametric statistical methods*. New York: Wiley; 1999.
- Holmes MD, Kutsy RL. Interictal, unifocal spikes in refractory extratemporal epilepsy predict ictal origin and postsurgical outcome. *Clin Neurophysiol* 2000; 111: 1802–8.
- Isokawa-Akesson M, Wilson CL, Babb TL. Inhibition in synchronously firing human hippocampal neurons. *Epilepsy Res* 1989; 3: 236–47.
- Keller CJ, Cash SS, Narayanan S, Wang C, Kuzniecky R, Carlson C, et al. Intracranial microprobe for evaluating neuro-hemodynamic coupling in unanesthetized human neocortex. *J Neurosci Methods* 2009; 179: 208–18.
- Kooi KA. Voltage-time characteristics of spikes and other rapid electroencephalographic transients: semantic and morphological considerations. *Neurology* 1966; 16: 59–66.
- Lewicki MS. Bayesian modeling and classification of neural signals. *Neural Comput* 1994; 6: 1005–30.
- Lieb JP, Woods SC, Siccardi A, Crandall PH, Walter DO, Leake B. Quantitative analysis of depth spiking in relation to seizure foci in patients with temporal lobe epilepsy. *Electroencephalogr Clin Neurophysiol* 1978; 44: 641–63.
- Marsaglia G, Wang J. Evaluating Kolmogorov's Distribution. *J Stat Software* 2003; 8: 1–4.
- Massey FJ. The Kolmogorov-Smirnov test for goodness of fit. *J Am Stat Association* 1951; 46: 68–78.
- Matsumoto H, Ajmone Marsan C. Cellular mechanisms in experimental epileptic seizures. *Science* 1964; 144: 193–4.
- Merchant H, Naselaris T, Georgopoulos AP. Dynamic sculpting of directional tuning in the primate motor cortex during three-dimensional reaching. *J Neurosci* 2008; 28: 9164–72.
- Niedermeyer E, Lopes da Silva F. *Electroencephalography: Basic Principles, Clinical Applications and Related Fields*. New York: Lippincott Williams and Wilkins; 1982.

- Pedley T. Epilepsy and the human electroencephalogram. In: Schwartzkroin P, Wheal H, editors. *Pathophysiology of Epilepsy*. London: Academic Press; 1984. p. 130.
- Penfield W, Jasper H. *Epilepsy and the functional anatomy of the human brain*. Boston: Little Brown; 1954.
- Prince DA, Wong RK. Human epileptic neurons studied in vitro. *Brain Res* 1981; 210: 323–33.
- Rayport M, Waller HJ. Technique and results of micro-electrode recording in human epileptogenic foci. *Electroencephalogr Clin Neurophysiol Suppl* 1967; 25: 143+.
- Raz A, Vaadia E, Bergman H. Firing patterns and correlations of spontaneous discharge of pallidal neurons in the normal and the tremulous 1-methyl-4-phenyl-1,2,3,6-tetrahydropyridine vervet model of parkinsonism. *J Neurosci* 2007; 20: 8559–71.
- Schevon CA, Ng SK, Cappell J, Goodman RR, McKhann G Jr, Waziri A, et al. Microphysiology of epileptiform activity in human neocortex. *J Clin Neurophysiol* 2008; 25: 321–30.
- Schwartzkroin PA, Turner DA, Knowles WD, Wyler AR. Studies of human and monkey "epileptic" neocortex in the in vitro slice preparation. *Ann Neurol* 1983; 13: 249–57.
- Staba RJ, Wilson CL, Bragin A, Fried I, Engel J Jr. Sleep states differentiate single neuron activity recorded from human epileptic hippocampus, entorhinal cortex, and subiculum. *J Neurosci* 2002; 22: 5694–704.
- Steriade M, Amzica F. Coalescence of sleep rhythms and their chronology in corticothalamic networks. *Sleep Res Online* 1998; 1: 1–10.
- Steriade M, Contreras D. Relations between cortical and thalamic cellular events during transition from sleep patterns to paroxysmal activity. *J Neurosci* 1995; 15: 623–42.
- Swadlow HA. Fast-spike interneurons and feedforward inhibition in awake sensory neocortex. *Cereb Cortex* 2003; 13: 25–32.
- Truccolo W, Friehs GM, Donoghue JP, Hochberg LR. Primary motor cortex tuning to intended movement kinematics in humans with tetraplegia. *J Neurosci* 2008; 28: 1163–78.
- Ulbert I, Halgren E, Heit G, Karmos G. Multiple microelectrode-recording system for human intracortical applications. *J Neurosci Methods* 2001; 106: 69–79.
- Ulbert I, Heit G, Madsen J, Karmos G, Halgren E. Laminar analysis of human neocortical interictal spike generation and propagation: current source density and multiunit analysis in vivo. *Epilepsia* 2004; 45 (Suppl 4): 48–56.
- Ulbert I, Karmos G, Heit G, Halgren E. Early discrimination of coherent versus incoherent motion by multiunit and synaptic activity in human putative MT+. *Hum Brain Mapp* 2001; 13: 226–38.
- Verzeano M, Crandall PH, Dymond A. Neuronal activity of the amygdale in patients with psychomotor epilepsy. *Neuropsychologia* 1971; 9: 331–44.
- Walczac TS, Jayakar P. Interictal Electroencephalography. In: Engel J, Pedley TA, editors. *Epilepsy: a comprehensive textbook*. New York: Raven Press; 1997. p. 831–48.
- Wang C, Ulbert I, Schomer DL, Marinkovic K, Halgren E. Responses of human anterior cingulate cortex microdomains to error detection, conflict monitoring, stimulus-response mapping, familiarity, and orienting. *J Neurosci* 2005; 25: 604–13.
- Ward AA, Thomas LB. The electrical activity of single units in the cerebral cortex of man. *Electroencephalogr Clin Neurophysiol* 1955; 7: 135–6.
- Waziri A, Schevon CA, Cappell J, Emerson RG, McKhann GM 2nd, Goodman RR. Initial surgical experience with a dense cortical microarray in epileptic patients undergoing craniotomy for subdural electrode implantation. *Neurosurgery* 2009; 64: 540–5; discussion 545.
- Williamson A, Spencer DD. Electrophysiological characterization of CA2 pyramidal cells from epileptic humans. *Hippocampus* 1994; 4: 226–37.
- Worrell GA, Gardner AB, Stead SM, Hu S, Goerss S, Cascino GJ, et al. High-frequency oscillations in human temporal lobe: simultaneous microwire and clinical macroelectrode recordings. *Brain* 2008; 131: 928–37.
- Wyler AR, Ojemann GA, Ward AA Jr. Neurons in human epileptic cortex: correlation between unit and EEG activity. *Ann Neurol* 1982; 11: 301–8.
- Ylinen A, Bragin A, Nadasdy Z, Jando G, Szabo I, Sik A, et al. Sharp wave-associated high-frequency oscillation (200 Hz) in the intact hippocampus: network and intracellular mechanisms. *J Neurosci* 1995; 15: 30–46.